IN VITRO SELECTION AND CHARACTERIZATION OF MONO-, DI-, AND TRIVALENT METAL-DEPENDENT DNAZYMES AND THEIR SENSING APPLICATIONS

BY

SEYED FAKHREDDIN TORABI

DISSERTATION

Submitted in partial fulfillment of the requirements
for the degree of Doctor of Philosophy in Biochemistry
in the Graduate College of the
University of Illinois at Urbana-Champaign, 2014

Urbana, Illinois

Doctoral Committee:

Professor Yi Lu, Chair
Professor Susan Martinis
Professor Scott Silverman
Professor Emad Tajkhorshid

ABSTRACT

Since the discovery of nucleic acid enzymes and aptamers that can perform functional roles other than storing genetic information; a new paradigm in nucleic acid chemistry has been opened. In 1990 the first artificially isolated functional nucleic acid was discovered through an *in vitro* process called SELEX, Systematic Evolution of Ligands by Exponential Enrichment. Aptamers are known as *in vitro* isolated functional nucleic acids that can bind their target ligands with high affinity and selectivity. Catalytic DNA or DNAzymes, another class of functional nucleic acids, were first isolated from pools of random DNA in 1994 using the *in vitro* selection procedure to catalyze the cleavage of a phosphodiester bond. Since the discovery of the first aptamer and DNAzyme, many more functional nucleic acids have been isolated and engineered to perform various functions, including binding to a wide variety of different ligands and catalysis of many different chemical reactions. Due to the superior properties of functional nucleic acids, they have found particular interest in environmental sensing and monitoring, biomedical diagnostics and therapy.

Iron is a critical component of oxygen transportation and electron transfer, and is tightly associated with functions of many enzymes. Deficiency in iron leads to anemia, which is especially detrimental to pregnant women. Knowing the concentration of both Fe(II) and Fe(III) will be beneficial for clinical diagnoses. A DNAzyme pair selective for Fe(II) and Fe(III) is of particular interest, because of their interconversion in an biological environment. Also comparison of the DNAzymes selective for each would provide a fundamental understanding about DNAzymes' abilities to distinguish between different oxidation states of the same metal ion. *In-vitro* selection experiments for Fe(II) and Fe(III)-dependent RNA-cleaving DNAzymes were carried out. *In-vitro* selection of Fe(II)-dependent DNAzyme selection was carried out in presence/absence of reduced

glutathione in oxygen free condition. For each condition the effect of counter selection was investigated using mixture of divalent metal ions including Pb^{2+}, Mn^{2+}, Cd^{2+}, Zn^{2+}, and Co^{2+}. Different pools were isolated that require Fe(II) for activity. *Cis*-acting DNAzymes were tested in presence of Fe(II) to find most active and selective Fe(II)-dependent DNAzymes. A number of DNAzymes converted into trans-cleaving DNAzymes through systematic truncation studies. Fe(II)-dependent DNAzymes including H5, the most active DNAzyme, were characterized. It was shown that the H5 DNAzyme selectivity reacts with Fe(II) in a mixture containing both Fe(II) and Fe(III). We are in the process of designing a fluorescent sensor for Fe(II) based on the H5 DNAzyme. This sensor will be tested for intracellular imaging of Fe(II) in living cells.

To obtain Fe(III)-dependent DNAzymes, different selection protocols and selection conditions were investigated. In order to select active Fe(III)-DNAzymes, various attempts were remained fruitless, including efforts of two previous Lu lab members. The choice of negative selection condition, Fe(III)-stabilizing agent and other selection parameters were shown to be vital to the success of Fe(III)-dependent DNAzyme selection. Finally, several classes of Fe(III)-dependent DNAzymes were selected in presence of 2-Bis(2-hydroxyethyl)amino-2-(hydroxymethyl)-1,3-propanediol (Bis-Tris) as a stabilizing agent for Fe(III) at pH 5.5. Activity of several clones from selected pools were examined in presence of Fe(III) to find the most active sequence. A number of active DNAzymes were converted into *trans*-cleaving DNAzymes including B12 and D13, the most active clones. Buffer, ligand, and pH requirements of both DNAzymes were investigated. It was shown that Fe(III)-dependent DNAzymes are highly selective and are able to react with Fe(III) without any interference from Fe(II). A turn-on fluorescent sensor for Fe(III) is designed based on the B12 DNAzyme sequence. We would like to test our fluorescent sensor capability in imaging Fe(III) in endosome.

Sodium ion detection is of particular interest. Infants suffer from diabetes insipidus (DI) are prone to wide sodium fluctuations, due to a high fluid diet and uncertainties in the assessment of hydration status. These individuals require daily assessment of serum and urine sodium. Monitoring sodium level is important in several other health conditions such as syndrome of inappropriate antidiuretic hormone secretion, hepatorenal syndrome, hypertension and different types of hyponatremia and hypernatremia. Two parallel *in vitro* selections were carried out to expand capability of DNAzymes in cleaving a ribonucleotide phosphodiester bond independent of any divalent or trivalent metal ion and, *specifically selective for the sodium ion*. Having efficient sodium specific DNAzyme can be used to design fast and simple point-of-care sodium sensors. A column-based strategy was used to isolate sodium-specific DNAzymes. NaA43 DNAzyme was isolated, truncated into a *trans*-acting DNAzyme, and biochemically characterized. Interestingly NaA43 is at least 10,000-fold selective for sodium over other monovalent ions such as lithium. A turn-on fluorescent sensor was designed based on NaA43 and tested in imaging sodium inside living cells. As a proof of concept we demonstrated that our sodium DNAzyme-based sensor can be used for cellular studies. We are designing a ratiometric fluorescent sensor based on NaA43 that can be used for quantitative assessment of sodium inside living cells. Additionally, a biosensor based on personal glucose meter and NaA43 was developed. It was shown that our NaA43-based sensor can be used to detect sodium in human serum with high accuracy (0.99).

Mercury is a highly toxic and widely distributed pollutant in the environment. It is known that mercury ion is able to bind to a class of functional DNA containing thymine-thymine mismatch. To develop a platform for detection of mercury ion, ability of functional DNA–linked gold nanoparticles was demonstrated for a fast and simple detection and quantification of Hg^{2+} ions in aqueous solution, with high sensitivity and selectivity over competing metal ions. DNA

functionalized gold nanoparticles were aggregated using a functional DNA containing several thymine-thymine mismatches. Mercury ions induce the folding of linker DNA strand by thymine–Hg^{2+}–thymine formation which disassemble aggregated gold nanoparticles rapidly and cause color change from purple to red. Such a system has been converted into dipstick tests using lateral flow devices to make it even more practical for on-site detection.

To my truelove Salehe

To my beloved parents

To my dear sisters

And

To the light of my life, my daughter

ACKNOWLEDGEMENTS

First, I would like to express my sincere appreciation to my research advisor, Prof. Yi Lu, whom without this research would not have been possible. He has given me the opportunity to adventure, research and learn. I will be forever in debt to him for all of his supports and guidance. I am thankful to my admirable committee members for their support throughout my graduate school time. I would like to thank Prof. Scott Silverman, who provided me the opportunity to discuss my scientific questions with him and learn from him; He inspired me to be a better scientist. I would like to thank Prof. Susan Martinis for her guidance and supports. I also would like to thank Prof. Emad Tajkhorshid whose enthusiasm for science and support have had a lasting effect on my life.

I am also thankful to my wonderful colleagues and all the past and current Lu lab members who made my graduate stay very memorable. I wish to thank Dr. Nandini Nagraj for patiently teaching me how to do activity assay. I thank Dr. Marjorie Cepeda, Hannah Ihms, Dr. Tian Lan, Dr. Eric Null, Dr. Priya Mazumdar, Dr. Brian Wong, Dr. Zidong Wang and all other senior lab mates who helped me in the first years. I also want to thank Claire McGhee, Peiwen Wu, Dr. JingJing Zhang, Kevin Hwang, and Lu Chen for their collaboration on the sensing projects based on sodium DNAzyme. I want to specially thank Li Huey Tan, Parisa Hosseinzadeh, and Kevin Hwang for being the most wonderful and helpful people I have ever met. I will never forget their kindness. Also I wish to thank Dr. Joy Sinha and Dr. Joonhee Han for all the help and useful discussions. I could continue on and on: thank you to all you Lu lab members for being incredible.

I wish to thank my dear friends who made Urbana feels like home. Seyed Saleh Yousefi, Mohammad Naghnaeian, Sara Bahramian, Ehsan Shafie, Negin Sattari, Narjes Tavoosi and Amin

Haghighat, I owe you all for your friendship and supports. I would like to specially thank my dearest friend Abdolhossein Sharafi who is like a brother to me.

I cannot find words to express my appreciation to my Mom, Fatemeh Zandi, and Dad, Seyed Mohammad Javad Torabi, who are my guide and my hero throughout my life. Mom and Dad, thank you, thank you, thank you for all that you have taught me about life, love, and God. Your love and presence means a world to me. I would like to thank my sisters, Fakhrossadat, Noorossadat, and Najmossadat for their unending love and support. Finally I wish to express my deepest appreciation to my truelove Salehe, my lovely wife, who deserves much appreciation. Without her I could not succeed. I am truly grateful of all your kindness, patience, and support you have given me. I wish to thank my darling daughter whose presence has delighted our world. And lastly, but most importantly, I thank Allah (God), the most Compassionate and the most Merciful, and our Prophet Mohammad, and his family and all his true followers. As Allah says "Surely, Allah is with the patient", I am sincerely grateful of Allah for the patience and strength he has given me to get through up and downs of life. I deeply ask Allah to bountifully give mercy, love, health, patience, and guidance to all my family, friends, colleagues, and all those people who helped and supported me to make this thesis possible and unforgettable experience for me.

TABLE OF CONTENTS

LIST OF FIGURES

LIST OF TABLES

1 Chapter 1. Introduction

1.1 DNA in Biology

Deoxyribonucleic acid, DNA, is known as "blueprint" of living organisms as it contains the required information to create the vast array of proteins, needed for cellular functions. In molecular biology, it is very well known that an individual characteristics (physical, biochemical, and physiological) are defined as a result of the DNA sequence interacting with the environment (*1*). According to the classic view of the central dogma of biology the coded genetic information stored in DNA is transcribed into ribonucleic acids, RNA, which contain the program for synthesis of proteins (*1*, *2*). Although the central dogma of biology reflects how information is organized in biological systems, many exceptions of this dogma are now known. One example is discovery of various types of functional RNA that are encoded by DNA regions that do not encode proteins (*3*).

Chemical structures of DNA and RNA are very similar. Both DNA and RNA are composed of nucleosides (themselves composed of a nitrogenous base linked to a ribose (RNA) or deoxyribose (DNA) sugar) joined by a phosphate backbone as shown in Figure 1.1. There are two types of nucleobases used in the structure of DNA including purines (adenine and guanine) and pyrimidines (cytosine and thymine). Uracil, used in RNA, and thymine share very similar chemical structure. A sequence of DNA or RNA is a long polymer of different nucleotides linked with phosphodiester bonds between each nucleotide. DNA usually forms a double-stranded helical structure through base pairing interactions. Adenine forms a base pair with thymine and guanine forms a base pair with cytosine. Interactions of bases in base pairing occur through hydrogen bonding. In contrast to DNA, RNA is usually found in a single stranded form which allows it to base pair with itself, forming complex structures with different functions.

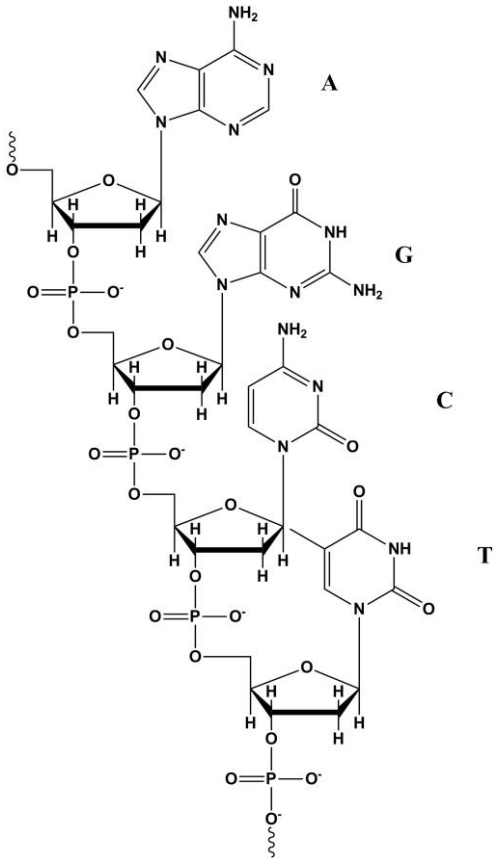

Figure 1.1 Chemical structures of nucleotides represented in a single stranded DNA.

1.2 Functional DNA

For more than 40 years, DNA was known to store genetic information based on the central dogma of molecular biology (*1, 4*). However after the first discovery of DNA aptamers and DNA enzymes (DNAzymes) in early 1990s (*5-7*), increasing number of functional DNA were isolated through *in vitro* selection (*8, 9*). Functional DNA are DNA molecules with functions beyond genetic storage. They are short single-stranded DNA molecules with enzymatic function (called DNAzymes or deoxyribozymes), biorecognition function (called aptamers) or both (called aptazymes). Aptamers are single stranded DNA molecules isolated from random-sequence DNA libraries. They can bind to a broad range of targets, from metal ions and organic molecules to

proteins and cells, with high specificity and affinity (*10, 11*). The isolation of the DNA aptamers is done through a combinatorial biology technique called systematic evolution of ligands by exponential enrichment (SELEX) (*12*). They are often analogous to antibodies due to their selectivity and sensitivity in binding a broad range of molecules (*13*). Due to their recognition properties, aptamers have been used in bioanalytical applications like molecular recognition elements and have been transformed into fluorescent, colorimetric, electrochemical, and magnetic sensors for a variety of different applications (*14-16*). Aptamers have several advantages over antibodies (*13*). These advantages include: a) after the sequence of the aptamer is identified it can be synthesized with automated DNA synthesis at a low cost and at a large scale; b) chemical modifications of DNA with various reactive and reporting functionalities can be done without interfering with DNA aptamer function; c) they can be denatured and renatured without loss of function; d) The DNA aptamers have higher shelf life than proteins or RNA molecules.

Another class of functional DNA molecules is DNAzymes that are DNA molecules with catalytic activity (*5, 8*). DNAzymes are obtained by an *in vitro* selection method from a large pool of random DNA molecules similar to the selection of aptamers. There have been hundreds of DNAzyme sequences isolated in many laboratories world-wide which can catalyze different chemical reactions (see Table 1.1). There have been tremendous efforts in turning the DNAzymes into the biological and chemical sensors for real time applications (*11, 16, 17*). The third class of functional DNA is allosteric DNAzymes or aptazymes. They are designed by combination of the functional regions of DNAzymes and aptamers in one system. They have a ligand binding motif for a specific small molecule and a catalytic fragment which can catalyze a chemical reaction as described above (*18, 19*).

Table 1.1 Examples of different DNAzymes isolated through *in vitro* selection.

Reaction	Cofactor	k_{max} (min^{-1})	Ref.
RNA cleavage	Pb^{2+}	1	(*5*)
	Mg^{2+}	0.01	(*20*)
	Ca^{2+}	0.1	(*21*, *22*)
	Mg^{2+}	10	(*22*)
	None	0.006	(*23*)
	L-histidine	0.2	(*24*)
	Zn^{2+}	~40	(*25*)
	Zn^{2+} [a]	~4	(*26*)
	Mg^{2+}	1.7	(*27*)
	None [b]	0.044 - 0.1	(*28-30*)
	Co^{2+}	7	(*31*)
	Cd^{2+}, Mn^{2+}, Ni^{2+}	~1	(*32*)
	UO_2^{2+}	~1.2	(*33*)
	Ce^{3+} [c]		(*34*)
DNA cleavage	Cu^{2+}	0.2	(*35*)
	Zn^{2+}	1	(*36*)
	Mn^{2+} and Zn^{2+}	0.045	(*37*)
RNA ligation	Mn^{2+}	~2.2	(*38*)
	Mg^{2+}	0.5	(*39*)
	Mg^{2+}	0.013	(*40*)
	Mg^{2+}	0.1	(*41*)
	Zn^{2+}	0.5	(*42*)
DNA ligation	Cu^{2+} or Zn^{2+}	0.07	(*43*)
	Mn^{2+}	4-Oct	(*44*)
DNA phosphorylation	Ca^{2+}	0.01	(*45*)
DNA depurination	IO_4^-		(*46*)
DNA adenylation	Cu^{2+}	0.003	(*47*)
Thymine dimer cleavage	None	4.5	(*48*)
Phosphoramidate bond cleavage	Mg^{2+}	$\sim 5\times10^{-4}$	(*49*)
N-glycosylation	Ca^{2+}	0.5	(*50*)
Porphyrin metallation	None	1.3	(*51*)
Carbon-carbon bond formation	Ca^{2+}	3	(*52*)
Reductive amination	Ni^{2+} and IO_4^-	0.006	(*53*)
Peptide-DNA conjugation	Zn^{2+}	0.007	(*54*)
Hydrolysis of amides	Zn^{2+} and Mn^{2+}	0.05	(*55*)
Tyrosine phosphorylation	Zn^{2+} and Mn^{2+}	0.004	(*56*)
Tyrosine and serine dephosphorylation	Zn^{2+}	0.7	(*57*)

[a] imidazole-modified DNAzyme, [b] DNAzyme modified with three protein-like functionalities, [c] DNAzyme reacts with all trivalent metal ions (lanthanides)

1.3 *In Vitro* Selection of DNAzymes

Although DNAzymes have not been found in nature, *in vitro* selection has revealed that single stranded DNA molecules can form complex structures with ability of catalyzing different chemical reactions (*8*). Basic principles of SELEX and *in vitro* selection are similar and the main difference is how functional DNA are separated from the rest of the initial random library. A general scheme of an *in vitro* selection process is represented in Figure 1.2.

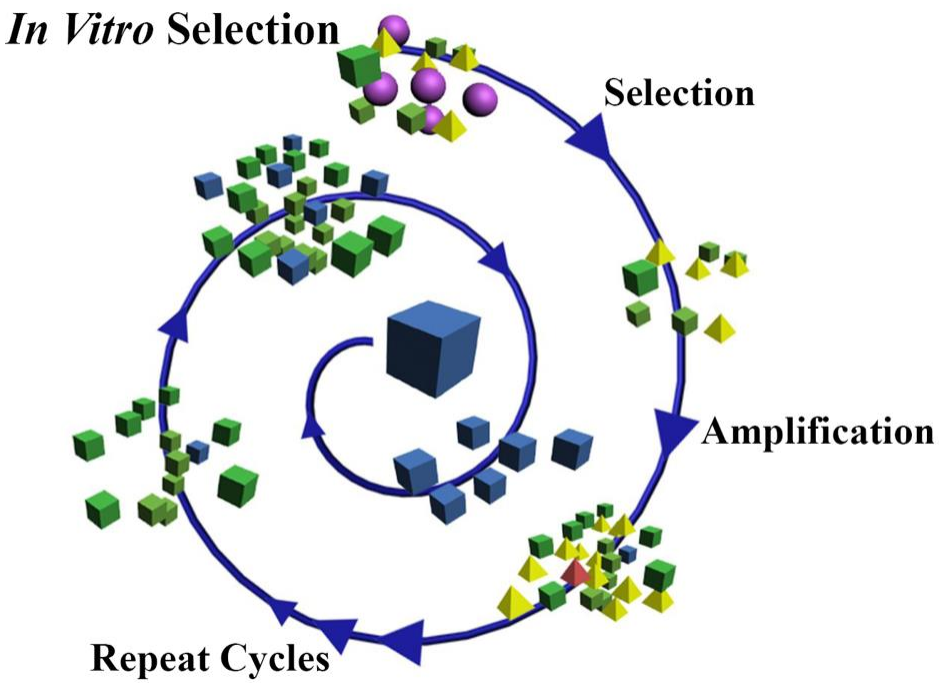

Figure 1.2 General schemes for the in vitro selection process. The initial rounds of the selection begins with a random DNA library (up to 10^{15} individual sequences). Through repeated cycles of selection and amplification functional sequences are obtained.

Among the several classes of isolated DNAzymes, RNA-cleaving DNAzymes are the most extensively used class in designing sensors (6) and developing DNA computational tools (7, 8). RNA-cleaving DNAzyme selection is similar to the process represented in Figure 2.1. Most of the

isolated RNA-cleaving DNAzymes are cofactor dependent (metal or nonmetal cofactors) with few exceptions (see Table 1.1). To isolate a metal dependent RNA-cleaving DNAzyme, the initial random pool (10^{14} to 10^{15} unique sequences) is incubated with a metal ion and cleaved vs. uncleaved sequences may be separated through immobilization of uncleaved DNA on beads (column-based selection) or by denaturing polyacrylamide gel electrophoresis (PAGE) (gel-based selection). In gel-based selection active sequences (cleaved pool) will be separated from nonfunctional DNA (uncleaved pool) based on their size difference. Cleaved sequences are then amplified and subjected to further rounds of selection. The initial random pool consists of constant regions (primer binding sites) and usually one random region. The random region is incorporated into the pool through solid surface synthesis. In this process instead of providing a specific nucleotide, equal mixture of all four nucleotides is provided. The possible number of random sequences are determined by 4^n where n is the length of the random region and 4 represents the four possible bases at each position (A, C, G, or T). It is feasible to cover all possible sequences in a DNA pool with ~ 25 nucleotides in the random region. Increasing size of the random region results in limiting the fraction of possible sequences that can be sampled in the pool. This incomplete sampling is due to the fact that it is impractical to work with kilograms of DNA. Although using relatively short random regions (<25 nucleotides) makes it possible to sample the sequence space completely, using longer random regions may allow to search for more complex structures (*58*). It has been shown that thorough sampling of the sequence space is not required to obtain functional DNA through *in vitro* selection (*59*).

1.4 Functional DNA Applications

In the past two decades, many different targets ranging from metal ions and small molecules to large and complex structures such as cancer cells have been used for selection of functional nucleic acids and due to the superior properties of selected molecules they have found particular interest in environmental sensing and monitoring, disease diagnostics and cancer therapy (*8, 14, 60, 61*). One of the main advantages utilizing SELEX-derived functional DNA is that in principle the selection process can be tailored to select functional DNA to almost any target of interest (*62*).

Metal specificity of DNAzymes has made them a proper tool in designing metal ion sensors (*61*). Unlike small-molecule or protein-based sensors, DNAzymes with high specificity for a metal ion of interest can be obtained from a combinatorial process, starting from a large DNA library containing up to 10^{15} different sequences (*5, 8*). Because of such high metal ion selectivity, these DNAzymes have been converted into sensors for many metal ions, such as Pb^{2+}, UO_2^{2+}, Hg^{2+}, and Cu^{2+}, based on fluorescence, colorimetry, or electrochemistry (*19, 32-34, 63-66*). The development of these sensors has significantly expanded the range of metal ions that can be detected in different samples. The major advantages of this type of sensor are that it does not require advanced knowledge in order to construct a metal-binding site, and the binding affinity and selectivity toward metal ions can be fine-tuned by introducing different levels of stringency during the selection process. Moreover, it is relatively simple to synthesize DNA and many different modifications and functional groups can be easily introduced into the DNA during synthesis. Furthermore, DNA is naturally water-soluble and biocompatible. All of these properties make DNAzyme sensors an attractive candidate for biosensing of metal ions. Recently, it is shown that

RNA-cleaving DNAzymes can be used for intracellular sensing of different metal ions such as Pb^{2+} (*67*), UO_2^{2+} (*68*), and Zn^{2+} (*69*) as well as histidine (*70*) .

1.5 Research Focus

The research to be presented is focused on isolation of metal specific DNAzymes for three different metal ions (Na^+, Fe^{2+}, and Fe^{3+}) through *in vitro* selection. **Chapter 2** discusses different *in vitro* selection attempts in isolating Fe(III)-specific DNAzymes. Several attempts in isolating these DNAzymes failed including my initial experiments as well as efforts from previous Lu lab members, Hannah Ihms, Peter Bruesehoff and Kevin Nelson. Results from the failed selections are presented in addition to the lessons learned from them. Additionally, several *in vitro* selections which resulted in isolation of Fe(III)-dependent DNAzymes are described. It is shown that selected pools do not show activity with different metal ions tested except Fe(III). Initial characterization of isolated sequences which resulted in identification of the most active DNAzymes are explained. Several Fe(III)-dependent DNAzymes are converted into *trans*-cleaving DNAzymes for designing DNAzyme based fluorescent biosensors. **Chapter 3** covers *in vitro* selection of Fe(II)-dependent DNAzymes. These experiments were carried out in an oxygen free environment to prevent oxidation of Fe(II) to Fe(III). Presented results include counter selection process used to improve selectivity of the selected pools for Fe(II) over other competing divalent metal ions. It is shown that counter selection is helpful in obtaining more selective DNAzymes. A systematic search strategy for truncation of the *cis*-cleaving DNAzymes to *trans*-cleaving DNAzymes is described. Most active trans-cleaving DNAzyme distinguishes Fe(II) from Fe(III) and is able to react with Fe(II) in a mixture containing both oxidation states. We are in the process of using both Fe(II) and Fe(III)-dependent DNAzymes for intracellular imaging of iron.

In **chapter 4**, to the best of our knowledge, the first *in vitro* selected Na^+-specific DNAzyme is represented. Several different DNAzymes isolated through *in vitro* selection; one of the most active sequences, NaA43, converted into a *trans*-cleaving DNAzyme. A fluorescent sensor was designed based on A43 sequence. Designed fluorescent sensor characterized and used for intracellular imaging of Na^+. **Chapter 5** describes detailed characterization of the NaA43 DNAzymes. Sequence-function relationship of the isolated sequences from active pools in combination with the mutational studies were used to identify catalytically conserved nucleotides in the DNAzyme. Biochemical characterization of the NaA43 DNAzymes is presented in this chapter.

Finally, **chapter 6** contains the design and experimental detail of a functional DNA based sensor for Hg^{2+}. This chapter describes combination of Hg^{2+} sensing DNA with gold nanoparticles in designing a colorimetric and lateral flow sensor for Hg^{2+}.

1.6 References

1. Thieffry, D., and Sarkar, S. (1998) Forty years under the central dogma, *Trends Biochem Sci 23*, 312-316.

2. Li, G. W., and Xie, X. S. (2011) Central dogma at the single-molecule level in living cells, *Nature 475*, 308-315.

3. Gerstein, M. B., Bruce, C., Rozowsky, J. S., Zheng, D., Du, J., Korbel, J. O., Emanuelsson, O., Zhang, Z. D., Weissman, S., and Snyder, M. (2007) What is a gene, post-ENCODE? History and updated definition, *Genome Res 17*, 669-681.

4. Crick, F. (1970) Central dogma of molecular biology, *Nature 227*, 561-563.

5. Breaker, R. R., and Joyce, G. F. (1994) A DNA enzyme that cleaves RNA, *Chem Biol 1*, 223-229.

6. Ellington, A. D., and Szostak, J. W. (1992) Selection in vitro of single-stranded DNA molecules that fold into specific ligand-binding structures, *Nature 355*, 850-852.

7. Bock, L. C., Griffin, L. C., Latham, J. A., Vermaas, E. H., and Toole, J. J. (1992) Selection of single-stranded DNA molecules that bind and inhibit human thrombin, *Nature 355*, 564-566.

8. Silverman, S. K. (2010) DNA as a versatile chemical component for catalysis, encoding, and stereocontrol, *Angew Chem Int Ed Engl 49*, 7180-7201.

9. Stoltenburg, R., Reinemann, C., and Strehlitz, B. (2007) SELEX--a (r)evolutionary method to generate high-affinity nucleic acid ligands, *Biomol Eng 24*, 381-403.

10. Wilson, D. S., and Szostak, J. W. (1999) In vitro selection of functional nucleic acids, *Annu Rev Biochem 68*, 611-647.

11. Liu, J., You, M., Pu, Y., Liu, H., Ye, M., and Tan, W. (2011) Recent developments in protein and cell-targeted aptamer selection and applications, *Curr Med Chem 18*, 4117-4125.

12. Tuerk, C., and Gold, L. (1990) Systematic evolution of ligands by exponential enrichment: RNA ligands to bacteriophage T4 DNA polymerase, *Science 249*, 505-510.

13. Keefe, A. D., Pai, S., and Ellington, A. (2010) Aptamers as therapeutics, *Nat Rev Drug Discov 9*, 537-550.

14. Kang, K. N., and Lee, Y. S. (2013) RNA aptamers: a review of recent trends and applications, *Adv Biochem Eng Biotechnol 131*, 153-169.

15. Cho, E. J., Lee, J. W., and Ellington, A. D. (2009) Applications of aptamers as sensors, *Annu Rev Anal Chem (Palo Alto Calif) 2*, 241-264.

16. Liu, J., Cao, Z., and Lu, Y. (2009) Functional nucleic acid sensors, *Chemical Reviews 109*, 1948-1998.

17. Torabi, S. F., and Lu, Y. (2014) Functional DNA nanomaterials for sensing and imaging in living cells, *Curr Opin Biotechnol 28*, 88-95.

18. Burgstaller, P., Jenne, A., and Blind, M. (2002) Aptamers and aptazymes: accelerating small molecule drug discovery, *Curr Opin Drug Discov Devel 5*, 690-700.

19. Knudsen, S. M., and Ellington, A. D. (2006) Aptazymes: Allosteric Ribozymes and Deoxyribozymes as Biosensors, In *The Aptamer Handbook*, pp 290-310, Wiley-VCH Verlag GmbH & Co. KGaA.

20. Breaker, R. R., and Joyce, G. F. (1995) A DNA enzyme with Mg(2+)-dependent RNA phosphoesterase activity, *Chem Biol 2*, 655-660.

21. Faulhammer, D., and Famulok, M. (1997) Characterization and divalent metal-ion dependence of in vitro selected deoxyribozymes which cleave DNA/RNA chimeric oligonucleotides, *Journal of molecular biology 269*, 188-202.

22. Santoro, S. W., and Joyce, G. F. (1997) A general purpose RNA-cleaving DNA enzyme, *Proceedings of the National Academy of Sciences of the United States of America 94*, 4262-4266.

23. Geyer, C. R., and Sen, D. (1997) Evidence for the metal-cofactor independence of an RNA phosphodiester-cleaving DNA enzyme, *Chemistry & biology 4*, 579-593.

24. Roth, A., and Breaker, R. R. (1998) An amino acid as a cofactor for a catalytic polynucleotide, *Proc Natl Acad Sci U S A 95*, 6027-6031.

25. Li, J., Zheng, W., Kwon, A. H., and Lu, Y. (2000) In vitro selection and characterization of a highly efficient Zn(II)-dependent RNA-cleaving deoxyribozyme, *Nucleic acids research 28*, 481-488.

26. Santoro, S. W., Joyce, G. F., Sakthivel, K., Gramatikova, S., and Barbas, C. F., 3rd. (2000) RNA cleavage by a DNA enzyme with extended chemical functionality, *J Am Chem Soc 122*, 2433-2439.

27. Feldman, A. R., and Sen, D. (2001) A new and efficient DNA enzyme for the sequence-specific cleavage of RNA, *J Mol Biol 313*, 283-294.

28. Ting, R., Thomas, J. M., Lermer, L., and Perrin, D. M. (2004) Substrate specificity and kinetic framework of a DNAzyme with an expanded chemical repertoire: a putative RNaseA mimic that catalyzes RNA hydrolysis independent of a divalent metal cation, *Nucleic acids research 32*, 6660-6672.

29. Hollenstein, M., Hipolito, C. J., Lam, C. H., and Perrin, D. M. (2009) A DNAzyme with Three Protein-Like Functional Groups: Enhancing Catalytic Efficiency of M2+-Independent RNA Cleavage, *Chembiochem : a European journal of chemical biology 10*, 1988-1992.

30. Hollenstein, M., Hipolito, C. J., Lam, C. H., and Perrin, D. M. (2013) Toward the combinatorial selection of chemically modified DNAzyme RNase A mimics active against all-RNA substrates, *ACS combinatorial science 15*, 174-182.

31. Mei, S. H., Liu, Z., Brennan, J. D., and Li, Y. (2003) An efficient RNA-cleaving DNA enzyme that synchronizes catalysis with fluorescence signaling, *J Am Chem Soc 125*, 412-420.

32. Liu, Z., Mei, S. H., Brennan, J. D., and Li, Y. (2003) Assemblage of signaling DNA enzymes with intriguing metal-ion specificities and pH dependences, *J Am Chem Soc 125*, 7539-7545.

33. Liu, J., Brown, A. K., Meng, X., Cropek, D. M., Istok, J. D., Watson, D. B., and Lu, Y. (2007) A catalytic beacon sensor for uranium with parts-per-trillion sensitivity and millionfold selectivity, *Proceedings of the National Academy of Sciences of the United States of America 104*, 2056-2061.

34. Huang, P. J., Vazin, M., and Liu, J. (2014) In Vitro Selection of a New Lanthanide-Dependent DNAzyme for Ratiometric Sensing Lanthanides, *Anal Chem 86*, 9993-9999.

35. Carmi, N., Balkhi, S. R., and Breaker, R. R. (1998) Cleaving DNA with DNA, *Proceedings of the National Academy of Sciences of the United States of America 95*, 2233-2237.

36. Gu, H., Furukawa, K., Weinberg, Z., Berenson, D. F., and Breaker, R. R. (2013) Small, highly active DNAs that hydrolyze DNA, *J Am Chem Soc 135*, 9121-9129.

37. Chandra, M., Sachdeva, A., and Silverman, S. K. (2009) DNA-catalyzed sequence-specific hydrolysis of DNA, *Nat Chem Biol 5*, 718-720.

38. Wang, Y., and Silverman, S. K. (2003) Deoxyribozymes that synthesize branched and lariat RNA, *J Am Chem Soc 125*, 6880-6881.

39. Coppins, R. L., and Silverman, S. K. (2004) A DNA enzyme that mimics the first step of RNA splicing, *Nat Struct Mol Biol 11*, 270-274.

40. Flynn-Charlebois, A., Wang, Y., Prior, T. K., Rashid, I., Hoadley, K. A., Coppins, R. L., Wolf, A. C., and Silverman, S. K. (2003) Deoxyribozymes with 2'-5' RNA ligase activity, *J Am Chem Soc 125*, 2444-2454.

41. Flynn-Charlebois, A., Prior, T. K., Hoadley, K. A., and Silverman, S. K. (2003) In vitro evolution of an RNA-cleaving DNA enzyme into an RNA ligase switches the selectivity from 3'-5' to 2'-5', *J Am Chem Soc 125*, 5346-5350.

42. Hoadley, K. A., Purtha, W. E., Wolf, A. C., Flynn-Charlebois, A., and Silverman, S. K. (2005) Zn2+-dependent deoxyribozymes that form natural and unnatural RNA linkages, *Biochemistry 44*, 9217-9231.

43. Cuenoud, B., and Szostak, J. W. (1995) A DNA metalloenzyme with DNA ligase activity, *Nature 375*, 611-614.

44. Sreedhara, A., Li, Y., and Breaker, R. R. (2004) Ligating DNA with DNA, *J Am Chem Soc 126*, 3454-3460.

45. Li, Y., and Breaker, R. R. (1999) Phosphorylating DNA with DNA, *Proc Natl Acad Sci U S A 96*, 2746-2751.

46. Hobartner, C., Pradeepkumar, P. I., and Silverman, S. K. (2007) Site-selective depurination by a periodate-dependent deoxyribozyme, *Chem Commun (Camb)*, 2255-2257.

47. Li, Y., Liu, Y., and Breaker, R. R. (2000) Capping DNA with DNA, *Biochemistry 39*, 3106-3114.

48. Chinnapen, D. J., and Sen, D. (2004) A deoxyribozyme that harnesses light to repair thymine dimers in DNA, *Proc Natl Acad Sci U S A 101*, 65-69.

49. Burmeister, J., von Kiedrowski, G., and Ellington, A. D. (1997) Cofactor-Assisted Self-Cleavage in DNA Libraries with a 3′–5′-Phosphoramidate Bond, *Angewandte Chemie International Edition in English 36*, 1321-1324.

50. Sheppard, T. L., Ordoukhanian, P., and Joyce, G. F. (2000) A DNA enzyme with N-glycosylase activity, *Proc Natl Acad Sci U S A 97*, 7802-7807.

51. Li, Y., and Sen, D. (1996) A catalytic DNA for porphyrin metallation, *Nat Struct Biol 3*, 743-747.

52. Chandra, M., and Silverman, S. K. (2008) DNA and RNA can be equally efficient catalysts for carbon-carbon bond formation, *J Am Chem Soc 130*, 2936-2937.

53. Wong, O. Y., Mulcrone, A. E., and Silverman, S. K. (2011) DNA-catalyzed reductive amination, *Angew Chem Int Ed Engl 50*, 11679-11684.

54. Chu, C. C., Wong, O. Y., and Silverman, S. K. (2014) A generalizable DNA-catalyzed approach to peptide-nucleic acid conjugation, *Chembiochem 15*, 1905-1910.

55. Brandsen, B. M., Hesser, A. R., Castner, M. A., Chandra, M., and Silverman, S. K. (2013) DNA-catalyzed hydrolysis of esters and aromatic amides, *J Am Chem Soc 135*, 16014-16017.

56. Walsh, S. M., Sachdeva, A., and Silverman, S. K. (2013) DNA catalysts with tyrosine kinase activity, *J Am Chem Soc 135*, 14928-14931.

57. Chandrasekar, J., and Silverman, S. K. (2013) Catalytic DNA with phosphatase activity, *Proc Natl Acad Sci U S A 110*, 5315-5320.

58. Velez, T. E., Singh, J., Xiao, Y., Allen, E. C., Wong, O. Y., Chandra, M., Kwon, S. C., and Silverman, S. K. (2012) Systematic evaluation of the dependence of deoxyribozyme catalysis on random region length, *ACS Comb Sci 14*, 680-687.

59. Silverman, S. K. (2008) Catalytic DNA (deoxyribozymes) for synthetic applications-current abilities and future prospects, *Chem Commun (Camb)*, 3467-3485.

60. Zhang, X. B., Kong, R. M., and Lu, Y. (2011) Metal ion sensors based on DNAzymes and related DNA molecules, *Annu Rev Anal Chem (Palo Alto Calif) 4*, 105-128.

61. Xiang, Y., and Lu, Y. (2014) DNA as sensors and imaging agents for metal ions, *Inorganic chemistry 53*, 1925-1942.

62. Bunka, D. H., and Stockley, P. G. (2006) Aptamers come of age - at last, *Nat Rev Microbiol 4*, 588-596.

63. Li, J., and Lu, Y. (2000) A Highly Sensitive and Selective Catalytic DNA Biosensor for Lead Ions, *Journal of the American Chemical Society 122*, 10466-10467.

64. Hollenstein, M., Hipolito, C., Lam, C., Dietrich, D., and Perrin, D. M. (2008) A Highly Selective DNAzyme Sensor for Mercuric Ions, *Angewandte Chemie International Edition 47*, 4346-4350.

65. Lan, T., and Lu, Y. (2012) Metal ion-dependent DNAzymes and their applications as biosensors, *Met Ions Life Sci 10*, 217-248.

66. Xiang, Y., and Lu, Y. (2014) DNA as sensors and imaging agents for metal ions, *Inorg Chem 53*, 1925-1942.

67. Zhang, L., Huang, H., Xu, N., and Yin, Q. (2014) Functionalization of cationic poly(p-phenylene ethynylene) with dendritic polyethylene enables efficient DNAzyme delivery for imaging Pb2+ in living cells, *Journal of Materials Chemistry B 2*, 4935-4942.

68. Wu, P., Hwang, K., Lan, T., and Lu, Y. (2013) A DNAzyme-gold nanoparticle probe for uranyl ion in living cells, *Journal of the American Chemical Society 135*, 5254-5257.

69. Hwang, K., Wu, P., Kim, T., Lei, L., Tian, S., Wang, Y., and Lu, Y. (2014) Photocaged DNAzymes as a General Method for Sensing Metal Ions in Living Cells, *Angew Chem Int Ed Engl*.

70. Meng, H. M., Zhang, X., Lv, Y., Zhao, Z., Wang, N. N., Fu, T., Fan, H., Liang, H., Qiu, L., Zhu, G., and Tan, W. (2014) DNA dendrimer: an efficient nanocarrier of functional nucleic acids for intracellular molecular sensing, *ACS Nano 8*, 6171-6181.

2 Chapter 2. *In vitro* selection of Fe(III)-dependent DNAzymes

2.1 Introduction

For many years DNA was known to store genetic information, as suggested by central dogma of molecular biology (*1-3*). However after the first discovery of DNA enzymes (DNAzymes) in 1994 (*4*), it has been proved that DNA is surprisingly versatile in function. Since then increasing number of DNAzymes have been isolated through *in vitro* selection (*5*). Among the numerous DNAzymes, RNA-cleaving DNAzymes are the most extensively used class with applications in designing sensors (*6*) and DNA computation tools (*7, 8*). With a few exceptions (*9, 10*), all RNA-cleaving DNAzymes are multivalent metal ion dependent. Very recently, an RNA-cleaving DNAzyme was reported which cleaves its substrate in an *Escherichia coli*-dependent manner (*11*). The *E. coli*-DNAzyme needs magnesium ions to function properly (*12*). It was shown that multivalent dependency of RNA-cleaving DNAzymes can be eliminated by introduction of new functionalities into the DNAzyme (*i.e*. amines, guanidines and imidazoles) (*13-16*). Although many metal dependent RNA-cleaving DNAzymes have been reported so far, few examples are highly selective for a specific metal cofactor (*e.g.* UO_2^{2+}-dependent DNAzyme (*17*), Pb^{2+}-dependent DNAzyme (GR5) (*4*), and Hg^{2+}-dependent DNAzyme) (*18*). Recently, two DNAzymes were isolated that are barely selective for a specific metal ion, but they utilize any lanthanide metals to catalyze the RNA cleavage reaction (*19, 20*). Although the selectivity of DNAzymes can be improved through negative/counter selection strategy (*21*), obtaining highly selective and metal-specific DNAzymes is still challenging.

Iron is an essential factor in living systems as it plays a critical role in many cellular processes including oxygen transport, energy metabolism, and DNA synthesis (*22, 23*). Iron, the most abundant transition metal ion in the body, acts as a critical redox cofactor in the active site

of key enzymes in biological pathways. Although iron is required in biological systems, excess of iron, which results in production of reactive oxygen species (ROS), is highly toxic. Production of ROS impairs cellular functions and damage cells, tissues, and organs. These effects are reported for iron-loading disease such as β-thalassemia and Fredreich's ataxia (*24-26*). Iron is present in both Fe(II) and Fe(III) oxidation forms in the cell. In mammalian cells, iron uptake is through endosomal pathway involving an iron transport protein, transferrin (Tf). Endosome maturation which is followed by reduction of pH results in release of Fe(III) from Tf and subsequent transport of the reduced Fe(II) form to the cytosol. Due to lack of proper probes to study intracellular iron, detailed mechanism of iron reduction and release in this process is not completely understood (*27*).

Variety of methods have been used to probe iron including electron paramagnetic resonance (EPR) spectroscopy, inductively coupled plasma mass spectroscopy (ICPMS) (*28*), atomic absorption spectroscopy (*29*), laser ablation inductively coupled plasma mass spectrometry (LA-ICP-MS) (*30*), and secondary ion mass spectrometry (nano-SIMS) (*31*). Recently, a collision reaction cell-inductively coupled plasma-mass spectrometry (CRC-ICP-MS) method is reported for detection of iron with capability of distinguishing between the two iron species, Fe(II) and Fe(III) (*32*). Most of these methods require sophisticated equipment and digestion of the sample before analysis. In addition they do not provide real-time information and can often detect only the total amount of metal ions (not different oxidation states) (*29*). Therefore, other tools such as fluorescent sensors for detecting iron in biological samples and cellular systems have been developed. Information obtained from using fluorescent sensors for Cu^{2+}, Ca^{2+}, and Zn^{2+} contributed significantly to understanding homeostasis and dynamics of these metal ions in cells or organisms (*33*).

Due to the paramagnetic quenching nature of iron most of probes for this metal show turn-off fluorescence response upon iron binding. Although this type of sensors have been used for iron sensing, turn-off property is an undesirable feature for analytical purposes because of lower dynamic range and potential false positives. These issues are mainly due to the non-specific quenching of probes by other paramagnetic competing metal ions or probe degradation in complex environments, such as in cells (*34, 35*). Few turn-on fluorescent probes for iron have been developed based on the equilibrium between a nonfluorescent spirolactam and fluorescent ring-opened amide forms of rhodamine (*36-38*). Although, development of Fe(III) turn-on fluorescent sensors is a breakthrough in the field of sensor design, these recently developed sensors suffer from high interference from Cr^{3+} (*38*) and medium interference from Fe(II) (*37*). Additionally they require a mixture of water/organic solvent for optimal performance (*37*). Therefore, design and development of turn-on fluorescent sensors for Fe(III) with high selectivity and proper sensitivity is still a challenge.

Fe(III) favors a six coordinate octahedral coordination geometry and has strong Lewis acidic character (pK_a values of 2.5) (*39*). Moreover, Fe(III) is classified as hard metal ion by hard soft acid based theory, which makes the phosphate and carbonyl oxygens of DNA potential ligands (*40*). However, studying interactions of Fe(III) and DNA has suggested that only oxygen atoms are coordinated to the Fe(III) ion (*41, 42*). Previous studies on interaction of Fe(III) with DNA have shown photo-induced reduction of Fe(III) to Fe(II) in the presence of chelators such as citrate and EDTA, resulted in the formation of single and double strand breaks in DNA without the addition of hydrogen peroxide (*43-46*). It has been proposed that genotoxicity of Fe(III) is due to the iron-induced DNA damage in cells (*47*). To the best of our knowledge, there is no report in literature of an Fe(III) specific DNAzyme. Since it is known that DNA interacts with Fe(III), it is

possible to search for a DNA sequence that can specifically sense Fe(III). We decided to obtain Fe(III)-dependent DNAzymes through *in vitro* selection process. Such DNAzymes could be readily converted into a DNAzyme-based fluorescent sensor for Fe(III). In this chapter I have described my efforts in isolation of Fe(III)-specific RNA-cleaving DNAzymes through *in vitro* selection.

2.2 Materials and Methods

2.2.1 Materials

All DNA oligos were purchased from Integrated DNA Technology Inc. (IDT) and purified by denaturing (8 M urea) 10 % polyacrylamide gel electrophoresis (PAGE) before use. Details of the nucleotide sequences used in different *in vitro* selections are provided in Tables 2.1, 2.2, and 2.3. Metal salts used in this study included: $Fe(NO_3)_3 \bullet xH_2O$ (x≈9) (Alfa Aesar, 99.999%), NaCl (Alfa Aesar, 99.999%), $MgCl_2.6H_2O$ (Alfa Aesar, 99.999%), $Ca(NO_3)_2.6H_2O$ (Alfa Aesar, 99.995%), $SrCl_2.6H_2O$ (Alfa Aesar, 99.996%), $BaCl_2.2H_2O$ (Alfa Aesar, 99.997%), $Mn(CH_3CO_2)_2.4H_2O$ (Alfa Aesar, 99.999%), $CoCl_2.6H_2O$ (Alfa Aesar, 99.9%), $NiCl_2.6H_2O$ (Alfa Aesar, 99.995%), $Cu(NO_3)_2.H_2O$ (Alfa Aesar, 99.999%), $ZnCl_2.H_2O$ (Alfa Aesar, 99.99%), $Cd(NO_3)_2.4H_2O$ (Alfa Aesar, 99.999%), $HgCl_2$ (Alfa Aesar, 99.999%), $Pb(CH_3CO_2)_2.3H_2O$ (Aldrich, 99.999%), $InCl_3$ (Aldrich, 99.999%), $La(NO_3)_3.6H_2O$ (Aldrich, 99.999%), $EuCl_3.6H_2O$ (Aldrich, 99.999%), $SmCl_3.6H_2O$ (Aldrich, 99.99%), and $YbCl_3.6H_2O$ (Aldrich, 99.998%). Salts and solutions used to adjust pH of buffer solutions included the following: $LiOH.H_2O$ (Alfa Aesar, 99.996%) $NaOH.H_2O$ (Alfa Aesar, 99.996%), KOH (Fisher Scientific), 65-70% HNO_3 (Alfa Aesar, 99.999%), and 36.5% HCl (Alfa Aesar, 99.999%). Other chemicals used to prepare different solutions included the following: Ethylenediaminetetraacetid acid, sodium free (EDTA) (Fluka, 99.0%), $EDTA.2Na.2H_2O$ (Fisher Scientific), Trisodium citrate (Alfa Aesar, 99%), urea (Affymetrix, MB grade), Tris (Affymetrix, MB grade), boric acid (Fisher Scientific, electrophoresis grade), and Bis-Tris (Sigma, 99.0%). Acrylamide/bisacrylamide 40% solution (29:1) was purchased from Bio-Rad. *Taq* DNA polymerase with standard *Taq* buffer, T4-polynucletide kinase, and deoxynucleotide (dNTP) solution mix were purchased from New England Biolabs. Radiolabeling of DNA carried out using ^{32}P labeled α-ATP and γ-ATP purchased from Perkin-Elmer. The original TA cloning® kit was purchased from Invitrogen. All buffer, metal

ion and gel stock solutions were prepared with Milli-Q water. The pH of the buffers was measured with Fisher Scientific Accumet AB15 pH meter.

Selection buffer for *in vitro* selection-1 was made as a 1× solution containing 50 mM Bis-Tris, 50 mM sodium citrate, 250 mM sodium chloride, 2 mM magnesium chloride, 1 mM ferric nitrate at pH 7.0. Ultrapure nitric acid was used for pH adjustment. A concentrated Fe(III) metal-stock solution was prepared containing 100 mM ferric nitrate in 100 mM ultrapure nitric.

Selection buffers for *in vitro* selection-2 and 3 were made as 2× solutions. Selection buffer-2, which was used for selection in neural condition, contained 25 mM Bis-Tris, 200 mM sodium chloride at pH 7.0. Selection buffer-3, which is used for selection in acidic condition, contained 40 mM sodium acetate, 5 mM Bis-Tris and 200 mM sodium chloride at pH 5.5. Ultrapure nitric acid was used for pH adjustment. The concentrated Fe(III) metal-stock solution contained 1 mM ferric nitrate in 100 mM ultrapure nitric. Right before each positive selection 2× Fe(III) solutions were made in selection buffers. *In vitro* selections were started by adding equal volume of 2× Fe(III) (in 1× selection buffer) to the DNA dissolved in 1× selection buffer.

2.2.2 Sequences

Table 2.1 Sequences of the oligonucleotides used for the in vitro selection-1, column-based selection at pH 7.0. Sequence of the random pool generated after PCR, full length pool, is also shown.

Name	Sequence of Oligonucleotide (5' to 3')
IDT template	GGAAGTACCGCATGGTAC-**N_{50}**-CGTGAGCCTACGATGAGAC
Full length pool	GTTCAGACTAATCATCACGTATrAGGAAGTACCGCATGGTAC-**N_{50}**-CGTGAGCCTACGATGAGAC
P1	GACTAATCATCACGTATAGGAAGTACCGCATG
P2	GTCTCATCGTAGGCTCAC
P3	GTTCAGACTAATCATCACGTATrA
P3-Bt	Biotin-GTTCAGACTAATCATCACGTATrA

Table 2.2 Sequences of the oligonucleotides used for the *in vitro* selection-2, gel-based selection at pH 7.0. Sequence of the random pool generated after PCR, full length pool, is also shown.

Name	Sequence of Oligonucleotide (5' to 3')
	pH 7.0 condition
IDT template	CCTCGACAGTTCTAG-**$N_{35/50}$**-GTCACATGCGTGACTCTCTCAACTAGAAGATATGC-SpC3
Full length pool	GTAATACGCATATCTTCTAGTTGrAGAGAGTCACGCATGTGAC- **$N_{35/50}$**-CTAGAACTGTCGAGGAGC
P1	GCATATCTTCTAGTTGAGAGAGTCACGCATG
P2	GCTCCTCGACAGTTCTAG
P2-iSp	GAC$(AAC)_4$- **Sp-C18**- GCTCCTCGACAGTTCTAG
P3	GTAATACGCATATCTTCTAGTTGrA

Table 2.3 Sequences of the oligonucleotides used for the *in vitro* selection-3, gel-based selection at pH 5.5. Sequence of the random pool generated after PCR, full length pool, is also shown.

Name	Sequence of Oligonucleotide (5' to 3')
	pH 5.5 condition
IDT template	CCGGACCTCCTTCAG-**$N_{35/50}$**-GACTCGTGCGAGTCTCCCTAACTGAAGTAAG-SpC3
Full length pool	GATACATAGCATCTTACTTCAGTTArGGGAGACTCGCACGAGTC- **$N_{35/50}$**-CTGAAGGAGGTCCGGTC
P1	GCATCTTACTTCAGTTAGGGAGACTCGCACG
P2	GACCGGACCTCCTTCAG
P2-iSp	GAC$(AAC)_4$- **Sp-C18**- GACCGGACCTCCTTCAG
P3	GATACATAGCATCTTACTTCAGTTArG

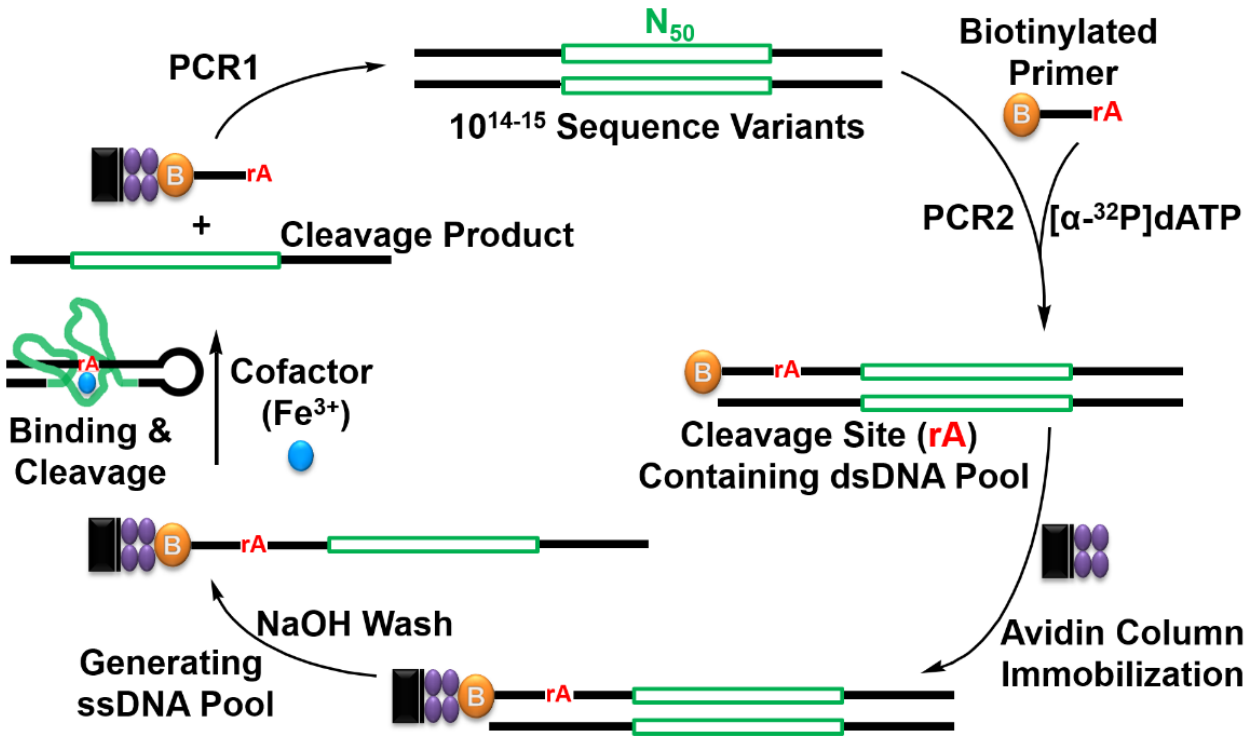

Figure 2.1 Scheme *in vitro* selection-1.

2.2.3 *In Vitro* Selection

2.2.3.1 *In Vitro* Selection-1

The *in vitro* selection-1 was carried out based on the protocol originally reported by Breaker and Joyce (column-based selection, Figure 2.1) (*4*). The initial selection pool was generated through template-directed extension and PCR amplifications (Figure 2.2). In the first step of PCR1, 250 pmol of DNA template and 250 pmol of primer P2 were mixed in 60 × 40 µl reaction mixtures and extended for two thermal cycles to complete the extension (1 min at 94°C, 1.5 min at 58°C and then 3 min at 72°C). The second step of PCR1 was performed by addition of 350 pmol of primer P1 and followed by two more cycles of amplification. Finally, in the third step, 2.3 nmol of P2 was added and 10 more cycles of amplification were carried out. Then, PCR2 was carried out by addition of 2.5 nmol of P3-Bt and 250 pmol of P2. P3-Bt primer was 5′-labeled with

biotin and incorporated the rA cleavage site into the DNA pool. The PCR reaction buffers also included 0.1 units/µl of Taq DNA polymerase (from New England Biolabs (NEB)), 1.5 mM $MgCl_2$, 50 mM KCl, 10 mM Tris-HCl (pH 8.3 at 25°C), and 0.2 mM of each dNTPs. PCR2 products were internally labeled with [α-^{32}P]-dATP (PerkinElmer) to keep track of DNA pools and cleavage products through selection process via liquid scintillation counting and denaturing PAGE analysis.

Amplification of the isolated DNA at the end of each selection round was carried out by two PCR reactions. In PCR1 isolated DNA was amplified with skewed ratio of P1 (1.0 µM) to P2 (0.1 µM). 10% of PCR1 reaction was used as template in PCR2 and amplified with skewed ratio of P3 (1.0 µM) to P1 (0.1 µM). PCR2 products were internally labeled with [α-^{32}P]-dATP (PerkinElmer) to keep track of DNA pools and cleavage products through selection process via liquid scintillation counting and denaturing PAGE analysis. Positive selections were started by addition of selection buffer-1 containing Fe(III). The *in vitro* selection-1 buffer contained 50 mM Bis-Tris, 50 mM sodium citrate, 250 mM sodium chloride, 2 mM magnesium chloride, and 1 mM ferric nitrate at pH 7.0. Selection column was capped from the bottom. After 1 h, the cap was removed and selection buffer contained cleavage products was collected to be used for the next PCR amplifications. Selection column was covered by aluminum foil to make sure mixture of Fe(III) and DNA is not exposed to light. Exposure of the mixture of DNA and Fe(III) could cause photo-induced DNA cleavage (*43*, *44*). In addition, it should be noted that it was troublesome to concentrate down collected samples through ethanol precipitation procedure. It was found that citrate precipitated alongside DNA and remained as a highly viscose solution after drying. Instead of ethanol precipitation, Amicon centrifugal filter tubes with 10,000 membrane molecular weight cutoff were used.

After each selection round and isolation of the cleavage product two PCR reactions were used to amplify DNA sequences and incorporate biotin modification as well as the rA cleavage site (Figure 2.3). Both PCR reactions were carried out with skewed primer ratio. The ratio of P1/P2 and P3-Bt/P2 was 10 in PCR1 and PCR2, respectively. PCR2 products were internally labeled with ^{32}P by addition of [α-^{32}P]-dATP in the reaction.

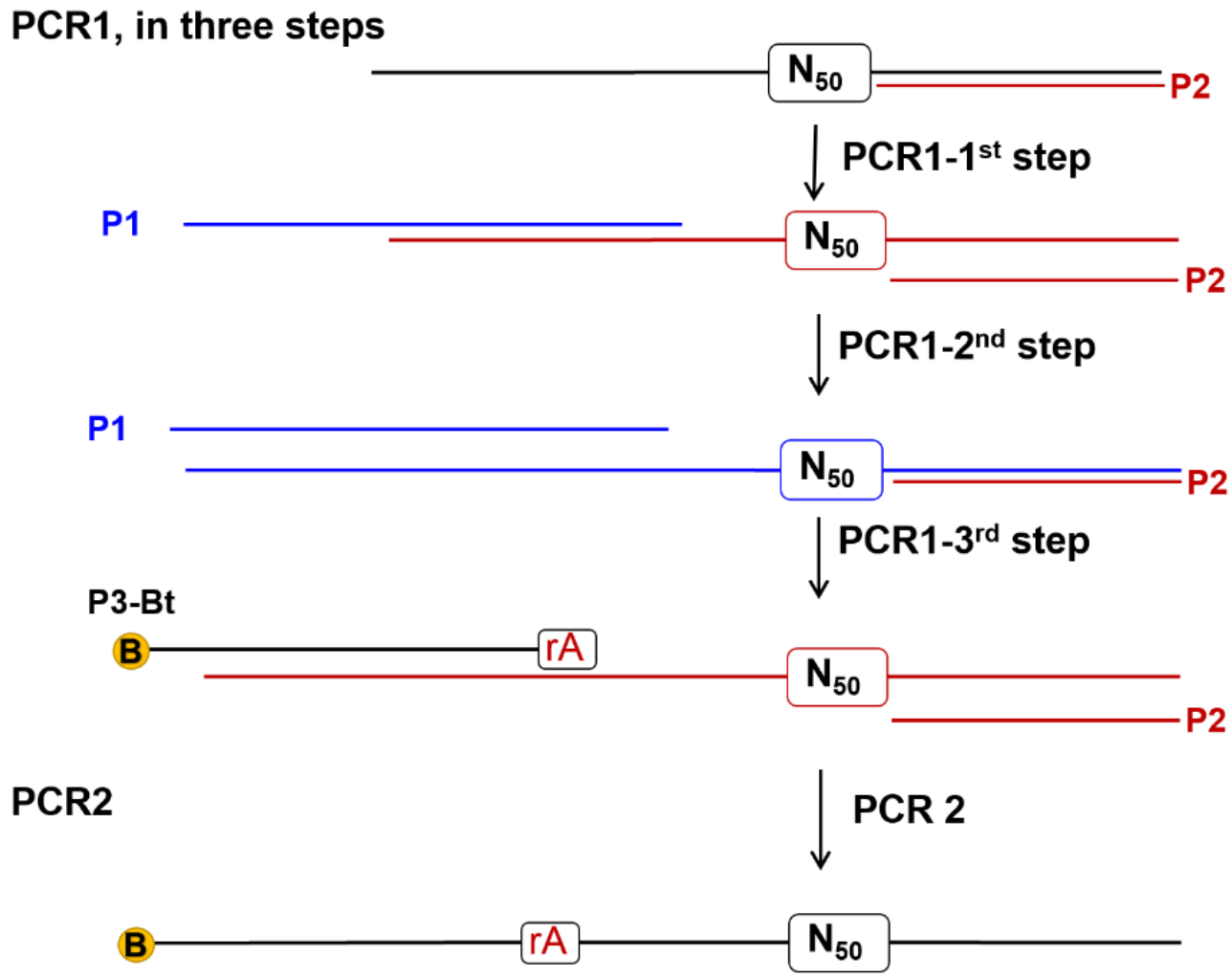

Figure 2.2 Generation of the initial pool for *in vitro* selection-1.

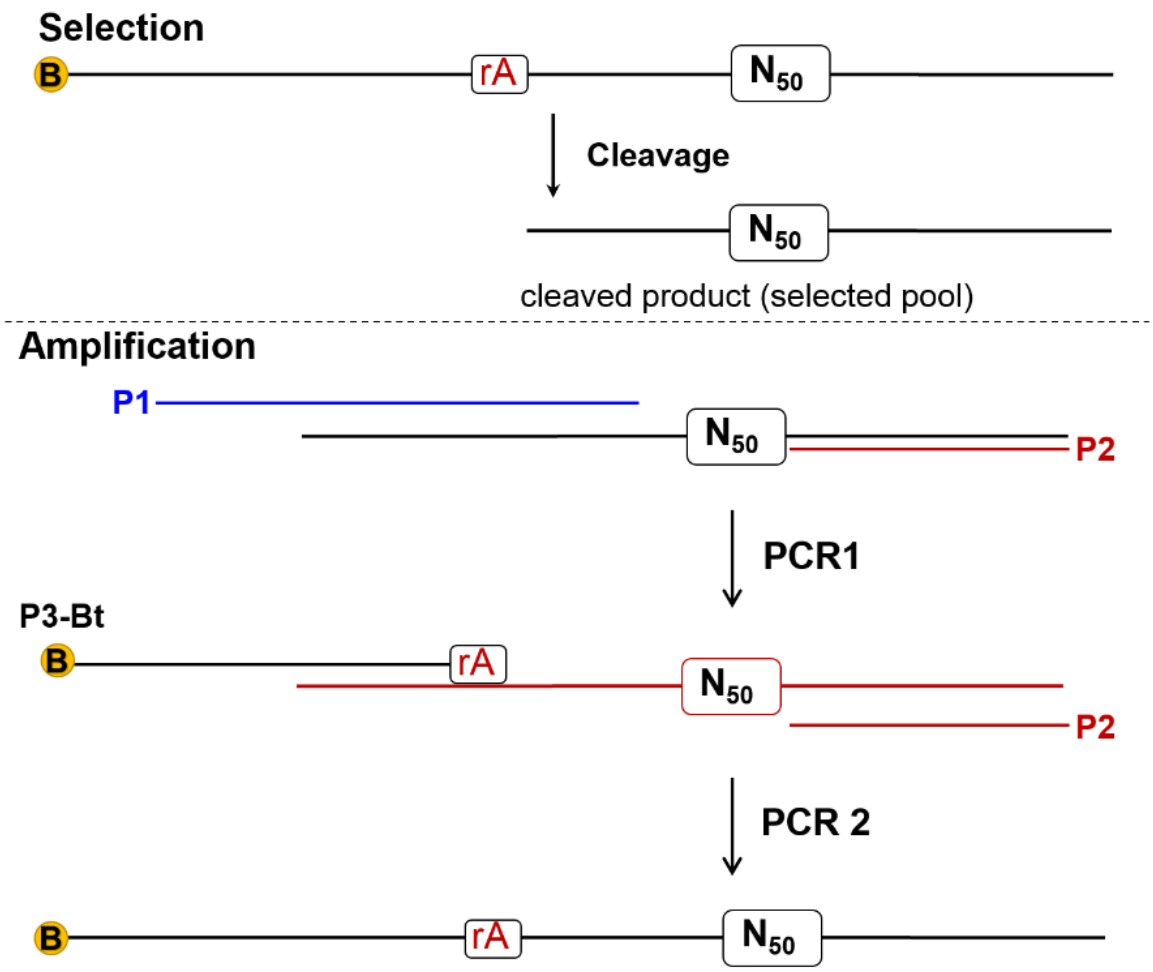

Figure 2.3 Amplification of selected sequences isolated at the end of each selection. Cleavage product is amplified in two PCR reactions.

2.2.3.2 *In Vitro* Selection-2 and 3

The *in vitro* selection-2 and 3 were carried out based on the protocol originally reported by Breaker and Joyce (Figure 2.1) (*4*) in combination with denaturing PAGE purification. Therefore, unlike column-based selection in which reaction takes place on beads, no immobilization was used. Instead, denaturing PAGE purification was used to separate cleavage products from uncleaved pools based on their size difference (gel-based method). This method is briefly described in Figure

2.4. Two different selection buffer with different pH values were used to carry out *in vitro* selection-2 and 3. The *In vitro* selection-2 buffer was adjusted to pH 7.0 while *in vitro* selection-3 was done at pH 5.5. In addition, rA and rG were used as the cleavage sites for *in vitro* selection-2 and 3, respectively. Moreover, for each buffer condition two different DNA pools with random region size of 35 or 50 nucleotides were used. The initial selection pools were generated through single linear PCR amplification. The PCR templates, synthesized by Integrated DNA Technologies, designed in a way to eliminate the need for multiple PCR amplifications to generate the initial pools. The DNA pools were generated by linear amplification of 360 pmol of the template mixed with 3.6 nmol of P3 primer in 90 × 40 µl followed by 10 thermal cycles to complete the pool generation (40 s at 94°C, 1.25 min at 53°C and then 1.1 min at 72°C). In generation of each pool, 4 µl of [α-^{32}P]-dATP (PerkinElmer) was used to internally label PCR products with ^{32}P. Amplification of the selected pools after each positive selection round was carried out similar to *in vitro* selection-1 through two PCR reactions (see section 2.3.1). Beside template and primers, each PCR reaction included 0.1 units/µl of Taq DNA polymerase (NEB), 1.5 mM $MgCl_2$, 50 mM KCl, 10 mM Tris-HCl (pH 8.3 at 25°C), and 0.2 mM of each dNTP. It should be noted that all parameters of different PCR reactions were optimized before initiation of the *in vitro* selection. This optimization process was required to minimize production of side products, obtain clean products, and increase yield of the correct PCR product.

Only for the initial rounds of different *in vitro* selections, the PCR products were precipitated with 10 % of a 3 M sodium acetate solution, at pH 5.2, and 2.7 × volume of cold ethanol. The samples were stored at −80 °C for at least 1 hour, then centrifuged, washed and lyophilized. Dried samples were dissolved in water and an equal amount of stop buffer was added. The stop buffer contained 8 M urea, 50 mM EDTA and 1× TBE (Tris, Boric acid, EDTA). The

reaction products were purified using a 10 % denaturing PAGE gel, using 1× TBE as the running buffer. The PCR product was run on the gel alongside DNA size markers corresponding to the cleaved (87-mer) and intact (110-mer) pool. For all other PCR2 products from round 2, samples were mixed with stop buffer and directly loaded on a 10% gel. The gel was then covered with a plastic wrap, a radioactive triangle location marker was placed on top of the gel, and exposed to a phosphorimager cassette. After imaging the exposed film, corresponding band to the 110-mer marker on the gel was excised, crushed, and extracted with a 10 mM Tris, 0.1 mM EDTA, and 100 mM sodium chloride solution (extraction buffer). Gel particles were frozen over 10 minutes at −80 °C and thawed in a room temperature water bath over 5 minutes to improve extraction process. The solution was centrifuged at 10,000 g for 1 minute to remove gel free solution which contains DNA. DNA samples were ethanol precipitated using the procedure mentioned earlier.

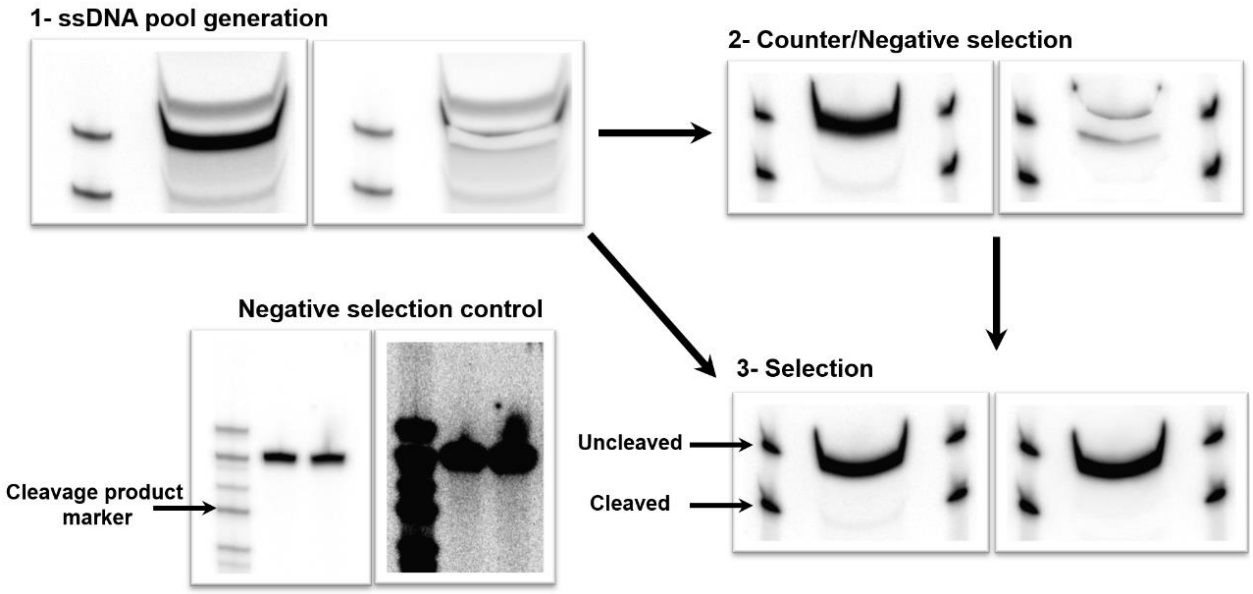

Figure 2.4 Different steps carried out in a gel-based *in vitro* selection. Every single step requires a PAGE purification. In the first two steps (1 and 2) uncleaved pool is excised from the gel to be used for the next step. In t he third step, which is carried out after the positive selection, cleaved product is excised and used as template for PCR amplification.

The dried pools were dissolved in 1× selection buffer and incubated for 24 h (negative selection). This step was carried out before all positive selection steps unless stated. Negative selection steps were carried out to remove nonspecific cleavage that may occur in an Fe(III)-independent manner. After the negative selection, uncleaved pools were PAGE purified, extracted from gel, ethanol precipitated, and dried to be used for positive selection. Dried pools were dissolved in 1× selection buffer and mixed with desired concentration of Fe(III) (for positive selections) for a certain period of time (see Table 2.6). To initiate selection Fe(III) was dissolved in selection buffer to make 2× Fe(III). Then equal volume of DNA samples were mixed with Fe(III) solution. Preparing 2× Fe(III) solutions was carried out right before positive selection. All positive selections were carried out in dark by covering tubes with aluminum foil to prevent unwanted light-induced DNA cleavage by Fe(III) (*43, 44*). After round 4, each of the *in vitro* selection experiments carried out with the rG cleavage site at pH 5.5 was branched into two conditions by continuing or not continuing negative selection steps. Negative selection steps never discontinued for selections carried out at pH 7.0 with the rA cleavage site. Cleaved DNA obtained in each positive selection was PAGE purified and used as a template for PCR amplification reactions. Stringency of positive selections were gradually increase by varying the reaction time and Fe(III) concentration. All selection reactions were stopped by addition of an equal amount of the stop buffer. All PAGE purifications were carried out using a 10 % gel alongside the DNA size markers used earlier.

2.2.4 Gel-based Activity Assays

Activity assay experiments were carried out after 5th round of the selection for several rounds in order to monitor enrichment of DNA pools with active/selective DNAzymes, fine tune stringency of positive selections, and identify the most active selected pools for cloning and

sequencing experiments. Single stranded DNA pools were PCR amplified and internally labeled with ^{32}P with the same protocol mentioned earlier. No annealing step was carried out before testing the activity of individual pools or *cis*-cleaving DNAzymes obtained later. DNA samples were dissolved in selection buffer and tested with different concentrations of Fe(III) and other metal ions. Each reaction was initiated by the addition of 2 µl of 20× Fe(III) solution (in 1 mM ultrapure nitric acid) to 18 µl of the DNA in 1.1× selection buffer. At known time points, 2 µl aliquots of the reaction mixture were withdrawn and added to 4 µl of a stop solution containing 50 mM EDTA, 8 M Urea, 1× TBE, 0.05 % xylene cyanol and 0.05 % bromophenol blue. The uncleaved and cleaved DNA pools were separated on a 10 % PAGE gel (36 W, 1.5h). The gel was then wrapped and exposed to a phosphorimager cassette. The cassette was then imaged using a Molecular Dynamics Storm 430 Phosphorimager (from Amersham Biosciences) and the fraction of cleavage was calculated using Image Quant software (Molecular Dynamics). To monitor activity of *trans*-cleaving DNAzymes, each substrate was radioactively labeled with [γ-^{32}P]-dATP using T4 kinase from NEB. The labeling mixture contained 10 pmol of the substrate, 1× forward reaction buffer, and 0.5 µL of T4 kinase and 1 µl of [γ-^{32}P]-dATP, the total volume being 20 µl. This solution incubated at 37 °C for 1.5 h. The cleavage product and uncleaved substrate DNA samples were separated on a 20 % PAGE gel. If gels were used for a single loading they were run at 40 W for 1.5 h.; if used for double loading, the first loaded samples ran at 40 W for 1h 10min and after subsequent loading samples were run for another 1 h at 40 W. Timing for double loading depends on the size of cleaved products and uncleaved substrate. The above mentioned timing is good for cleavage products from 8 to 12 nucleotides and uncleaved substrate from 24 to 34 nucleotides.

Rate of cleavage was determined by plotting cleavage percentage versus time and fitting the data points to a double exponential equation:

$$Y_t = Y + A \times e^{-k_{obs,1} \times t} + B \times e^{-k_{obs,2} \times t}$$

In this equation Y is the percentage of the substrate cleaved at completion (t = ∞), Y_t is the % of product at time t, −A and −B are the amplitude of the observed cleavage at each at each phase. $k_{obs,1}$ and $k_{obs,2}$ are the observed first-order rate constants for the fast and slow phases. All of the reported k_{obs} values in this chapter are the observed rates for the fast phase ($k_{obs,1}$).

2.3 Results and Discussion

2.3.1 *In Vitro* Selection-1

2.3.1.1 Selection Condition

A DNAzyme selection usually is carried out in the presence of monovalent metal ions. Monovalent metal ions provide charge shielding for the DNAzyme phosphate backbone and help in stabilization of complementary regions formed in the DNAzyme structures (*48, 49*). With the exception of Na^+-specific DNAzyme, which I have isolated very recently, no monovalent metal ion specific RNA-cleaving has been reported. Due to the lack of specific interaction between DNA and monovalent metal ions, variety of different monovalent metals with different concentrations have been used in *in vitro* selection buffers. In some cases only one type of monovalent metal such as NaCl were used in selection buffers (concentration range from 150 mM (*50*) to 1 M (*10, 51*)). In other cases a mixture of two monovalent metals with equal concentrations were used (*i.e.* 0.5 M NaCl and KCl) (*52*). In addition, a few DNAzymes were selected in the presence of $MgCl_2$ in the selection buffer, although the desired metal cofactors were other metals such as Pb^{2+} (*4*) or Zn^{2+} (*50*). Therefore, I decided to use 200 mM NaCl in Fe(III) selection buffers. Only *in vitro* selection-1 was carried out in the presence of 2 mM $MgCl_2$ and 200 mM NaCl.

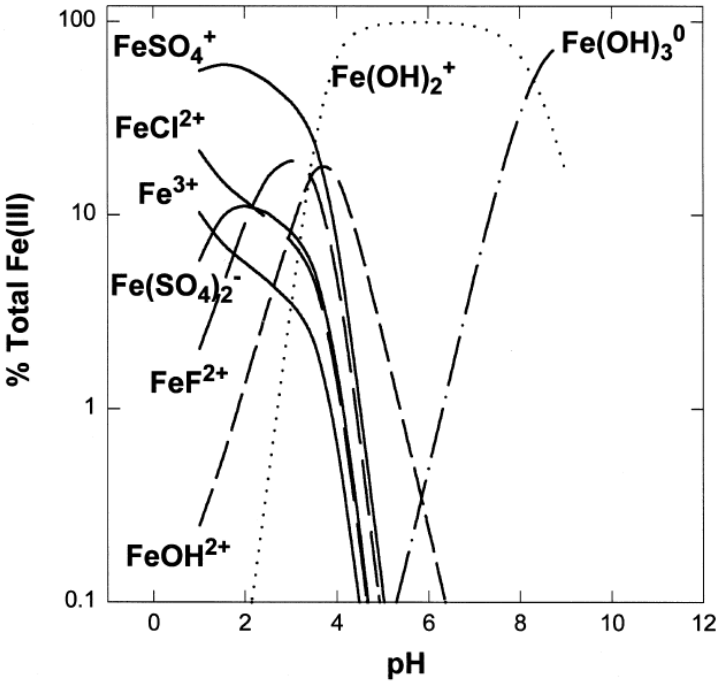

Figure 2.5 The speciation of Fe(III) in seawater as a function of pH. Adapted from (*53*).

Fe(III) is insoluble in aqueous solutions at neutral pH and it can form highly stable ferric hydroxide with solubility of $K_{sp} \sim 10^{-39}$ (*54*). Free aqueous Fe(III) is stable at pH values lower than 2 and upon increase in pH iron solubility decreases significantly (Figure 2.5) (*55*). To select DNAzyme that can function at neutral pH, it is preferred to run the *in vitro* selection of Fe(III)-dependent DNAzymes in physiological pH. Although obtaining DNAzymes with acidic pH as their optimal condition can be useful for Fe(III) sensing in biological systems. Such a DNAzyme is beneficial for sensing iron in lysosomes. These compartments are acidic vesicles (pH ~ 4 - 5) with critical role in cellular iron metabolism (*56*). One approach to solubilize Fe(III) in selection buffer is addition of chelators that stabilize Fe(III) and prevent formation of insoluble ferric hydroxide. Table 2.4 represents a list of biologically relevant ligands that can stabilize Fe(III) and the stability constants of their complex with Fe(III).

Previous attempts in our lab in isolating Fe(III)-dependent DNAzymes have failed in spite of using numerous selection conditions and strategies (*57*, *58*). Different selection conditions were tested including; different buffers/pH (5.5, 6.0, 7.0, and 7.4), different selection strategies (gel or column-based), and different ligands (citrate, lactate, or none). Major problems with these attempts were reported to be contamination, buffer activity, lack of PCR amplification, gel purification anomaly, or no activity. In addition, citrate was used successfully in the *in vitro* selection of UO_2^{2+}-dependent DNAzyme as a ligand (*17*). It is known that citrate stabilizes Fe(III) and increase its solubility up to 0.8 M at neutral pH (*59*). In Figure 2.6, pH-distribution of Fe(III) species is shown.

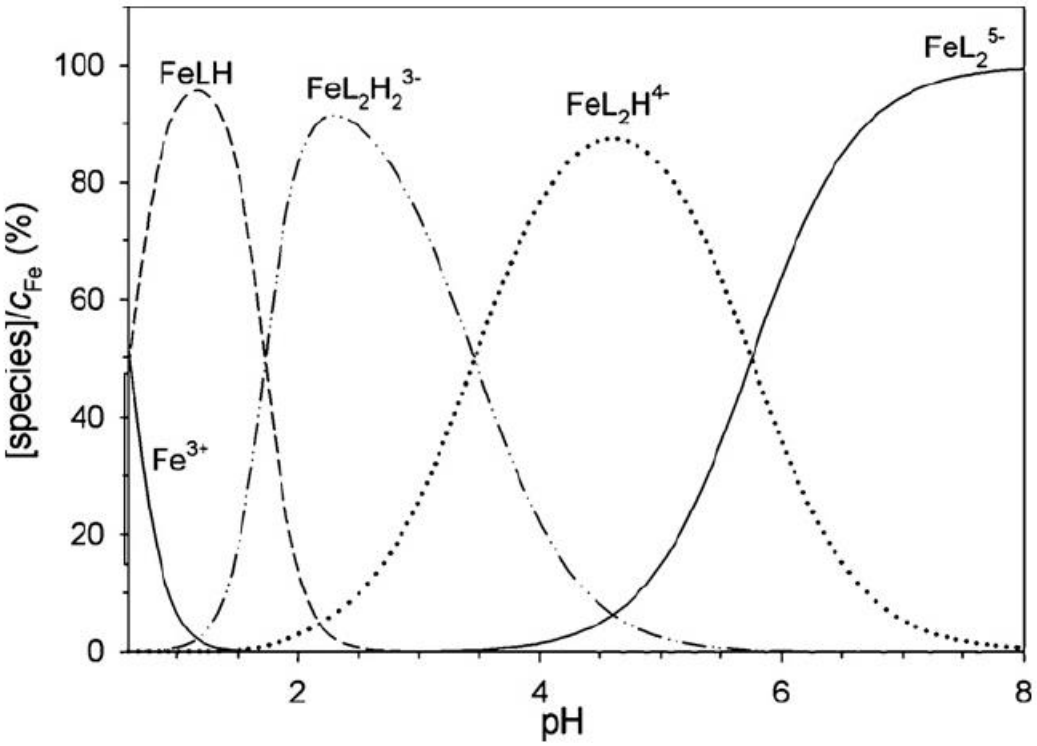

Figure 2.6 pH-distribution of Fe(III)-citrate species. Adapted from (*60*).

Table 2.4 Stability constant (complex formation constant) of Fe(III) and different ligands. All values correspond to Fe(III) unless stated otherwise.

ligand	Stability constant	Reference
AMP (Fe(II))	4.80×10^{1}	(*61*)
2,6-Dihydroxybenzoic acid	2.23×10^{2}	(*62*)
L-Methionine	4.00×10^{2}	(*63*)
Malate	1.41×10^{3}	(*61*)
Ascorbate	1.90×10^{3}	(*61*)
Succinate	1.93×10^{3}	(*61*)
Propionic acid	2.80×10^{3}	(*64*)
Hystamine	5.20×10^{3}	(*65*)
L-Lysine	3.10×10^{4}	(*64, 66*)
L-Histidine	5.00×10^{4}	(*67*)
Glycolic acid	5.00×10^{4}	(*68*)
Guanosine	6.30×10^{4}	(*69*)
ATP (Fe(II))	1.34×10^{5}	(*70*)
ADP (Fe(III),Fe(II))	5.00×10^{5}	(*71*)
Lactate	2.50×10^{6}	(*64*)
2,4-Dihydroxybenzoic acid	1.40×10^{7}	(*62*)
L-Threonine	4.00×10^{8}	(*63*)
L-Asparagine	4.00×10^{8}	(*63*)
TMP-5	4.00×10^{8}	(*72*)
Ornithine	5.00×10^{8}	(*66*)
L-Phenylalanine	7.90×10^{8}	(*67*)
Leucine	1.00×10^{9}	(*73*)
Glycylglycine	1.20×10^{9}	(*64*)
L-Serine	1.60×10^{9}	(*63*)
Oxalic acid	2.50×10^{9}	(*64*)
Valine	4.00×10^{9}	(*73*)
Tryptophan	1.00×10^{10}	(*67*)
L-Cysteine	7.00×10^{10}	(*63*)
Iminodiacetic acid	7.90×10^{10}	(*74*)
Alanine	9.50×10^{10}	(*73*)
Proline	1.00×10^{11}	(*64*)
Citrate	7.10×10^{11}	(*71*)
Glyphosate	1.25×10^{16}	(*75*)
Salicylic acid	2.80×10^{16}	(*62*)
o-Cresotic acid	5.60×10^{16}	(*62*)
HEDTA	6.30×10^{19}	(*76*)
2,3-Dihydroxybenzoic acid	3.20×10^{20}	(*62*)
Pyrophosphate	1.60×10^{22}	(*64*)
catecholate	1.00×10^{23}	(*77*)
EDTA	1.00×10^{26}	(*71*)

In a recent study on Fe(III) citrate speciation in aqueous solution, it was found that formation of stable oligomeric Fe(III)-citrate species is dominant when citrate : Fe(III) ratio is lower than 4:1 (*78*). On the other hand, increase in this ratio enhanced the dominance of the mononuclear iron complexes. In the previous *in vitro* selection attempts in our lab, in which citrate was used to stabilize Fe(III), 4:1 was the highest ratio of citrate : Fe(III). It is possible that formation of stable oligomeric Fe(III)-citrate species was one of the reasons resulted in lack of success in the previous selections. Therefore, I decided to use citrate : Fe(III) ratio of 50:1 to avoid formation of oligomeric species.

2.3.1.2 Design of the Random Pool

In Figure 2.7 the design of the random pool used in selection of Fe(III)-dependent DNAzymes is shown. The random pool included a single riboadenosine (rA) as the cleavage site which was embedded in the middle of two Watson-Crick "pairing regions" (*79*). The 5′ end of the random pool was modified with biotin which was used to immobilize DNA sequences on NeutrAvidin beads. Pairing regions were engineered in the random pool to bring random region of the pool in close proximity of the cleavage site. Previous attempts in our laboratory to isolate Pb^{2+} or UO_2^{2+}-dependent DNAzymes from random libraries lacking engineered pairing regions were not successful (*57*). In addition, it was shown that selecting DNAzymes from random libraries lacking pairing regions negatively influenced isolation of DNAzymes that exploit metal ion cofactors for their catalysis (*10*). Therefore, design of random pools may play an important role in increasing the likelihood of obtaining active DNAzymes with cofactor dependent activity (*80*). Random region was connected to the cleavage site through a stable tetraloop. This tetraloop was chosen from a thermodynamically stable DNA tetraloop library (*81*) to ensure formation of this pairing region in the selection condition.

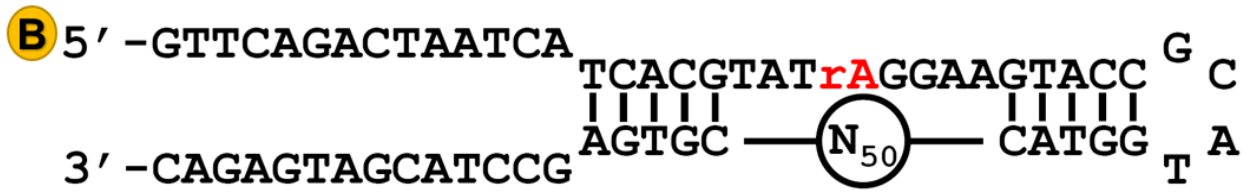

Figure 2.7 The design of the DNA pool used in *in vitro* selection-1.

2.3.1.3 *In Vitro* Selection Experiments

In vitro selection experiments were carried out using column-based selection reported before (*4*). Active sequences (cleaved pool, 87-mer) were eluted from inactive DNA sequences (uncleaved pool, 110-mer), which were immobilized on the beads through biotin-NeutrAvidin interaction. Fraction of cleaved pool at each round of the selection was determined from the radiation count of different samples by liquid scintillation counting (LSC). To prevent undesired photo-induced DNA break in the presence of Fe(III), selection columns were covered by aluminum foil.

Table 2.5 Conditions used in *in vitro* selection-1. Starting at round 7 two different negative selection conditions were carried out (A: 2 h and B: 12 h).

Selection round	Incubation time (min)	[Fe(III)] (mM)
1-6	60	1
7-8 A/B	60	0.5
9-12 B	60	0.5

From round three to six cleavage signal gradually increased from ~ 0.1 to 1.7 %, while signal over background ratio decreased from ~ 2.4 to 0.7. Background was determined for each selection round by incubating immobilized pools with selection buffer without Fe(III) over 1 h. After eluting background followed by several washing steps with selection buffer, Fe(III) was

added to initiate the positive selection. Observed decreased in signal over background may be an

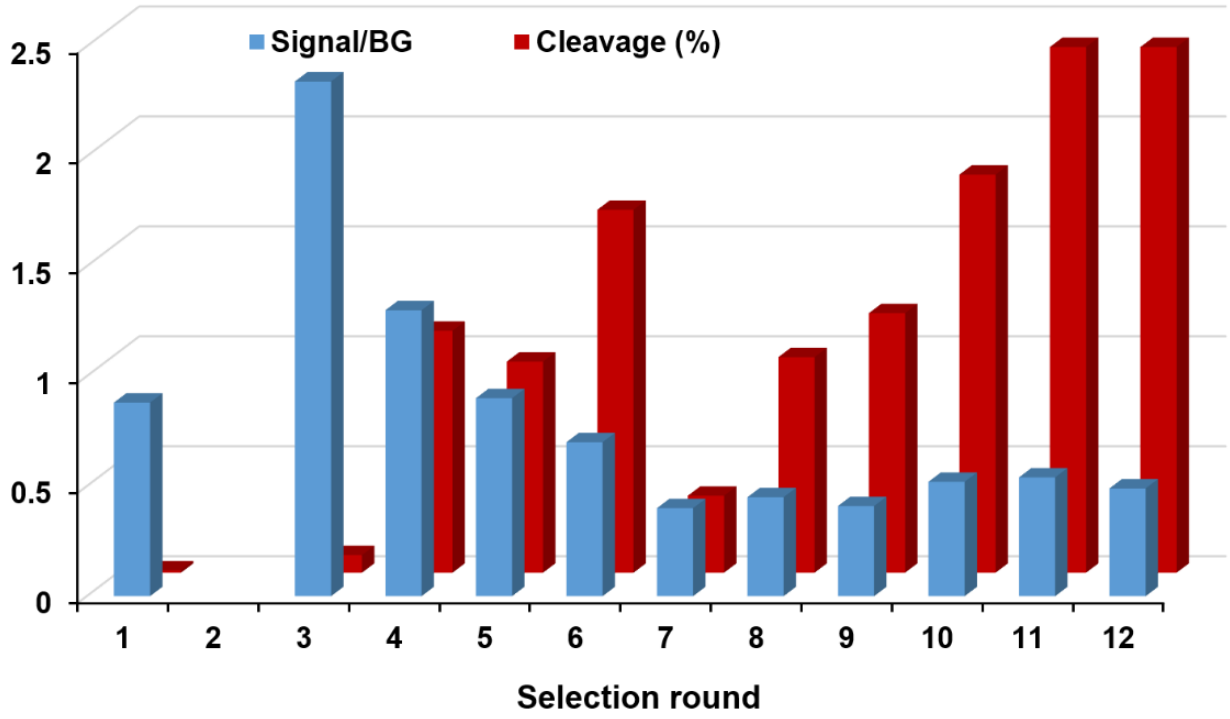

Figure 2.8 *In vitro* selection-1 progress. Two parameters were represented, cleavage product obtained at each round of the selection (cleavage %) and signal over background. Background cleavage was the fraction of pool cleaved with selection buffer in the absence of Fe(III).

indication of evolution of species that can catalyze cleavage reaction in an Fe(III)-independent manner. To decrease background activity, starting from round seven, selection was branched into two different conditions. Negative selections were carried out by incubating the immobilized pools with selection buffer for 2 h (condition A) or 12 h (condition B). After removing cleavage products in the negative selection step, beads were washed extensively. Then positive selection was initiated by addition of Fe(III) to the beads. While condition A was discontinued after two rounds, condition B was continued up to round 12. Despite carrying out six rounds of negative selection, I was not able to improve signal over background ratio. Increase in the cleavage signal over the last six

rounds of positive selection, suggested that the pool was enriched with DNA sequences that are buffer active. Activity assay experiments were carried out to further investigate the activity observed in selected pools. It was found that neither Fe(III) nor Mg^{2+} was the cause of observed cleavage activity. Therefore this selection was stopped.

2.3.2 *In Vitro* Selection-2

2.3.2.1 Selection Condition

Our attempts in using citrate to stabilize Fe(III) in *in vitro* selection were not fruitful, although, citrate was used previously to stabilize uranyl ion in *in vitro* selection procedure to isolate the UO_2^{2+}-dependent DNAzyme (*17*). Initial rounds of selection for the UO_2^{2+}-dependent DNAzyme were carried out in the presence of 5 mM uranyl and 10 mM citrate in the selection buffer at pH 5.5. It is known that uranyl forms a negatively charged complex with two citrate ions in pH ~ 5.5 with log K_f ~ 11.2 (*82, 83*). In addition, uranyl-DNA or RNA complex was found to be very stable with log K_f ~ 9.7 (*84*). Since the UO_2^{2+}-dependent DNAzyme was selected in the presence of uranyl-citrate complex which is negatively charged, it is likely that uranyl can interact with DNA with a binding affinity higher than uranyl-citrate.

In contrast to the UO_2^{2+}-dependent DNAzyme, all of *in vitro* selection attempts for Fe(III)-dependent DNAzymes in the presence of citrate have failed in our lab. Like uranyl, Fe(III) forms negatively charged complexes with citrate (*60*). Additionally, it was shown that increase in the pH resulted in formation of species with higher number of negative charges (*85*). As DNA-Fe(III) and citrate-Fe(III) complex stability is reported to be log K_f ~ 4 - 5 (*86, 87*) and log K_f ~ 11 (*71*), respectively, it is possible that none of our selections was able to isolate a DNA sequence that can compete with citrate-Fe(III) complex. If this hypothesis is correct, then the chance of isolating

Fe(III)-dependent DNAzymes in the presence of a Fe(III) ligand with affinity lower than citrate-Fe(III) may be higher.

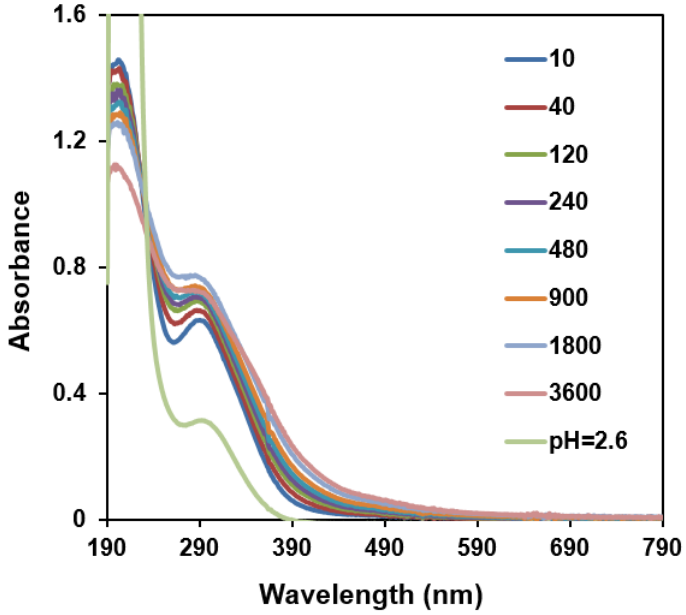

Figure 2.9 UV-vis spectra of 0.2 mM Fe(III) in water at pH 4.0. As a control Fe(III) spectra at pH 2.6, in which Fe(III) is stable, is shown in light green. Spectra collected at different time points (seconds).

To find a proper ligand for Fe(III), I studied the UV–vis spectra of Fe(III) in different conditions. It was found that either $FeNH_4(SO_4)_2$ or $Fe(NO_3)_3$ as a source of Fe(III) gives similar results. Therefore, sources of Fe(III) did not make any difference. I tested two different pH conditions (5.5 and 7.0) using different buffers including MOPS, Bis-Tris, and acetate. Additionally, I investigated number of ligands including alanine, threonine, valine, ATP, GMP, citrate, lactate, salicylate and EDTA. The goal of this study was to find out a condition and a ligand in which UV–vis spectra of Fe(III) does not show a significant change over time. EDTA, salicylate, citrate (Table 2.4), high affinity Fe(III) ligands, were tested as controls. These strong chelators can stabilize Fe(III) even at neutral pH. As shown in Figure 2.9, Fe(III) is not stable in the absence of

ligands at pH 4.0. After testing different ligands and buffers, it was found that Bis-Tris can stabilize Fe(III) at both tested pH values (Figure 2.10).

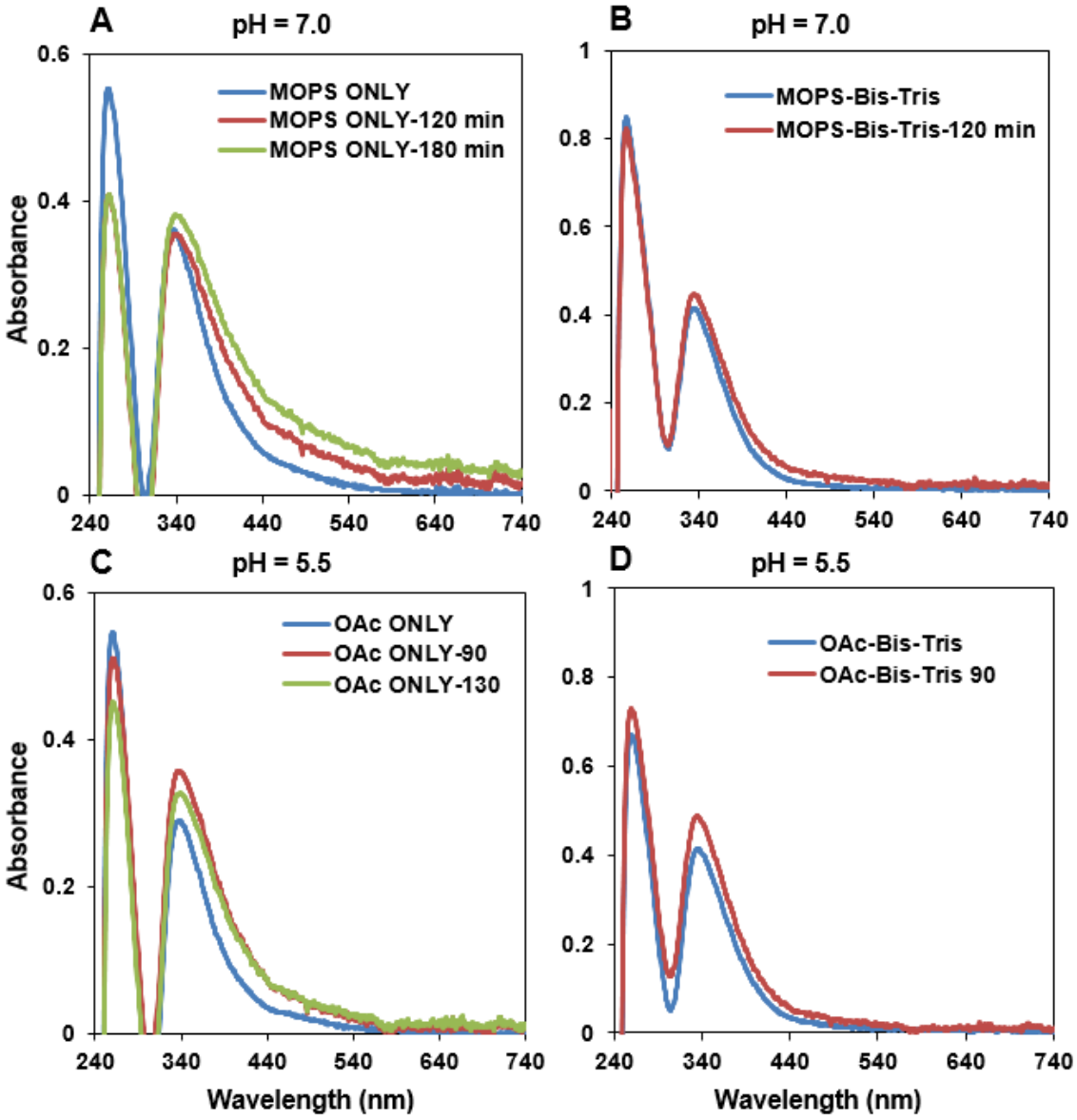

Figure 2.10 UV-vis spectra of 0.1 mM Fe(III) in MOPS and acetate at pH 7.0 and 5.5, respectively. In A and C no ligand is added, while in B and D 5 mM Bis-Tris was added. Spectra collected at different time points (minutes).

Bis-Tris, generally used as a buffering agent with a pK_a of ~ 6.5, was used previously in studying mussel foot protein (mfp) which can bind Fe(III) and regulate formation of adhesive plaques by mussel (*88*). In these studies one (*89*) or 10 (*88*) mM Bis-Tris was used to stabilize Fe(III) at concentrations from 10 to 100 µM at pH 5.5. In another example stabilization of Fe(III) (40 to 350 µM) at pH 7.0 was carried out by using 5 mM Bis-Tris (*90*). It was proposed that Bis-Tris can function as a weak chelator to keep Fe(III) accessible in the media by preventing formation of high molecular weight aggregates. Results from UV-vis studies are in agreement with stabilization of Fe(III) by Bis-Tris proposed previously.

2.3.2.2 Design of the Random Pools

In Figure 2.11 the design of the random pools used in *in vitro* selection-2 is shown. Two different DNA pools that were used are only different in their random region size. Like *in vitro* selection-1, the random pool included a single riboadenosine (rA) as the cleavage site which was embedded in the middle of two pairing regions. The stable tetraloop used here is identical to the one used in the design of the previous random pool (*in vitro* selection-1). No biotin modification was incorporated in the pool, because *in vitro* selection-2 was carried out using the gel-based method.

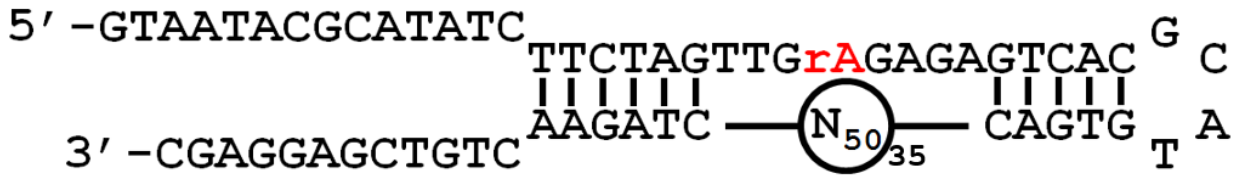

Figure 2.11 The design of the DNA pool used in *in vitro* selection-2.

2.3.2.3 *In Vitro* Selection

In vitro selection experiments were carried out using denaturing PAGE protocol developed before (*17*) to separate active DNAzyme sequences (cleaved pool, 87-mer) from inactive DNA sequences (uncleaved pool, 110-mer) with slight modification. The random pool was generated by PCR reactions to incorporate rA cleavage site and internally label the pool with ^{32}P. The first round of the selection was carried out using 360 pmol DNA template (~ 10^{14} different sequences). The DNA pool generated by PCR was 15 nt shorter than the antisense strand because the reverse primer used in PCR reactions contained a Taq polymerase stopper with 15 nt extension. Before starting each round of the selection, a negative selection step carried out to decrease the chance of isolating DNA sequences with Fe(III)-independent activity. In negative selection DNA pool was incubated in the selection buffer (200 mM NaCl in 25 mM Bis-Tris pH 7.0) in the absence of Fe(III) for 24 h. Then uncleaved DNA sequences were separated from cleaved pool through denaturing PAGE and used for positive selection in the presence of Fe(III). DNA pools were dissolved in 1× selection buffer and then reactions were started by addition of equal volume of 2× Fe(III) in selection buffer. For each positive selection a negative control was carried out. In negative control DNA pools were incubated in the selection buffer in the absence of Fe(III) to monitor background cleavage in the selection buffer. Cleavage obtained in negative control was used to determine the background cleavage.

Six and seven rounds of selection were carried out for N35 and N50 random pool, respectively. All positive selections were performed with 50 μM Fe(III) for one hour. Selection with N35 pool started to show an observable cleavage product at round 5 during the negative selection. In the next round of the selection I observed cleavage band with N35 pool. In spite of significant increase in cleavage at round six, this cleavage was mostly due to the background

activity (see the signal/background ratio, Figure 2.12). Similarly, activity of N50 pool was observed at the same time of decrease in signal/background ratio (Figure 2.12). Altogether, these results indicate that the cleavage activities observed in both pools were Fe(III)-independent. This nonspecific activity was evolved, in spite of stringent negative selections carried out before all positive selections.

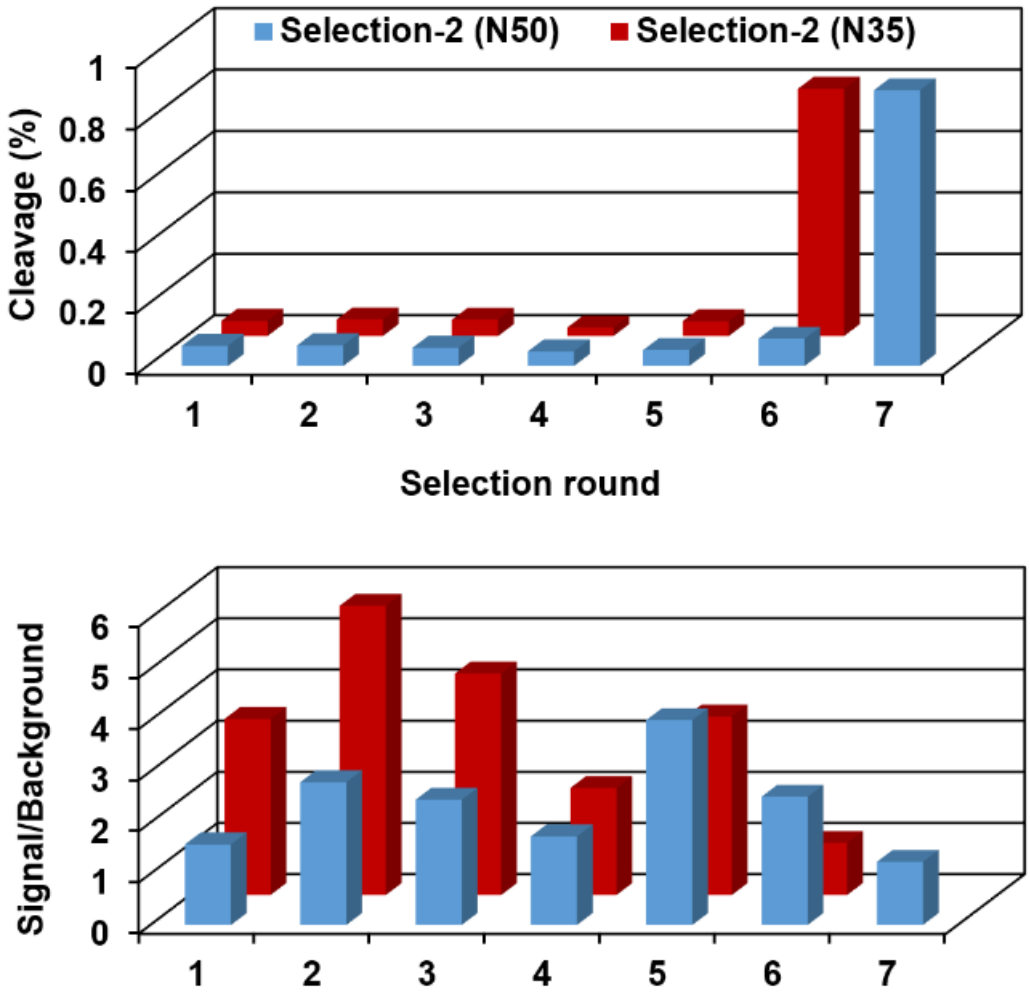

Figure 2.12 Selection progress in terms of cleavage (%) and signal/background ratio.

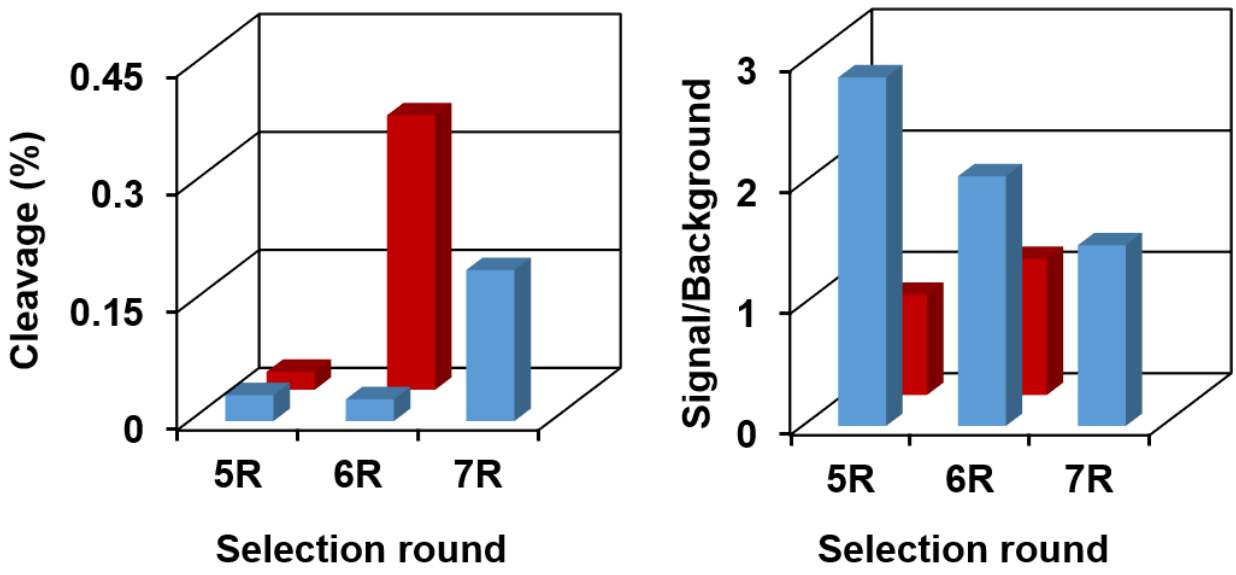

Figure 2.13 Selection progress in terms of cleavage (%) and signal/background ratio after three consecutive negative selections.

To improve efficiency of the negative selection steps and minimize the survival chance of nonspecific activity, I decided to run multiple consecutive negative selection steps with annealing process. Selected pools at round four were amplified and used for three consecutive negative selections. In each negative selection step DNA pools were dissolved in 1× selection buffer and then heated at 90 °C for 2 minutes followed by cooling down to the room temperature over 20 minutes. The pools were incubated for 12 hours and then uncleaved pools were PAGE purified to be used for the next negative selection step. As shown in Figure 2.13, evolving nonspecific activity did not stop by introducing more stringent negative selections. To further investigate the possibility of having Fe(III)-dependent activity I have tested the activity of both N35 and N50 pools with 500 µM Fe(III). It was found that cleavage activities obtained with 500 µM Fe(III) are no more than the background cleavage. Evolution of nonspecific activity through selection, regardless of the stringency of the negative selections, may mean that Fe(III) is not accessible to DNA or if there

are some Fe(III) species available they are less effective than background in causing cleavage. As a result, this *in vitro* selection condition was not continued further.

2.3.3 *In Vitro* Selection-3

2.3.3.1 Selection Condition

Since our attempts in isolating Fe(III)-dependent DNAzyme at pH 7.0 failed, I decided to run *in vitro* selection experiments at pH 5.5. Although at this pH available hydrated Fe(III) is less than 0.1 pM, addition of a weak stabilizing agent such as Bis-Tris may improve availability of Fe(III) to the potential DNAzymes that can survive several rounds of selection. Our UV-vis studies (section 2.2.1) has shown Bis-Tris can stabilize Fe(III) at pH 5.5. Therefore, it is more likely to isolate Fe(III)-dependent DNAzymes using acidic condition in presence of Bis-Tris. Selection buffer used in *in vitro* selection-3 consisted of 40 mM sodium acetate, 5 mM Bis-Tris pH 5.5 and 200 mM sodium chloride.

2.3.3.2 Design of the Random Pools

In Figure 2.14 the design of the random pools used in *in vitro* selection-3 is shown. The two different pools used are only different in their random region size (N35 and N50). Unlike the other pools I used before, the random pool designed for *in vitro* selection-3 included a single riboguanosine (rG) as the cleavage site which was embedded in the middle of two pairing regions. It was reported that cleavage of rG at the cleavage site is easier than other possible ribonucleotides (*91*). Therefore, rG was chosen at the cleavage site to increase the chance of isolating active DNAzymes with Fe(III). Sequence of the stable tetraloop chosen here is different from what was utilized in the design of the previous pools. Similar to *in vitro* selection-2, no biotin modification was incorporated in the pool, as gel-based methodology was performed here.

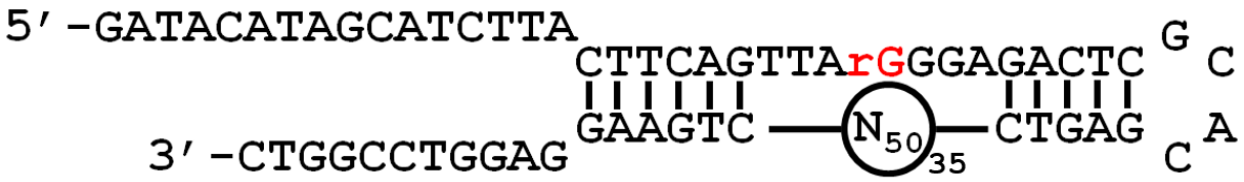

Figure 2.14 The design of the DNA random pool used in *in vitro* selection-3.

Table 2.6 Fe(III)-dependent DNAzyme *in vitro* selection conditions. In one condition a negative selection step was carried out for 24 h before positive selections. In the other condition, after round three, the negative selection discontinued (round 4NN to 9NN).

Selection round	Incubation time (min)	[Fe(III)] (μM)
	Negative selection	
1-4	60	50
5	15	50
6	3	50
7-9	3	5
	No negative Selection	
4-5-NN	60	50
6-NN	10	50
7-NN	3	50
8-9-NN	3	5

2.3.3.3 *In Vitro* Selection

In vitro selection experiments were carried similar to the one described in section 2.2.1, except using different selection conditions. Nine selection rounds were carried out for both N35 and N50 random pools. Each selection was branched into two different conditions after round three. In one condition no more negative selection was carried out, while in the other condition the negative selections were continued until the end of the selection. As shown in Table 2.6, different Fe(III) concentrations and selection times were used in the four described selections. Similar to the previous *in vitro* selections, a negative selection control was carried out alongside each positive selection to determine the background cleavage. In addition, few other control experiments were

performed such as testing final cleavage obtained with 5 and 50 µM Fe(III) in one hour. All four pools showed lower signal over background in the last round of the selections (Figure 2.15). Therefore, no further positive selection was performed.

Selectivity of the pools for Fe(III) over Fe(II) were tested at round six. Although more than 10% cleavage was observed with 10 µM Fe(III), no activity was found with Fe(II) from 10 to 100 µM. In addition, I tested activity of the selected pools from the last two rounds of the selection with 50 µM of different metal ions including Mg^{2+}, Ca^{2+}, Sr^{2+}, Ba^{2+}, Mn^{2+}, Co^{2+}, Ni^{2+}, Cu^{2+}, Zn^{2+}, Cd^{2+}, Pb^{2+}, Eu^{3+}, Sm^{3+}, In^{3+}, Tb^{3+}, and Yb^{3+}. Our results showed none of tested metal ions can cause cleavage except Fe(III). Therefore, enriched pools were highly selective for Fe(III) over other competing metal ions.

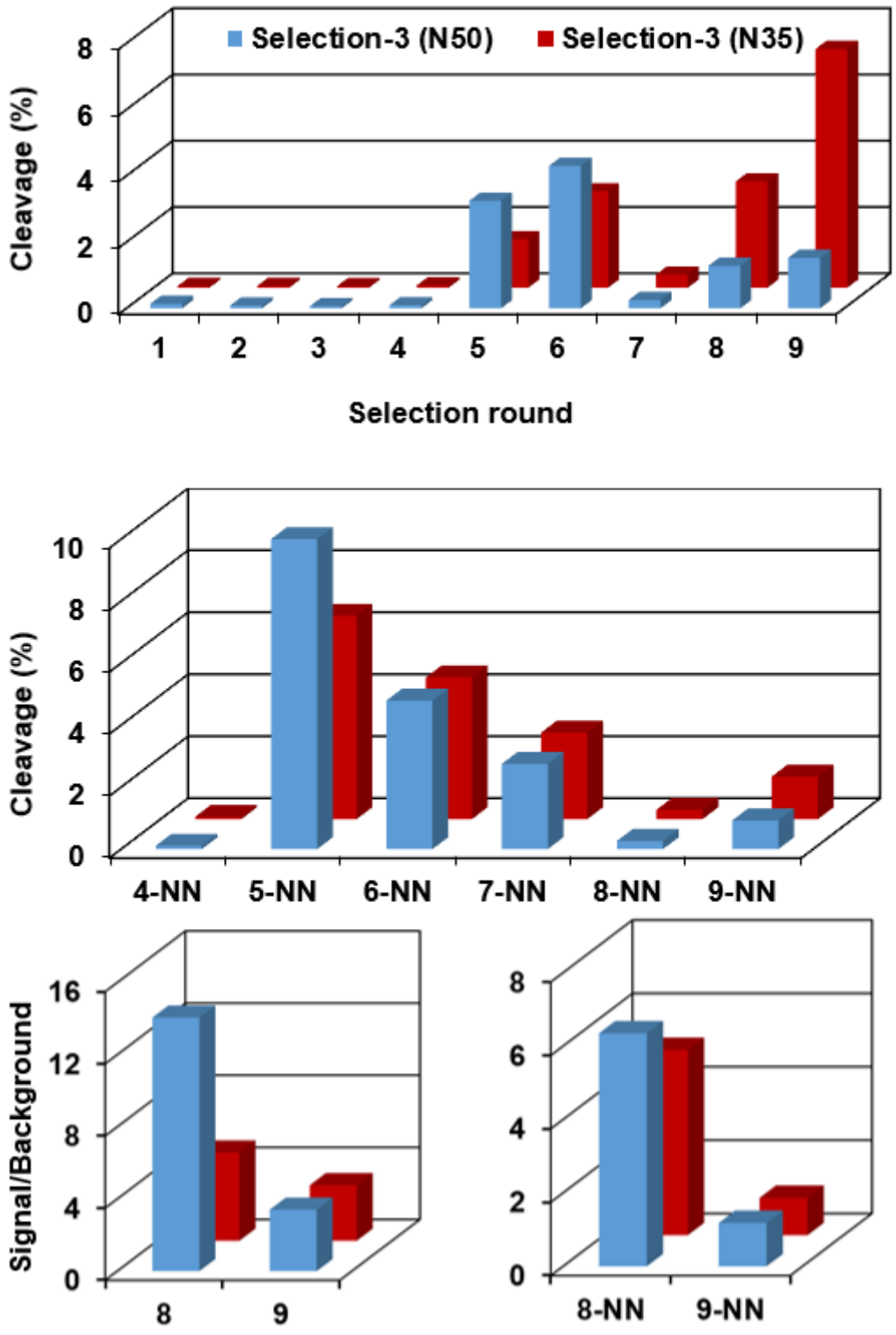

Figure 2.15 Selection progress in terms of cleavage (%) and signal/background. Two different pools with different random regions, N35 and N50, are shown in blue and red, respectively. Selection rounds carried out without prior negative selection are shown with "NN".

2.3.4 Cloning and Sequencing

Base on the cleavage activity of the selected pools, results obtained in control experiments, and the activity assays carried out with different Fe(III) concentrations, the most active pools with least background activity were chosen for cloning and sequencing. Cloning was carried out using PCR products with primers with no rG or Taq stopper. Same PCR reactions were carried out using selection primers to control activity of the species used for cloning. Negative PCR controls, with no template, were performed to assure no contamination is the cause of observed amplifications. Table 2.7 represents selection conditions, number of obtained clones and their one letter code.

Table 2.7 Assigned letters to different Fe(III) selected pools

Selection condition	Number of sequenced clones	Letter code
N35	39	A
N50	40	B
N35 (NN)	39	C
N50 (NN)	39	D

DNA sequences obtained from sequencing aligned based on their sequence similarity for each individual pool. Sequence identity of the thermodynamically stable DNA tetraloop, which was engineered in the design of the random pools, remained intact in more than 96% of the obtained clones. Few sequence were identified with mutations in their primer regions. Conservation of the stable tetraloop suggests that formation of this stable structure did not interfere with catalytic activity of the evolved sequences. Presence of the tetraloop in the active sequences can help in the prediction of active secondary structures. Sequence alignment of each individual pool is represented in Figures 2.16 to 2.19.

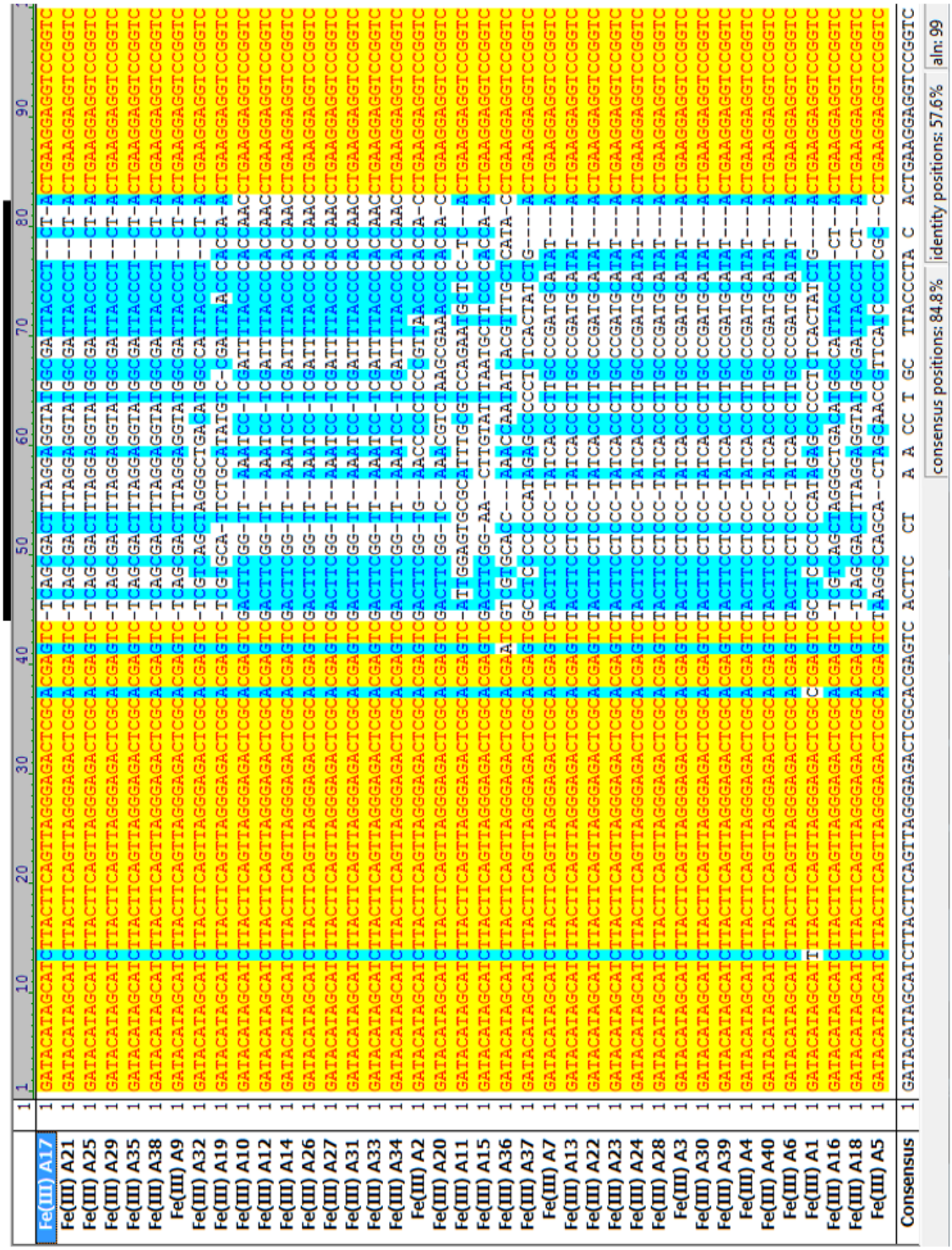

Figure 2.16 Sequence alignment of 39 clones isolated from selection condition A. Red text with yellow background indicates identical regions and dark blue text on a light blue background represent conserved sequences. Black on a white background signifies non-similar regions. The location of the N35 random region is indicated with a black line.

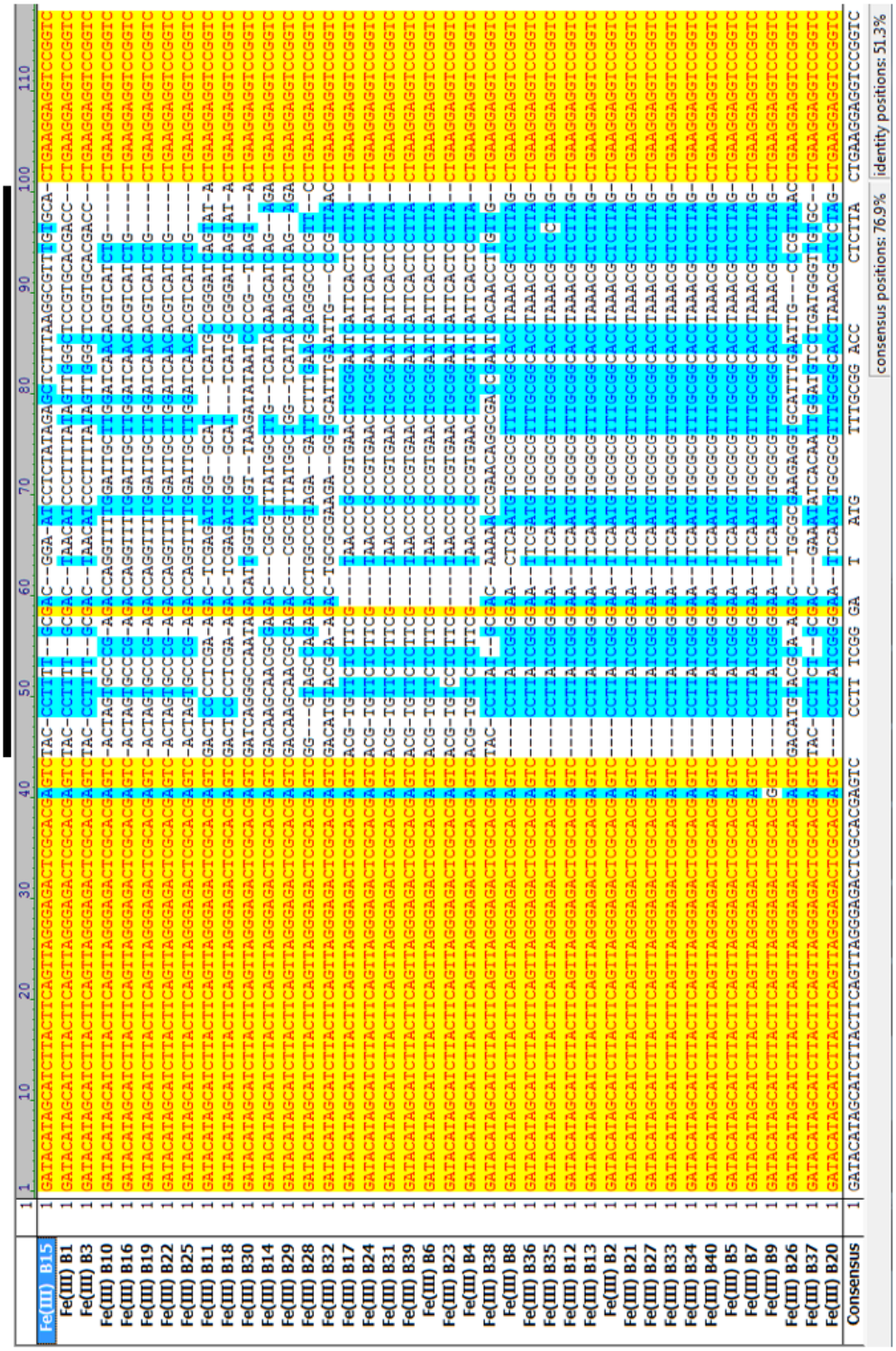

Figure 2.17 Sequence alignment of 40 clones isolated from selection condition B. Red text with yellow background indicates identical regions and dark blue text on a light blue background represent conserved sequences. Black on a white background signifies non-similar regions. The location of the N35 random region is indicated with a black line.

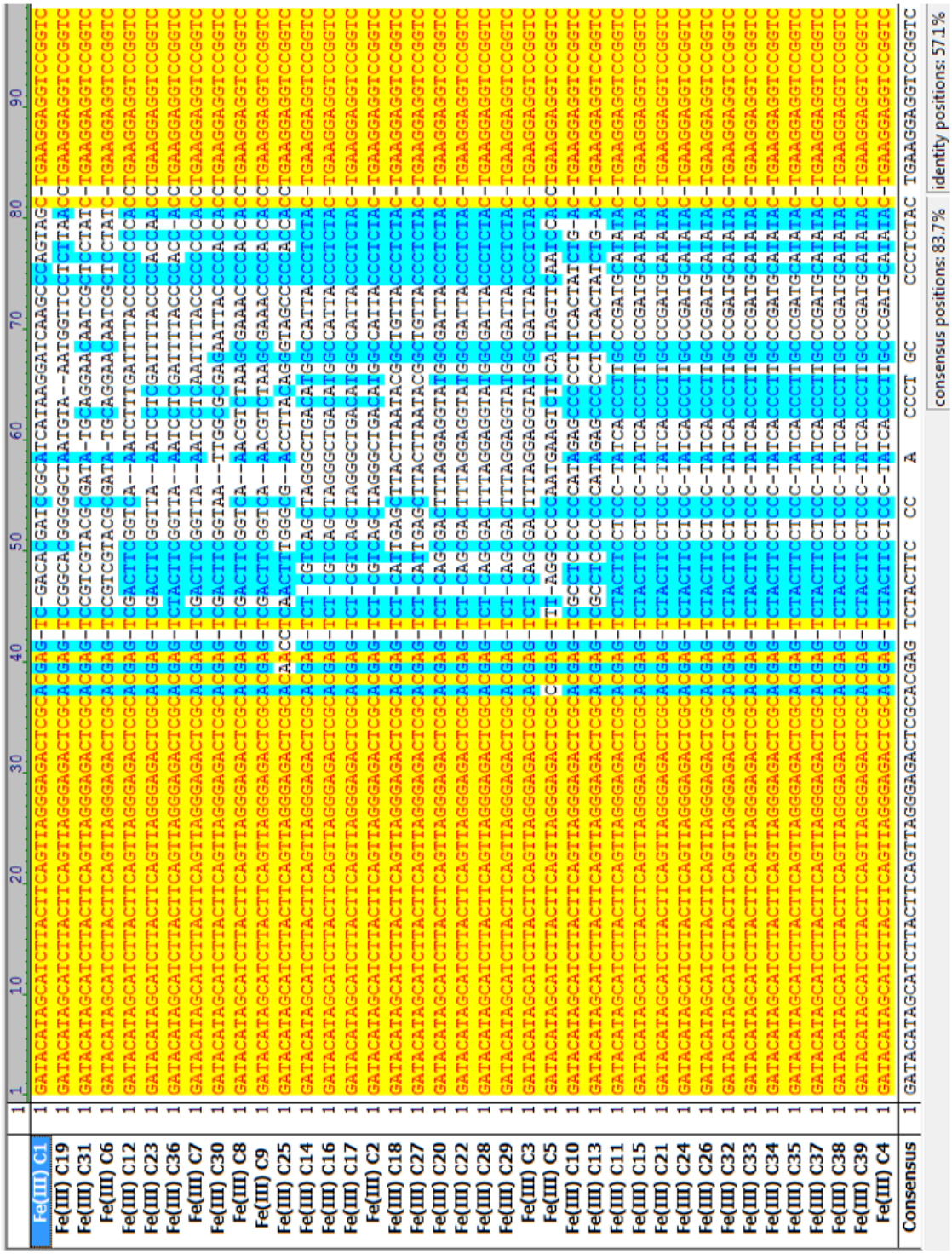

Figure 2.18 Sequence alignment of 39 clones isolated from selection condition C. Red text with yellow background indicates identical regions and dark blue text on a light blue background represent conserved sequences. Black on a white background signifies non-similar regions. The location of the N35 random region is indicated with a black line.

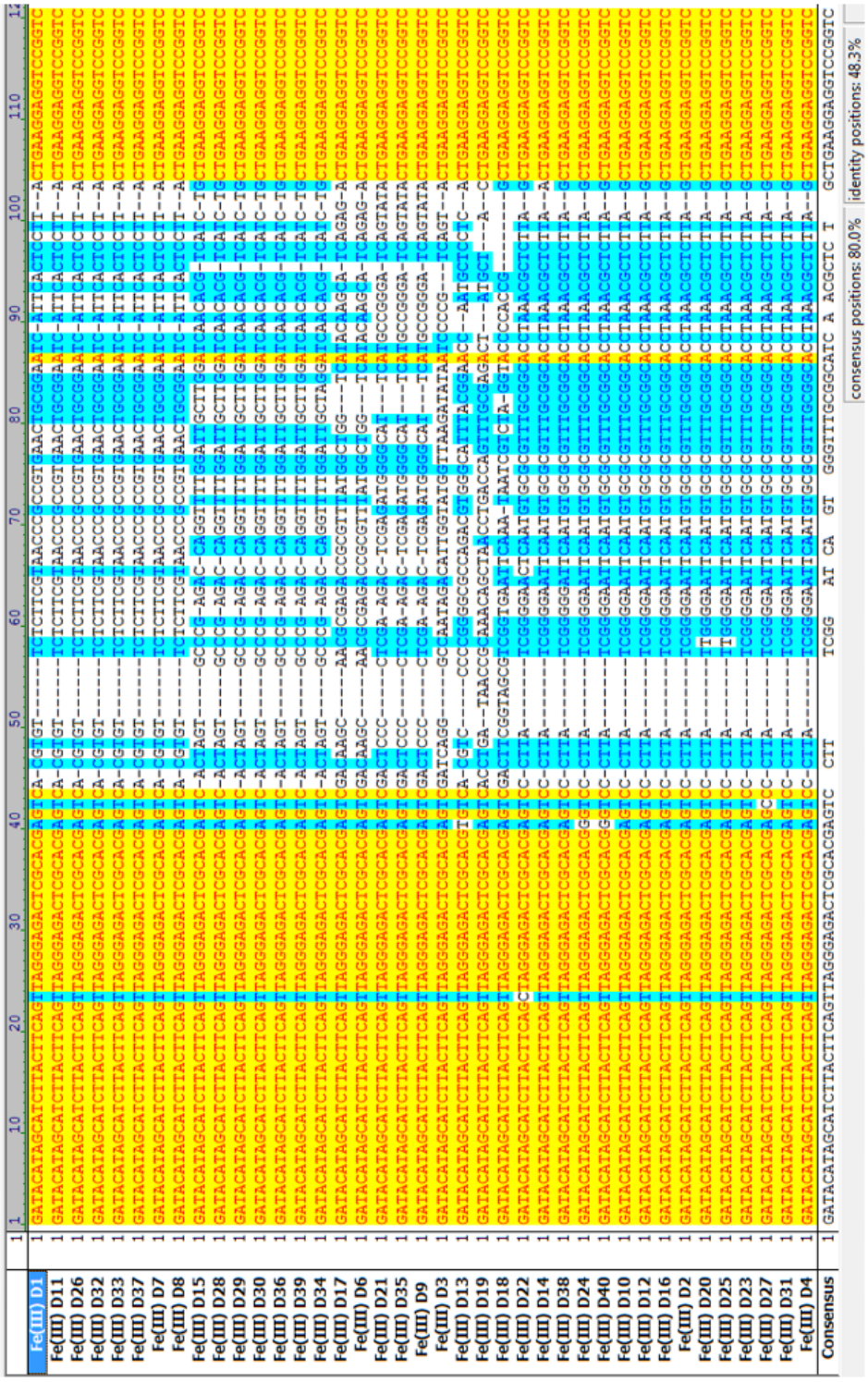

Figure 2.19 Sequence alignment of 39 clones isolated from selection condition D. Red text with yellow background indicates identical regions and dark blue text on a light blue background represent conserved sequences. Black on a white background signifies non-similar regions. The location of the N35 random region is indicated with a black line.

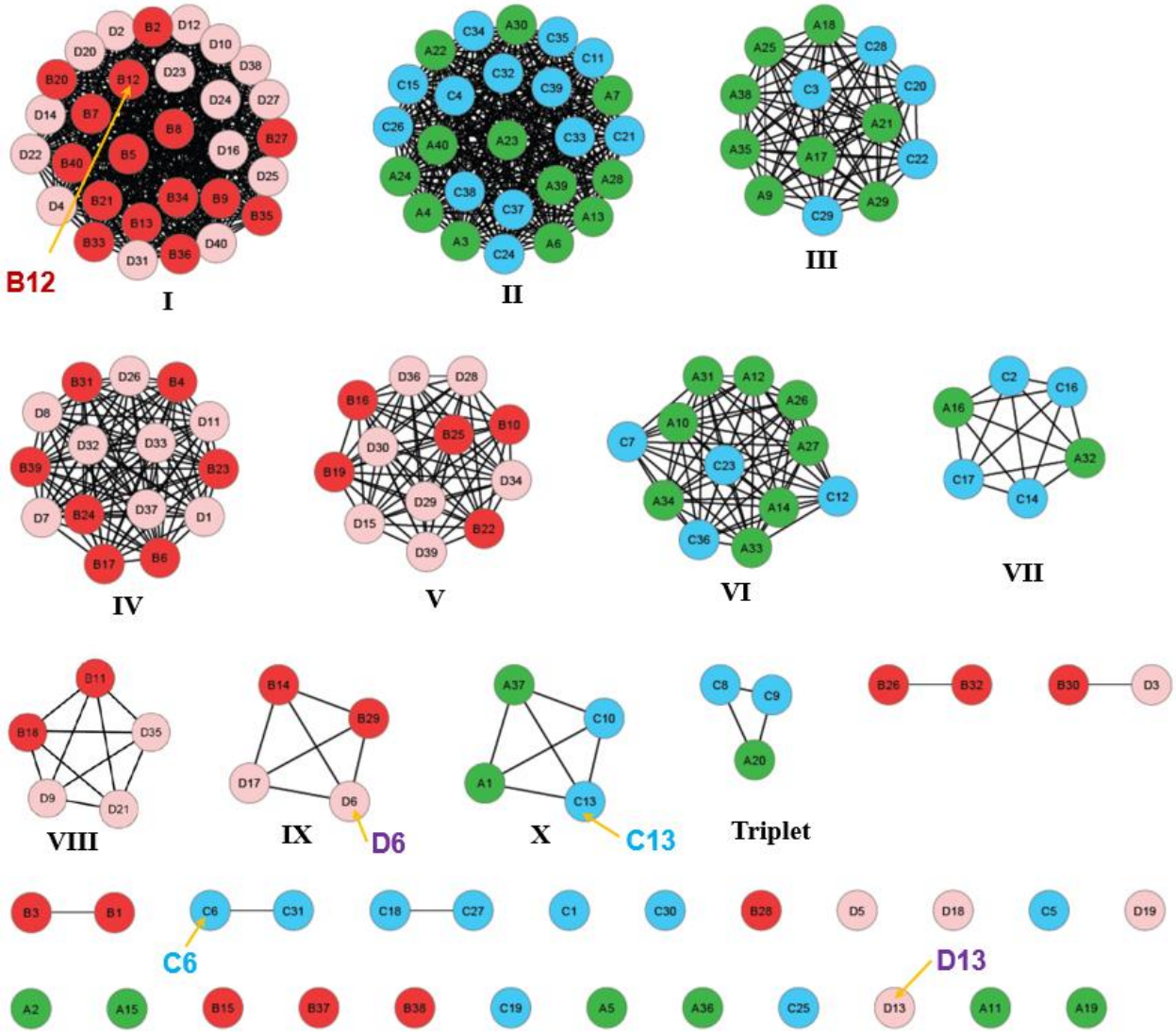

Figure 2.20 Sequence similarity network (SSN) including 157 sequences obtained from 4 different Fe(III)-dependent DNAzyme selections. This network was obtained with a threshold at BLAST E-value of 10^{-30}: only edges associated with E-values more significant than 10^{-30} are included in the network. Lengths of connecting edges correlate with the relative dissimilarities of each pair of sequences. Green, red, blue, and pink nodes represent sequences from condition A, B, C, and D, respectively.

Sequence Similarity Networks (SSN), originally designed for organizing sequence similarity of proteins (*92*, *93*), was utilized to identify sequence similarity of obtained sequences. I used SSN that presents interconnected sequences as clusters within 2D space providing a good

visual representation of sequence similarity relationships between four different pools (Figure 2.20). A node represents each sequence and two sequences are connected with a line if their pair-wise BLAST e-value is below 10^{-30} cutoff. Clusters contained four or more sequences have been named from I to X (Figure 2.20). This segregation is likely because of the 15 nucleotides size difference in between the pools. However, by relaxing the cutoff threshold to 10^{-7}, five other sequences, including four from N35 pools, were identified to be closely related to cluster I (Figure2.21). Later it was found that these sequences are functionally related.

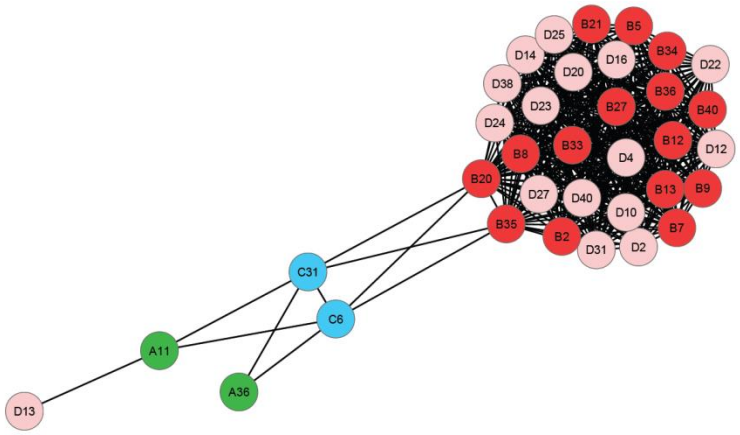

Figure 2.21 SSN including cluster I and 5 other sequences that found to be functionally related. The threshold of this network was set at a BLAST E-value of 10^{-7}. Green, red, blue, and pink nodes represent sequences from condition A, B, C, and D, respectively.

The sequences in the first five populated clusters (I-V), 95 individual sequences, are almost identical within each cluster with none or only a few single nucleotide differences. Only 12% of the population remained unclustered as singletons in the SSN (orphan sequences). In addition, it was found that stopping or continuing negative selection after round three had no effect on the similarity of the obtained sequences. Figure 2.22 shows sequence similarity of clones from cluster

I and II with 30 and 25 members, respectively. In addition, sequence similarity of unclustered sequences is shown in Figure 2.23.

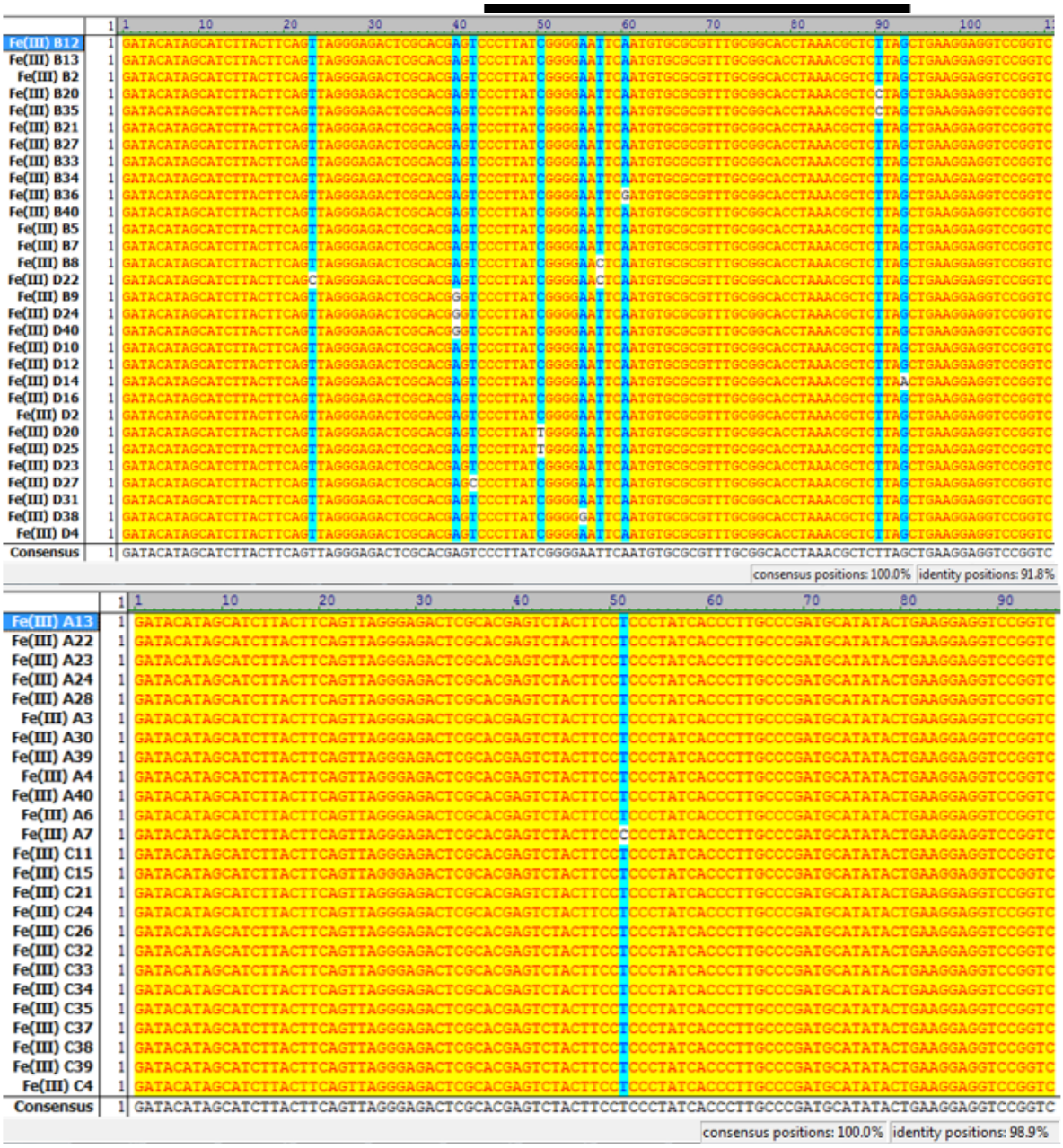

Figure 2.22 Sequence alignment of 30 and 25 sequences from cluster I (top) and II (bottom), respectively.

Figure 2.23 Sequence alignment of unclustered sequences based on SSN with BLAST e-value of 10^{-30}.

2.3.5 Activity of Individual Clones

A number of clones were tested for cleavage activity with Fe(III) in *cis*-cleaving format to understand the sequence-function relationship of the isolated DNAzymes. These clones included at least one representative from identified clusters in addition to all unclustered sequences. As chosen clones are from different clusters, they shared relatively low sequence similarity (Figure 2.24). Single stranded DNAzymes were internally labeled with ^{32}P and dissolved in the selection buffer (described in detail in the method section). Activity of each *cis*-cleaving DNAzyme was tested with 5, 20, and 50 µM Fe(III). I found that few sequences show background activity (B1, B15, B37, and D19). In addition, several sequences including A9, A20, B38, C2, C25, C30, and D18 were found to be inactive. Except A9 and C2 the rest inactive or background active sequences belong to unclustered clones. As shown in Figure 3.25, the fastest rate (~ 1 min^{-1}) was observed

with clone D13 (unclustered) at 20 µM Fe(III). Clone B12 (cluster I) was the second active sequence with low final cleavage (~30%) under the same condition. Moreover, D13 was the most active clone at lower Fe(III) concentration (5 µM) with ~ 60% cleavage at one hour.

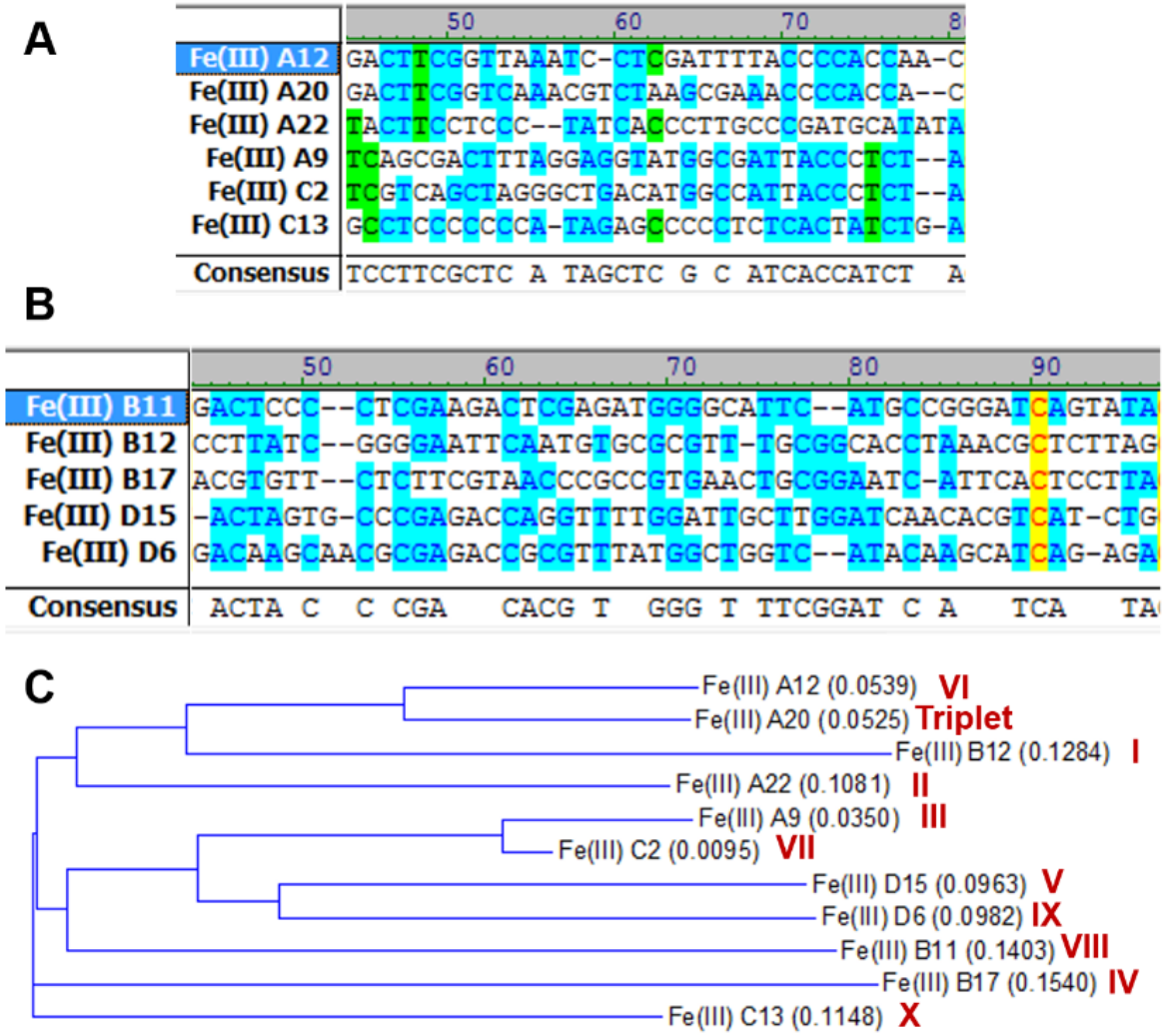

Figure 2.24 Sequence representatives from different clusters. (A) Sequence alignment of 6 different clones used for activity assay analysis from N35 pools. (B) Sequence alignment of 5 different clones used for activity assay analysis from N50 pools. (C) Phylogeny tree of representative clones and their cluster number is shown. One representative from each triplet is included as well. Red text with yellow shade indicates identical regions and dark blue on a light blue background represents conserved sequences. Black on a white background signifies non-similar regions. The location of the N35 random region is indicated with a black line. Black text with green background indicates block of similar regions.

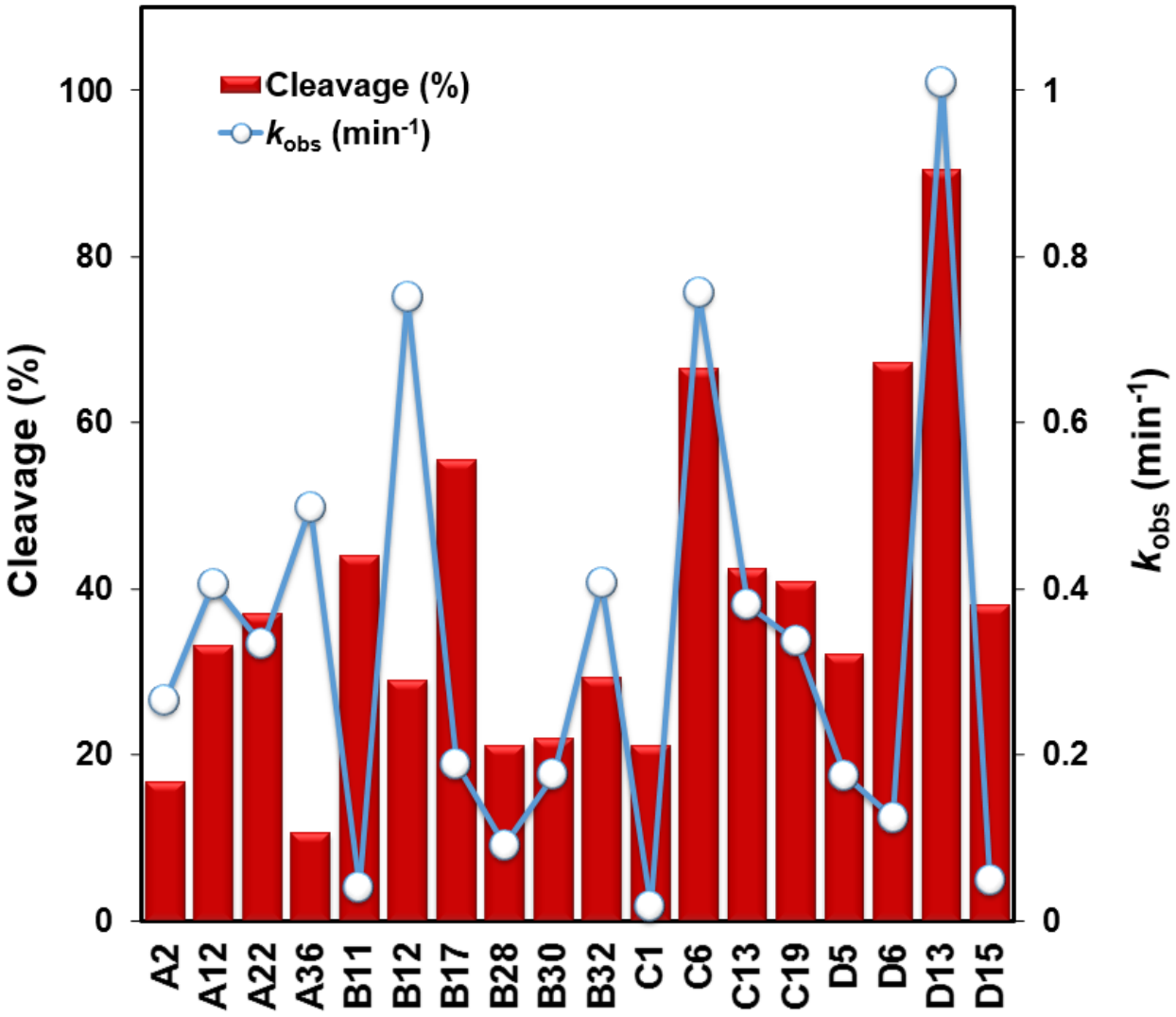

Figure 2.25 Activity of 18 most active *cis*-cleaving Fe(III)-dependent DNAzymes. Final cleavage percentage obtained in 1 hour reaction time with 20 µM Fe(III) (red bars, left axis) and determined k_{obs} values (open circles) under the same condition.

Cleavage activity and obtained k_{obs} values for 18 most active clones are represented in Figure 2.25. All clones were tested with 20 µM Fe(III) and their final cleavage activity after one hour is shown in Figure 2.25. B12, C6, and D13 were found to be the most active clones. In addition, maximum cleavage product was observed from D13. Based on the obtained k_{obs} and final

cleavage product I chose 5 of the most active clones, B12, C6, C13, D6, and D13, for truncation studies.

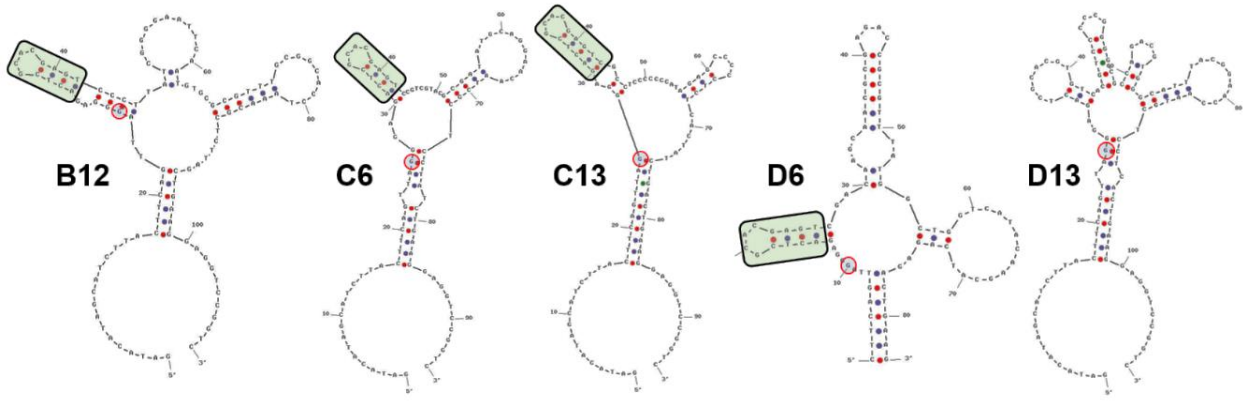

Figure 2.26 Predicted secondary structures for *cis*-cleaving DNAzymes B12, C6, C13, and D6 which contains the stable tetraloop (boxed in black). The only exception is D13. Cleavage site, rG, is indicated by red circles. Only C13 and D6 structures showed here were found to be the active structures. In case of C13 and D6 boxed region used for truncation.

2.3.5.1 Secondary Structures Determination and *Cis* to *Trans* Truncation

The random pool of *in vitro* selection-3 contained two pairing regions (Figure 2.14), intended to bring random region to the vicinity of the cleavage site. A thermodynamically stable tetraloop (*81*) was used to form a hairpin and assure formation of a stable stem loop which may simplify prediction of secondary structures of the isolated clones. In contrast to Fe(II)-DNAzymes, sequence of the stable tetraloop remained unmodified in the most active Fe(III) clones, B12, C6, C13, and D6 with one exception, D13 (Figure 2.26). This may suggest that the formation of stable tetraloop did not interfere with activity of the selected sequences. However, truncation studies showed that the tetraloop was formed in only two (C13 and D6) out of five active structures. Truncation based on the presence of the tetraloop for B12, D13, and C6 resulted in inactive *trans*-

cleaving DNAzymes. Secondary structure of the five most active *cis*-cleaving DNAzymes, predicted using UNAFold web package (*94*), are shown in Figure 3.22.

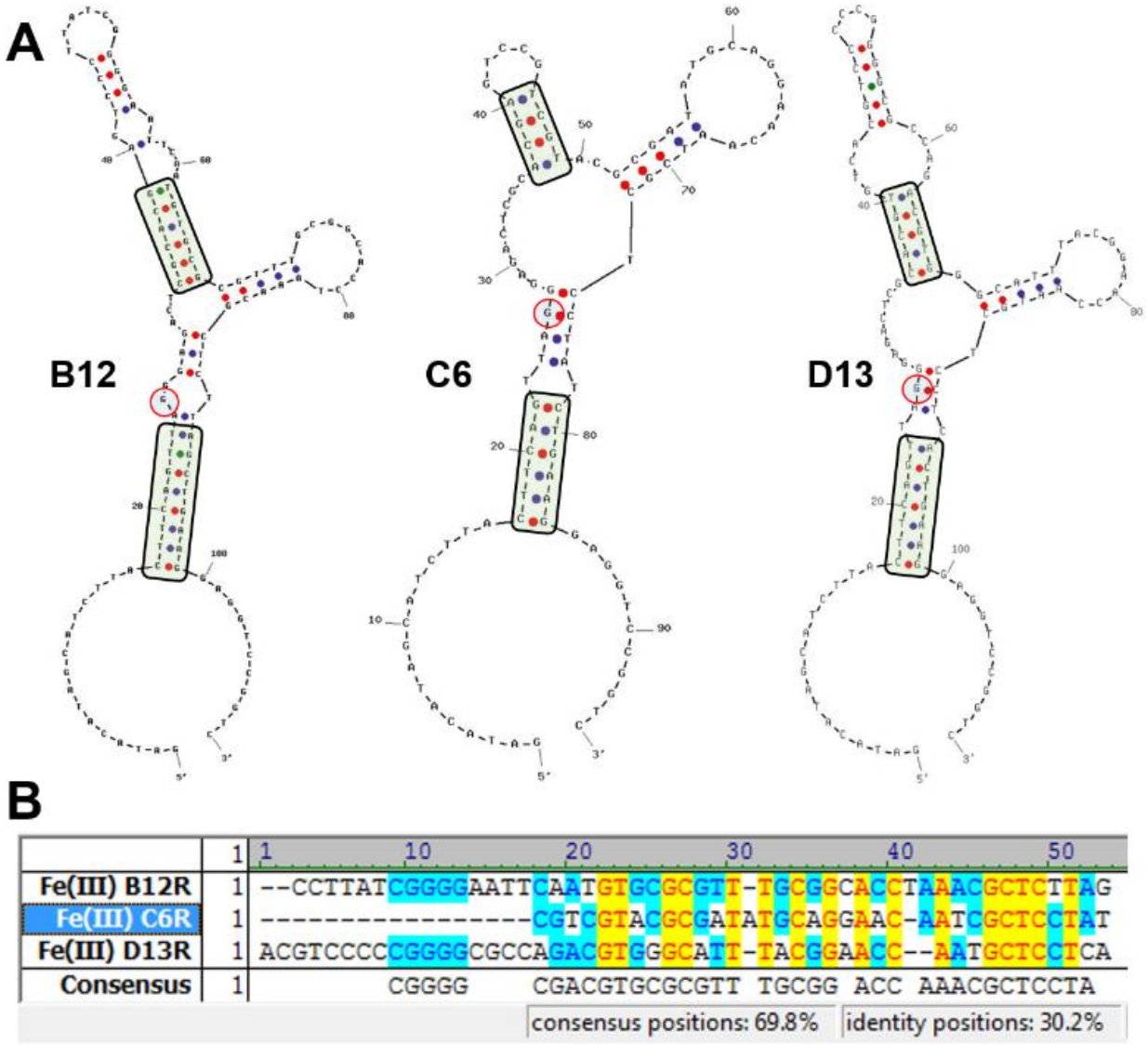

Figure 2.27 Predicted secondary structures and sequence alignment of B12, C6, and D13. (A) Predicted secondary structures resulted in an active *trans*-cleaving DNAzyme after truncation. (B) Sequence alignment of random regions from B12, C6, and D13.

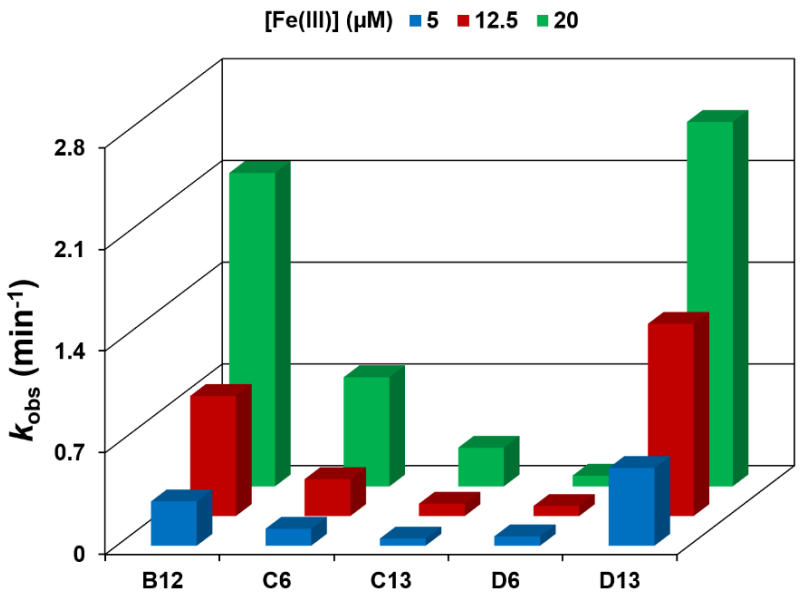

Figure 2.28 Activity of *trans*-cleaving B12, C6, C13, D6 and D13 DNAzymes. Cleavage activity of each DNAzyme was monitored with 5, 12.5, and 20 μM Fe(III) in 40 mM acetate, 5 mM Bis-Tris pH 5.5 and 200 mM NaCl.

Figure 2.27 shows that B12, C6 and D13 clones share a similar secondary structures. Truncation sites that resulted in an active *trans*-cleaving DNAzymes are boxed in black. Interestingly, all three DNAzymes share a highly similar sequence in their enzyme strand. B12 and D13 are 15 nucleotides longer than C6, as it is shown in Figure 2.27B. Interestingly, this extra 15 nucleotides is not part of the enzyme strand in both B12 and D13 DNAzymes. Comparison of enzyme strand in the *trans*-cleaving DNAzymes shows that except D6, in the other four DNAzymes a relatively short DNA sequence is found to act as Fe(III) DNAzyme. After converting *cis*-DNAzymes to *trans*-cleaving DNAzymes using truncations sites shown in Figures 2.26 and 2.27, both arms were extended to form a stable DNAzyme-substrate complex. Substrates were end labeled with ^{32}P and annealed with DNAzymes at 80 °C for 3 minutes followed by cooling down to the room temperature over 20 minutes. Activity of each DNAzyme was tested under single-turnover conditions with 5, 12.5 and 20 μM Fe(III). As shown in Figure 2.28, B12 and D13 are more active than other 3 DNAzymes.

2.3.6 *Trans*-Cleaving DNAzyme Characterization

2.3.6.1 Ligand Dependency

Isolating Fe(III)-dependent DNAzymes in *in vitro* selection-3 proved that addition of Bis-Tris and running selection reactions at pH=5.5 were effective in stabilizing Fe(III) in solution while keeping it accessible to the DNAzymes. First, I tested the activity of the *trans*-cleaving version of B12, C6, C13, D6, and D13 with varying concentrations of Fe(III) from 1 to 100 µM (Figure 2.29). It was found that C13 is more sensitive to lower Fe(III) concentrations, although no activity was observed with 1 µM Fe(III). Activity of C13 and D6 was inhibited at higher Fe(III) concentrations (*i.e.* 50 and 100 µM). B12 and D13 were found to be much faster than the other three DNAzymes. To find out ligand dependency of DNAzymes, D6 and C13 activity with 20 µM Fe(III) was tested under single-turnover condition in the presence of different concentrations of Bis-Tris (0.1, 1, and 5 mM) or citrate (20, 100, 500 µM) in 40 mM sodium acetate pH 5.5 and 200 mM sodium chloride. Additionally, C13 and D6 activity was tested with 20 µM Fe(III) in the presence of 1 mM alanine, threonine, lactate, ATP, or GMP. Interestingly, cleavage activity was observed only in the presence of Bis-Tris and none of the other provided ligands could replace Bis-Tris. Moreover, highest cleavage activity was observed in the presence of 5 mM Bis-Tris. Further increase in Bis-Tris concentration to 20 mM did not change activity of the DNAzymes. B12 and C13 activity with 20 µM Fe(III) was reduced by lowering Bis-Tris concentration from 5 to 0.1 mM. Likewise, when activity of all five DNAzymes were tested with lower Fe(III) concentrations (*i.e.* 1 µM), lowering Bis-Tris concentration from 5 to 0.1 mM did not improve sensitivity of the DNAzymes. This may suggest that lack of reactivity with 1 µM Fe(III) is not due to the presence of high concentration of Bis-Tris.

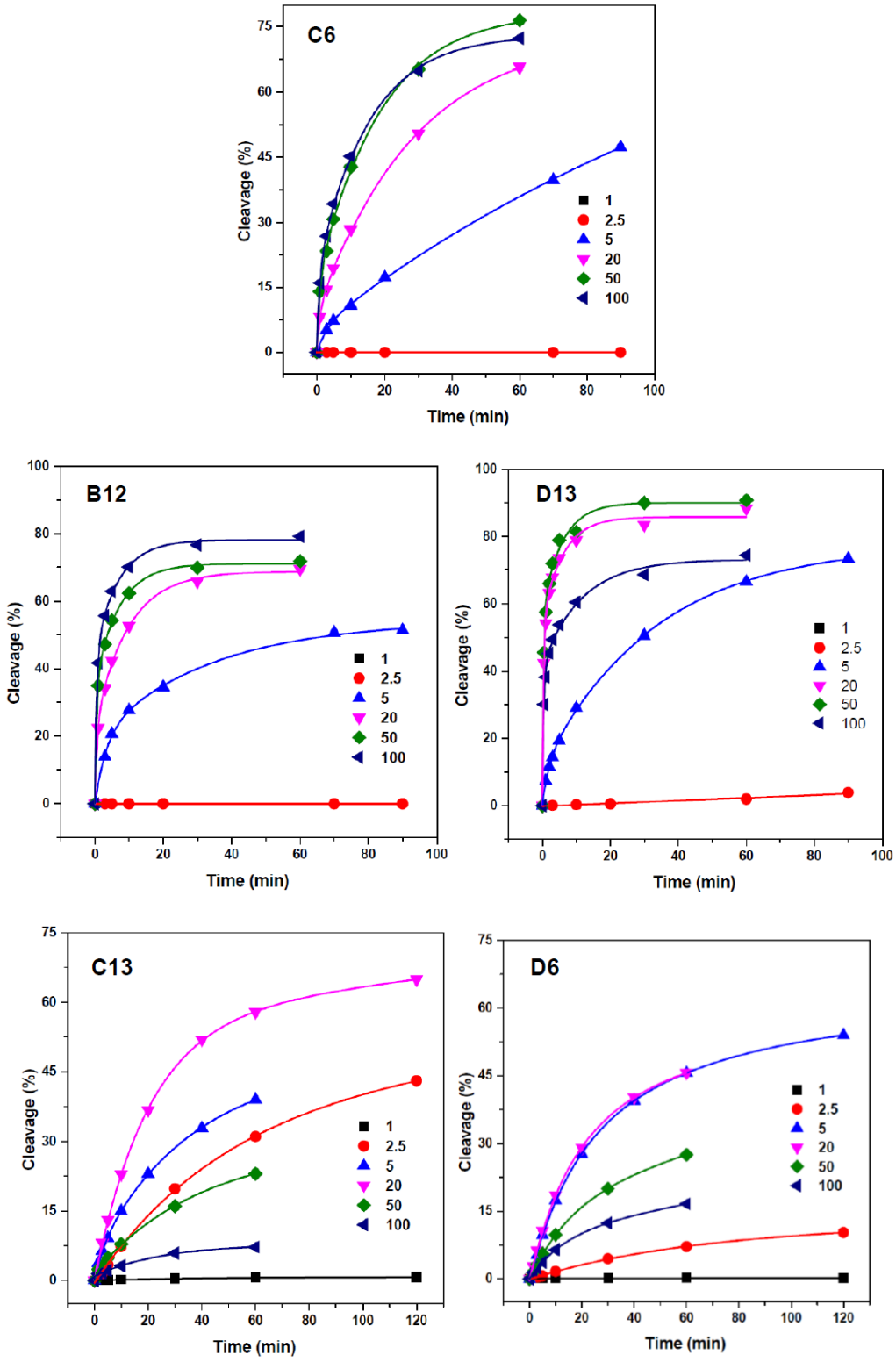

Figure 2.29 Fe(III)-dependent activity of *trans*-cleaving DNAzymes; B12, C6, C13, D6, and D13.

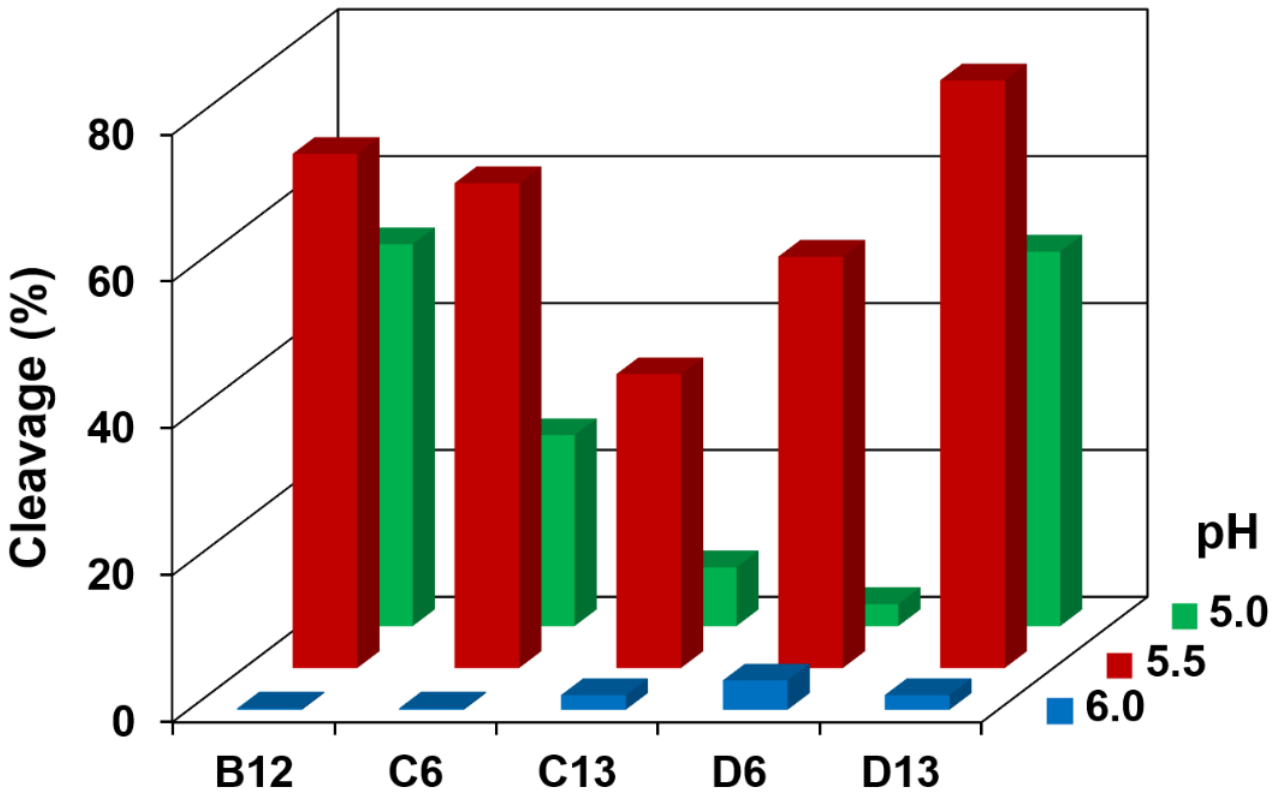

Figure 2.30 Final cleavage activity of B12, C6, C13, D6, and D13 over 1 h with 20 µM Fe(III). 40 mM sodium acetate and 5 mM Bis-Tris were used for pH 5.0 and 5.5. 40 mM Bis-Tris was used for pH 6.0. All buffers contained 200 mM sodium chloride.

2.3.6.2 Effect of pH on DNAzyme Activity

Effect of pH on reactivity of B12, C6, C13, D6, and D13 was tested at pH 5.0, 5.5, and 6.0 under single-turnover condition. As shown in Figure 2.30, cleavage obtained with 20 µM Fe(III) within 1 h influenced significantly by pH. Since Bis-Tris was shown to be a requirement for Fe(III) DNAzymes activity, the pH 6.0 buffer was made from Bis-Tris and no additional ligand was added. All DNAzymes work best at pH 5.5 and minimal cleavage activity was observed at pH 6.0. Additionally, only B12, C6, and D13 are active at pH 5.0, while C13 and D6 are barely active at this pH. Observing similar behavior in the pH dependent activity of B12, C6, and D13 might be due to their high sequence similarity (Figure 2.27). D13 pH dependent activity was investigated in

more detail. When D13 activity was tested at pH 5.75, it was found that the rate of cleavage reaction is decreased by less than 3-fold (2.5 to 1.0 min^{-1}). Further increase in pH from 5.75 to 6.0 resulted in three orders of magnitude reduction in the reaction rate (1.0 to 0.001 min^{-1}).

Significant reduction in the activity observed by 0.25 unit increase in the pH may solely be due to the pH effect or combination of the pH effect and a change in buffer components. To address this issue the activity of D13 was tested in a buffer containing 5 mM Bis-Tris and 40 mM sodium acetate pH 6.0. Interestingly, it was found that D13 requires presence of both Bis-Tris and acetate for optimal activity. The DNAzyme was highly active at pH 5.5 and 6.0 when both acetate and Bis-Tris were present in the activity assay solution. To further investigate dependency of the D13 DNAzyme on Bis-Tris and acetate for its activity, I have tested D13 cleavage activity with 20 µM Fe(III) in the presence of different chemicals which some of them have similar chemical structure or functional group as in acetate or Bis-Tris (Figure 2.31).

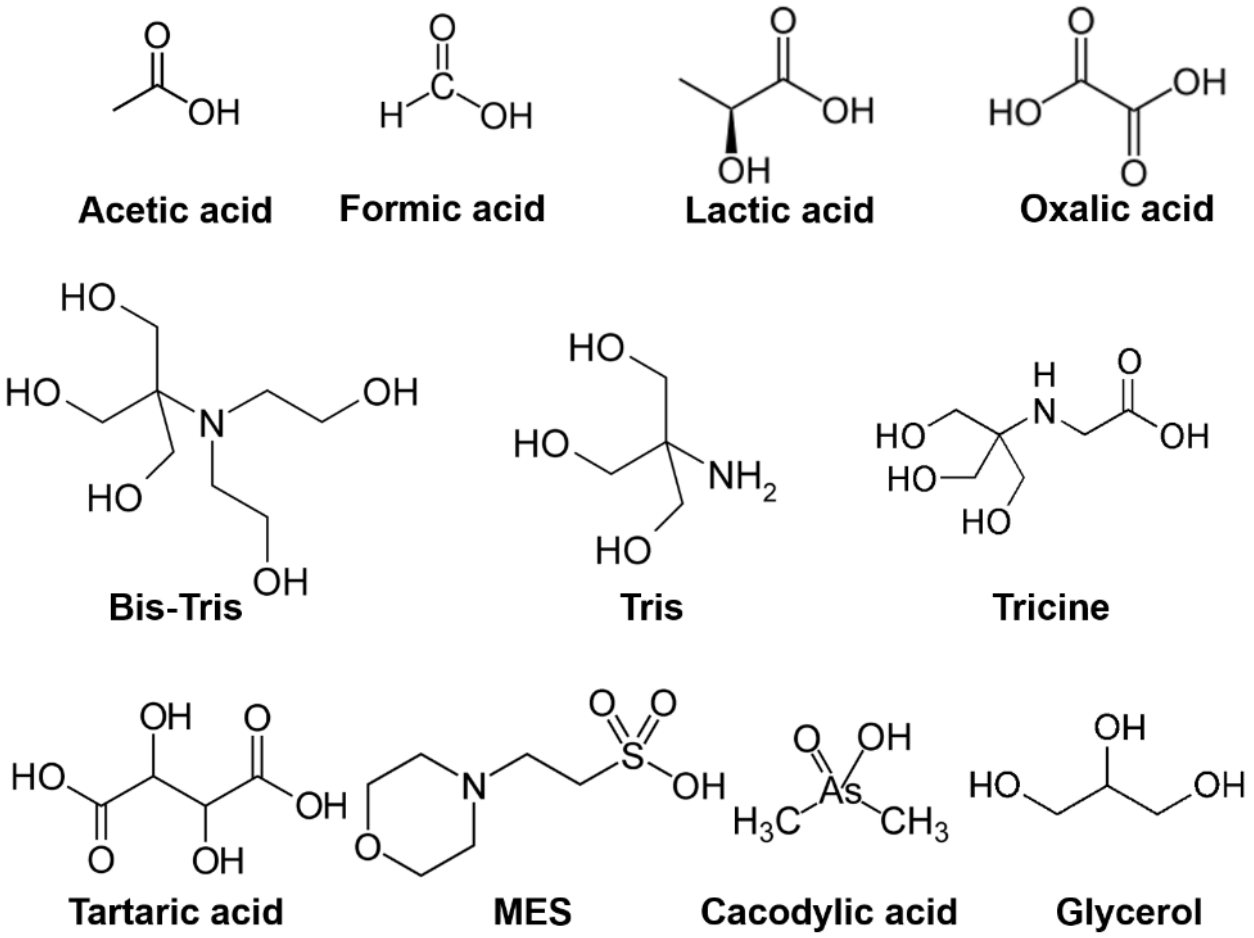

Figure 2.31 Different chemicals used to identify functional groups that required for the activity of D13. Acetic acid (pK_a = 4.8), formic acid (pK_a = 3.8), lactic acid (pK_a = 3.9), oxalic acid (pK_a =1.3 and 4.1), Bis-Tris (pK_a = 6.5), Tris (pK_a = 8.1), Tricine (2.3 and 8.2), tartaric acid (pK_a = 3.2 and 4.9), MES (pK_a = 6.2), cacodylic acid (pK_a = 6.3), and glycerol.

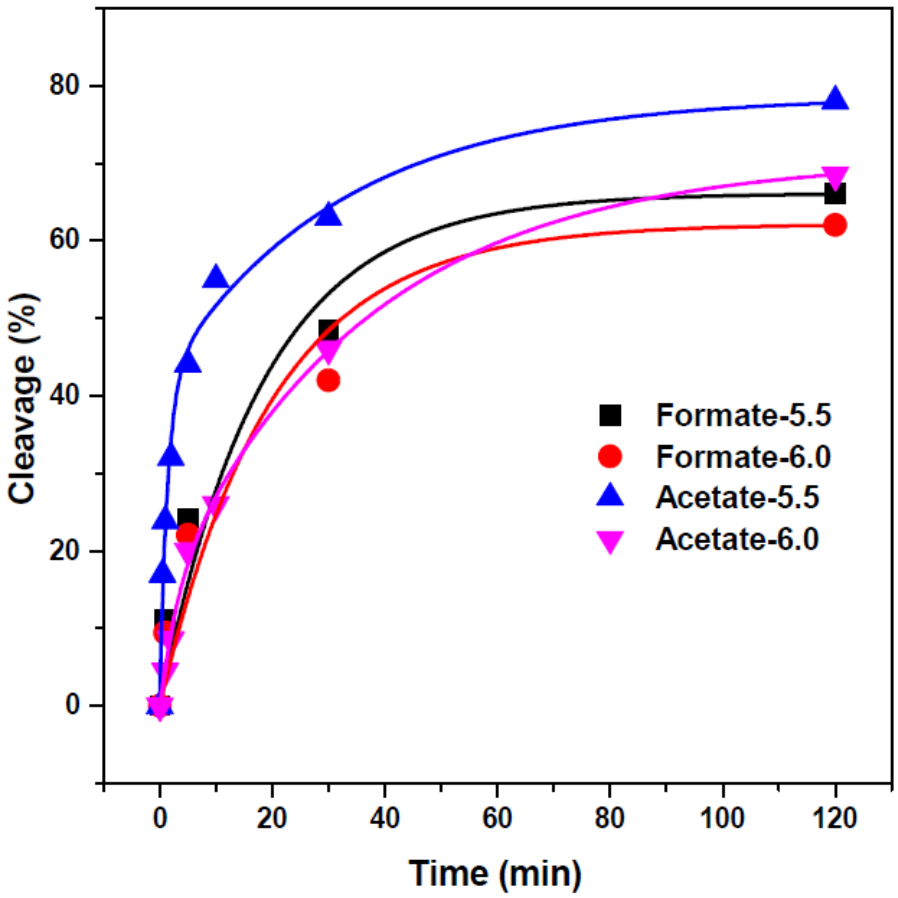

Figure 2.32 D13 DNAzyme activity in the presence of 20 mM acetate or formate at two different pH values (5.5 and 6.0). All reactions contained 5 mM Bis-Tris.

To replace acetate several carboxylic acids was tested including formic acid, lactic acid, oxalic acid, and tartaric acid. Tris and glycerol were examined as they have functional groups similar to Bis-Tris. Activity of the DNAzyme was investigated in the presence of tricine, since this molecule is similar to Bis-Tris in having three hydroxymethyl groups and also like acetate has a carboxylic group. MES and cacodylic acid were used as two other buffers for preparation of the solutions at pH ~ 6. All of the mentioned conditions and buffers are represented in Table 2.8. These results show that except formate, none of other studied carboxylic acids supports D13 cleavage activity. Another condition in which D13 was still active was found to be MES pH 5.5 in the

presence of Bis-Tris (low catalytic activity was observed). Finally, in the presence of only Bis-Tris D13 showed suboptimal activity. Altogether, it was found that optimal condition for activity of D13 is in the presence of Bis-Tris and either of acetate or formate (Figure 2.32).

Table 2.8 Number of different conditions used to test the activity of the D13 DNAzyme.

Condition	pH	D13 cleavage
Acetate	5.0, 5.5, 6.0, and 6.5	Active [a]
Formate	5.5 and 6.0	Active
Lactate	5.5 and 6.0	Inactive
Oxalate	5.5 and 6.0	Inactive
Tartrate	5.5 and 6.0	Inactive
Acetate and Tris [b]	5.5 and 6.0	Inactive
Acetate and glycerol [c]	5.5	Inactive
Tricine [d]	6.0 and 6.5	Inactive
MES	5.5	Active [e]
MES	6.0 and 6.5	Inactive
Cacodylate	5.5, 6.0, and 6.5	Inactive
MOPS [f]	7.0	Inactive
Bis-Tris [g]	5.5 and 6.0	Active
Bis-Tris [g]	6.5	Inactive

Concentration of the buffer component in all cases was 20 mM and their pH adjusted by addition of ultrapure hydrochloric acid or sodium hydroxide before use. All conditions were tested with in the presence of 5 mM Bis-Tris with 20 µM Fe(III) (except in [b] and [c]). [a] At pH 6.5 D13 is still active, however activity was very low (5% cleavage in 2 h). [b,c] In these two condition Tris or glycerol (5 mM) was used instead of Bis-Tris. [d] Tricine was tested with and without Bis-Tris and in both case no activity was observed. [e] low activity was notice in MES in the presence of Bis-Tris (15% cleavage in 2 h). In the absence of Bis-Tris D13 was inactive. [f] MOPS is used to test D13 activity in pH 7.0. When both acetate and Bis-Tris were present in the solution ~ 1% cleavage activity was detected in 2 h. g Activity of D13 was tested in Bis-Tris (no acetate was added). At pH 5.5 DNAzyme was active and at pH 6.0 very low activity was noticed (~ 5% in 2 h). No cleavage activity was observed at pH 6.5.

The effect of pH on the cleavage rate of D13 is shown in Figure 2.33. All buffers contained both acetate and Bis-Tris, required for optimal activity of D13. A bell-shaped pH profile was obtained for D13 with optimal activity at pH 5.5, the pH at which the DNAzyme was originally selected. Either decrease or increase in the pH by 0.5 unit resulted in 10 to 20-fold reduction in the catalytic rate. Although D13 is still active at pH 6.5, no noticeable cleavage activity was observed at pH 7.0. This bell-shape pH behavior with optimal activity at pH of the *in vitro* selection condition has been observed for other DNAzymes (*95*, *96*). Negative effect of increase in pH on the activity of metal dependent DNAzymes such as the leadzyme and uranyl-dependent DNAzyme has been attributed to the poor solubility of the metal cofactor at higher pH values (*96*, *97*). A linear decrease of the activity with increase in pH, at values higher than 5.5, with a slope of ~ −3 may be partly due to the poor solubility of Fe(III) and production of ferric hydroxo species (*98*).

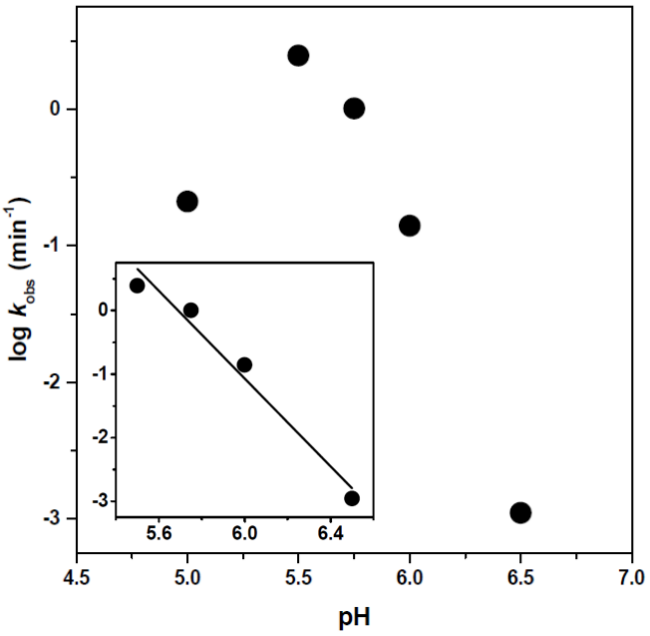

Figure 2.33 Effect of pH on the activity of the D13 DNAzyme. Cleavage rate was obtained with 20 µM Fe(III) in 20 mM sodium acetate and 5 mM Bis-Tris pH 5.0 to 7.0 and 200 mM NaCl. No activity was observed at pH 7.0. Linear portion of the pH profile is shown as an inset. Activity decreased linearly by increase in pH with a slope of −3.4. R-square value for the linear fit is 0.96.

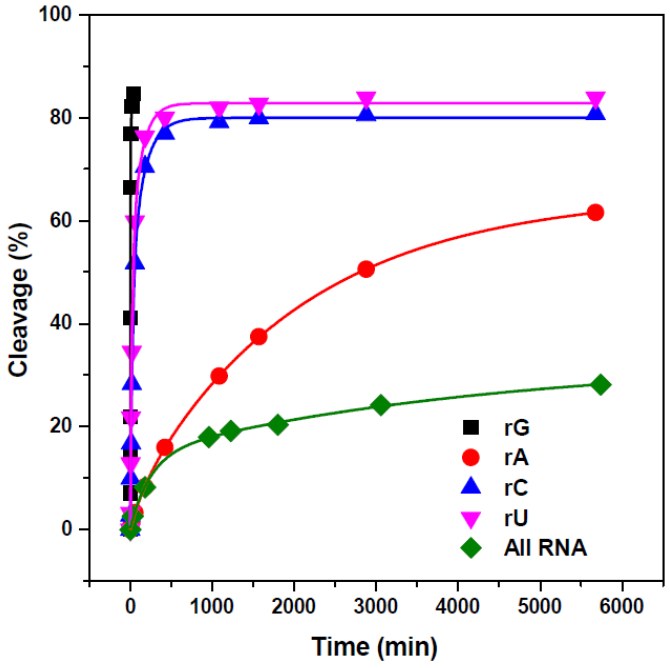

Figure 2.34 Effect of ribonucleotide identity in the cleavage site on rate of the B12 DNAzyme. Cleavage percentage were monitored with 20 µM Fe(III) in 20 mM sodium acetate, 5 mM Bis-Tris pH 5.5 and 200 mM NaCl. Rate of catalysis for rG, rA, rC, rU, and all RNA substrate was calculated to be 1.0, 0.006, 0.04, 0.06, and 0.004 min^{-1}, respectively.

2.3.6.3 Choice of Cleavage Site

In vitro selection-3 was carried out with a random pool containing a single rG as the cleavage site. It was shown that RNA-cleaving DNAzymes prefer certain ribonucleotide at their cleavage site (*91, 99*). Catalytic ability of the B12 DNAzyme was investigated in cleaving substrates with other ribonucleotides in the cleavage site including riboadenosine (rA), ribocytosine (rC), or ribouridine (rU). Cleavage rate of all ^{32}P end labeled substrates were examined under single-turnover condition (Figure 2.34). It was found that B12 was able to cleave all four possible ribonucleotides in the cleavage with higher preference for rG, which was originally used in the selection (rG>>rC>rU>>rA). In addition I assayed catalytic ability of B12 in cleaving all RNA substrate. It was found that cleavage of the all RNA substrate by B12 is two

orders of magnitude slower than the rate of cleaving the chimeric substrate. It is reported that RNA-cleaving DNAzymes that have been selected to cleave RNA/DNA chimeric substrates, can cleave all RNA substrate very inefficiently with catalytic rates ~ 1000-fold slower than the rate of cleaving wild type substrate (*100, 101*).

Table 2.9 List of the mutations examined in the catalytic core of B12.

	3										13										23				Activity
B12E	C	G	T	T	T	G	C	G	G	C	A	C	C	T	A	A	A	C	G	C	T	C	T	T	A	G	5.0
G24.5A [a]	-	-	-	-	-	-	-	-	-	-	-	-	-	-	-	-	-	-	-	-	-	-	-	-	-	A	4.8
G24.5A/T24.2C	-	-	-	-	-	-	-	-	-	-	-	-	-	-	-	-	-	-	-	-	-	-	C	-	-	A	4.8
G24.5A/T24.2A [a]	T	-	-	-	-	-	-	-	-	-	-	-	-	-	-	-	-	-	-	-	-	-	A	-	-	A	3.5
T7,A17Δ	-	-	-	-	X	-	-	-	-	-	-	-	-	X	-	-	-	-	-	-	-	-	C	-	-	A	0.7
T6-7,A17-18Δ	-	-	-	X	X	-	-	-	-	-	-	-	-	X	X	-	-	-	-	-	-	-	C	-	-	A	None
G4,C20Δ	-	X	-	-	-	-	-	-	-	-	-	-	-	-	-	-	-	X	-	-	-	-	C	-	-	A	None
C3,G4,C20,G21Δ	X	X	-	-	-	-	-	-	-	-	-	-	-	-	-	-	-	X	X	-	-	-	C	-	-	A	None
G4,T5,A9,C20Δ	-	X	X	-	-	-	-	-	-	-	-	-	-	-	-	-	X	X	-	-	-	-	C	-	-	A	None
Stem-scramble	G	T	A	A	C	-	-	-	-	-	-	-	-	-	G	T	T	A	C	-	-	-	C	-	-	A	0.6
Split (G-T16Δ)	-	-	-	-	-	3′							5′	-	-	-	-	-	-	-	-	-	C	-	-	A	None
Loop-scramble-1	-	-	-	-	-	A	G	C	C	G	C	G	T	C	-	-	-	-	-	-	-	-	C	-	-	A	None
G-G10Δ	-	-	-	-	-	X	X	X	-	-	-	-	-	-	-	-	-	-	-	-	-	-	C	-	-	A	2.1
G11-A13Δ	-	-	-	-	-	-	-	-	X	X	X	-	-	-	-	-	-	-	-	-	-	-	C	-	-	A	2.2
C14-T16Δ	-	-	-	-	-	-	-	-	-	-	-	X	X	X	-	-	-	-	-	-	-	-	C	-	-	A	2
C22A	-	-	-	-	-	-	-	-	-	-	-	-	-	-	-	-	-	-	-	A	-	-	C	-	-	A	Very low [b]
T23G	-	-	-	-	-	-	-	-	-	-	-	-	-	-	-	-	-	-	-	-	G	-	C	-	-	A	Very low [b]
T23C	-	-	-	-	-	-	-	-	-	-	-	-	-	-	-	-	-	-	-	-	C	-	C	-	-	A	None
C22G,T23A	-	-	-	-	-	-	-	-	-	-	-	-	-	-	-	-	-	-	G	A	-	-	C	-	-	A	None
T23Δ	-	-	-	-	-	-	-	-	-	-	-	-	-	-	-	-	-	-	-	-	X	-	C	-	-	A	None
C22Δ	-	-	-	-	-	-	-	-	-	-	-	-	-	-	-	-	-	-	-	X	-	-	C	-	-	A	None
Scramble	T	T	A	C	G	A	G	C	C	G	G	T	C	C	C	G	T	A	A	-	-	-	C	-	-	A	None
C14-A17Δ	-	-	-	-	-	-	-	-	-	-	-	X	X	X	X	-	-	-	-	-	-	-	C	-	-	A	Very low [b]
C3A	A	-	-	-	-	-	-	-	-	-	-	-	-	-	-	-	-	-	-	-	-	-	C	-	-	A	Very low [b]
C3-G10Δ	X	X	X	X	X	X	X	X	-	-	-	-	-	-	-	-	-	-	-	-	-	-	C	-	-	A	None
D13 Catalytic core-1	G	C	C	A	T	T	T	A	C	G	G	A	A	C	C	A	A	T	G	C	T	-	C	-	-	A	Very low [b]
D13 Catalytic core-2	C	C	A	T	T	T	A	C	G	G	A	A	C	C	A	A	T	G	C	C	T	-	C	-	-	A	Very low [b]
Loop-scramble-2	-	-	-	-	-	A	T	T	-	T	-	T	-	A	-	-	-	-	-	-	-	-	C	-	-	A	Very low [b]

Dark shaded area indicates a region of five nucleotides from 3′ end of the DNAzyme that forms a pairing region with the substrate. [a] Except these two mutants, all other mutants contain G24.5A/T24.2C mutation which form a complete pairing region. This mutation is as active as the wild type B12. [b] Very low activity indicates mutants which had less than 15% cleavage activity in ~ 100 hour .

2.3.6.4 Mutational Analysis of the B12 DNAzyme

To further investigate sequence requirements for catalytic activity of the Fe(III)-dependent DNAzyme, I designed mutated *trans*-cleaving DNAzymes based on the B12 sequence (Table 2.9). These mutational studies included a number of single point mutations, deletions, and multiple mutations (or shuffling). B12 belongs to cluster I (Figure 2.22), the most populated cluster identified from SSN of all isolated sequences. All members of this cluster share an identical catalytic core and cannot be used for mutational studies. As shown in Figure 2.27, the rG cleavage site is placed in an internal loop in the secondary structure of B12, predicted by UNAFold (*94*). To explore if formation of the internal loop is required for the activity of the DNAzyme, few mutations were introduced in the B12 DNAzyme strand to remove the internal loop by forming a complete pairing region. G24.5A/T24.2C mutant that forms a Watson-Crick base pairing with the rG cleavage site is as active as the wild type B12. Therefore, the B12 DNAzyme can cleave the substrate even if rG is predicted to be in the double stranded region. Further mutations in the catalytic core of B12 resulted in significant reduction in the activity of the DNAzyme (at least three orders of magnitude). As represented in Table 2.9, B12 is intolerable to mutations in the catalytic core. This intolerance indicates that catalytic core of the B12 DNAzyme is highly conserved.

2.3.7 Fe(II) Interference

To investigate the selectivity of the B12 DNAzyme in sensing Fe(III) as a cofactor and distinguishing Fe(III) from Fe(II), I tested Fe(III)-dependent cleavage activity of B12 in a mixture containing both Fe(III) and Fe(II). No cleavage activity was observed at pH 6.0 when B12 incubated with 100 μM Fe(II). In addition, no significant change observed in the Fe(III)-dependent activity of B12 when Fe(II) was also present in the solution. Therefore, no interference was

observed from the presence of 100 µM Fe(II) in the activity of B12 with 20 µM Fe(III) (Figure 2.35) Similarly, it was found that Fe(II) does not interfere with the Fe(III)-dependent activity of D13. These results, suggest that the B12 and D13 DNAzymes can distinguish two different oxidation states of iron, are selective for Fe(III) over Fe(II), and detect Fe(III) in a mixture of both oxidation states with minimal interference from Fe(II).

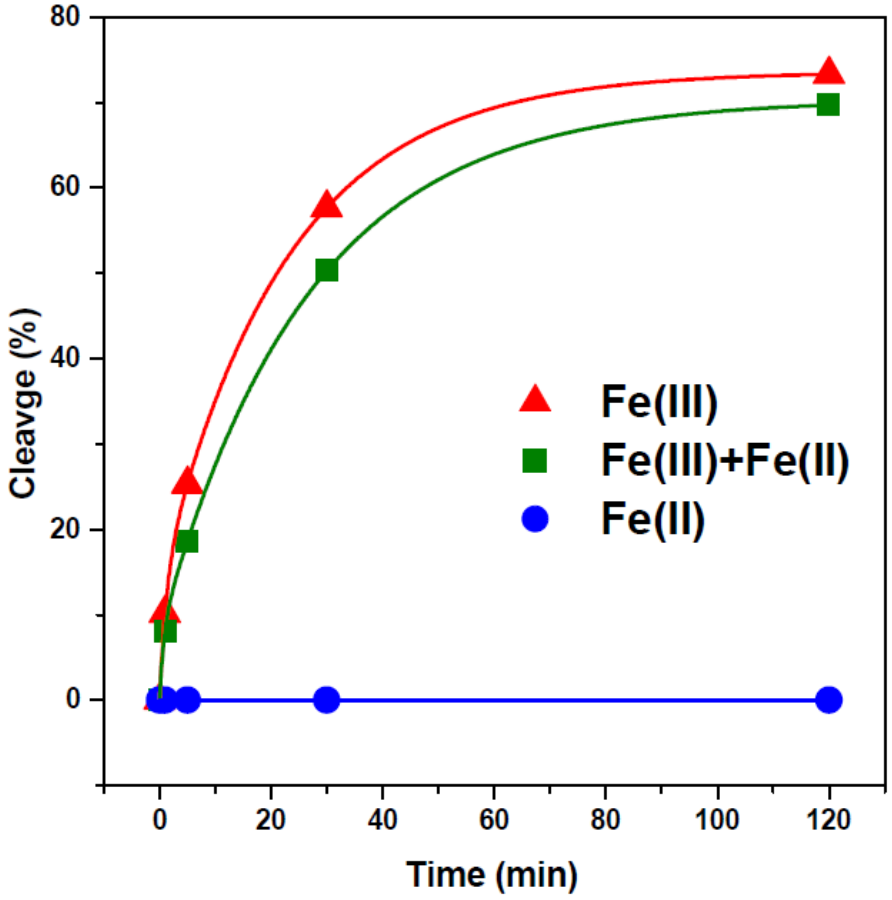

Figure 2.35 Activity of B12 DNAzyme in the presence of Fe(II). Cleavage reaction monitored with 20 µM Fe(III) in 20 mM acetate buffer pH 6.0, 5 mM Bis-Tris and 200 mM NaCl in the presence or absence of 100 µM Fe(II). No cleavage activity was noticed with 100 µM Fe(II) (blue circles).

Catalytic activity of the B12 and D13 DNAzymes were tested in the presence of 10% human cell lysate or 50 µM citrate at pH 6.0. It was found that human cell lysate or 50 µM citrate inhibited the activity of B12 and D13. Addition of more Fe(III) to the solution was shown to restore the cleavage activity. Previously, it was shown that citrate has inhibitory effect on the activity of metal dependent DNAzymes such as uranyl DNAzyme (*96*). Therefore, in the presence of strong chelators more of the metal ion cofactor is required to see the cleavage activity.

2.4 Conclusions

Several *in vitro* selection conditions were carried out to isolate Fe(III)-dependent RNA-cleaving DNAzymes. Different strategies such as column-based and gel-based selection were performed. It was found that negative selection should be incorporated into the selection protocol, at least in the first few rounds, to prevent evolution of the nonspecific cleavage activity. Selection attempts at pH 7.0 using different Fe(III) stabilizing agents including citrate and Bis-Tris did not succeed in isolation of Fe(III)-dependent DNAzymes. On the other hand, *in vitro* selections carried out at pH 5.5 in the presence of 5 mM Bis-Tris as a weak Fe(III) stabilizing agent resulted in several active DNAzymes. Activity assay experiments showed that observed cleavage activity was caused by Fe(III) and none of the other tested metal ions resulted in a noticeable cleavage.

157 sequences were obtained from active pools, and grouped into ten major clusters based on their sequence similarity. Screening experiments were used to identify the most active clones for further analysis. Although B12, one of the most active clones, belongs to the most populated cluster, interestingly two other active clones (D13 and C6) were not clustered with other sequences. It was found that B12, C6, D13 belong to the same structural class and all have a short catalytic region (~ 25 nucleotides). Truncation attempts were performed based on the design of the initial random pool and the secondary structures predicted by UNAFold to convert active *cis*-cleaving DNAzymes into a *trans*-cleaving version for biosensor applications.

Interestingly, Fe(III) DNAzymes required presence of Bis-Tris and either acetate or formate for optimal activity. The D13 DNAzyme was observed to have a bell-shaped pH profile in a pH range from 5.0 to 6.5 while no activity was observed at pH 7.0. It was found that all ribonucleotides can be used in the cleavage site, although rG, which was present originally in the design of the random pool, is preferred over the other ribonucleotides. Cleavage of all RNA

substrate with the B12 DNAzymes was found to be two orders of magnitude slower than the DNA/RNA chimeric substrate. No significant interference was found when Fe(III)-dependent cleavage activity was tested in the presence of 100 μM Fe(II). Our results show that the D13 Fe(III)-dependent DNAzyme potentially can be used for designing a DNAzyme-based sensor for Fe(III) with biological applications. We are in the process of designing a fluorescent sensor for Fe(III) based on this DNAzyme. Our goal is to utilize a DNAzyme based fluorescent sensor to image Fe(III) inside living cells. In mammalian cells Fe(III) uptake is through endocytic pathway in which Fe(III) is released in acidic (pH ~5) environment of endosomes. Our hypothesis is that a sensor deigned based on the Fe(III)-dependent DNAzyme can operate as a probe to image the release of Fe(III) in the late endosome.

2.5 References

1. Guerrier-Takada, C., Gardiner, K., Marsh, T., Pace, N., and Altman, S. (1983) The RNA moiety of ribonuclease P is the catalytic subunit of the enzyme, *Cell 35*, 849-857.

2. Crick, F. (1970) Central dogma of molecular biology, *Nature 227*, 561-563.

3. Paul, N., Springsteen, G., and Joyce, G. F. (2006) Conversion of a ribozyme to a deoxyribozyme through in vitro evolution, *Chem Biol 13*, 329-338.

4. Breaker, R. R., and Joyce, G. F. (1994) A DNA enzyme that cleaves RNA, *Chem Biol 1*, 223-229.

5. Silverman, S. K. (2010) DNA as a versatile chemical component for catalysis, encoding, and stereocontrol, *Angew Chem Int Ed Engl 49*, 7180-7201.

6. Liu, J., Cao, Z., and Lu, Y. (2009) Functional nucleic acid sensors, *Chemical Reviews 109*, 1948-1998.

7. Elbaz, J., Lioubashevski, O., Wang, F., Remacle, F., Levine, R. D., and Willner, I. (2010) DNA computing circuits using libraries of DNAzyme subunits, *Nat Nanotechnol 5*, 417-422.

8. Wang, F., Lu, C. H., and Willner, I. (2014) From cascaded catalytic nucleic acids to enzyme-DNA nanostructures: controlling reactivity, sensing, logic operations, and assembly of complex structures, *Chem Rev 114*, 2881-2941.

9. Geyer, C. R., and Sen, D. (1997) Evidence for the metal-cofactor independence of an RNA phosphodiester-cleaving DNA enzyme, *Chemistry & biology 4*, 579-593.

10. Carrigan, M. A., Ricardo, A., Ang, D. N., and Benner, S. A. (2004) Quantitative Analysis of a RNA-Cleaving DNA Catalyst Obtained via in Vitro Selection†, *Biochemistry 43*, 11446-11459.

11. Aguirre, S. D., Ali, M. M., Kanda, P., and Li, Y. (2012) Detection of bacteria using fluorogenic DNAzymes, *J Vis Exp*.

12. Ali, M. M., Aguirre, S. D., Lazim, H., and Li, Y. (2011) Fluorogenic DNAzyme probes as bacterial indicators, *Angew Chem Int Ed Engl 50*, 3751-3754.

13. Hollenstein, M., Hipolito, C. J., Lam, C. H., and Perrin, D. M. (2009) A self-cleaving DNA enzyme modified with amines, guanidines and imidazoles operates independently of divalent metal cations (M2+), *Nucleic acids research 37*, 1638-1649.

14. Hollenstein, M., Hipolito, C. J., Lam, C. H., and Perrin, D. M. (2009) A DNAzyme with Three Protein-Like Functional Groups: Enhancing Catalytic Efficiency of M2+-Independent RNA Cleavage, *Chembiochem : a European journal of chemical biology 10*, 1988-1992.

15. Hollenstein, M., Hipolito, C. J., Lam, C. H., and Perrin, D. M. (2009) A self-cleaving DNA enzyme modified with amines, guanidines and imidazoles operates independently of divalent metal cations (M2+), *Nucleic acids research 37*, 1638-1649.

16. Hollenstein, M., Hipolito, C. J., Lam, C. H., and Perrin, D. M. (2013) Toward the combinatorial selection of chemically modified DNAzyme RNase A mimics active against all-RNA substrates, *ACS combinatorial science 15*, 174-182.

17. Liu, J., Brown, A. K., Meng, X., Cropek, D. M., Istok, J. D., Watson, D. B., and Lu, Y. (2007) A catalytic beacon sensor for uranium with parts-per-trillion sensitivity and millionfold selectivity, *Proceedings of the National Academy of Sciences of the United States of America 104*, 2056-2061.

18. Hollenstein, M., Hipolito, C., Lam, C., Dietrich, D., and Perrin, D. M. (2008) A Highly Selective DNAzyme Sensor for Mercuric Ions, *Angewandte Chemie International Edition 47*, 4346-4350.

19. Huang, P. J., Vazin, M., and Liu, J. (2014) In Vitro Selection of a New Lanthanide-Dependent DNAzyme for Ratiometric Sensing Lanthanides, *Anal Chem 86*, 9993-9999.

20. Huang, P. J., Lin, J., Cao, J., Vazin, M., and Liu, J. (2014) Ultrasensitive DNAzyme beacon for lanthanides and metal speciation, *Anal Chem 86*, 1816-1821.

21. Bruesehoff, P. J., Li, J., Augustine, A. J., 3rd, and Lu, Y. (2002) Improving metal ion specificity during in vitro selection of catalytic DNA, *Combinatorial chemistry & high throughput screening 5*, 327-335.

22. Hentze, M. W., Muckenthaler, M. U., and Andrews, N. C. (2004) Balancing acts: molecular control of mammalian iron metabolism, *Cell 117*, 285-297.

23. Yu, Y., Gutierrez, E., Kovacevic, Z., Saletta, F., Obeidy, P., Suryo Rahmanto, Y., and Richardson, D. R. (2012) Iron chelators for the treatment of cancer, *Curr Med Chem 19*, 2689-2702.

24. Wong, C., and Richardson, D. R. (2003) Beta-thalassaemia: emergence of new and improved iron chelators for treatment, *Int J Biochem Cell Biol 35*, 1144-1149.

25. Alper, G., and Narayanan, V. (2003) Friedreich's ataxia, *Pediatr Neurol 28*, 335-341.

26. Siddique, A., and Kowdley, K. V. (2012) Review article: the iron overload syndromes, *Aliment Pharmacol Ther 35*, 876-893.

27. Kalinowski, D. S., and Richardson, D. R. (2005) The evolution of iron chelators for the treatment of iron overload disease and cancer, *Pharmacol Rev 57*, 547-583.

28. Stadler, N., Lindner, R. A., and Davies, M. J. (2004) Direct detection and quantification of transition metal ions in human atherosclerotic plaques: evidence for the presence of elevated levels of iron and copper, *Arterioscler Thromb Vasc Biol 24*, 949-954.

29. Cerchiaro, G., Manieri, T. M., and Bertuchi, F. R. (2013) Analytical methods for copper, zinc and iron quantification in mammalian cells, *Metallomics 5*, 1336-1345.

30. M-M, P., Weiskirchen, R., Gassler, N., Bosserhoff, A. K., and Becker, J. S. (2013) Novel bioimaging techniques of metals by laser ablation inductively coupled plasma mass spectrometry for diagnosis of fibrotic and cirrhotic liver disorders, *PLoS One 8*, e58702.

31. Moore, K. L., Lombi, E., Zhao, F. J., and Grovenor, C. R. (2012) Elemental imaging at the nanoscale: NanoSIMS and complementary techniques for element localisation in plants, *Anal Bioanal Chem 402*, 3263-3273.

32. Spolaor, A., Vallelonga, P., Gabrieli, J., Cozzi, G., Boutron, C., and Barbante, C. (2012) Determination of Fe2+ and Fe3+ species by FIA-CRC-ICP-MS in Antarctic ice samples, *Journal of Analytical Atomic Spectrometry 27*, 310-317.

33. Carter, K. P., Young, A. M., and Palmer, A. E. (2014) Fluorescent sensors for measuring metal ions in living systems, *Chem Rev 114*, 4564-4601.

34. Domaille, D. W., Que, E. L., and Chang, C. J. (2008) Synthetic fluorescent sensors for studying the cell biology of metals, *Nat Chem Biol 4*, 168-175.

35. Tenopoulou, M., Kurz, T., Doulias, P. T., Galaris, D., and Brunk, U. T. (2007) Does the calcein-AM method assay the total cellular 'labile iron pool' or only a fraction of it?, *Biochem J 403*, 261-266.

36. Chereddy, N. R., Suman, K., Korrapati, P. S., Thennarasu, S., and Mandal, A. B. (2012) Design and synthesis of rhodamine based chemosensors for the detection of Fe3+ ions, *Dyes and Pigments 95*, 606-613.

37. OuYang, H., Gao, Y., and Yuan, Y. (2013) A highly selective rhodamine-based optical–electrochemical multichannel chemosensor for Fe3+, *Tetrahedron Letters 54*, 2964-2966.

38. Chen, W. D., Gong, W. T., Ye, Z. Q., Lin, Y., and Ning, G. L. (2013) FRET-based ratiometric fluorescent probes for selective Fe3+ sensing and their applications in mitochondria, *Dalton Trans 42*, 10093-10096.

39. Vallejos, S., Munoz, A., Ibeas, S., Serna, F., Garcia, F. C., and Garcia, J. M. (2013) Solid sensory polymer substrates for the quantification of iron in blood, wine and water by a scalable RGB technique, *Journal of Materials Chemistry A 1*, 15435-15441.

40. Kas'ianenko, N. A., Plotnikova, L. V., Zanina, A. V., Anderzhanov, A., and Defrenne, S. (2002) [Complexes of DNA with trivalent metal ions in presence of manganese ions], *Biofizika 47*, 433-437.

41. Bertoncini, C., Meneghini, R., Cruz, D. Z., Martins Alves, M. C., and Tolentino, H. (1999) Studies of Fe(II) and Fe(III)-DNA complexes by XANES spectroscopy, *J Synchrotron Radiat 6*, 417-418.

42. Trotta, A., Barbieri Paulsen, A., Silvestri, A., Ruisi, G., Assunta Girasolo, M., and Barbieri, R. (2002) The dynamics of (57)Fe nuclei in Fe(III)-DNA condensates, *J Inorg Biochem 88*, 14-18.

43. Larson, R. A., Lloyd, R. E., Marley, K. A., and Tuveson, R. W. (1992) Ferric-ion-photosensitized damage to DNA by hydroxyl and non-hydroxyl radical mechanisms, *J Photochem Photobiol B 14*, 345-357.

44. Park, Y., Noh, H. A., and Cho, H. (2012) Effect of low-energy electron irradiation on DNA damage by Fe3+ ion, *Radiat Res 177*, 775-780.

45. Stohs, S. J., and Bagchi, D. (1995) Oxidative mechanisms in the toxicity of metal ions, *Free Radic Biol Med 18*, 321-336.

46. Chao, C. C., and Aust, A. E. (1993) Photochemical reduction of ferric iron by chelators results in DNA strand breaks, *Arch Biochem Biophys 300*, 544-550.

47. Knobel, Y., Weise, A., Glei, M., Sendt, W., Claussen, U., and Pool-Zobel, B. L. (2007) Ferric iron is genotoxic in non-transformed and preneoplastic human colon cells, *Food Chem Toxicol 45*, 804-811.

48. Draper, D. E. (2004) A guide to ions and RNA structure, *RNA 10*, 335-343.

49. Shamsi, M., and Kraatz, H.-B. (2013) Interactions of Metal Ions with DNA and Some Applications, *J Inorg Organomet Polym 23*, 4-23.

50. Santoro, S. W., Joyce, G. F., Sakthivel, K., Gramatikova, S., and Barbas, C. F., 3rd. (2000) RNA cleavage by a DNA enzyme with extended chemical functionality, *J Am Chem Soc 122*, 2433-2439.

51. Santoro, S. W., and Joyce, G. F. (1997) A general purpose RNA-cleaving DNA enzyme, *Proceedings of the National Academy of Sciences of the United States of America 94*, 4262-4266.

52. Carmi, N., Balkhi, S. R., and Breaker, R. R. (1998) Cleaving DNA with DNA, *Proceedings of the National Academy of Sciences of the United States of America 95*, 2233-2237.

53. Millero, F. J. (1998) Solubility of Fe(III) in seawater, *Earth and Planetary Science Letters 154*, 323-329.

54. Meighan, M., MacNeil, J., and Falconer, R. (2008) Determining the Solubility Product of Fe(OH)3: An Equilibrium Study with Environmental Significance, *Journal of Chemical Education 85*, 254.

55. Liu, X., and Millero, F. J. (1999) The solubility of iron hydroxide in sodium chloride solutions, *Geochimica et Cosmochimica Acta 63*, 3487-3497.

56. Kurz, T., Terman, A., Gustafsson, B., and Brunk, U. T. (2008) Lysosomes in iron metabolism, ageing and apoptosis, *Histochem Cell Biol 129*, 389-406.

57. Nelson, K. E. (2005) In vitro selection and metal selectivity of transition metal dependent DNAzymes, In *Biochemistry*, University of Illinois at Urbana-Champaign, Urbana-Champaign.

58. Ihms, H. E. (2012) The In Vitro Selection and Biochemical Characterization of MetalloDNAzymes, In *Chemistry*, University of Illinois at Urbana-Champaign, Urbana-Champaign.

59. Wen, Y. H., Zhang, H. M., Qian, P., Zhou, H. T., Zhao, P., Yi, B. L., and Yang, Y. S. (2006) Studies on Iron ($Fe3+/Fe2+$) -Complex/Bromine ($Br2/Br-$) Redox Flow Cell in Sodium Acetate Solution, *Journal of The Electrochemical Society 153*, A929-A934.

60. Vukosav, P., Mlakar, M., and Tomisic, V. (2012) Revision of iron(III)-citrate speciation in aqueous solution. Voltammetric and spectrophotometric studies, *Anal Chim Acta 745*, 85-91.

61. Gorman, J. E., and Clydesdale, F. M. (1984) Thermodynamic and Kinetic Stability Constants of Selected Carboxylic Acids and Iron, *Journal of Food Science 49*, 500-503.

62. Lajunen, L. H. J., Portanova, R., Piispanen, J., and Tolazzi, M. (1997) Critical evaluation of stability constants for alpha-hydroxycarboxylic acid complexes with protons and metal ions and the accompanying enthalpy changesPart I: Aromatic ortho-hydroxycarboxylic acids (Technical Report), *Pure and Applied Chemistry 69*, 329-382.

63. Berthon, G. (1995) Critical evaluation of the stability constants of metal complexes of amino acids with polar side chains (Technical Report), *Pure and Applied Chemistry 67*, 1117-1240.

64. Gaithersburg, M. D. (2004) NIST critically selected stability constants.

65. Sjöberg, S. (1997) Critical evaluation of stability constants of metal-imidazole and metal-histamine systems (Technical Report), *Pure and Applied Chemistry 69*, 1549-1570.

66. Yamauchi, O., and Odani, A. (1996) Stability constants of metal complexes of amino acids with charged side chains - Part I: Positively charged side chains (Technical Report), *Pure and Applied Chemistry 68*, 469-496.

67. Pettit, L. D. (1984) Critical survey of formation constants of complexes of histidine, phenylalanine, tyrosine, L-DOPA and tryptophan, *Pure and Applied Chemistry 56*, 247-292.

68. Portanova, P., Lajunen, L. H. J., Tolazzi, M., and Piispanen, J. (2003) Critical evaluation of stability constants for alpha-hydroxycarboxylic acid complexes with protons and metal ions and the accompanying enthalpy changes. Part II. Aliphatic 2-hydroxycarboxylic acids (IUPAC Technical Report), *Pure and Applied Chemistry 75*, 495-540.

69. Netto, L. E., Ferreira, A. M., and Augusto, O. (1991) Iron(III) binding in DNA solutions: complex formation and catalytic activity in the oxidation of hydrazine derivatives, *Chem Biol Interact 79*, 1-14.

70. Richter, Y., and Fischer, B. (2003) Characterization and elucidation of coordination requirements of adenine nucleotides complexes with Fe(II) ions, *Nucleosides Nucleotides Nucleic Acids 22*, 1757-1780.

71. Miller, D. M., Spear, N. H., and Aust, S. D. (1992) Effects of deferrioxamine on iron-catalyzed lipid peroxidation, *Arch Biochem Biophys 295*, 240-246.

72. Smith, R. M., Martell, A. E., and Chen, Y. (1991) Critical evaluation of stability constants for nucleotide complexes with protons and metal ions and the accompanying enthalpy changes, *Pure and Applied Chemistry 63*, 1015-1080.

73. Sovago, I., Kiss, T., and Gergely, A. (1993) Critical survey of the stability constants of complexes of aliphatic amino acids (Technical Report), *Pure and Applied Chemistry 65*, 1029-1080.

74. Anderegg, G., Arnaud-Neu, F., Delgado, R., Felcman, J., and Popov, K. (2005) Critical evaluation of stability constants of metal complexes of complexones for biomedical and environmental applications* (IUPAC Technical Report), *Pure and Applied Chemistry 77*, 1445-1495.

75. Popov, K., Rönkkömäki, H., and Lajunen, L. H. J. (2001) Critical evaluation of stability constants of phosphonic acids (IUPAC Technical Report), *Pure and Applied Chemistry 73*, 1641-1677.

76. (2007) Trilon® D Liquid - the Performance Chemicals division.

77. Perron, N. R., Wang, H. C., Deguire, S. N., Jenkins, M., Lawson, M., and Brumaghim, J. L. (2010) Kinetics of iron oxidation upon polyphenol binding, *Dalton Trans 39*, 9982-9987.

78. Silva, A. M., Kong, X., Parkin, M. C., Cammack, R., and Hider, R. C. (2009) Iron(III) citrate speciation in aqueous solution, *Dalton Trans*, 8616-8625.

79. Breaker, R. R., and Joyce, G. F. (1995) A DNA enzyme with Mg(2+)-dependent RNA phosphoesterase activity, *Chem Biol 2*, 655-660.

80. Silverman, S. K. (2005) In vitro selection, characterization, and application of deoxyribozymes that cleave RNA, *Nucleic Acids Res 33*, 6151-6163.

81. Nakano, M., Moody, E. M., Liang, J., and Bevilacqua, P. C. (2002) Selection for thermodynamically stable DNA tetraloops using temperature gradient gel electrophoresis reveals four motifs: d(cGNNAg), d(cGNABg),d(cCNNGg), and d(gCNNGc), *Biochemistry 41*, 14281-14292.

82. Boughammoura, S., and M'halla, J. (2012) Uranyl-citrate Speciation Diagram in Aqueous Solutions, *International Journal of Nuclear Energy Science and Engineering* 11-22.

83. Lenhart, J. J., Cabaniss, S. E., MacCarthy, P., and Honeyman, B. D. (2000) Uranium(VI) complexation with citric, humic and fulvic acids, *Radiochimica Acta 88*, 345-354.

84. Van Horn, J. D., and Huang, H. (2006) Uranium(VI) bio-coordination chemistry from biochemical, solution and protein structural data, *Coordination Chemistry Reviews 250*, 765-775.

85. Hamada, Y. Z., Carlson, B. L., and Shank, J. T. (2003) Potentiometric and UV–Vis Spectroscopy Studies of Citrate with the Hexaquo Fe3 + and Cr3 + Metal Ions, *Synthesis and Reactivity in Inorganic and Metal-Organic Chemistry 33*, 1425-1440.

86. Babkina, S. S., and Ulakhovich, N. A. (2005) Complexing of heavy metals with DNA and new bioaffinity method of their determination based on amperometric DNA-based biosensor, *Anal Chem 77*, 5678-5685.

87. Ouameur, A. A., Arakawa, H., Ahmad, R., Naoui, M., and Tajmir-Riahi, H. A. (2005) A Comparative study of Fe(II) and Fe(III) interactions with DNA duplex: major and minor grooves bindings, *DNA Cell Biol 24*, 394-401.

88. Hwang, D. S., Zeng, H., Masic, A., Harrington, M. J., Israelachvili, J. N., and Waite, J. H. (2010) Protein- and metal-dependent interactions of a prominent protein in mussel adhesive plaques, *J Biol Chem 285*, 25850-25858.

89. Zeng, H., Hwang, D. S., Israelachvili, J. N., and Waite, J. H. (2010) Strong reversible Fe3+-mediated bridging between dopa-containing protein films in water, *Proc Natl Acad Sci U S A 107*, 12850-12853.

90. Taylor, S. W., Chase, D. B., Emptage, M. H., Nelson, M. J., and Waite, J. H. (1996) Ferric Ion Complexes of a DOPA-Containing Adhesive Protein from Mytilus edulis, *Inorganic Chemistry 35*, 7572-7577.

91. Schlosser, K., Gu, J., Sule, L., and Li, Y. (2008) Sequence-function relationships provide new insight into the cleavage site selectivity of the 8-17 RNA-cleaving deoxyribozyme, *Nucleic Acids Res 36*, 1472-1481.

92. Atkinson, H. J., Morris, J. H., Ferrin, T. E., and Babbitt, P. C. (2009) Using sequence similarity networks for visualization of relationships across diverse protein superfamilies, *PLoS One 4*, e4345.

93. Apeltsin, L., Morris, J. H., Babbitt, P. C., and Ferrin, T. E. (2011) Improving the quality of protein similarity network clustering algorithms using the network edge weight distribution, *Bioinformatics 27*, 326-333.

94. Markham, N. R., and Zuker, M. (2008) UNAFold: software for nucleic acid folding and hybridization, *Methods in molecular biology 453*, 3-31.

95. Liu, Z., Mei, S. H., Brennan, J. D., and Li, Y. (2003) Assemblage of signaling DNA enzymes with intriguing metal-ion specificities and pH dependences, *J Am Chem Soc 125*, 7539-7545.

96. Brown, A. K., Liu, J., He, Y., and Lu, Y. (2009) Biochemical characterization of a uranyl ion-specific DNAzyme, *Chembiochem 10*, 486-492.

97. Pan, T., Dichtl, B., and Uhlenbeck, O. C. (1994) Properties of an in vitro selected Pb2+ cleavage motif, *Biochemistry 33*, 9561-9565.

98. Sanchiz, J. n., Esparza, P., Domínguez, S., Brito, F., and Mederos, A. (1999) Solution studies of complexes of iron(III) with iminodiacetic, alkyl-substituted iminodiacetic and nitrilotriacetic acids by potentiometry and cyclic voltammetry, *Inorganica Chimica Acta 291*, 158-165.

99. Cruz, R. P., Withers, J. B., and Li, Y. (2004) Dinucleotide junction cleavage versatility of 8-17 deoxyribozyme, *Chem Biol 11*, 57-67.

100. Ota, N., Warashina, M., Hirano, K., Hatanaka, K., and Taira, K. (1998) Effects of helical structures formed by the binding arms of DNAzymes and their substrates on catalytic activity, *Nucleic Acids Res 26*, 3385-3391.

101. Li, J., Zheng, W., Kwon, A. H., and Lu, Y. (2000) In vitro selection and characterization of a highly efficient Zn(II)-dependent RNA-cleaving deoxyribozyme, *Nucleic acids research 28*, 481-488.

3 Chapter 3. *In vitro* selection of Fe(II)-dependent DNAzymes

3.1 Introduction

DNAzymes, deoxyribozymes or catalytic DNA are the newest member of metalloenzyme family, since their first discovery in 1994 (*1*). DNAzymes are single stranded DNA molecules that can catalyze a variety of chemical reactions including RNA/DNA cleavage, RNA/DNA ligation, phosphoryl transfer, peptide bond formation, peptide-nucleic acid conjugation, etc (*2-6*). They can provide significant rate enhancements as high as 10^{12}-fold over the corresponding uncatalyzed reactions (*7*). So far, there is no precedent for naturally evolved DNAzymes, but they have been isolated through a process called *in vitro* selection (*8*).

In vitro selection is an extremely useful combinatorial technique that can be used to select oligonucleotides with a desired ligand-binding or catalytic activity from a large library of random sequences (up to 10^{14}). *In vitro* selection, also known as systematic evolution of ligands by exponential enrichment (SELEX), have been used to isolate nucleic acid molecules, namely aptamers, with the ability to bind specific targets, which can range from small organic molecules to whole cells (*9-11*). In SELEX or *in vitro* selection process, the starting random DNA or RNA pool is iteratively subjected to selection pressure to isolate either a desired catalytic activity or binding function (*8, 12, 13*). At the end of each selection round, sequences with the desired activity are separated from the rest of the pool. Once the desired sequences have been separated, they are amplified using PCR to enrich the pool and fed into the next round of the selection. The sequences that survive the selection pressure through several rounds of selection and display highest activity are identified for further characterization.

Most of the identified DNAzymes require metal ions as a cofactor for their catalytic function. Among all of the DNAzymes, RNA-cleaving DNAzymes, have shown promises to be highly sensitive and selective sensors for metal ions (*14-16*). This class of DNAzymes is of special interest for developing sensors and biosensors due to their specificity for their metal cofactors. 10-23 and 8-17 DNAzymes are two of the most common motifs isolated RNA-cleaving DNAzymes (*16*). The 10-23 DNAzyme has been used for therapeutic applications due to its ability to cleave RNA sequences with high catalytic efficiency (*17, 18*). The 8-17 DNAzyme, has been isolated by three different research groups under various selection conditions (*19-21*). Although 8-17 shows the highest activity with Pb^{2+}, however, it is also active with other divalent metal ions such as Zn^{2+} (*22*). Several other DNAzymes have been reported which show activity in the presence of UO_2^{2+} (*23*), Zn^{2+} (*20*), Cu^{2+} (*24*), Co^{2+} (*25, 26*), and lanthanides (*27*). Many of these DNAzymes have been converted into DNAzyme-based sensors for detection of their preferred metal cofactor.

Iron is the most abundant transition metal in the body and plays a critical role in variety of biological processes such as respiration, energy metabolism, DNA synthesis, immunity, and pathogenesis (*28-30*). Iron has a complex role as a controlled substance with both medicinal and destructive potential. One of the reactions that iron participates in, the Fenton reaction, produces reactive oxygen species (ROSs):

$$Fe^{2+} + H_2O_2 \rightarrow Fe^{3+} + {}^{\bullet}OH + OH^{-}$$

The past decade has been described *as* "golden age" of iron metabolism, since many new iron-associated proteins and pathways associated with intracellular iron regulation have been discovered. These discoveries have been applied in deciphering molecular relationships between iron and cancer (*31*). Based on the evidences obtained in the past five years, altered iron metabolism is a key metabolic *'hallmark of cancer'* (*32*). A more comprehensive picture of iron

uptake, storage and efflux changes in malignant cells would significantly benefit for the recognition of key elements that can be therapeutically manipulated (*31, 33*). Increased levels of iron in the body are associated with increased cancer risk (*34*). It is reported that genetically induced accumulation of excess iron (iron overload) is associated with significantly higher risk of cancer such as hepatocellular carcinoma (*35*). In addition, it was found that breast cancer cells and tumor have high levels of the labile iron pool (*36*).

Most common methods to measure free iron in biological samples are based on iron chelators and cannot differentiate ferric from ferrous forms of iron (*37*). Another disadvantage of chelator-based iron detection methods is DNA breakage which can be induced by iron-chelator complexes (*38, 39*). In addition, current clinical total blood iron tests do not distinguish between protein-bound and "free" iron, nor do they retain any information on speciation. In these methods, all protein-bound iron ions are removed from its protein carrier, and reduced or oxidized as a single pool for detection. Therefore, developing selective Fe(II) and Fe(III) sensors can be used to determine the concentration and speciation of the "free" ionic iron population in the biological samples, thus complementing the currently available information from previous tests. Most of early fluorescent sensors for Fe(II) or Fe(III) exhibit turn-off fluorescence response to iron binding (*40, 41*). One major challenge with turn-off sensors is that fluorescence quenching can be a nonspecific process. Moreover, relatively small number of Fe(II) probes are available. Some of available probes for Fe(II) suffer from several drawbacks such as formation of redox-active and toxic complexes with iron (*41, 42*). Recently several turn-on fluorescent sensors have been reported for Fe(II) or Fe(III). There are a number of disadvantages reported for these probes including poor water solubility (*43*), require acidic condition (*44*), unable to distinguish Fe(II) from Fe(III) (*45*), or their irreversible mode of detection (*46, 47*). In contrast to Fe(II), there are

many probes reported for Fe(III). However, limited number of them have shown applicability in biological systems (*15*). Similar to Fe(II) probes, most of available Fe(III) probes are turn-off sensors; although recently a few turn-on fluorescent sensors for Fe(III) have been developed (*48*). These novel rhodamine-based sensors suffer from reactivity with Cr^{3+} and some interference from Fe(II) (*49*). Overall unlike zinc and copper, proper iron probes suitable for biological applications are still underdeveloped (*15*).

Our objective in this project is the *in vitro* selection of DNAzymes specific for different oxidation states of iron. Through careful selection design, I tried to isolate selective DNAzymes with the ability of distinguishing Fe(II) from Fe(III). These DNAzymes will be used in the design of DNAzyme based sensors for different biological applications such as point of care detection and live cell imaging. In this chapter our efforts on isolating Fe(II)-dependent DNAzymes have been described.

3.2 Materials and Methods

3.2.1 Materials

All DNA sequences including PCR primers and random pools were purchased from Integrated DNA Technologies and denaturing PAGE purified before use. All the used metal salts are listed as follows: $FeCl_2$ (Alfa Aesar, 99.99%), (NaCl (Alfa Aesar, 99.999%), $MgCl_2.6H_2O$ (Alfa Aesar, 99.999%), $Ca(NO_3)_2.6H_2O$ (Alfa Aesar, 99.995%), $SrCl_2.6H_2O$ (Alfa Aesar, 99.996%), $BaCl_2.2H_2O$ (Alfa Aesar, 99.997%), $Mn(CH_3CO_2)_2.4H_2O$ (Alfa Aesar, 99.999%), $CoCl_2.6H_2O$ (Alfa Aesar, 99.9%), $NiCl_2.6H_2O$ (Alfa Aesar, 99.995%), $Cu(NO_3)_2.H_2O$ (Alfa Aesar, 99.999%), $ZnCl_2.H_2O$ (Alfa Aesar, 99.99%), $Cd(NO_3)_2.4H_2O$ (Alfa Aesar, 99.999%), and $Pb(CH_3CO_2)_2.3H_2O$ (Aldrich, 99.999%). Other chemicals used to prepare different solutions included the following: Ethylenediaminetetraacetid acid, sodium free (EDTA) (Fluka, 99.0%), EDTA.2Na.$2H_2O$ (Fisher Scientific), Trisodium citrate (Alfa Aesar, 99%), urea (Affymetrix, MB grade), Tris (Affymetrix, MB grade), boric acid (Fisher Scientific, electrophoresis grade), and Bis-Tris (Sigma, 99.0%). Acrylamide/bisacrylamide 40% solution (29:1) was purchased from Bio-Rad Laboratories, Inc. *Taq* DNA polymerase with standard *Taq* buffer, T4-polynucletide kinase, and deoxynucleotide (dNTP) solution mix were purchased from New England Biolabs. Radiolabeling of DNA carried out using ^{32}P labeled α-ATP and γ-ATP purchased from Perkin-Elmer. The original TA cloning® kit was purchased from Invitrogen. All buffer, metal ion and gel stock solutions were prepared with Milli-Q water. The pH of the buffers was measured with Fisher Scientific Accumet AB15 pH meter.

The selection buffers were made as a 2× solution of 50 mM Bis-Tris, 400 mM sodium chloride at pH 7.0. Ultrapure hydrochloric acid (from Alfa-Aesar) was used for adjustment of the

pH. The concentrated Fe(II) metal-stock solution contained 100 mM ferrous chloride in 1.2 mM ultrapure hydrochloric acid and prepared fresh every time before selection or activity assay experiments in the glove bag with degassed and oxygen free solutions. Subsequent dilutions in Milli-Q water were made to obtain 2× metal solutions of appropriate concentrations.

3.2.2 Sequences

Table 3.1 Sequences of the oligonucleotides used for the *in vitro* selection and the random pool generated after PCR.

Name	Sequence of Oligonucleotide (5' to 3')
IDT template	GGAAGGAATCGTACGATTCC-**N_{50}**-CGTGATGCCTCTACCTC
Full length pool	GACTGGTATCAATCTCACGTATrAGGAAGGAATCGTACGATTCC-**N_{50}**-CGTGATGCCTCTACCTC
P1	GTA TCA ATC TCA CGT ATA GGA AGG AAT CGT AC
P2	CGT GAT GCC TCT ACC TC
P2-iSp	$(AAC)_5$ **-Sp-C18-** CGT GAT GCC TCT ACC TC
P3	GAC TGG TAT CAA TCT CAC GTA TrA

3.2.3 *In Vitro* Selection

The *in vitro* selection method was adopted based on the protocol originally reported by Breaker and Joyce (*1*) in combination with denaturing PAGE-based separation method (*50*). The initial pool used for all four different selection conditions was identical. It contained a randomized N_{50} region flanked by 2 primer-binding regions, one containing the single riboadenosine (rA) which serves as a cleavage site. The P2-iSp primer contained a hexaethyleneglycol spacer (Spacer-C18, from Integrated DNA Technologies). This modification stops Taq polymerization reaction from further extension. The internal C18 spacer is followed by $(AAC)_5$, which results in production of the antisense strand with 15 nucleotides longer than the sense strand (DNA random pool).

Therefore, single stranded DNA random pool were separated from the antisense strand using denaturing PAGE.

The initial random pool for the first selection round was generated in two steps using PCR machine (C1000 Touch™ Thermal Cycler from Bio-Rad Laboratories, Inc). PCR1 was carried out in 96 PCR tubes with 0.1 µM of IDT DNA template in three steps. In the first step, 0.1 µM primer P2-iSp was added to the PCR mixture containing 0.1 µM of DNA template to undergo two cycles of extension. Second step was carried out by addition of 0.15 µM primer P1 and two more extension cycles. Finally, in the third step 0.9 µM of primer P2-iSp was added and 10 cycles of extension were carried out. PCR2 was carried out by addition of 1 µM primer P3 (for incorporation of the RNA base) and 0.1 µM of primer P2-iSp followed by 10 cycles of amplification. Before PCR2 and 2 µl of [γ-^{32}P]-dATP was added to the PCR reaction. The PCR products were then precipitated with 10 % of a 3 M sodium acetate solution, at pH 5.2, and 2.7 × volume of cold ethanol. The samples were stored at -80 °C for at least 1 h, then centrifuged, washed and lyophilized. It should be noted that subsequent PCR amplifications, which was used to amplify selected DNA at the end of each selection round, were slightly different. In those reactions PCR1 was carried out in a single step with 1 µM of primer P2-iSp and P2. Then PCR2 was done with 5% of PCR1 reaction as DNA template with 0.1 µM of primer P2-iSp and 1 µM P3.

Dried samples were dissolved in water and an equal amount of stop buffer was added. The stop buffer contained 8 M urea, 50 mM EDTA and 1× TBE (Tris, Boric acid, EDTA). The reaction products were purified using a 10 % denaturing PAGE gel, with the use of 1× TBE as the running buffer. The PCR product was run on the gel alongside DNA size markers corresponding to the cleaved (87-mer) and intact (110-mer) pool. The gel was then covered with a plastic wrap, a radioactive triangle location marker was placed on top of the gel, and exposed to a phosphorimager

cassette. After imaging the exposed film, band corresponds to the 110-mer marker on the gel was excised, crushed, and extracted with a 10 mM Tris, 0.1 mM EDTA, and 300 mM sodium chloride solution (extraction buffer). Gel particles were frozen over 10 minutes at -80 °C and thawed in a room temperature water bath over 5 minutes to improve extraction process. The solution was centrifuged at 10,000 g for 1 minute to remove gel free solution which contains DNA. DNA samples were ethanol precipitated using the procedure mentioned earlier.

The dried pools after the initial pool generation for the first selection round (and PCR amplifications for subsequent selection rounds) were dissolved in 1× selection buffer and incubated with a desired concentration of Fe(II) (for positive selections) or a mixture of competing divalent metal ions (for counter selections) for 18 h. The initial negative selection which was carried out before round 1, was done by incubating the DNA pool in selection buffer without addition of any divalent metal ion for 24 h. Counter selections were carried out by incubating the DNA pools with 1 mM Mn^{2+}, Cd^{2+}, Zn^{2+}, Co^{2+}, and 0.2 mM of Pb^{2+} in selection buffer over 18 h. Overall, four different selection conditions were carried out and each named with a letter (E, F, G, and H) (see Table 3.4). After negative and counter selection steps, uncleaved DNA pools were PAGE purified and used for the subsequent positive selection. Cleaved DNA produced in each positive selection was PAGE purified and used as a template for PCR amplification reactions. Stringency of positive selections gradually increased by varying the reaction time and Fe(II) concentration. All selection reactions were stopped by the addition of an equal amount of the stop buffer. All PAGE purifications were carried out using a 10 % gel alongside the DNA size markers used earlier.

3.2.4 Gel-Based Activity Assays

Activity assay experiments were carried out after 5th round of the selection for several rounds, in order to monitor enrichment of DNA pools with active/selective DNAzymes and fine tuning of the stringency of positive selections. Single stranded DNA pools were PCR amplified and internally labeled with ^{32}P with the same protocol mentioned earlier. No annealing step was carried out before testing the activity of the selected pools or *cis*-cleaving DNAzymes obtained from cloning experiments. DNA samples were dissolved in selection buffer and tested with different concentrations of Fe(II) and other metal ions. Each reaction was initiated by the addition of an equal volume of 2× metal solution (in 1× selection buffer) to the DNA in 1× selection buffer. Therefore, no dilution occurred in ionic strength of solutions upon addition of cofactor metal ions. At known time points, 2 µl aliquots of the reaction mixture were withdrawn and added to 4 µl of a stop solution containing 50 mM EDTA, 8 M Urea, 1× TBE, 0.05 % xylene cyanol and 0.05 % bromophenol blue. The uncleaved and cleaved DNA pools were separated on a 10 % PAGE gel (36 W, 1.5h). The gel was then wrapped and exposed to a phosphorimager cassette. The cassette was then imaged using a Molecular Dynamics Storm 430 Phosphorimager (from Amersham Biosciences) and the fraction of cleavage was calculated using Image Quant software (Molecular Dynamics). To monitor activity of *trans*-cleaving DNAzymes, each substrate was radioactively labeled with [γ-^{32}P]-dATP using T4 kinase from NEB. The labeling mixture contained 10 pmol of the substrate, 1× forward reaction buffer, 0.5 µL of T4 kinase and 1 µl of [γ-^{32}P]-dATP, the total volume being 20 µl. This solution was incubated at 37 °C for 1.5 h.

Rate of cleavage was determined by plotting cleavage percentage versus time and fitting the data points to the following equation:

$$\% P_t = \% P_0 + \% P_\infty (1-e^{-k_{obs} \times t})$$

In this equation % P_0 is the initial percent of cleavage product (t = 0), % P_∞ is the % of product at the end point of the reaction (t = ∞) ,% P_t is the % of product at time t, and k_{obs} is the apparent rate of cleavage.

3.3 Results and Discussion

3.3.1 Selection Condition

It is known that Fe(II) easily oxidize to Fe(III) in an aqueous solution in the presence of oxygen (*51*). In order to isolate Fe(II)-dependent DNAzymes with capability of distinguishing Fe(II) from Fe(III), it is crucial to minimize contamination of the selection reaction with Fe(III). Our major goal in designing a selection condition for Fe(II)-dependent DNAzyme selection is to keep Fe(II) in its reduced oxidation state in the presence of a biological ligand which potentially forms a complex with Fe(II) in real systems. One way to keep Fe(II) in the reduced oxidation state is to use biologically relevant ligands that are known to stabilize Fe(II). Citrate, one the most potent biologically relevant chelators with high abundance, is expected to be one of the major ligands forming complex with multivalent metal ions in biological systems (*52*). However, it was demonstrated that the rate of Fe(II)-autoxidation is significantly increased in the presence of effective chelators such as citrate (*53*). Hence, citrate is not a good ligand to be present in Fe(II) selection buffer.

Ascorbic acid (AA) is a biologically relevant ligand used to stabilize iron in the Fe(II) oxidation state and reduces Fe(III) to Fe(II), if present in the solution (*51, 54*). Although AA is potent in stabilizing Fe(II) ligand, it was found that the efficiency of Fe(II)-stabilization by AA is greatly influenced by pH, *i.e.* at pH 6.0 or higher AA is no longer able to stabilize Fe(II) or reduce Fe(III) to Fe(II) (*55, 56*). Since neutral pH is the preferred pH for Fe(II)-dependent DNAzyme selection, therefore AA is not a proper Fe(II)-stabilizing ligand for *in vitro* selection. Another biologically relevant ligand that could stabilize Fe(II) is glutathione (GSH). Since GSH is highly abundant in cytosol (2 – 10 mM), it was predicted that ~ 82% of cytoplasmic Fe(II) is in complex with GSH and the second major cytoplasmic Fe(II) species is hexaaquo-Fe(II) (*57, 58*).

Additionally, based on a computer simulation it was predicted that Fe(II)–carbonate complexes and hexaaquo-Fe(II) are the predominant Fe(II) species in human blood plasma (*59*). Therefore, I decided to use GSH as the Fe(II)-stabilizing ligand in the selection buffer.

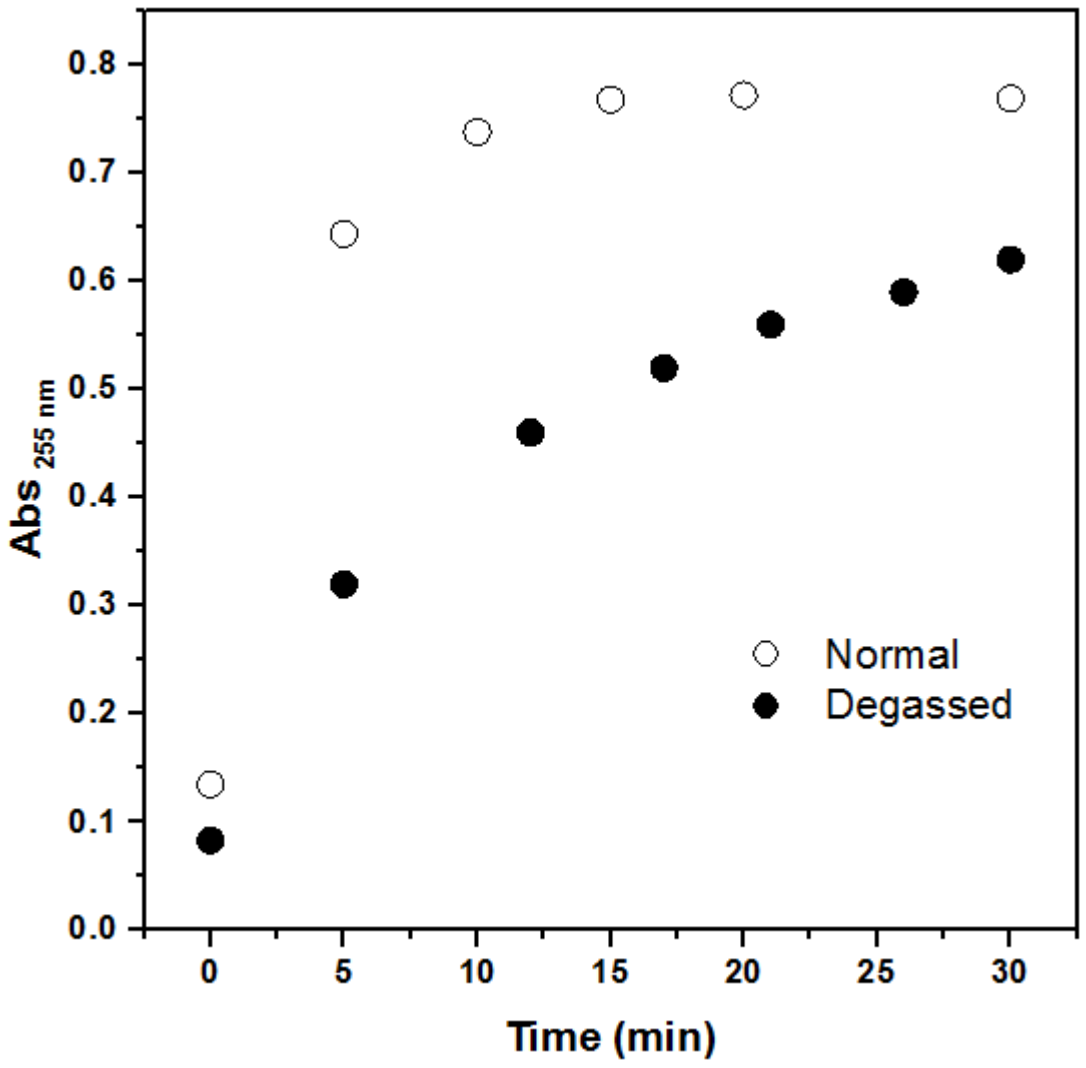

Figure 3.1 Oxidation of Fe(II) solutions in degassed (filled circles) and air equilibrated buffer (open circles) in 10 mM Bis-Tris pH 7.0 over 30 minutes.

In order to explore whether Fe(II)-dependent DNAzyme selection can be carried out in a degassed solution in an open to air environment, rate of Fe(II) oxidation was measured in such a

solution and compared with rate of Fe(II) oxidation in an air equilibrated solution. Experiments were carried out with 0.1 mM Fe(II) in 10 mM Bis-Tris buffer pH 7.0. As a control UV-Vis spectra of Fe(III) dissolved in the same solution was tested. It was found that Fe(III) showed an absorption peak at ~ 255 nm. Figure 3.1 shows increase in the absorption at 255 nm over time. Although rate of oxidation was slower in the degassed solution; however, substantial oxidation occurred over 30 minutes. Since incubation times in *in vitro* selection experiments are usually longer than 30 minutes specifically at earlier rounds of the selection; therefore, degassing and presence of GSH is not sufficient to keep iron in the Fe(II) oxidation state in the open to air environment. Therefore, I decided to do the selection in an oxygen free environment which was a glove bag filled with argon and 2% hydrogen.

3.3.2 Design of the Random Pool

The random pool used in selection of Fe(II)-dependent DNAzymes was designed to have a single riboadenosine (rA) as the cleavage site which was embedded in the middle of two Watson-Crick "pairing regions" (Figure 3.2) (*60*). Pairing regions were engineered in the random pool to bring random region of the pool in close proximity of the cleavage site. Previous attempts in our laboratory to isolate Pb^{2+} or UO_2^{2+}-dependent DNAzymes from random libraries lacking engineered pairing regions did not succeeded. In addition, it was shown that selecting DNAzymes from random libraries lacking pairing regions negatively influences isolation of DNAzymes that exploit metal ion cofactors for their catalysis (*61*). Therefore, design of random pools may play an important role in increasing the likelihood of obtaining active DNAzymes with cofactor dependent activity (*8*).

Fe(II) random pool was designed to have five base pairs in the pairing region in the 5′ end of the cleavage site. The pairing region on the 3′ end of the cleavage site consisted of 6 base pairs

forming a tetraloop and connecting enzyme and substrate strands together. The sequence of the tetra loop was chosen to form a thermodynamically stable DNA tetraloop (*62*) to assure formation of this pairing region in real condition. UNAFold (*63*) and DINAMelt (*64*) web server were used to confirm that DNA template and PCR primers do not form undesired structures (*i.e.* self-complements, hairpins, and hetero-dimers with relatively high melting temperature under PCR conditions). These precautions were taken into consideration as previously it was shown in our lab that PCR anomaly and unwanted DNA amplification during PCR might result in failure of *in vitro* selection experiments.

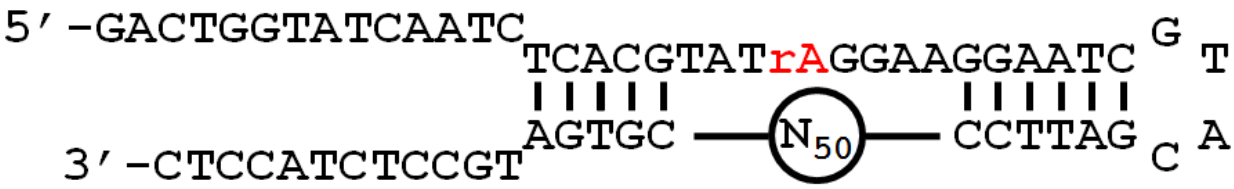

Figure 3.2 Designed random pool for *in vitro* selection of Fe(II)-dependent DNAzymes. A single riboadenosine cleavage site is inserted between two pairing regions.

3.3.3 *In Vitro* Selection

In vitro selection experiment was carried out using denaturing PAGE protocol, developed before (*23*), to separate active DNAzyme sequences (cleaved pool, 87 nt) from inactive DNA sequences (uncleaved pool, 110 nt) with a slight modification. The random pool was generated by PCR reactions to incorporate rA cleavage site and internally labelled with ^{32}P. The first round of the selection was carried out using 350 pmol DNA template (~ 10^{14} different sequences). DNA pool generate by PCR was 15 nt shorter than the antisense strand as the reverse primer used in PCR reactions contained a Taq polymerase stopper with 15 nt extension. As shown in Figure 3.3 before each selection round, single stranded DNA pool was separated from their complementary

strands using denaturing PAGE purification. Before starting the first round of the selection, a negative selection step carried out to decrease the chance of isolating DNA sequences with Fe(II)-independent catalytic activity. In negative selection PAGE purified DNA pool was incubated in the same Fe(II) selection buffer (200 mM NaCl in 25 mM Bis-Tris pH 7.0) in the absence of Fe(II) for 24 h. Then uncleaved DNA sequences were separated from cleaved one using denaturing PAGE and for positive selection in the presence of Fe(II).

I*n vitro* selection of Fe(II)-dependent DNAzyme was carried out using two different conditions under the oxygen free condition in a glove bag. In the first condition, random DNA pool was incubated with Fe(II) and no GSH was incorporated in the selection buffer (Condition F) and in the second condition selection was carried out in the presence of 1 mM reduced GSH (condition H). Each selection was started with a random pool with diversity ~ 10^{14} different DNA sequence. First round of positive selections were carried out by incubating random pool with 0.5 mM Fe(II) for 1 h. From the second round of the selection no negative selection step was carried out. Instead, in a control experiment called "negative selection control" DNA pools were incubated in the selection buffer in the absence of Fe(II) to monitor any cleavage that might occur in an Fe(II)-independent manner.

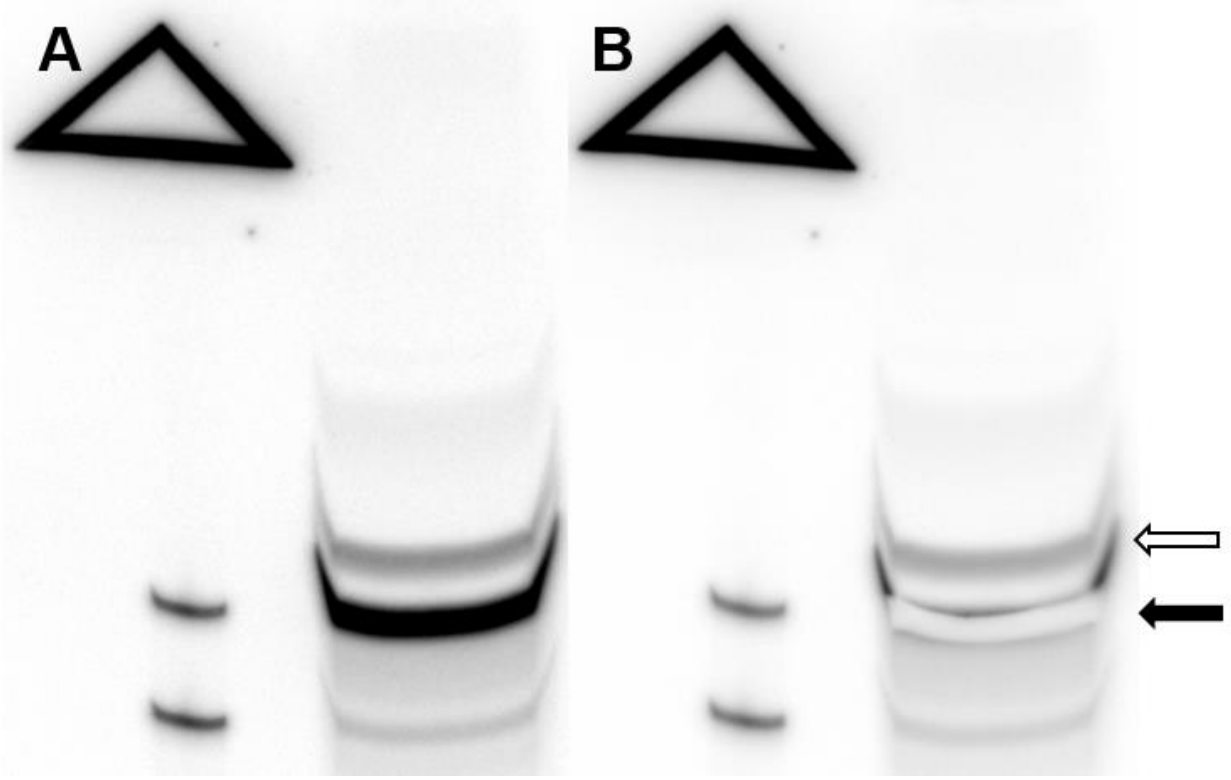

Figure 3.3 Denaturing PAGE separation of single stranded DNA pool after PCR reaction. (A) Before (A) and after (B) excising DNA pool out of the gel. Opened arrow represents complementary DNA from the PCR reaction. Closed arrow represents the single stranded DNA pool. Black triangle is prepared with soaking piece of paper with the same shape in radioactive solution, dried and wrapped to be used for aligning gel images with actual gels.

After third round of the selection, for the first time, a faint cleavage band was observed in both selection conditions which accounted for ~ 0.2 % cleavage over the course of the *in vitro* selection. I introduced more stringent selection condition from round 4 by reducing selection time to 30 min and also reducing Fe(II) concentration to 0.25 mM (Table 3.2). Since the amount of cleavage product was increase significantly in round 4, I continued to carry out more stringent selection in the next round.

Table 3.2 Fe(II)-dependent DNAzyme *in vitro* selection condition.

Selection round	Incubation time (min)	[Fe(II)] (μM)
1	60	500
2	60	500
3	40	500
4	30	250
5	10	100
6	5	50
7	5	10
8	5	10
9	5	5

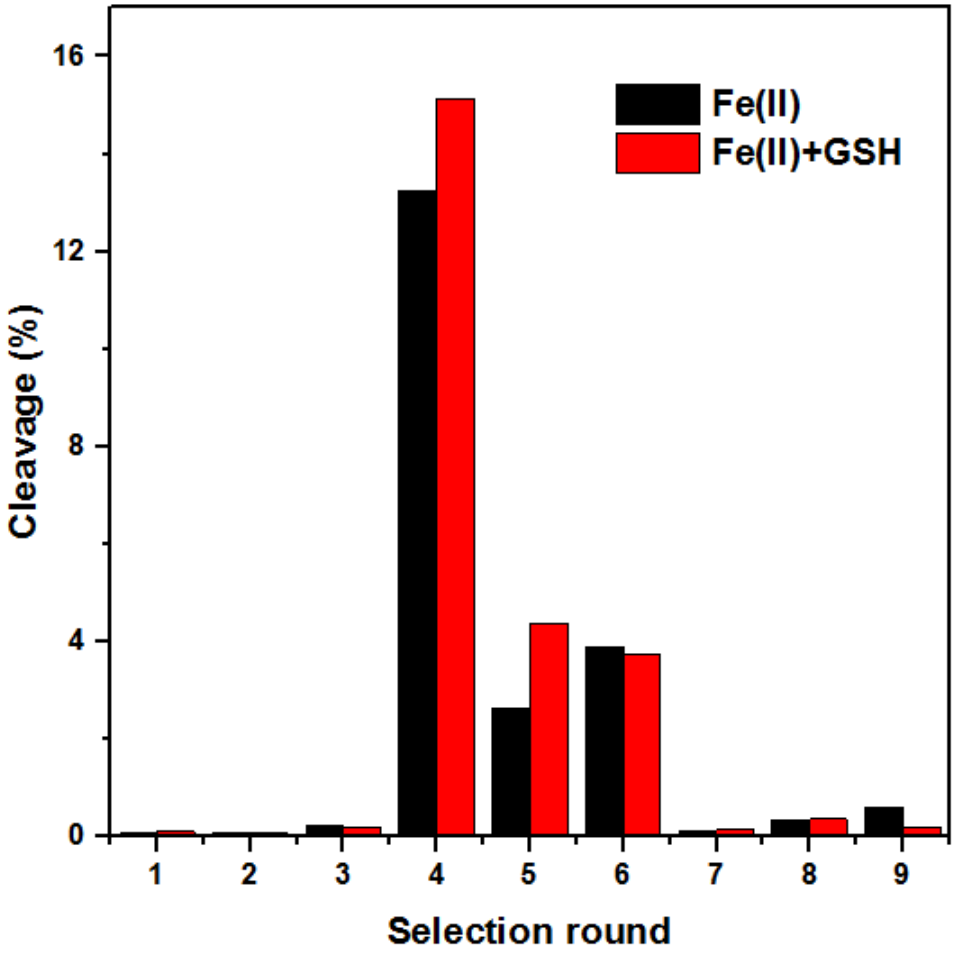

Figure 3.4 *In vitro* selection progress in terms of cleavage products observed in different rounds.

Table 3.3 Fe(II)-dependent DNAzyme *in vitro* selection condition. From round 3 before each positive selection one counter selection step was introduced. In counter selection steps, DNA sequences that were active in a mixture of 1 mM Mn^{2+}, Co^{2+}, Zn^{2+}, Cd^{2+}, and Pb^{2+} were removed. No counter selection was introduced before the first 2 rounds of the selection.

Selection round	Incubation time (min)	[Fe(II)] (μM)
1	60	500
2	60	500
3-R	40	500
4-R	30	250
5-R	30	250
6-R	10	100
7-R	5	50
8-R	5	50
9-R	5	25

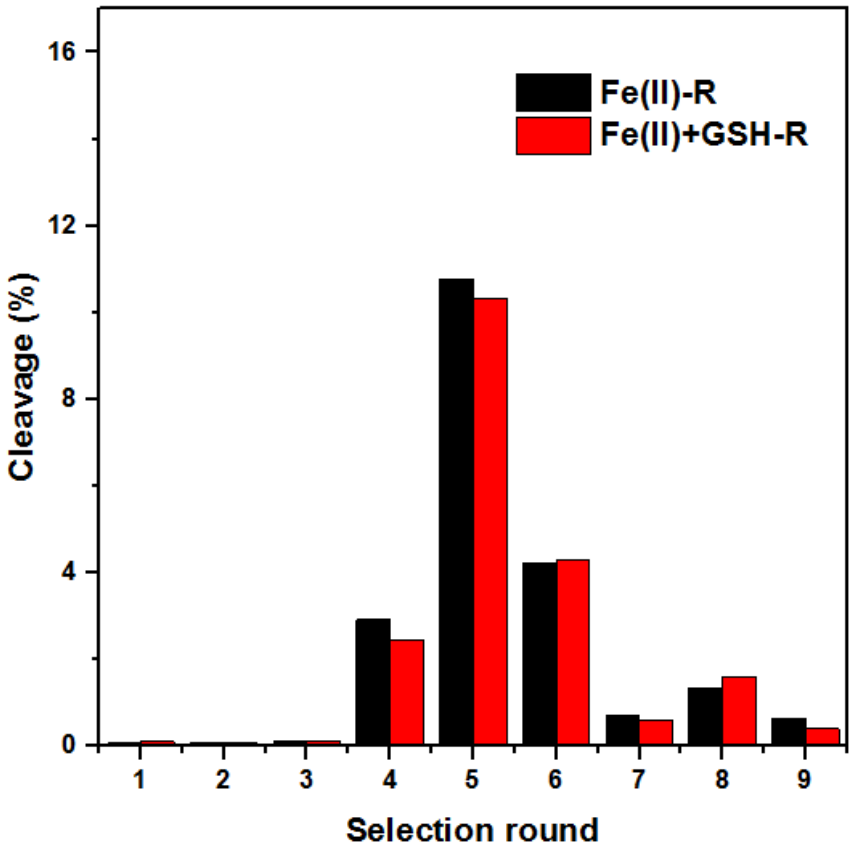

Figure 3.5 *In vitro* selection progress in terms of cleavage products observed in different rounds. "R" in the legends represent incorporation of a counter selection before each positive selection, started from round 3.

Selected pools from round 5 were tested for their activity with Fe(II) and several other metal ions including Mg^{2+}, Ca^{2+}, Sr^{2+}, Ba^{2+}, Mn^{2+}, Co^{2+}, Ni^{2+}, Cu^{2+}, Zn^{2+}, Cd^{2+}, Pb^{2+}, and Fe^{3+}. Although selected pools were more active with Fe(II), they showed activity with few other divalent metal ions such as Mn^{2+}, Co^{2+}, Zn^{2+}, and Cd^{2+} (Figure 3.6). In order to improve selectivity of the DNA pools for Fe(II) over other competing metal ions, counter selection strategy was used. Counter selection helps to remove DNA sequences that are active with other divalent metal ions. To increase efficiency of counter selection, I went back and introduced this step before round 3, which was the first round that cleavage product was observed. After PCR amplification of selected pool from round 2 and generation of single stranded DNA, the pools were incubated in selection buffer with a mixture of 1 mM Mn^{2+}, Co^{2+}, Zn^{2+}, Cd^{2+}, and Pb^{2+} for 18 h. Cleaved DNA sequences in counter selection step were removed from the pools by denaturing PAGE purification and then used to perform round three positive selection in the presence of Fe(II). From this round on, one counter selection step was introduced before each positive selection round. In addition, the original selection without any counter selection was continued with the *in vitro* selection conditions shown in Table 3.2 and selection progress is represented in terms of cleavage percentage in Figures 3.4. The selection rounds with counter selection (labelled with "R") were performed with the conditions shown in Table 3.3 and the selection progress is represented in terms of cleavage percentage in Figures 3.5.

To investigate the effect of introducing counter selection steps, I compared the activity of the selected pools from round 5 with Fe(II) and several other metal ions including Mg^{2+}, Ca^{2+}, Sr^{2+}, Ba^{2+}, Mn^{2+}, Co^{2+}, Ni^{2+}, Cu^{2+}, Zn^{2+}, Cd^{2+}, Pb^{2+}, and Fe^{3+} (Figure 3.6 with no counter selection and Figure 3.7 with counter selection). Activity of the pools were tested with 0.1 and 2 mM Fe(II) and with 2 mM of the other divalent metal ions except Pb^{2+} where 0.1mM was used. Figure 3.7

shows significant decrease in the activity of counter selected pools with competing divalent metal ions (*i.e.* Mn^{2+}, Co^{2+}, Zn^{2+}, Cd^{2+}, and Pb^{2+}) as compared to the pool without counter selection Figure 3.6. In addition, a small decrease was also observed in the Fe(II)-dependent activity. This reduction might be due to the stringent counter selection steps carried out before positive selection rounds. In the counter selection step, some DNA sequences which were able to catalyze cleavage reaction in the presence of both Fe(II) and competing divalent metal ions have been removed from the active population. The most competing metal ion was found to be Mn^{2+} and counter selected pools showing ~ 20-folds selectivity for Fe(II) over Mn^{2+} (Figure 3.8).

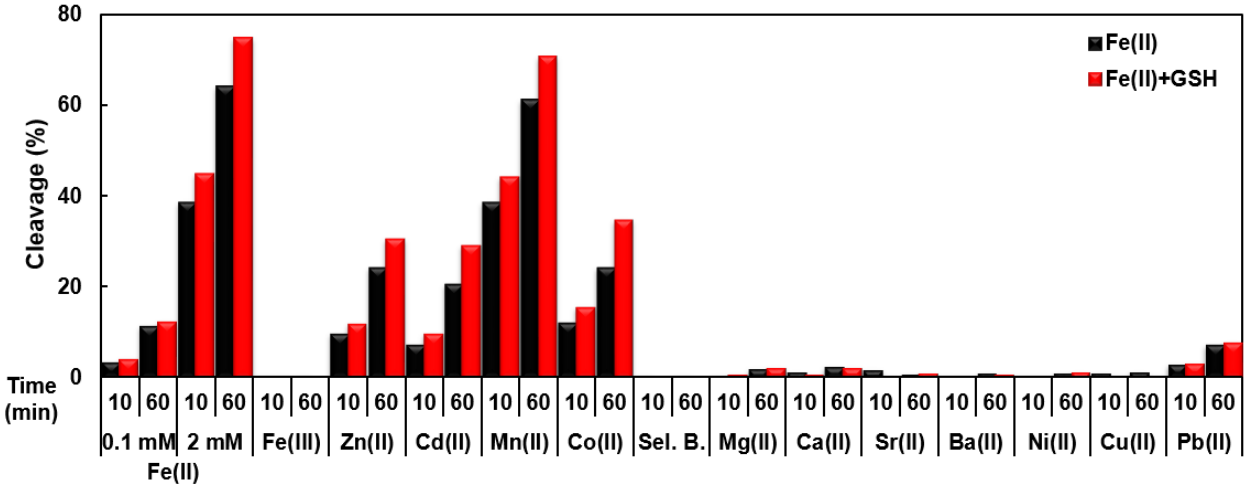

Figure 3.6 Activity of selected pools form round 5. Percentage of cleavage product is represented over 10 and 60 min. Two different concentrations of Fe(II), 0.1 and 2 mM, were tested. Cleavage activity of the pools were tested in the presence of 0.250 mM Fe(III) or 0.1 mM Pb^{2+}. All other divalent metal ions were tested at 2 mM. "Sel. B." represents cleavage activity observed in selection buffer in the absence of Fe(II).

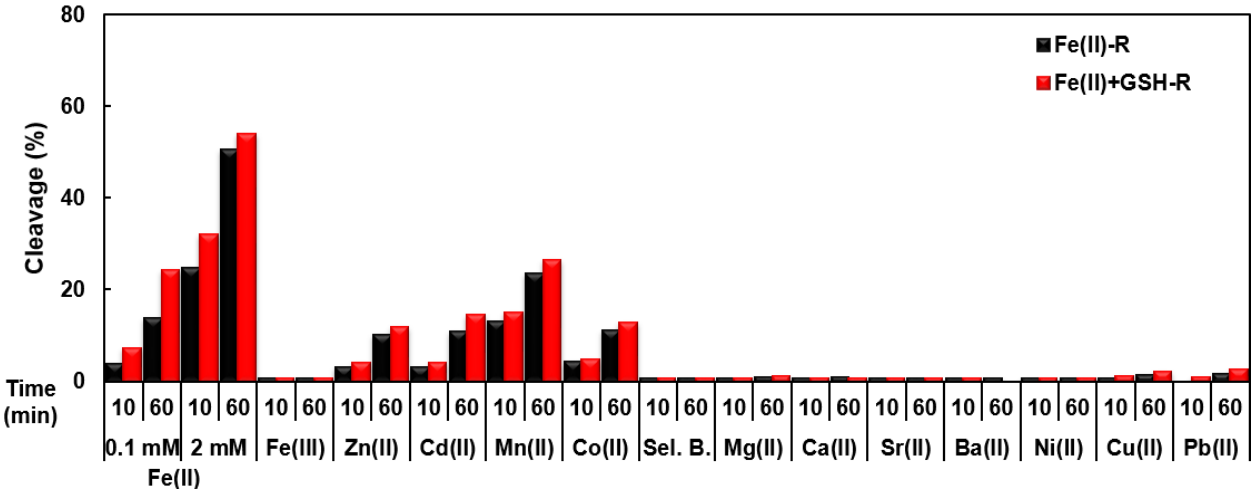

Figure 3.7 Activity of selected pools form round 5 after introduction of 3 counter selection steps. Percentage of cleavage product is represented over 10 and 60 min. Two different concentrations of Fe(II), 0.1 and 2 mM, were tested. Cleavage activity of the pools were tested in the presence of 0.250 mM Fe(III) or 0.1 mM Pb^{2+}. All other divalent metal ions were tested at 2 mM. "Sel. B." represents cleavage activity observed in selection buffer in the absence of Fe(II).

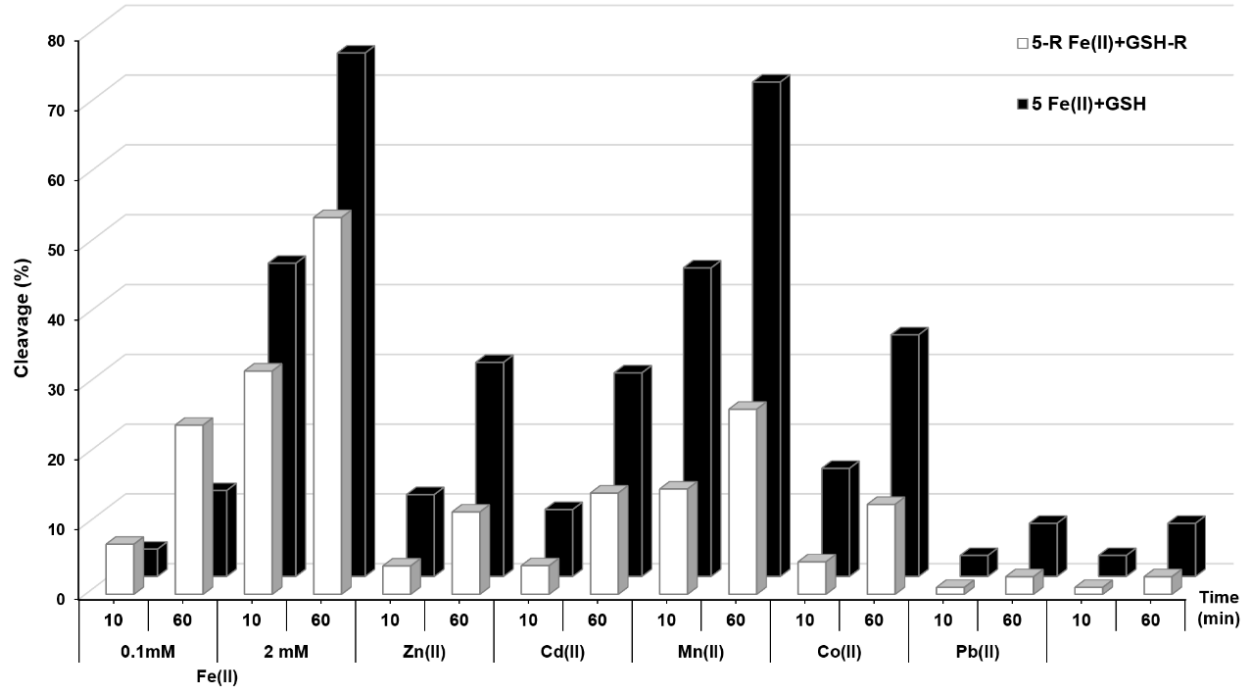

Figure 3.8 Comparing the activity of selected pools in the presence of GSH with and without counter selection steps.

Selection was carried out to round 9 for all four different pools. At this round some cleavage activity was found in the negative selection controls. This non-specific cleavage was found to be less significant for the counter selected pools. Amplified pools for round 10 showed background activity of 1 to 7% in selection buffer. Therefore, Fe(II)-dependent DNAzyme selections were stopped and no more rounds were carried out. Based on the activity assay results and selection signal over background (Figure 3.9), selected pools from round 8 were chosen for cloning and sequencing experiments.

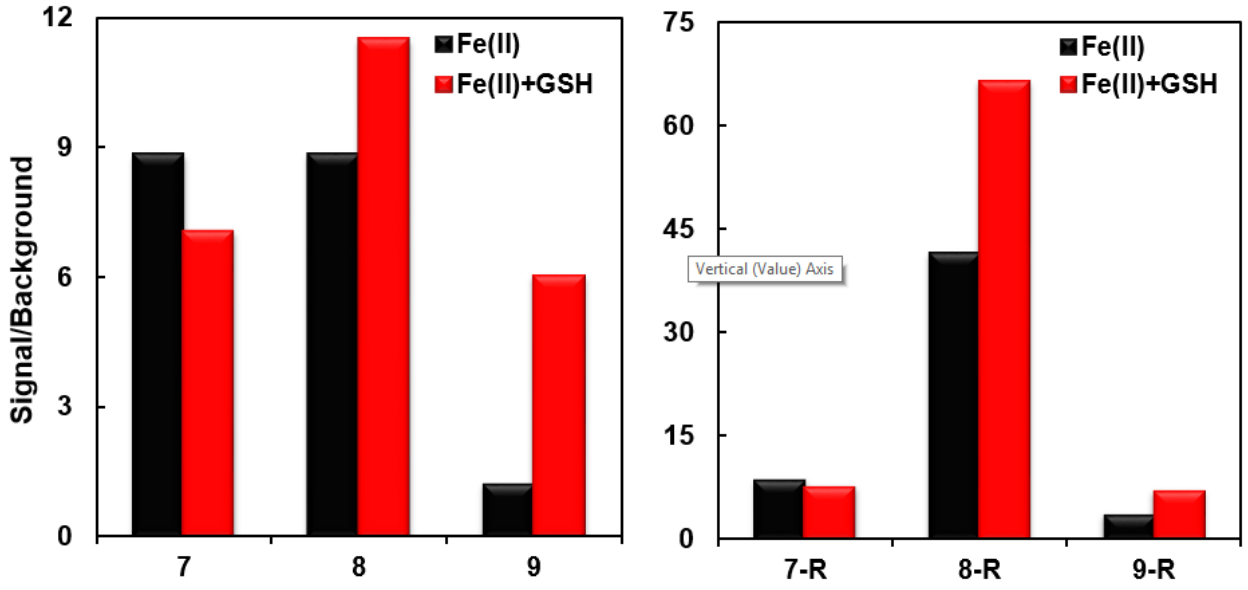

Figure 3.9 Signal over background from the last three round of different selections. Signal represent cleavage product produced in the presence of Fe(II) under selection conditions. Background is the fraction of cleavage product which observed from negative control selection.

3.3.4 Cloning and Sequencing

Base on the activity of the pools in positive selection and negative selection control and also activity assay experiments carried out with the pools from selection rounds, the most active pool with least background activity were selected for cloning and sequencing. Cloning was carried

out using PCR products with primers with no rA or Taq stopper. Same PCR reactions were carried out with selection primers to control overall activity of the species used for cloning. Negative PCR control with no selected DNA pool as PCR template is critical to make sure there is no contamination and cloned DNA sequences belong to the active population enriched over several selection rounds. Table 3.4 represents the selection condition, number of clones and their one letter code.

Table 3.4 Assigned letters for different Fe(II) selected pools

Selection condition	Number of sequenced clones	Letter code
Fe(II)	34	E
Fe(II)+GSH	40	F
Fe(II)-R	36	G
Fe(II)+GSH-R	39	H

Obtained DNA sequences from each individual pool were aligned based on their sequence similarity. Although a thermodynamically stable DNA tetraloop was engineered in the design of Fe(II) DNA pool, only 38 clones were found to have an intact tetraloop. In the rest of closes there was at least one mutation in this region. Primer regions remained relatively intact, in spite of few exceptions with mutations or deletions in their primer binding regions. Sequence identity of tetraloop regions remained intact in the case of Na^+-dependent (chapter 4) and Fe(III)-dependent DNAzymes. Observing sequences with relatively high variation in their tetraloop region might imply that formation of this stable structure was not in favor of forming catalytically active structures. Since this region in the Fe(II) pool was not part of the PCR primers, a potential selection pressure might have caused evolution of species without stable tetraloop over several selection rounds. Sequence alignment of each individual pool are represented in Figures 3.10 to 3.13.

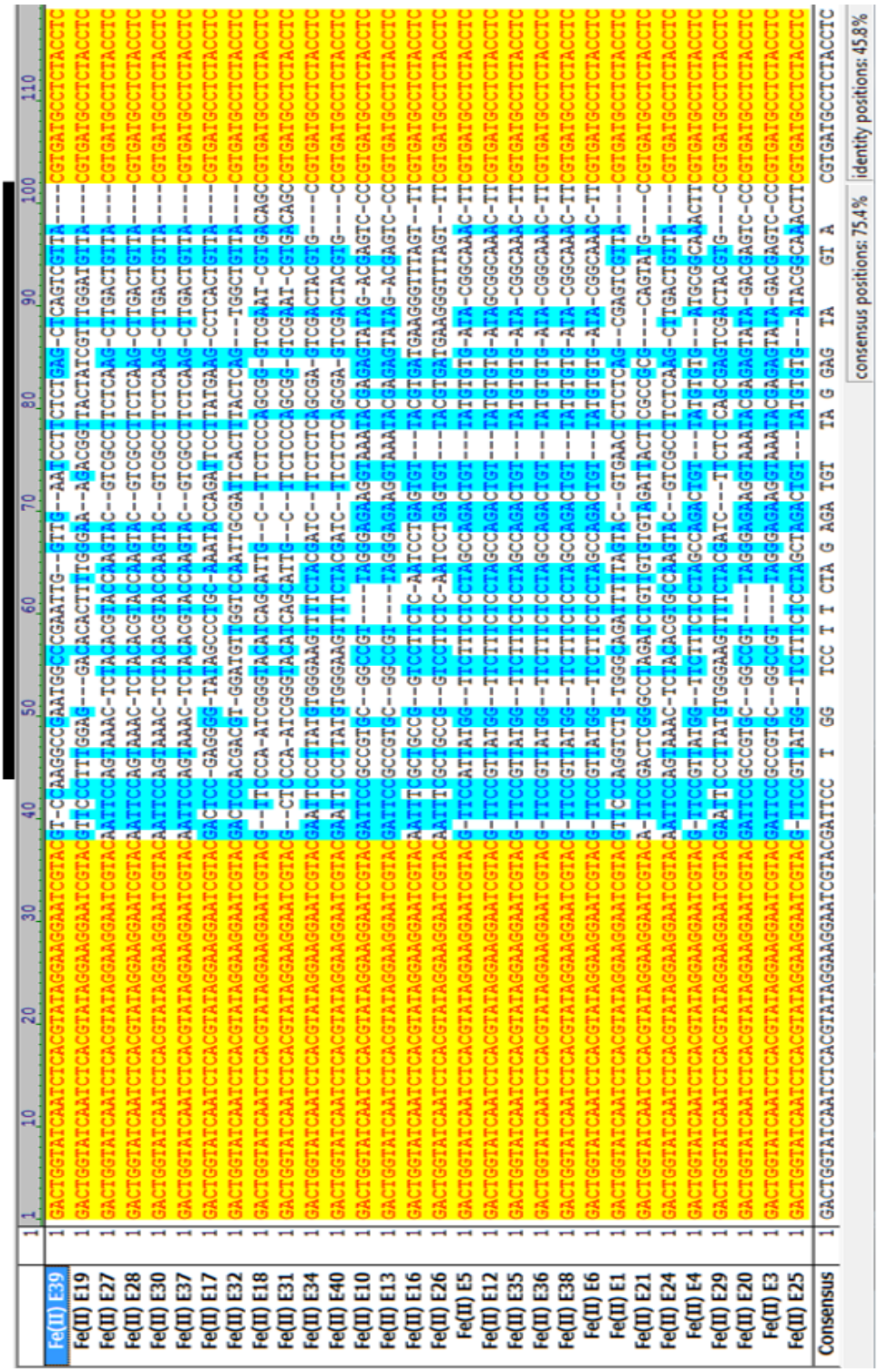

Figure 3.10 Sequence alignment of 34 clones isolated from selection condition E. Red text with yellow background indicates identical regions and dark blue text on a light blue background represent conserved sequences. Black on a white background signifies non-similar regions. The location of the N50 random region is indicated with a black line.

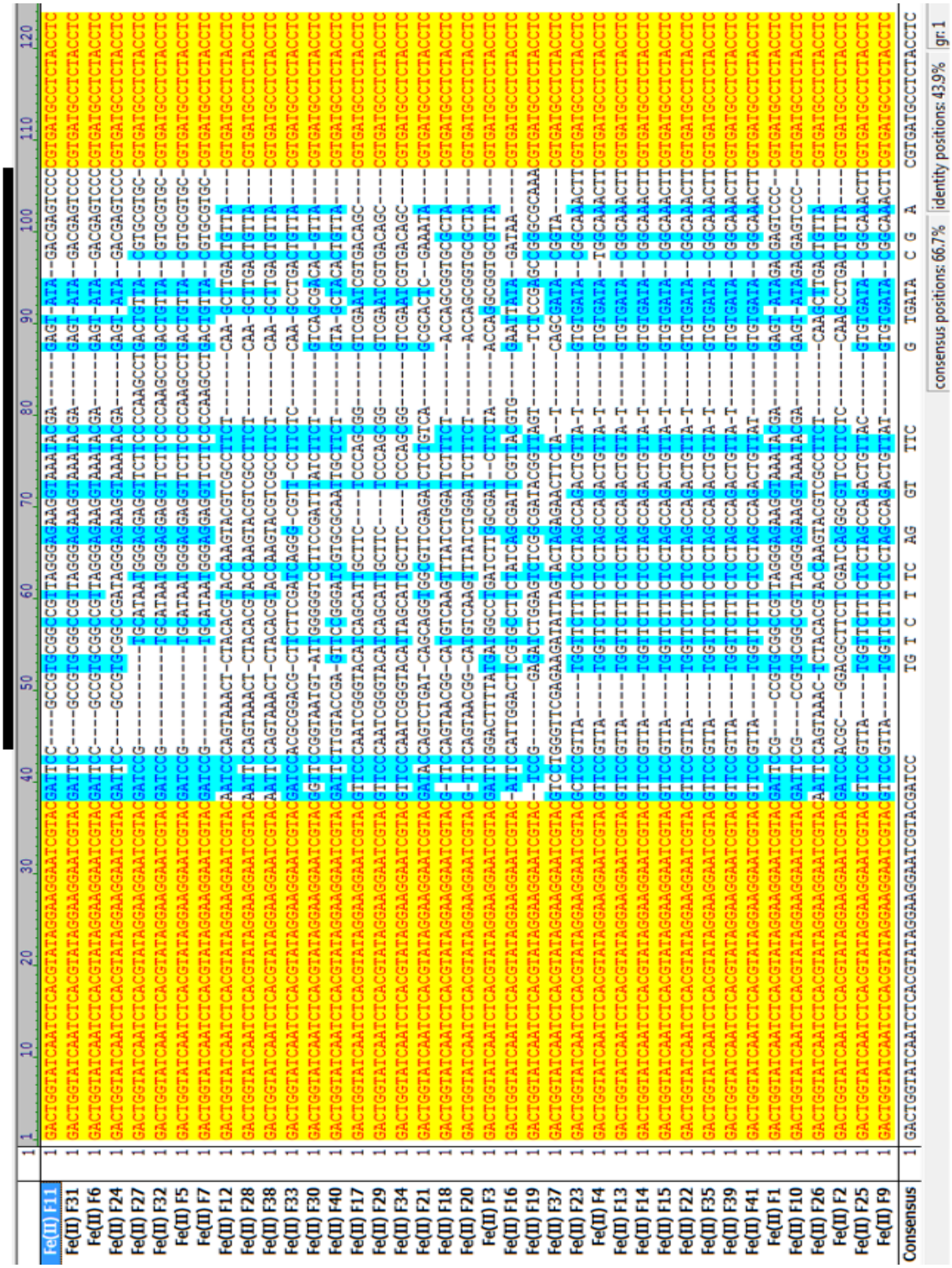

Figure 3.11 Sequence alignment of 40 clones isolated from selection condition F. Red text with yellow background indicates identical regions and dark blue text on a light blue background represent conserved sequences. Black on a white background signifies non-similar regions. The location of the N50 random region is indicated with a black line.

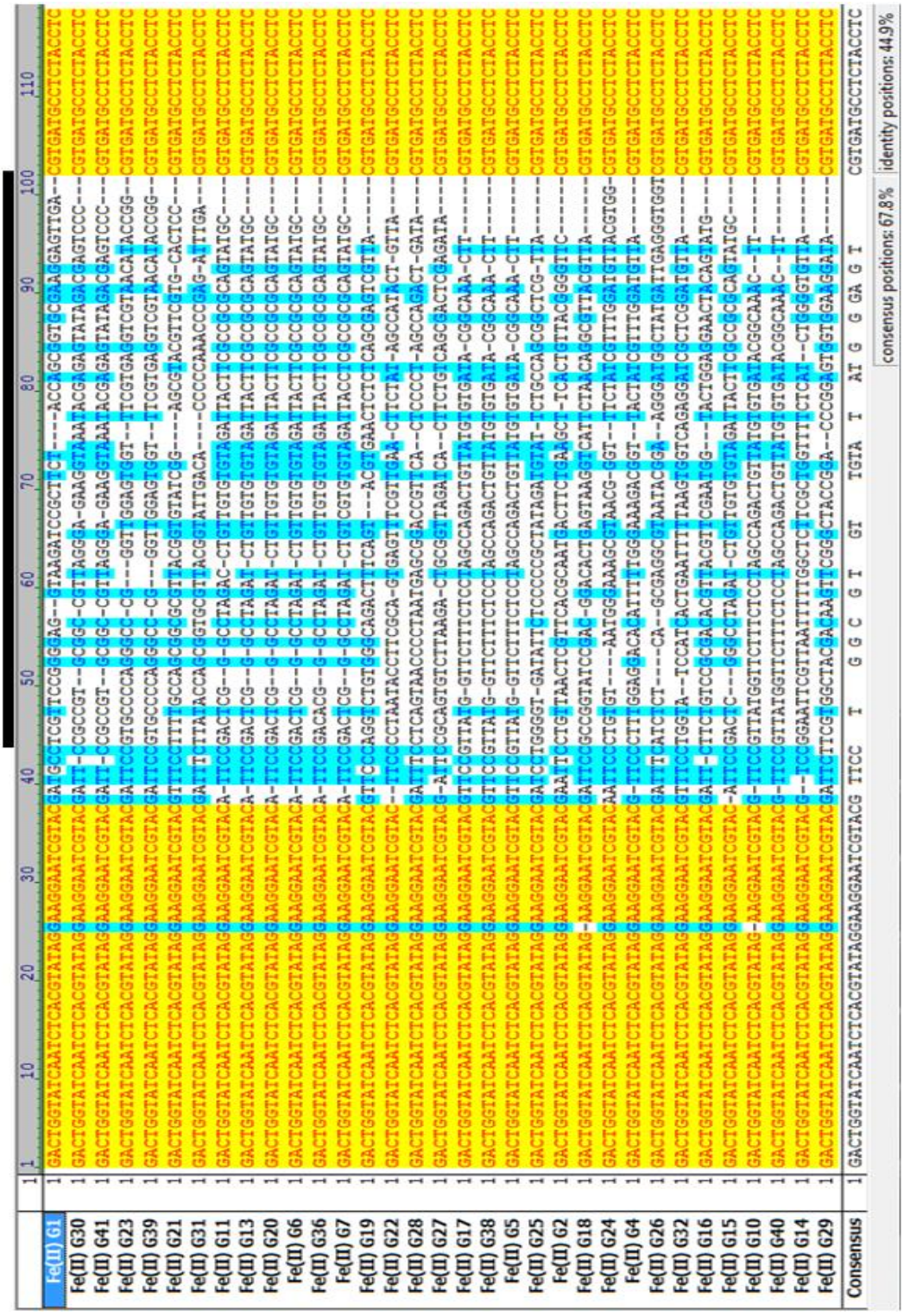

Figure 3.12 Sequence alignment of 36 clones isolated from selection condition G. Red text with yellow background indicates identical regions and dark blue text on a light blue background represent conserved sequences. Black on a white background signifies non-similar regions. The location of the N50 random region is indicated with a black line.

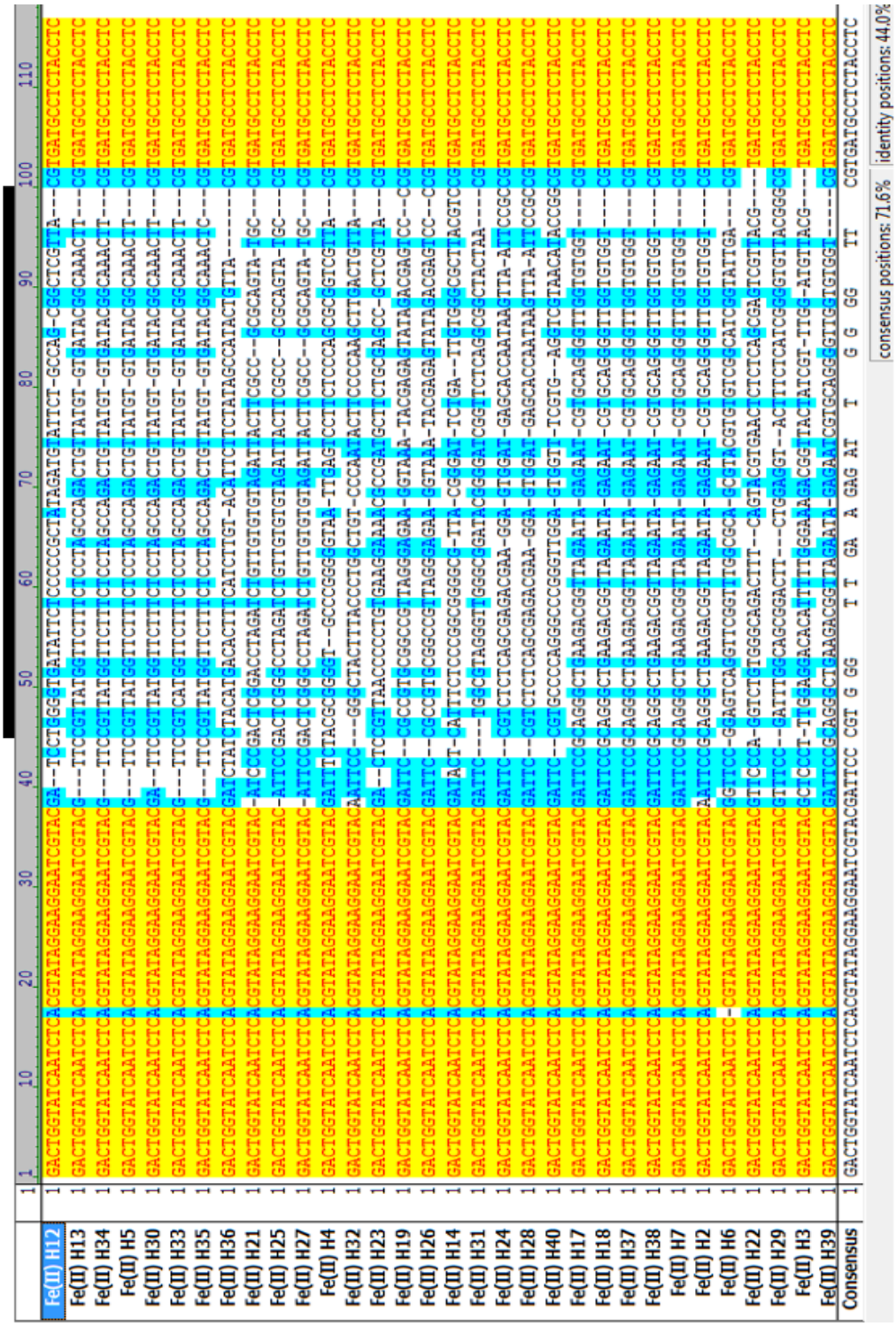

Figure 3.13 Sequence alignment of 39 clones isolated from selection condition H. Red text with yellow background indicates identical regions and dark blue text on a light blue background represent conserved sequences. Black on a white background signifies non-similar regions. The location of the N50 random region is indicated with a black line.

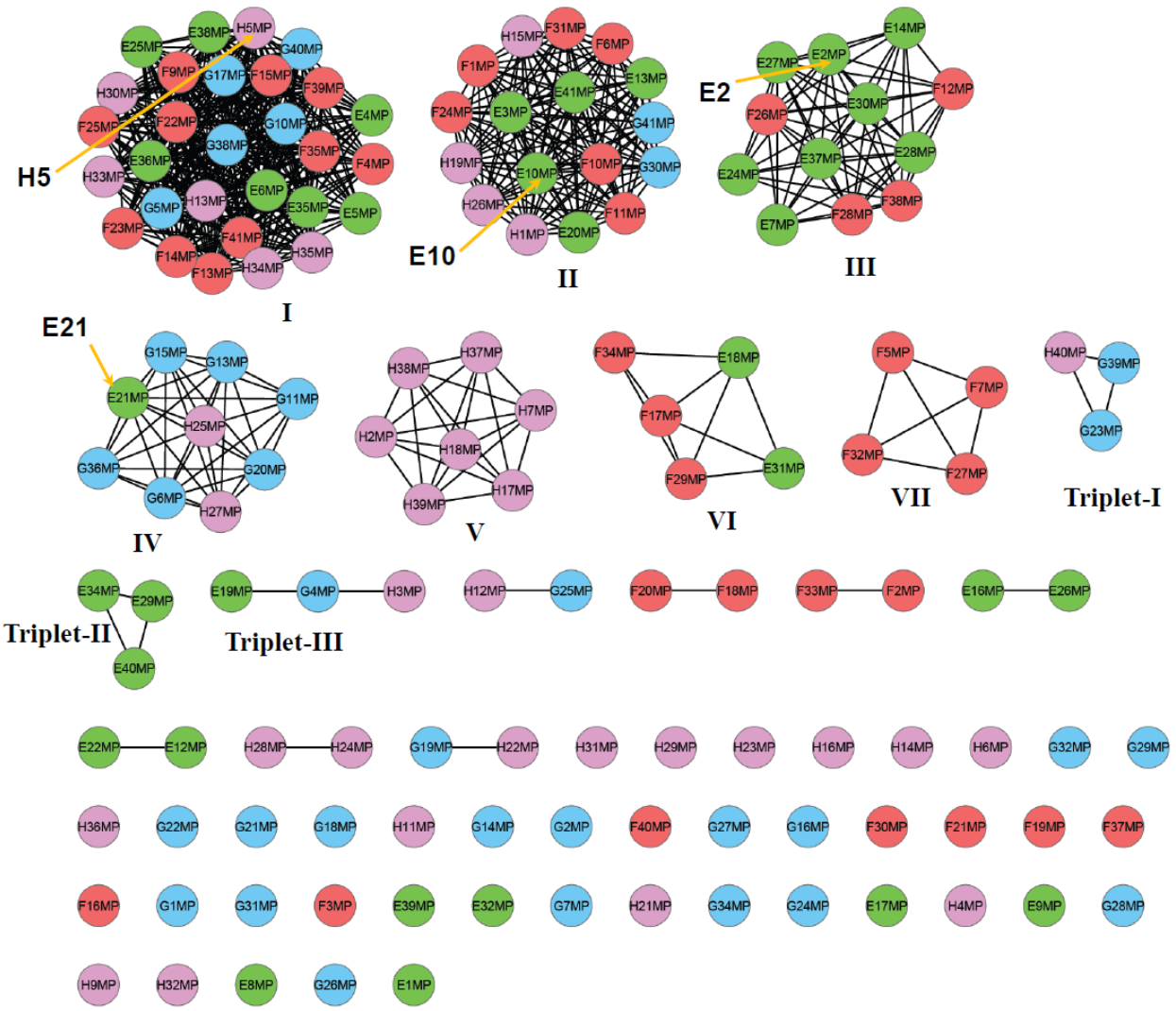

Figure 3.14 Sequence similarity network (SSN) including 149 sequences obtained from 4 different Fe(II)-dependent DNAzyme selections. This network was thresholded at a BLAST E-value of 10^{-25}: only edges associated with E-values more significant than 10^{-25} are included in the network. Lengths of connecting edges correlate with the relative dissimilarities of each pair of sequences. Green, red, blue, and purple nodes represent sequences from condition E, F, G, and H, respectively.

The sequence similarity of obtained sequences were represented using Sequence Similarity Networks (SSN), originally utilized for organizing sequence similarity of protein sequences (*65, 66*). Since I had four different groups of DNA sequences isolated from different selection conditions, I used SSN which presents interconnected sequences as clusters within 2D space which provides a good visual representation of the sequence similarity relationships. Figure 3.14 demonstrates the SSN of all sequences obtained from four different selection conditions at the BLAST e-value of 10^{-25}. Each node represents a unique sequence and each edge represents the similarity between connected sequences. At this e-value threshold, the sequences in the various clusters share at least 90% sequence identity. This network is constructed from obtained sequences after removing primer regions. Clusters with 3 or more members are named from I to VII (Figure 3.14). The two major populated clusters includes sequences from all the 4 different selection conditions. On the other hand, there are several clusters consisted of sequences from counter selected conditions (*i.e.* cluster IV and V). Figure 3.15 shows 91% sequence similarity of clones from cluster I (29 members). Interestingly, 41 singletons in the SSN are the sequences with low sequence similarity (only 40% identity which corresponds to the primer regions) (Figure 3.16).

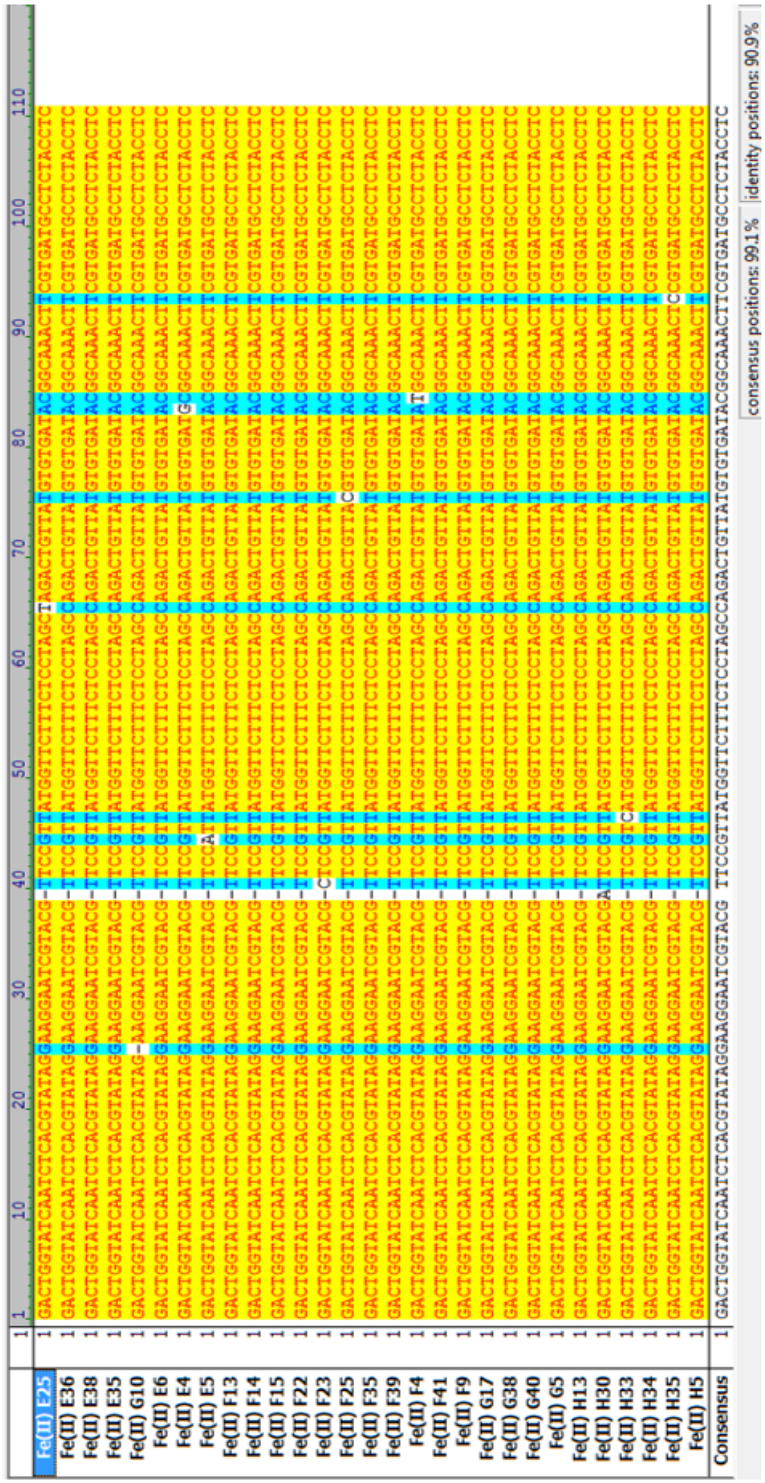

Figure 3.15 Sequence alignment of 29 sequences belong to cluster I. High degree of sequence identity in the random region shows enrichment of selected pools with this specific class of sequences. Red text with yellow background indicates identical regions and dark blue text on a light blue background represent conserved sequences. Black on a white background signifies non-similar regions. The location of the N50 random region is indicated with a black line.

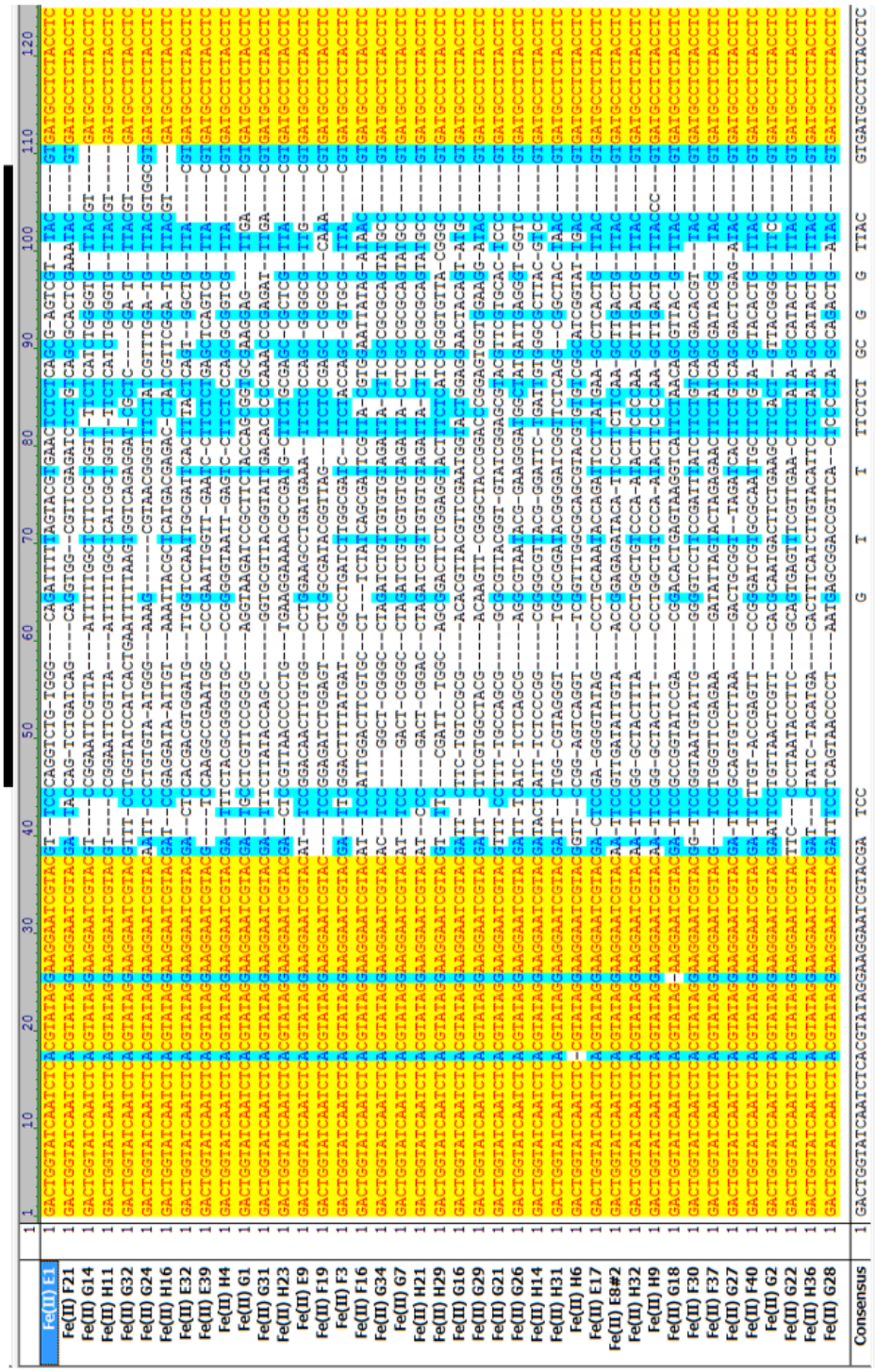

Figure 3.16 Sequence alignment of 41 orphan sequences not clustered with any other sequences. They represent low sequence similarity in the random region and high level variation in the tetraloop region (left side of the random region). Red text with yellow background indicates identical regions and dark blue text on a light blue background represent conserved sequences. Black on a white background

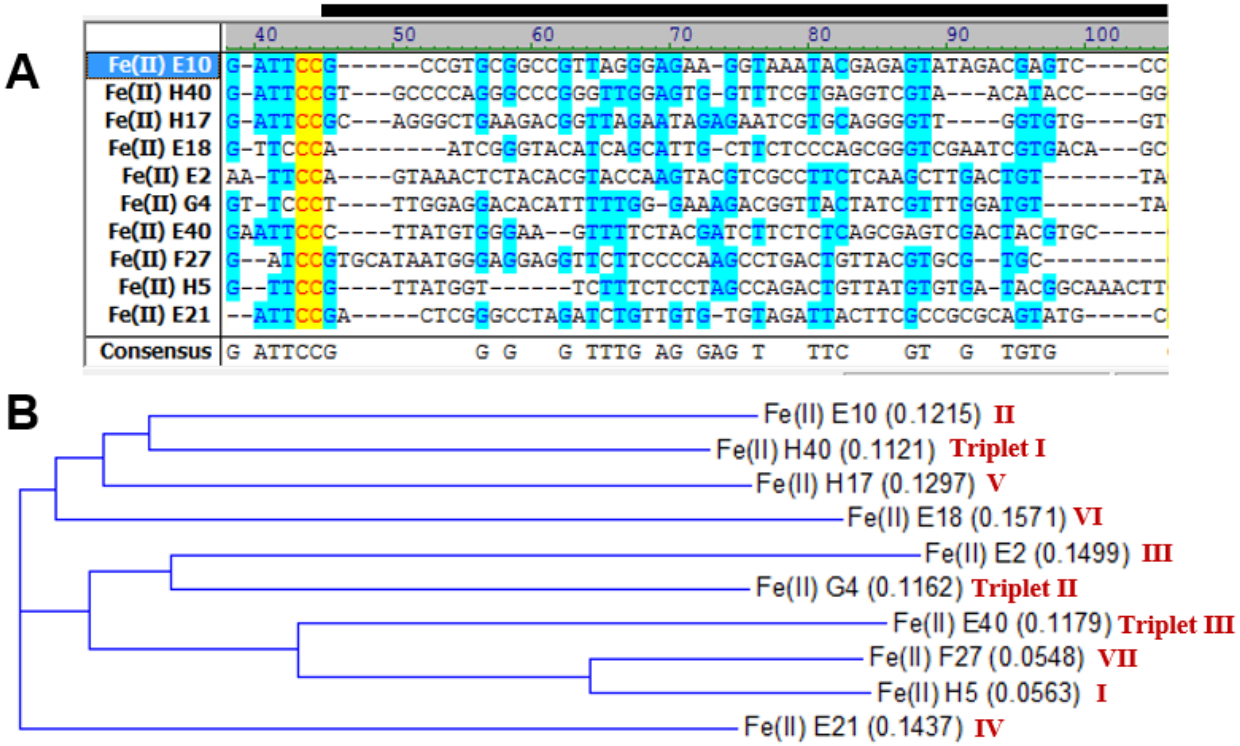

Figure 3.17 Sequence representatives from different clusters. (A) Sequence alignment of 10 different clones used for activity assay analysis. (B) Phylogeny tree of representative clones and their cluster number is shown. One representative from each triplet is included as well.

3.3.5 Activity of Individual Clones

Activity of a number of sequences including representative sequences from each cluster were tested in the *cis*-cleaving format to understand the sequence-function relationship of the isolated DNAzymes. Since these sequences were chosen from individual clusters, they have low sequence similarity (Figure 3.17). Single stranded DNAzymes were internally labeled with ^{32}P as described above, PAGE-purified, and dissolved in a final concentration of 25 mM Bis-Tris buffer (pH 7.0) with 200 mM NaCl. Activity of each DNAzyme was tested with 10 and 100 µM Fe(II) under oxygen free environment in the glove bag. As shown in Figure 3.18A, the fastest rate (~ 0.03 min^{-1}) was observed with clone H5 (cluster I) at 100 µM Fe(II). Clone E10 from cluster II

was slightly less active than H5 under the same condition. On the other hand, at lower Fe(II) concentration E10 was found to be more active than other clones with ~ 22% cleavage product in 2 h. The least active clone at both Fe(II) concentrations was found to be H40 (triplet I). In addition, clones E18 (cluster VI), E40 (triplet III), and H17 (cluster V) were found to be barely active with 10 μM Fe(II). None of the tested clones showed buffer activity over 2 h course of the reaction. Figure 3.18A and B shows k_{obs} and final cleavage values at 2 h reaction time for the tested clones. All 41 different orphans and representatives of 7 different duplets were tested with 100 μM Fe(II) over 1 h reaction time and none of them was found to be as active as H40. Therefore, orphan and duplet clones were not considered for further characterizations.

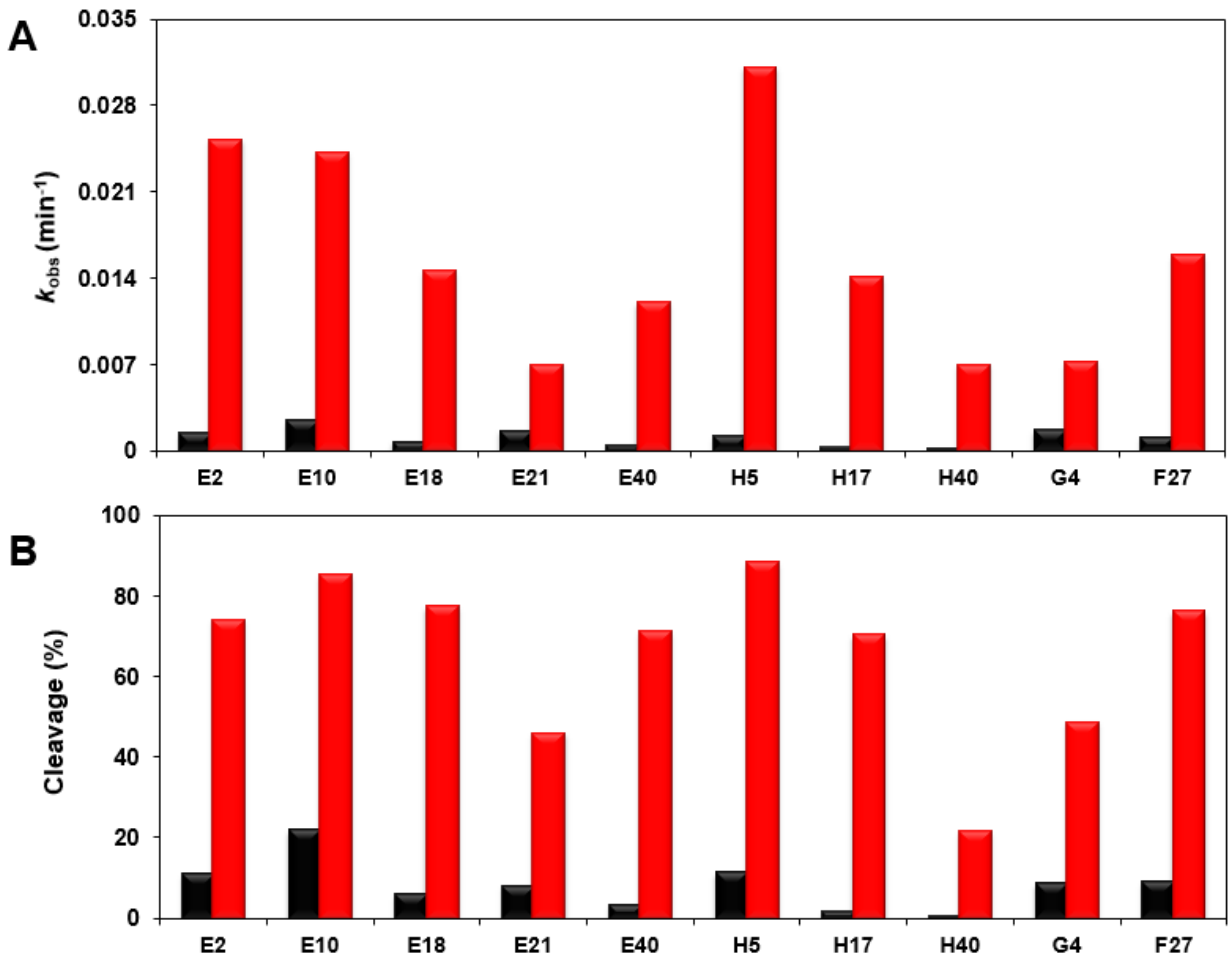

Figure 3.18 Activity of clones E2, E10, E18, E21, E40, H5, H17, H40, G4, and F27 with 10 (black bars) and 100 µM (red bars) Fe(II). (A) k_{obs} values for different clones. (B) Final cleavage product obtained over 2 h reaction time.

To explore Fe(II)-dependent activity of the most active clones with wider range of Fe(II) concentration, I tested E2, E10, E21, F27, G4, and H5 with 1 µM and 500 µM Fe(II). H5 clone showed highest rate of catalysis with 500 µM Fe(II) (Figure 3.19A) and E10 was found to be the most sensitive clone and showed highest activity with 1 µM Fe(II) (Figure 3.19B).

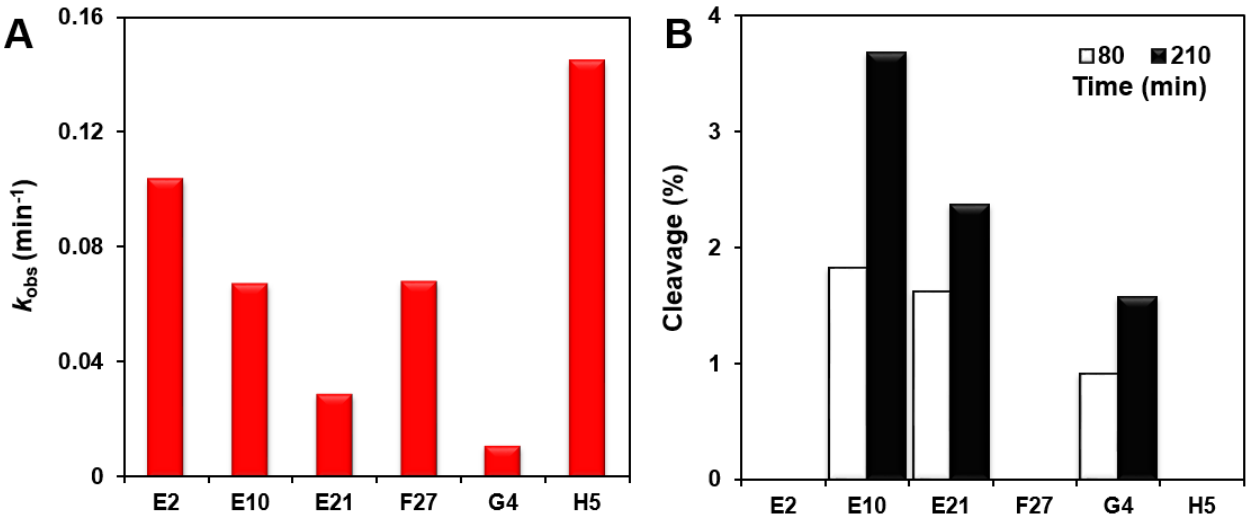

Figure 3.19 Activity and sensitivity of clones E2, E10, E21, F27, G4, and H5. (A) Obtained k_{obs} values for different clones with 500 µM Fe(II). (B) Cleavage activity of clones with 1 µM Fe(II).

In addition, selectivity of the 6 most active clones for Fe(II) over other competing divalent metal ions were tested. Each clone was incubated for 1 h with 100 µM Fe(II), Co^{2+}, Zn^{2+}, Mn^{2+}, Cd^{2+}, or Pb^{2+}. As shown in Figure 3.20, E21 (cluster IV) is the most selective clone for Fe(II) over other divalent metal ions. Altogether, highest and lowest activities were observed with Co^{2+} and Pb^{2+}, respectively. E21 clone belongs to cluster IV which members were mainly isolated from counter selected pools. This finding may suggest that carrying out counter selection improves selectivity. Although, it should be noted that catalytic rates of clones obtained from counter selected pools were relatively lower than other clones.

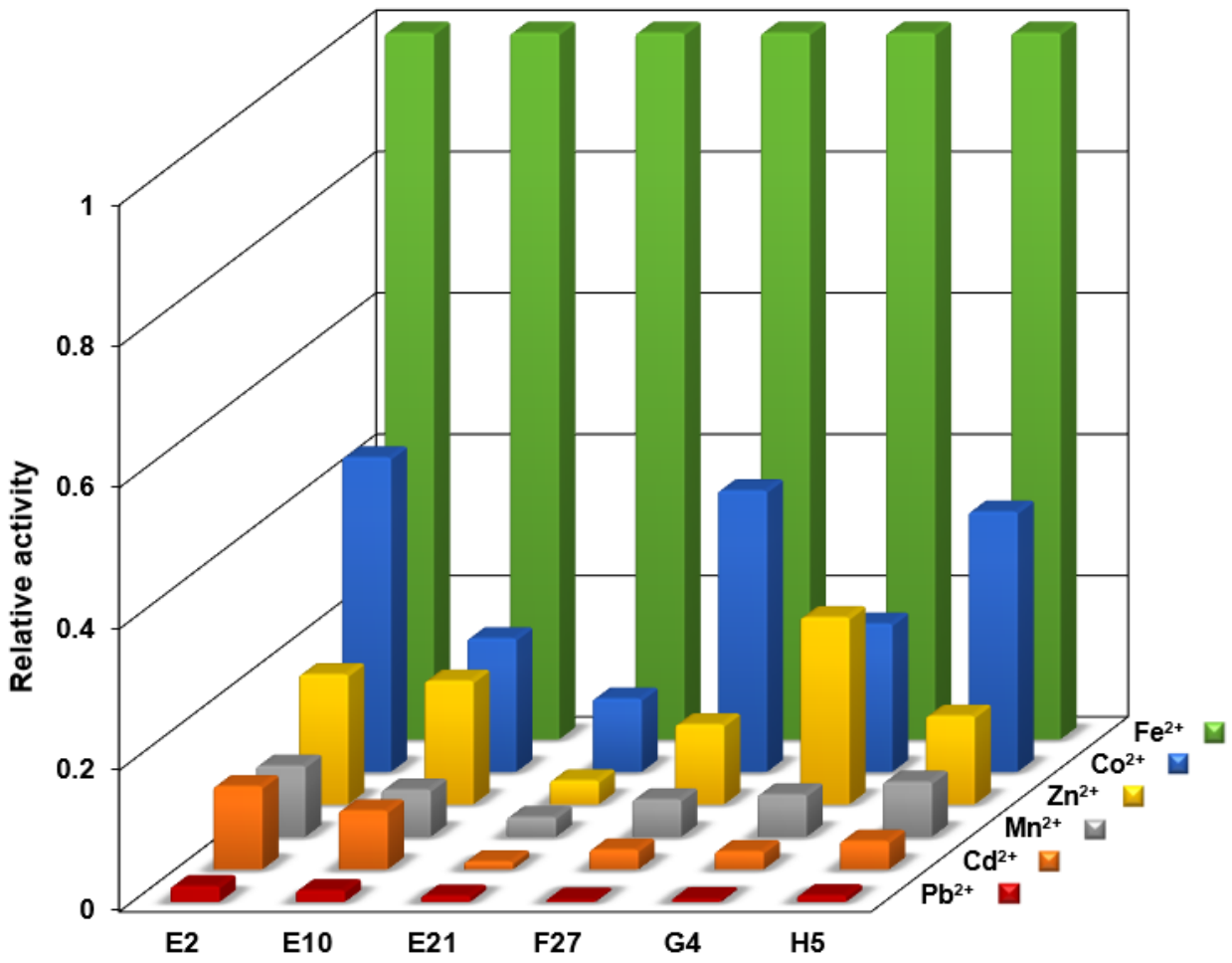

Figure 3.20 Activity of clones E2, E10, E21, F27, G4, and H5 with other metal ions. Normalized percent cleavage of different clones is depicted in the presence of 100 µM Co^{2+}, Zn^{2+}, Mn^{2+}, Cd^{2+}, or Pb^{2+} after 1 h in 25 mM Bis-Tris pH 7.0, 200 mM NaCl.

3.3.6 Secondary Structure and *Cis* to *Trans* Truncation

Fe(II) DNA random pool was designed with two pairing regions (Figure 3.2), intended to bring random region to the vicinity of the cleavage site. Sequence of one of these pairing regions was chosen from a library of thermodynamically stable tetraloops (*62*) to ensure formation of a stable stem loop which might ease prediction of secondary structures of isolated clones. Interestingly, out of the 6 most active clones found in the activity assays, only E10 was identified

with intact thermodynamically stable tetraloop (Figure 3.17A). Preference of active sequences to have a modified tetraloop or lose the designed tetraloop may indicate that the structurally constrained motif of a stable tetraloop was not in favor of catalytic activity. Secondary structure of *cis*-cleaving DNAzymes, predicted using UNAFold web package (*63*) are shown in Figure 3.21.

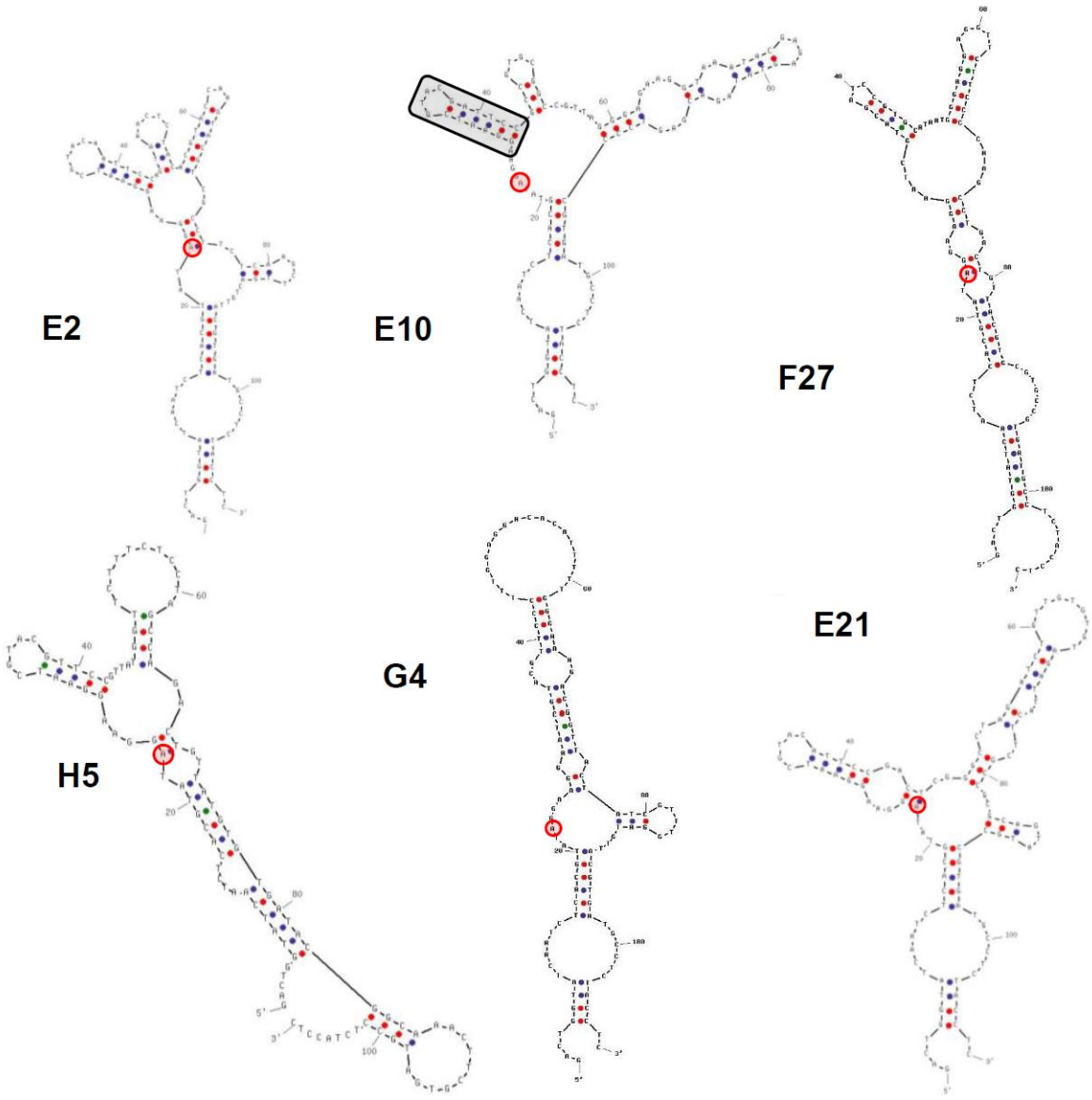

Figure 3.21 Predicted secondary structures for the 6 most active clones. Position of the rA cleavage site is circled in red. E10 is the only sequence which retained the stable tetraloop (boxed in black). Other sequences do not have the tetraloop or they contain a modified stem loop.

The first attempt to truncate *cis*-cleaving form of E2 and E10 was based on the design of the initial random pool. Both of the pairing regions were found in the predicted secondary structure of E10. Although E2 sequence was modified in the stable tetraloop region, a modified tetraloop was predicted to form relatively in the same position of the engineered stable tetraloop. Therefore, both DNAzymes were truncated at these two pairing region and converted to a *trans*-cleaving DNAzyme (E2-T1 and E10-T1). Both arms extended to increase the length of base pairing region to ensure the formation of a stable DNAzyme/substrate complex (Figure 3.22).

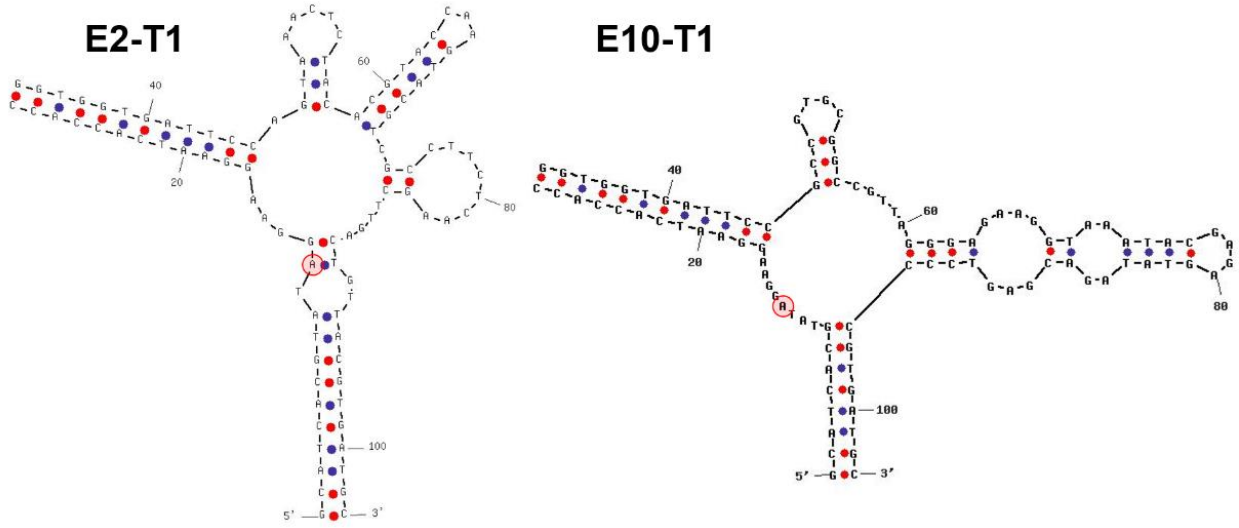

Figure 3.22 Predicted secondary structures for trans-cleaving DNAzymes E2-T1 and E10-T1. Position of the rA cleavage site is circled in red.

Activity of E2-T1 and E10-T1 DNAzymes were tested under single-turnover condition (DNAzyme/substrate ~ 200) with 1, 10, 100 and 500 µM Fe(II) in 25 mM Bis-Tris pH 7.0, 200 mM NaCl. 5′ end ^{32}P labeled substrates were annealed with DNAzymes by heating at 80 °C for 3 minutes and cooling down to the room temperature over 20 minutes. Reactions were started by addition of Fe(II) and quenched by mixing with stop solution at each time point. As shown in

Figure 3.23, both trans-cleaving DNAzymes were active, however, their activity was reduced significantly in comparison to *cis*-cleaving DNAzymes. This significant reduction in the activity of *trans*-cleaving DNAzymes in comparison to *cis*-versions suggests that a critical part of the DNAzymes were deleted upon truncation. I also found that increase in NaCl concentration up to 500 mM or addition of 2 mM $MgCl_2$ in the activity assay solution has no effect in improving activity of E2-T1 or E10-T1.

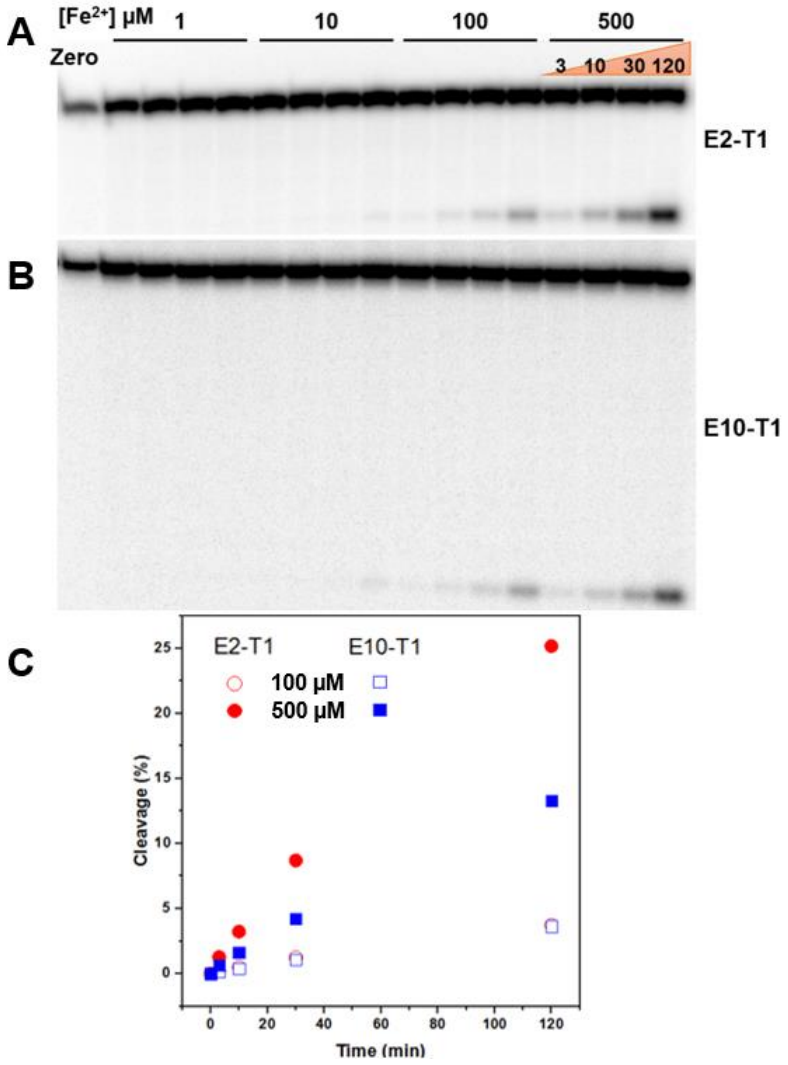

Figure 3.23 Activity of trans-cleaving E2-T1 and E10-T1 DNAzymes. Gel images of E2-T1 (A) and E10-T1 (B) activity assays with 1, 10, 100, and 500 µM Fe(II). (C) Analysis of cleavage percentage obtained in A and B.

In truncation studies, the goal is to find a loop which is not critical for the activity of the DNAzyme. Therefore, cutting this loop would separate DNAzyme from the substrate strand without loss of activity (*20, 67*). In contrast to E2 and E10 DNAzymes, which remained active after truncation, E21 and H5 truncation attempts failed to generate active *trans*-cleaving DNAzymes even when it was tested at 500 μM of Fe(II). To further investigate which loop can be truncated to form an active *trans*-cleaving DNAzyme, I studied truncations of E10, E21, and H5 systematically. Using UNAFold web package (*65*) and by varying different parameters such temperature, Na^+ concentration, etc., I tried to retrieve as many predicted secondary structures as possible. One main criterion considered was to screen predicted structures for potentially active ones and ignore the less likely structural conformation. Based on this criterion, I did not consider secondary structures that have the cleavage site folded back on itself or folded independent of the other half of the molecule as potentially active structures. Then, all predicted structures that could be truncated in the same way would be grouped in one structural class. Therefore, by finding all possible structural classes, different options will be identified for truncation and converting *cis*-cleaving DNAzyme to a *trans* version. Table 3.5 shows number of structural classes and their members for E2, E10, E21, and H5 DNAzymes. Different structural classes that were identified for E21 sequence are shown in Figure 3.24. In many cases, like E21, each class of structures have multiple truncation sites. I first started truncating from outside to delete as less as possible from the original sequence. After finding an active structural class, combination of different truncation sites were tested to find out shorter catalytic regions.

Table 3.5 Number of different structural classes and individual structures predicted by UNAFold web package. Each class represents at least one potential truncation site.

	E2	E10	E21	H5
Number of structural classes	5	6	7	5
Number of individual structures	42	27	31	16

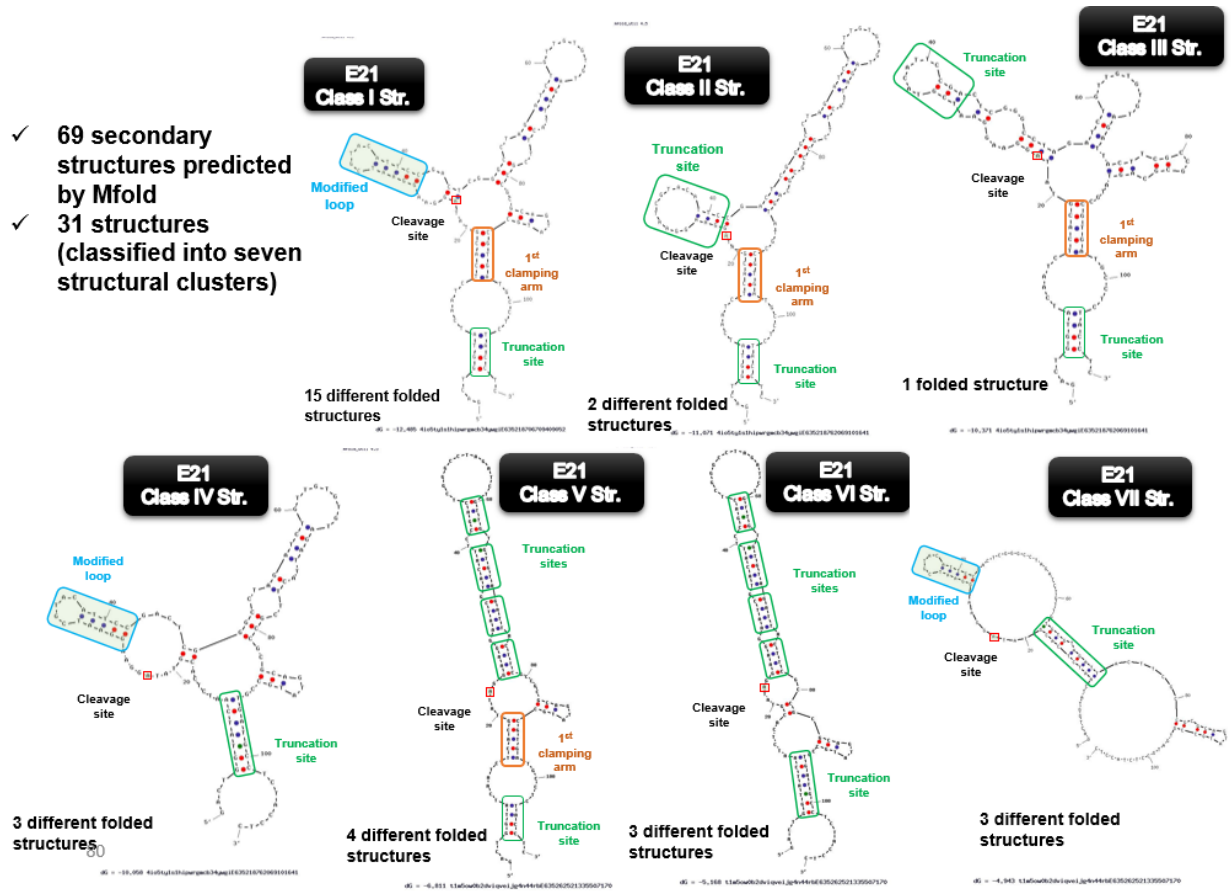

Figure 3.24 Different structural classes identified for E21. Out of 69 predicted secondary structures, 31 were classified into 7 different structural classes. Some classes (*i.e.* V and VI) have several potential truncation sites.

I identified active structural classes for E10, E21 and H5 and then converted all 3 *cis*-cleaving DNAzymes into *trans*-cleaving DNAzymes with similar catalytic activity to their original sequences. Substrate arms were extended to ensure formation of stable DNAzyme/substrate complex. Predicted secondary structures of E10, E21, and H5 *trans*-cleaving DNAzymes are shown on Figure 3.25. One common feature in all three DNAzymes is having a relatively long substrate.

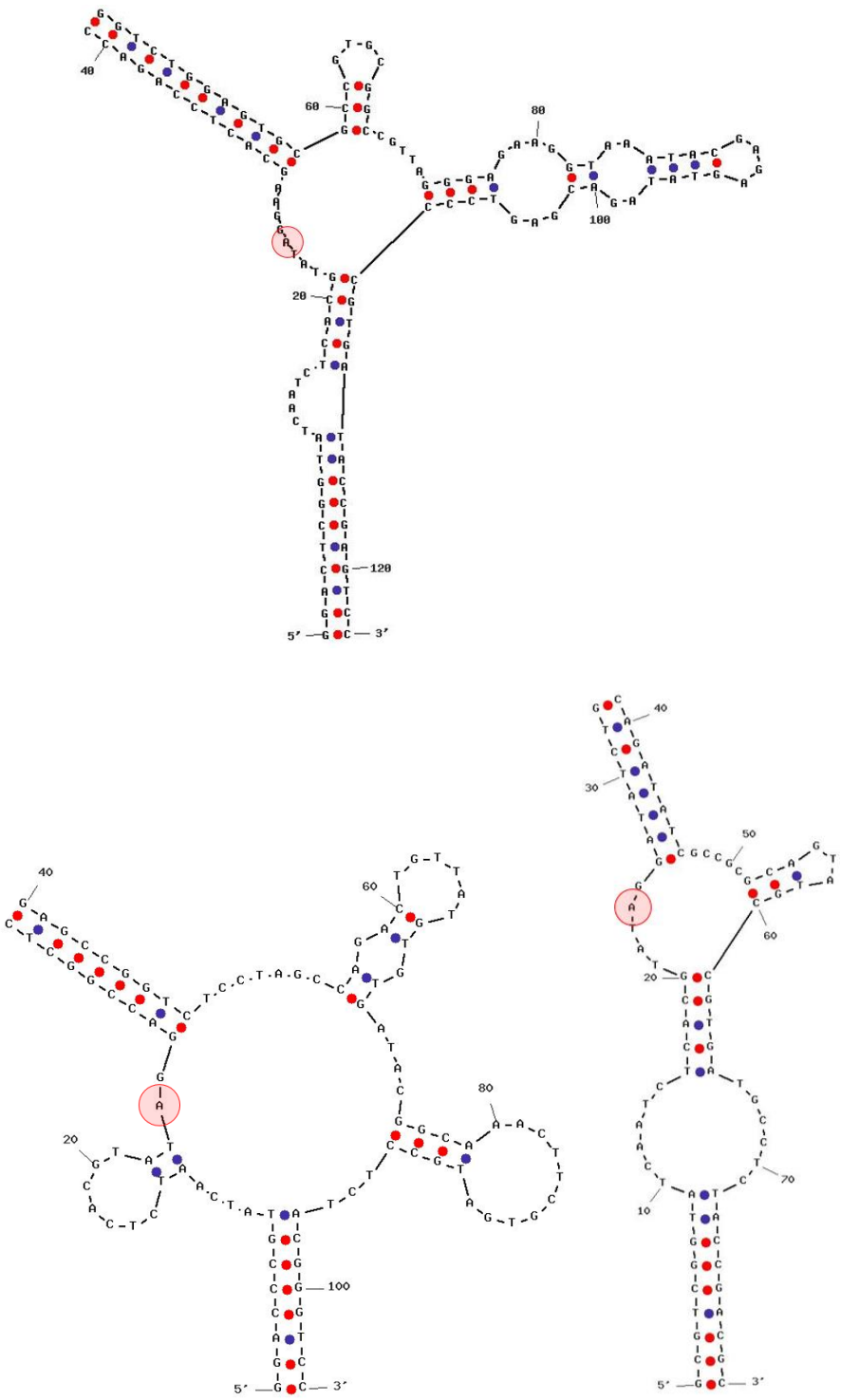

Figure 3.25 Secondary structure of *trans*-cleaving Fe(II) DNAzymes. E10 (top), E21 (bottom right) and H5 (bottom left).

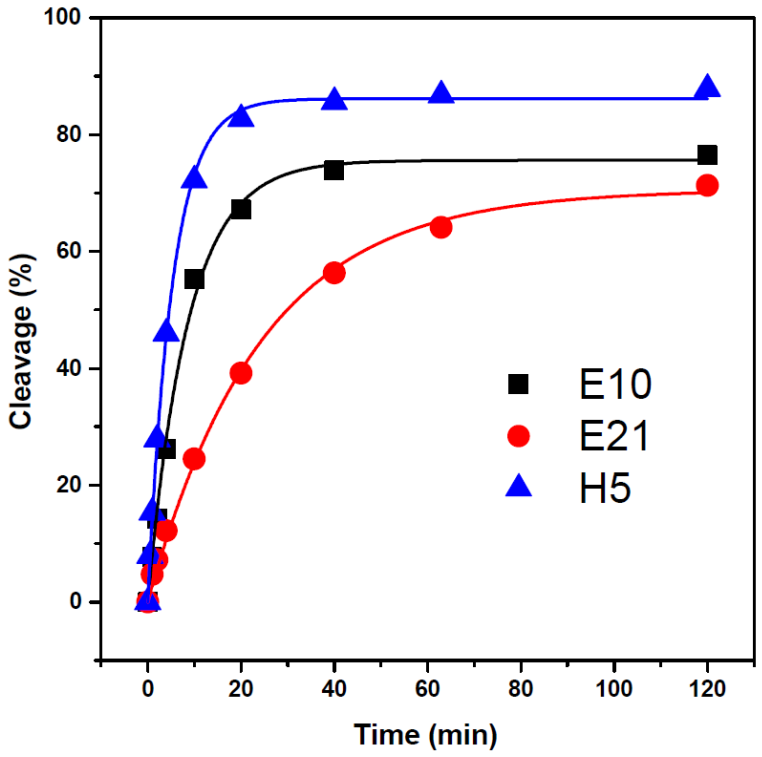

Figure 3.26 Activity of *trans*-cleaving E10, E21, and H5 DNAzymes. Cleavage percentage were monitored with 500 µM Fe(II) in 25 mM Bis-Tris pH 7.0 and 200 mM NaCl. Rate of catalysis for E10, E21, and H5 was calculated to be 0.11, 0.04, and 0.20 min^{-1}, respectively.

3.3.7 H5 DNAzyme Characterization

3.3.7.1 Choice of Cleavage Site

Since H5 was the most active Fe(II)-dependent trans-cleaving DNAzyme identified, it was chosen for further characterizations. It was shown that RNA-cleaving DNAzymes prefer certain ribonucleotide as their cleavage site (*68, 69*). Fe(II)-dependent DNAzymes were selected with a random pool designed with a single rA as the cleavage site. To find out whether H5 DNAzyme can catalyze cleavage of other ribonucleotides in the cleavage site, I tested the cleavage of substrates with ribocytosine (rC), riboguanosine (rG), or ribouridine (rU) as their cleavage sites. Cleavage rate of all ^{32}P end labeled substrates were tested under single-turnover condition (Figure

3.27). It was found that H5 was able to cleave all four possible ribonucleotides in the cleavage with higher preference for rA, which was originally used in the selection (rA>>rU>rG>>rC). In addition I tested the ability of H5 to cleave all RNA substrate. Interestingly, I observed that H5 cleaved all RNA substrate efficiently (only 7-fold slower than the chimeric wild type substrate). RNA-cleaving DNAzymes that have been selected to cleave RNA/DNA chimeric substrates, can cleave all RNA substrate very inefficiently with catalytic rate ~ 1000-fold slower than the rate of cleaving wild type substrate (*20*, *70*).

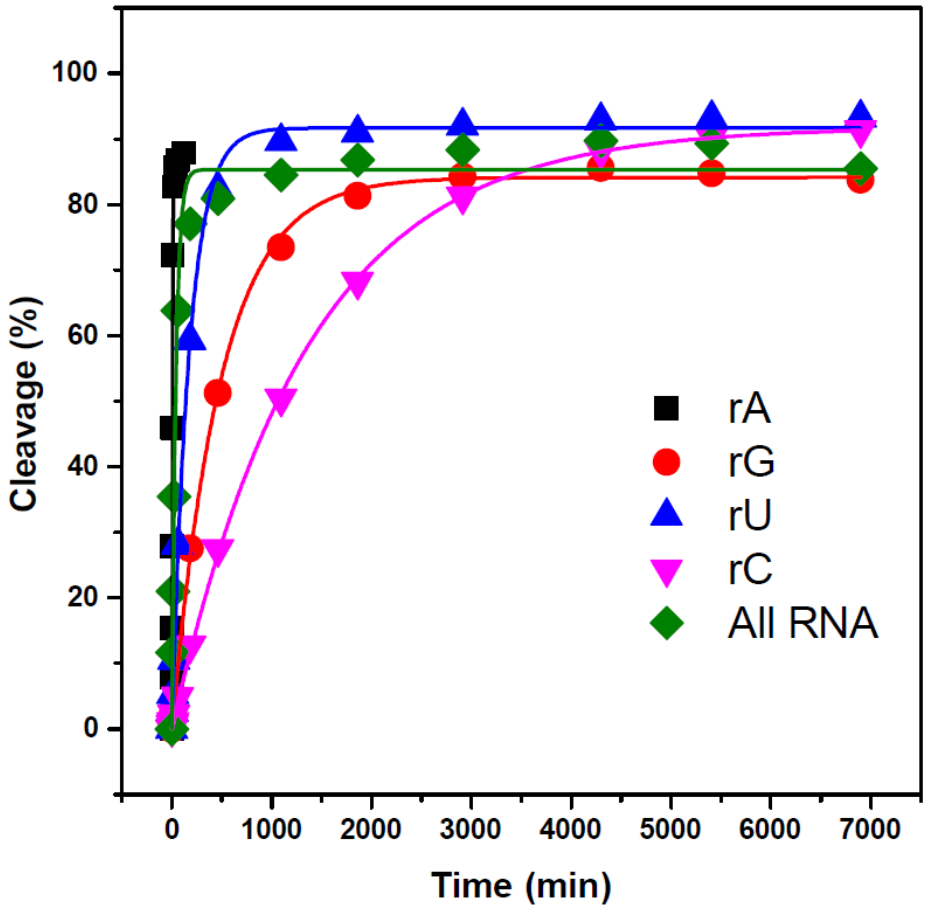

Figure 3.27 Effect of ribonucleotide identity on cleavage rate of H5 DNAzyme. Cleavage percentage were monitored with 500 µM Fe(II) in 25 mM Bis-Tris pH 7.0 and 200 mM NaCl. Rate of catalysis for rA, rG, rU, rC, and all RNA substrate was calculated to be 0.20, 0.002, 0.006, 0.0007, and 0.03 min^{-1}, respectively.

3.3.7.2 Effect of pH on Activity

The dependence of reaction rate (k_{obs}) on pH (pH/log k_{obs} profile) in the presence of 100 µM Fe(II) was studied in two different buffers spanning a range of pH from 5.5 to 7.0 under single-turnover conditions. Studying pH/catalytic activity profile of DNAzymes reveals whether chemical-cleavage or conformational change is the rate limiting step (*71*, *72*). As shown in Figure 3.28, the log value of k_{obs} increased linearly with a slope of 1.2 and 1.1 as pH increased for H5 and E10, respectively. Obtaining the slope of unity in pH profile of E10 and H5 suggests that the rate-limiting step of the reaction is cleavage step and the obtained k_{obs} represents the rate of the chemical cleavage (*73*).

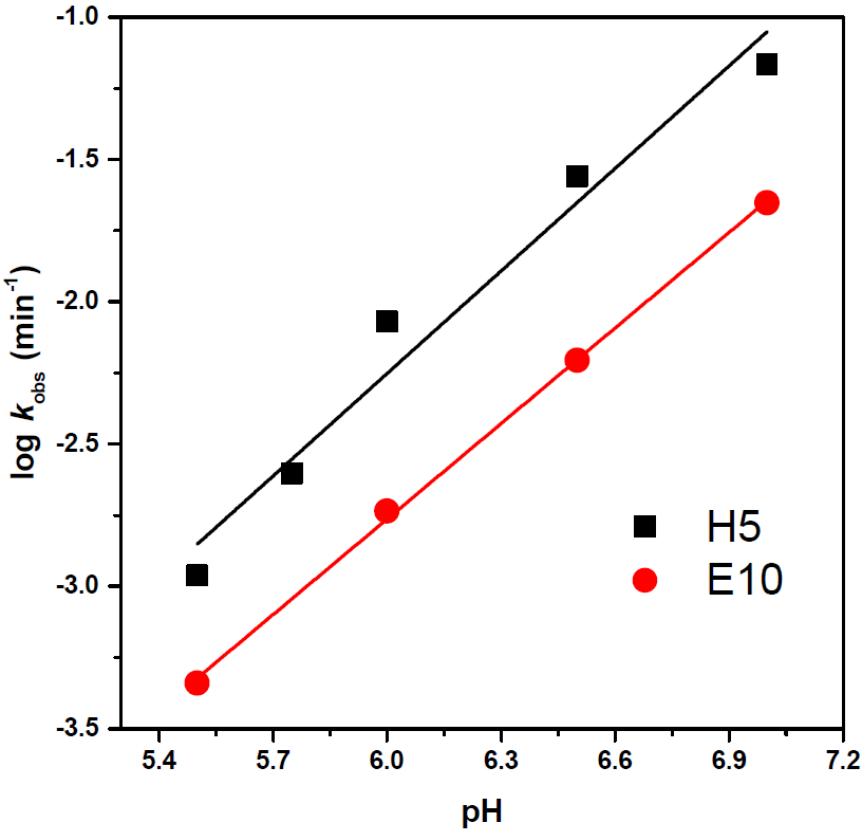

Figure 3.28 Effect of pH on the activity of E10 and H5 DNAzymes. Cleavage rate was obtained with 100 µM Fe(II) in 25 mM sodium acetate pH 5.5 or 5.75, Bis-Tris pH 6.0, 6.5, or 7.0 and 200 mM NaCl.

3.3.7.3 Activity of H5 DNAzyme in Cell Lysate

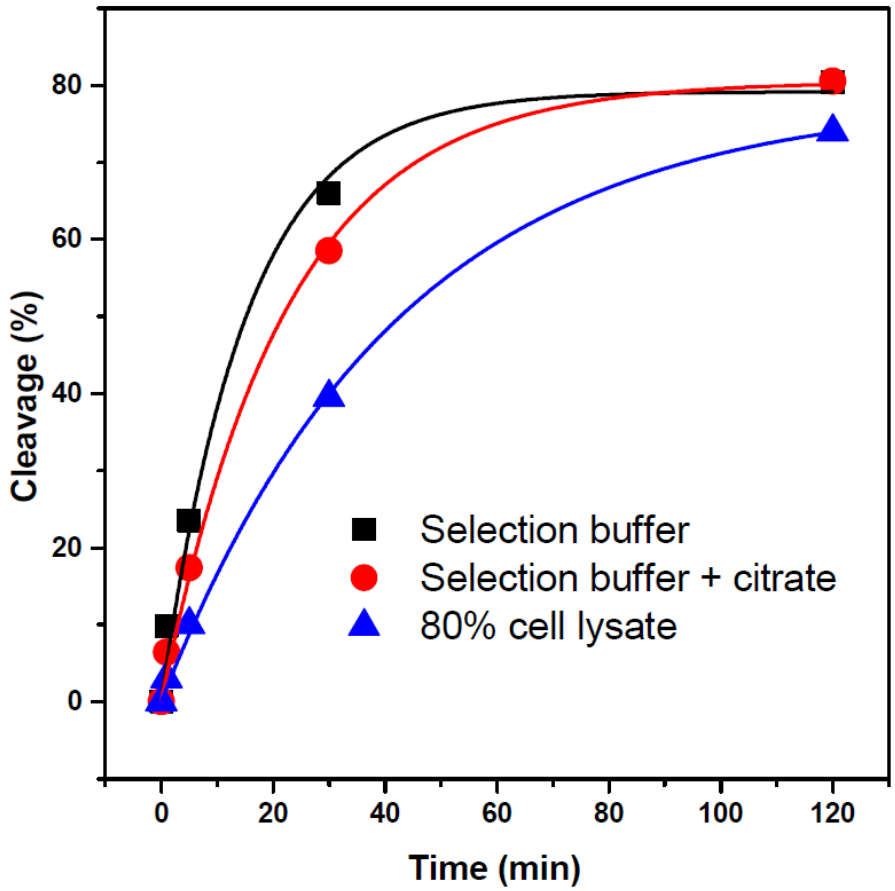

Figure 3.29 Activity of H5 DNAzyme in the presence of citrate and 80% human cell lysate. Cleavage rate was obtained with 100 µM Fe(II) in selection buffer (25 mM Bis-Tris pH 7.0 and 200 mM NaCl) or selection buffer and 50 µM citrate or 80% human cell lysate.

Iron is the most abundant transition metal in the body and plays a critical role in a variety of biological processes such as respiration, energy metabolism, DNA synthesis, immunity, and pathogenesis (*28-30*). Therefore, we were interested to explore the possibility of using Fe(II)-dependent DNAzymes as Fe(II) sensor by testing the activity of H5 DNAzyme in the presence of cell lysate or citrate which is known to be one the most potent and highly abundant cellular chelators (*52*). Fe(II)-dependent activity of H5 was tested with 100 µM Fe(II) in the presence of citrate as well as in 80% human cell lysate and compared to the DNAzyme activity in selection

buffer. Cleavage activity of the H5 DNAzyme was monitored under single-turnover condition by using ^{32}P labeled substrate. As shown in Figure 3.29, no significant change was observed by addition of citrate. Minimum interference by citrate suggests that H5 DNAzyme could potentially sense intracellular labile iron. In agreement with citrate interference study, H5 remained active with Fe(II) in 80% human cell lysate and no significant interference with Fe(II)-dependent activity was observed from cell lysate components (Figure 3.29).

3.3.7.4 Fe(III) Interference

To investigate the ability of the H5 DNAzyme in sensing Fe(II) and distinguishing the reduced oxidation of iron from Fe(III), I tested Fe(II)-dependent cleavage activity of H5 in a mixture containing both Fe(II) and Fe(III). No cleavage activity was observed at pH 7.0 with Fe(III) when H5 incubated with 20 µM Fe(III). In addition, no significant change observed in the Fe(II)-dependent activity of H5 when Fe(III) was also present in the solution. Since Fe(III) solubility decreases significantly by increase in pH, lack of H5 activity with Fe(III) might be due to the unavailability of Fe(III) at neutral pH. To address this issue, I tested activity of the H5 DNAzyme at a pH and condition in which Fe(III)-dependent DNAzyme is active. Therefore, unavailability of Fe(III) is no longer an issue. Fe(III)-dependent DNAzyme was shown to be active with 20 µM Fe(III) in 20 mM acetate buffer pH 6.0, 5 mM Bis-Tris and 200 mM NaCl. As shown in Figure 3.30, the H5 DNAzyme activity with 100 µM Fe(II) did not change by addition of 20 µM Fe(III). In addition, no activity observed with 20 µM Fe(III). These results, suggests that the H5 DNAzyme can distinguish two different oxidation states of iron, is selective for Fe(II) over Fe(III), and detect Fe(II) in a mixture of both oxidation states with minimal interference from Fe(III).

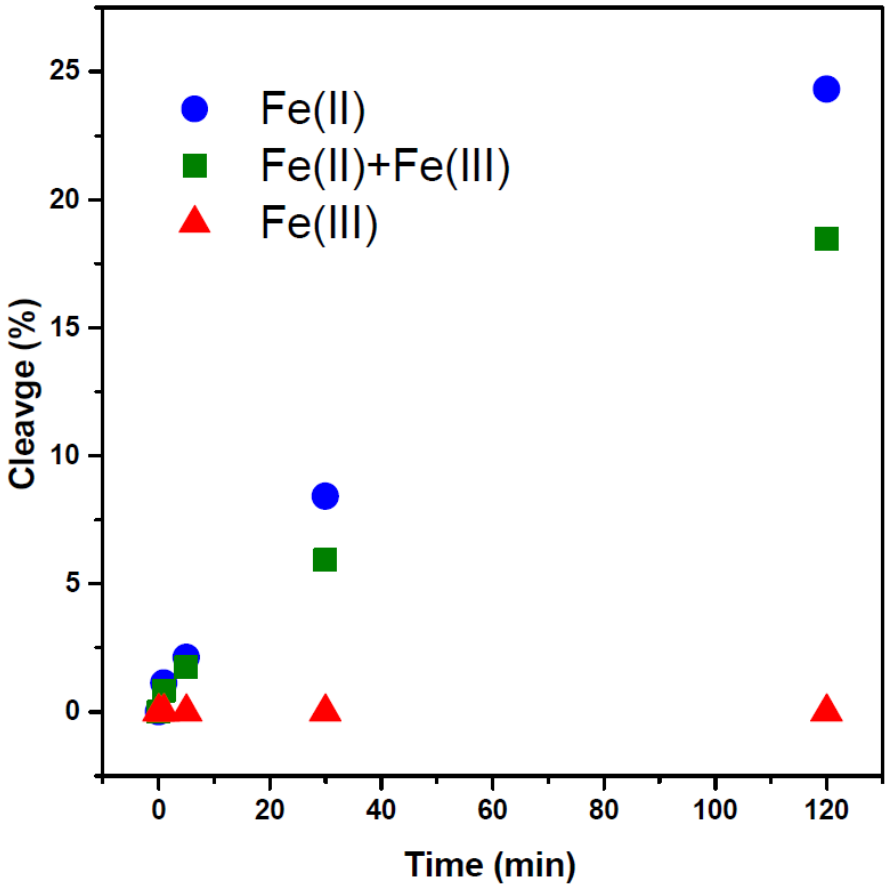

Figure 3.30 Activity of H5 DNAzyme in the presence of Fe(III). Cleavage reaction monitored with 100 µM Fe(II) in 20 mM acetate buffer pH 6.0, 5 mM Bis-Tris and 200 mM NaCl in the presence or absence of 20 µM Fe(III). No cleavage caused by 20 µM Fe(III) (red triangles).

3.4 Conclusions

Four *in vitro* selection conditions were carried out using Fe(II) as a cofactor in order to isolate Fe(II)-dependent RNA-cleaving DNAzymes. To avoid Fe(III) contamination, all four selections were performed under oxygen free environment. Two out of four conditions were performed by introducing counter selection steps before each positive selection. All four selections carried out for 9 rounds and resulted in active pool with Fe(II)-dependent cleavage activity. Activity assay experiments in combination with selection results were used to identify the most active library form each selection for cloning and sequencing experiments.

149 sequences were obtained from the four selections, and grouped into seven major clusters based on their sequence similarity. Screening experiments were used to identify the most active clones for further analysis. Interestingly, stable tetraloop which was engineered in the design of the initial pool, was modified in majority of the active sequences, including H5 DNAzyme. The most active clones were from highly populated clusters and none of unclustered sequences showed activity. Primary truncation attempts based on the design of initial random pool and the secondary structures predicted by UNAFold failed to convert active *cis*-cleaving DNAzymes into a *trans*-cleaving version for biosensor applications. Systematic structural search and classification strategy was used to identify active secondary structures to convert them into a *trans*-cleaving DNAzymes. E10, E21 and H5 *trans*-cleaving DNAzymes were designed and tested for activity with Fe(II). The H5 DNAzyme, the most active sequence, was also observed to have high activity (~ 0.2 min^{-1}) with 500 µM Fe(II) at pH 7.0. This *trans*-cleaving DNAzyme was used for further characterization.

The H5 DNAzyme was observed to have a linear pH profile in a range from 5.5 to 7.0 with a slope close to unity. It was observed that all ribonucleotides can be used in the cleavage site, although rA which was originally used in the selection is preferred over other ribonucleotides.

Interestingly, cleavage of all RNA substrate was efficiently catalyzed by the H5 DNAzyme with cleavage rate only ~7-fold slower than the wild type DNA/RNA chimeric substrate. No significant interference was found when Fe(II)-dependent cleavage activity was tested in the presence of citrate as well as in 80% human cell lysate. In addition, H5 was able to distinguish Fe(II) from Fe(III) and catalyze cleavage reaction in the presence of a mixture of both Fe(II) and Fe(III) with minimal interference. Our results show that the H5 Fe(II)-dependent DNAzyme has all the criteria required for a selective and sensitive DNAzyme-based Fe(II) sensor for biological applications such as intracellular imaging.

3.5 References

1. Breaker, R. R., and Joyce, G. F. (1994) A DNA enzyme that cleaves RNA, *Chem Biol 1*, 223-229.

2. Silverman, S. K. (2008) Catalytic DNA (deoxyribozymes) for synthetic applications-current abilities and future prospects, *Chem Commun (Camb)*, 3467-3485.

3. Franzen, S. (2010) Expanding the catalytic repertoire of ribozymes and deoxyribozymes beyond RNA substrates, *Curr Opin Mol Ther 12*, 223-232.

4. Chu, C. C., Wong, O. Y., and Silverman, S. K. (2014) A generalizable DNA-catalyzed approach to peptide-nucleic acid conjugation, *Chembiochem 15*, 1905-1910.

5. Chandrasekar, J., and Silverman, S. K. (2013) Catalytic DNA with phosphatase activity, *Proc Natl Acad Sci U S A 110*, 5315-5320.

6. Silverman, S. K. (2010) DNA as a versatile chemical component for catalysis, encoding, and stereocontrol, *Angew Chem Int Ed Engl 49*, 7180-7201.

7. Chandra, M., Sachdeva, A., and Silverman, S. K. (2009) DNA-catalyzed sequence-specific hydrolysis of DNA, *Nat Chem Biol 5*, 718-720.

8. Silverman, S. K. (2005) In vitro selection, characterization, and application of deoxyribozymes that cleave RNA, *Nucleic Acids Res 33*, 6151-6163.

9. Stoltenburg, R., Reinemann, C., and Strehlitz, B. (2007) SELEX--a (r)evolutionary method to generate high-affinity nucleic acid ligands, *Biomol Eng 24*, 381-403.

10. Shamah, S. M., Healy, J. M., and Cload, S. T. (2008) Complex target SELEX, *Acc Chem Res 41*, 130-138.

11. Tuerk, C., and Gold, L. (1990) Systematic evolution of ligands by exponential enrichment: RNA ligands to bacteriophage T4 DNA polymerase, *Science 249*, 505-510.

12. Sen, D., and Geyer, C. R. (1998) DNA enzymes, *Curr Opin Chem Biol 2*, 680-687.

13. Wilson, D. S., and Szostak, J. W. (1999) In vitro selection of functional nucleic acids, *Annu Rev Biochem 68*, 611-647.

14. Zhang, X. B., Kong, R. M., and Lu, Y. (2011) Metal ion sensors based on DNAzymes and related DNA molecules, *Annu Rev Anal Chem (Palo Alto Calif) 4*, 105-128.

15. Xiang, Y., and Lu, Y. (2014) DNA as sensors and imaging agents for metal ions, *Inorg Chem 53*, 1925-1942.

16. Lan, T., and Lu, Y. (2012) Metal ion-dependent DNAzymes and their applications as biosensors, *Met Ions Life Sci 10*, 217-248.

17. Cairns, M. J., Saravolac, E. G., and Sun, L. Q. (2002) Catalytic DNA: a novel tool for gene suppression, *Curr Drug Targets 3*, 269-279.

18. Santoro, S. W., and Joyce, G. F. (1997) A general purpose RNA-cleaving DNA enzyme, *Proceedings of the National Academy of Sciences of the United States of America 94*, 4262-4266.

19. Faulhammer, D., and Famulok, M. (1997) Characterization and divalent metal-ion dependence of in vitro selected deoxyribozymes which cleave DNA/RNA chimeric oligonucleotides, *Journal of molecular biology 269*, 188-202.

20. Li, J., Zheng, W., Kwon, A. H., and Lu, Y. (2000) In vitro selection and characterization of a highly efficient Zn(II)-dependent RNA-cleaving deoxyribozyme, *Nucleic acids research 28*, 481-488.

21. Faulhammer, D., and Famulok, M. (1996) The Ca2+ Ion as a Cofactor for a Novel RNA-Cleaving Deoxyribozyme, *Angewandte Chemie International Edition in English 35*, 2837-2841.

22. Brown, A. K., Li, J., Pavot, C. M., and Lu, Y. (2003) A lead-dependent DNAzyme with a two-step mechanism, *Biochemistry 42*, 7152-7161.

23. Liu, J., Brown, A. K., Meng, X., Cropek, D. M., Istok, J. D., Watson, D. B., and Lu, Y. (2007) A catalytic beacon sensor for uranium with parts-per-trillion sensitivity and millionfold selectivity, *Proceedings of the National Academy of Sciences of the United States of America 104*, 2056-2061.

24. Carmi, N., and Breaker, R. R. (2001) Characterization of a DNA-cleaving deoxyribozyme, *Bioorg Med Chem 9*, 2589-2600.

25. Bruesehoff, P. J., Li, J., Augustine, A. J., 3rd, and Lu, Y. (2002) Improving metal ion specificity during in vitro selection of catalytic DNA, *Comb Chem High Throughput Screen 5*, 327-335.

26. Nelson, K. E., Ihms, H. E., Mazumdar, D., Bruesehoff, P. J., and Lu, Y. (2012) The importance of peripheral sequences in determining the metal selectivity of an in vitro-selected Co(2+) -dependent DNAzyme, *Chembiochem 13*, 381-391.

27. Huang, P. J., Vazin, M., and Liu, J. (2014) In Vitro Selection of a New Lanthanide-Dependent DNAzyme for Ratiometric Sensing Lanthanides, *Anal Chem 86*, 9993-9999.

28. Weinberg, E. D. (2007) Iron loading in humans: A risk factor for enhanced morbidity and mortality, *Journal of Nutritional and Environmental Medicine 16*, 43-51.

29. Stadler, N., Lindner, R. A., and Davies, M. J. (2004) Direct detection and quantification of transition metal ions in human atherosclerotic plaques: evidence for the presence of elevated levels of iron and copper, *Arterioscler Thromb Vasc Biol 24*, 949-954.

30. Hasinoff, B. B. (2003) The intracellular iron sensor calcein is catalytically oxidatively degraded by iron(II) in a hydrogen peroxide-dependent reaction, *J Inorg Biochem 95*, 157-164.

31. Andrews, N. C. (2008) Forging a field: the golden age of iron biology, *Blood 112*, 219-230.

32. Hanahan, D., and Weinberg, R. A. (2011) Hallmarks of cancer: the next generation, *Cell 144*, 646-674.

33. Chifman, J., Kniss, A., Neupane, P., Williams, I., Leung, B., Deng, Z., Mendes, P., Hower, V., Torti, F. M., Akman, S. A., Torti, S. V., and Laubenbacher, R. (2012) The core control system of intracellular iron homeostasis: a mathematical model, *J Theor Biol 300*, 91-99.

34. Torti, S. V., and Torti, F. M. (2013) Iron and cancer: more ore to be mined, *Nat Rev Cancer 13*, 342-355.

35. Elmberg, M., Hultcrantz, R., Ekbom, A., Brandt, L., Olsson, S., Olsson, R., Lindgren, S., Loof, L., Stal, P., Wallerstedt, S., Almer, S., Sandberg-Gertzen, H., and Askling, J. (2003) Cancer risk in patients with hereditary hemochromatosis and in their first-degree relatives, *Gastroenterology 125*, 1733-1741.

36. Coleman, P. G. (1991) Ageing and life history: the meaning of reminiscence in late life, *Sociol Rev Monogr*, 120-143.

37. Nilsson, U. A., Bassen, M., Savman, K., and Kjellmer, I. (2002) A simple and rapid method for the determination of "free" iron in biological fluids, *Free Radic Res 36*, 677-684.

38. Whyte, J. F., and Thistle, N. A. (1976) Male incontinence: the inside story on external collection, *Nursing 6*, 66-67.

39. Ayene, I. S., Koch, C. J., and Krisch, R. E. (2007) DNA strand breakage by bivalent metal ions and ionizing radiation, *Int J Radiat Biol 83*, 195-210.

40. Bhatt, K. D., Gupte, H. S., Makwana, B. A., Vyas, D. J., Maity, D., and Jain, V. K. (2012) Calix receptor edifice; scrupulous turn off fluorescent sensor for Fe(III), Co(II) and Cu(II), *J Fluoresc 22*, 1493-1500.

41. Carter, K. P., Young, A. M., and Palmer, A. E. (2014) Fluorescent sensors for measuring metal ions in living systems, *Chem Rev 114*, 4564-4601.

42. Petrat, F., de Groot, H., and Rauen, U. (2000) Determination of the chelatable iron pool of single intact cells by laser scanning microscopy, *Arch Biochem Biophys 376*, 74-81.

43. Praveen, L., Reddy, M. L. P., and Varma, R. L. (2010) Dansyl-styrylquinoline conjugate as divalent iron sensor, *Tetrahedron Letters 51*, 6626-6629.

44. Chen, J. L., Zhuo, S. J., Wu, Y. Q., Fang, F., Li, L., and Zhu, C. Q. (2006) High selective determination iron(II) by its enhancement effect on the fluorescence of pyrene-tetramethylpiperidinyl (TEMPO) as a spin fluorescence probe, *Spectrochim Acta A Mol Biomol Spectrosc 63*, 438-443.

45. Garcia-Beltran, O., Mena, N., Yanez, O., Caballero, J., Vargas, V., Nunez, M. T., and Cassels, B. K. (2013) Design, synthesis and cellular dynamics studies in membranes of a new coumarin-based "turn-off" fluorescent probe selective for Fe2+, *Eur J Med Chem 67*, 60-63.

46. Au-Yeung, H. Y., Chan, J., Chantarojsiri, T., and Chang, C. J. (2013) Molecular imaging of labile iron(II) pools in living cells with a turn-on fluorescent probe, *J Am Chem Soc 135*, 15165-15173.

47. Hirayama, T., Okuda, K., and Nagasawa, H. (2013) A highly selective turn-on fluorescent probe for iron(ii) to visualize labile iron in living cells, *Chemical Science 4*, 1250-1256.

48. Carter, K. P., Young, A. M., and Palmer, A. E. (2014) Fluorescent Sensors for Measuring Metal Ions in Living Systems, *Chemical Reviews 114*, 4564-4601.

49. OuYang, H., Gao, Y., and Yuan, Y. (2013) A highly selective rhodamine-based optical–electrochemical multichannel chemosensor for Fe3+, *Tetrahedron Letters 54*, 2964-2966.

50. Williams, K. P., and Bartel, D. P. (1995) PCR product with strands of unequal length, *Nucleic Acids Res 23*, 4220-4221.

51. Tesfaldet, Z. O., van Staden, J. F., and Stefan, R. I. (2004) Sequential injection spectrophotometric determination of iron as Fe(II) in multi-vitamin preparations using 1,10-phenanthroline as complexing agent, *Talanta 64*, 1189-1195.

52. Krom, B. P., Warner, J. B., Konings, W. N., and Lolkema, J. S. (2000) Complementary metal ion specificity of the metal-citrate transporters CitM and CitH of Bacillus subtilis, *J Bacteriol 182*, 6374-6381.

53. Welch, K. D., Davis, T. Z., and Aust, S. D. (2002) Iron autoxidation and free radical generation: effects of buffers, ligands, and chelators, *Arch Biochem Biophys 397*, 360-369.

54. Petrat, F., Paluch, S., Dogruoz, E., Dorfler, P., Kirsch, M., Korth, H. G., Sustmann, R., and de Groot, H. (2003) Reduction of Fe(III) ions complexed to physiological ligands by lipoyl dehydrogenase and other flavoenzymes in vitro: implications for an enzymatic reduction of Fe(III) ions of the labile iron pool, *J Biol Chem 278*, 46403-46413.

55. Hsieh, Y. H., and Hsieh, Y. P. (2000) Kinetics of Fe(III) reduction by ascorbic acid in aqueous solutions, *J Agric Food Chem 48*, 1569-1573.

56. Hsieh, Y. H. P., and Hsieh, Y. P. (1997) Valence State of Iron in the Presence of Ascorbic Acid and Ethylenediaminetetraacetic Acid, *Journal of Agricultural and Food Chemistry 45*, 1126-1129.

57. Hider, R. C., and Kong, X. (2013) Iron speciation in the cytosol: an overview, *Dalton Trans 42*, 3220-3229.

58. Hider, R. C., and Kong, X. L. (2011) Glutathione: a key component of the cytoplasmic labile iron pool, *Biometals 24*, 1179-1187.

59. Konigsberger, L. C., Konigsberger, E., May, P. M., and Hefter, G. T. (2000) Complexation of iron(III) and iron(II) by citrate. Implications for iron speciation in blood plasma, *J Inorg Biochem 78*, 175-184.

60. Breaker, R. R., and Joyce, G. F. (1995) A DNA enzyme with Mg(2+)-dependent RNA phosphoesterase activity, *Chem Biol 2*, 655-660.

61. Carrigan, M. A., Ricardo, A., Ang, D. N., and Benner, S. A. (2004) Quantitative Analysis of a RNA-Cleaving DNA Catalyst Obtained via in Vitro Selection†, *Biochemistry 43*, 11446-11459.

62. Nakano, M., Moody, E. M., Liang, J., and Bevilacqua, P. C. (2002) Selection for thermodynamically stable DNA tetraloops using temperature gradient gel electrophoresis reveals four motifs: d(cGNNAg), d(cGNABg),d(cCNNGg), and d(gCNNGc), *Biochemistry 41*, 14281-14292.

63. Markham, N. R., and Zuker, M. (2008) UNAFold: software for nucleic acid folding and hybridization, *Methods in molecular biology 453*, 3-31.

64. Markham, N. R., and Zuker, M. (2005) DINAMelt web server for nucleic acid melting prediction, *Nucleic acids research 33*, W577-581.

65. Atkinson, H. J., Morris, J. H., Ferrin, T. E., and Babbitt, P. C. (2009) Using sequence similarity networks for visualization of relationships across diverse protein superfamilies, *PLoS One 4*, e4345.

66. Apeltsin, L., Morris, J. H., Babbitt, P. C., and Ferrin, T. E. (2011) Improving the quality of protein similarity network clustering algorithms using the network edge weight distribution, *Bioinformatics 27*, 326-333.

67. Ihms, H. E., and Lu, Y. (2012) In vitro selection of metal ion-selective DNAzymes, *Methods in molecular biology 848*, 297-316.

68. Cruz, R. P., Withers, J. B., and Li, Y. (2004) Dinucleotide junction cleavage versatility of 8-17 deoxyribozyme, *Chem Biol 11*, 57-67.

69. Schlosser, K., Gu, J., Sule, L., and Li, Y. (2008) Sequence-function relationships provide new insight into the cleavage site selectivity of the 8-17 RNA-cleaving deoxyribozyme, *Nucleic Acids Res 36*, 1472-1481.

70. Ota, N., Warashina, M., Hirano, K., Hatanaka, K., and Taira, K. (1998) Effects of helical structures formed by the binding arms of DNAzymes and their substrates on catalytic activity, *Nucleic Acids Res 26*, 3385-3391.

71. Dahm, S. C., Derrick, W. B., and Uhlenbeck, O. C. (1993) Evidence for the role of solvated metal hydroxide in the hammerhead cleavage mechanism, *Biochemistry 32*, 13040-13045.

72. Zhou, D. M., Zhang, L. H., and Taira, K. (1997) Explanation by the double-metal-ion mechanism of catalysis for the differential metal ion effects on the cleavage rates of 5'-oxy and 5'-thio substrates by a hammerhead ribozyme, *Proc Natl Acad Sci U S A 94*, 14343-14348.

73. Knitt, D. S., and Herschlag, D. (1996) pH dependencies of the Tetrahymena ribozyme reveal an unconventional origin of an apparent pKa, *Biochemistry 35*, 1560-1570.

4 Chapter 4. *In vitro* selection of Na^+-dependent DNAzymes

4.1 Introduction

Metal ions play crucial roles in a variety of biochemical processes. As a result, the concentrations of cellular metal ions have to be highly regulated in different parts of cells, as both deficiency and surplus of metal ions can disrupt normal function (1-4). In order to better understand the functions of metal ions in biology, it is important to detect metal ions selectively in living cells; such an endeavor will not only result in better understanding of cellular processes, but also novel ways to reprogram the process to achieve novel functions for biotechnological applications.

Among the range of metal ions in cells, sodium (Na^+) serves particularly important functions, as changes in its concentrations influence cellular processes of numerous living organisms and cells (5-8), such as epithelial and other excitable cells (9). As one of the most abundant metal ions in intracellular fluid (10) Na^+ affects cellular processes by triggering the activation of many signal transduction pathways, as well as influencing the actions of hormones (11). Therefore it is important to carefully monitor the concentrations of Na^+ in cells. Toward this goal, instrumental analyses by atomic absorption spectroscopy (AAS) (12), X-ray fluorescence microscopy (XFM) (13), and ^{23}Na NMR (14) have been used to detect the concentration of intracellular Na^+. However, it is difficult to use these methods to obtain real time dynamics of Na^+ distribution in living cells. Fluorescent sensors provide an excellent choice to overcome this difficulty, as they can provide sensitive detection with high spatial and temporal resolution. However, despite significant efforts in developing fluorescent metal ion sensors, such as those based on either genetically-encoded probes or small molecular sensors, most fluorescent sensors reported so far can detect divalent metal ions such as Ca^{2+}, Zn^{2+}, Cu^{2+}, Fe^{2+} (15-21). Among the

limited number of Na^+ sensors, such as sodium-binding benzofuran isophthalate (SBFI) (22), Sodium Green (23), CoroNa Green/Red (24, 25), and Asante NaTRIUM Green-1/2 (ANG-1/2) (26), most of them are not selective for Na^+ over K^+ (22-25, 27, 28) or have a low binding affinity for Na^+ (with K_d higher than 100 mM) (25, 27-31). Furthermore, the presence of organic solvents is frequently required to achieve the desired sensitivity and selectivity for many of the Na^+ probes (32-34), making it difficult to study Na^+ under physiological conditions. Therefore, it is still a major challenge to design fluorescent sensors with strong affinity for Na^+ and high selectivity over other mono- and multi-valent metal ions that work under physiological conditions.

To meet this challenge, our group and others have taken advantage of an emerging class of metalloenzymes called DNAzymes (deoxyribozymes or catalytic DNA) and turn them into metal ion probes. DNAzymes were first discovered in 1994 through a combinatorial process called *in vitro* selection (35). Since then, many DNAzymes have been isolated via this selection process. Among them, RNA-cleaving DNAzymes are of particular interest for metal ion sensing, due to their fast reaction rate and because the cleavage which is catalyzed by a metal ion cofactor can easily be converted into a detectable signal (36-38). Unlike the rational design of either small-molecule or genetically-encoded protein sensors, DNAzymes with desired sensitivity and specificity for a metal ion of interest can be selected from a large library of DNA molecules, containing up to 10^{15} distinct sequences (35, 39). A major advantage of DNAzymes as metal ion sensors is that metal-selective DNAzymes can be obtained without prior knowledge of necessary metal ion binding sites or specific metal-DNA interaction (40, 41). In addition, through the *in vitro* selection process, metal ion binding affinity and selectivity can be improved by tuning the stringency of selection pressure and introducing negative selection against competing metal ions (39, 40). Finally, DNA is easily synthesized with a variety of useful modifications and its

biocompatibility makes DNAzyme-based sensors excellent tools for live-cell imaging of metal ions. As a result, several metal-specific DNAzymes have been isolated and converted into sensors for their respective metal ion cofactors, including Pb^{2+} (35, 42, 43), Cu^{2+} (44, 45), Zn^{2+} (46), UO_2^{2+} (47), and Hg^{2+} (48). They have recently been delivered into cells for monitoring UO_2^{2+} (41, 49), Pb^{2+} (50), Zn^{2+} (51), and histidine (52) in living cells.

However, in contrast to the previously reported DNAzymes with divalent metal ion selectivity, no DNAzymes have been reported to have high selectivity towards a specific monovalent metal ion. Although DNAzymes that are independent of divalent metal ions have been obtained (53-55), including those employing modified nucleosides with protein-like functionalities (*i.e.* guanidinium and imidazole) (56-58), no DNAzymes have been found to be selective for a specific monovalent metal ion over other monovalent metal ions. For example, the DNAzyme with the highest reported selectivity for Na^+ still binds Na^+ over K^+ with only 1.3-fold selectivity (54). More importantly, those DNAzymes require very high concentration of monovalent ions (molar ranges) to function and display very slow catalytic rates, (e.g., 10^{-3}) (53-55). Such poor selectivity, sensitivity and slow catalytic rate render these DNAzymes unsuitable for cellular detection of Na^+, due to interference from other monovalent ions such as K^+ (which is present in concentrations about 10-fold higher than Na^+), and the need to image the Na^+ fast.

In this study, we report the *in vitro* selection and characterization of an RNA-cleaving DNAzyme with exceptionally high selectivity (> 10,000-fold) for Na^+ over other competing metal ions, with dynamic range covering the physiological Na^+ concentration range (0.135-50 mM) and fast catalytic rate (k_{obs} ~ 0.1 min^{-1}). This Na^+-specific DNAzyme was transformed into a DNAzyme-based fluorescent sensor in imaging intracellular Na^+ in living cells, by adopting an

efficient DNAzyme delivery method using a cationic polypeptide, together with a photo-caging strategy to allow controllable activation of the probe inside cells.

4.2 Materials and Methods

4.2.1 Materials

4.2.1.1 Chemicals

All oligonucleotides were purchased from Integrated DNA Technology Inc. (IDT) and purified by denaturing (8 M urea) 10 % polyacrylamide gel electrophoresis (PAGE) before use. Sensor oligonucleotides were synthesized and HPLC-purified by IDT. Details of the nucleotide sequences are provided in Sequences section. Other metal salts used included the following: $LiCl.H_2O$ (Alfa Aesar, 99.996%), NaCl (Alfa Aesar, 99.999%), KCl ((Alfa Aesar, 99.995%), RbCl (Alfa Aesar, 99.975%), CsCl (Alfa Aesar, 99.999%), $NH_4CH_3CO_2$ (Aldrich, 99.999%), $MgCl_2.6H_2O$ (Alfa Aesar, 99.999%), $Ca(NO_3)_2.6H_2O$ (Alfa Aesar, 99.995%), $SrCl_2.6H_2O$ (Alfa Aesar, 99.996%), $BaCl_2.2H_2O$ (Alfa Aesar, 99.997%), $Mn(CH_3CO_2)_2.4H_2O$ (Alfa Aesar, 99.999%), $CoCl_2.6H_2O$ (Alfa Aesar, 99.9%), $NiCl_2.6H_2O$ (Alfa Aesar, 99.995%), $Cu(NO_3)_2.H_2O$ (Alfa Aesar, 99.999%), $ZnCl_2.H_2O$ (Alfa Aesar, 99.99%), $Cd(NO_3)_2.4H_2O$ (Alfa Aesar, 99.999%), $HgCl_2$ (Alfa Aesar, 99.999%), $Pb(CH_3CO_2)_2.3H_2O$ (Aldrich, 99.999%), $InCl_3$ (Aldrich, 99.999%), $La(NO_3)_3.6H_2O$ (Aldrich, 99.999%), $EuCl_3.6H_2O$ (Aldrich, 99.999%), $SmCl_3.6H_2O$ (Aldrich, 99.99%), and $YbCl_3.6H_2O$ (Aldrich, 99.998%). Salts and solutions used to adjust pH of buffer solutions included the following: $LiOH.H_2O$ (Alfa Aesar, 99.996%) $NaOH.H_2O$ (Alfa Aesar, 99.996%), KOH (Fisher Scientific), and 36.5% HCl (Alfa Aesar, 99.999%). Other chemicals used to prepare different solutions included the following: Ethylenediaminetetraacetic acid, sodium free (EDTA) (Fluka, 99.0%), $EDTA.2Na.2H_2O$ (Fisher Scientific), Trisodium citrate (Alfa Aesar, 99%), urea (Affymetrix, MB grade), Tris (Affymetrix, MB grade), boric acid (Fisher Scientific, electrophoresis grade), and Bis-Tris (Sigma, 99.0%). Acrylamide/bisacrylamide 40% solution (29:1) was obtained from Bio-Rad. *Taq* DNA polymerase with standard *Taq* buffer, T4-

polynucletide kinase, and deoxynucleotide (dNTP) solution mix were obtained from New England Biolabs. ^{32}P labeled α-ATP and γ-ATP for DNA radiolabeling was obtained from Perkin-Elmer. All buffer, metal ion and gel stock solutions were prepared with Milli-Q water. The pH of the buffers was measured with Fisher Scientific Accumet AB15 pH meter.

4.2.1.2 Sequences

Table 4.1 Sequences of the oligonucleotides used for the *in vitro* selection.

Name	Sequence of Oligonucleotide (5' to 3')
IDT template	GGAAGTACCGCATGGTAC-**N$_{50}$**-CGTGAGCCTACGATGAGAC
P1	GTCTCATCGTAGGCTCAC
P2	GACTAATTCATCACGTATAGGAAGTACCGCATG
P3	Biotin-GTTCAGACTAATCATCACGTATrA
P4	GAC(AAC)$_4$-**Sp**-C**18**- GTCTCATCGTAGGCTCAC
P5	GTTCAGACTAATCATCACGTATrA

Table 4.2 NaA43 *trans*-cleaving form with four different binding arms as represented in Figure 4.15

Name	Sequence of Oligonucleotide (5' to 3')
NaA43S#1	GGATCACGTATrAGGAAGTACCGCC
NaA43E#1	GGCGGTACCAGGTCAAAGGTGGGTGAGGGGACGCCAAGAGTCCCCGCG GTTACGTGATCC
NaA43S#2	CTCTATGTATrAGGAAGTACCGCCGC
NaA43E#2	GCGGCGGTACCAGGTCAAAGGTGGGTGAGGGGACGCCAAGAGTCCCCG CGGTTACATAGAG
NaA43S#3	ACTCACTATrAGGAAGAGATGGACGTG
NaA43E#3	CACGTCCATCTCCAGGTCAAAGGTGGGTGAGGGGACGCCAAGAGTCCC CGCGGTTAGTGAGT
NaA43S#4	GGATGTATrAGGAAGTACCGCC
NaA43E#4	GGCGGTACCAGGTCAAAGGTGGGTGAGGGGACGCCAAGAGTCCCCGCG GTTACATCC

Table 4.3 NaA43 Fluorescence sensor oligos

Name	Sequence of Oligonucleotide (5' to 3')
NaA43S FAM/IABkFQ	6-FAM/CTCTATCTATrAGGAAGTACCGCCGC/IABkFQ
NaA43E IABkFQ	GCGGCGGTACCAGGTCAAAGGTGGGTGAGGGGACGCCAAGAGTCCCCG CGGTTAGATAGAG/IABkFQ

Table 4.4 Co-localization study oligos

Name	Sequence of Oligonucleotide (5' to 3')
FAM-dANaA43S	6-FAM/ACTCACTATAGGAAGAGATGGACGTG
NaA43E-Col	ACGTCCATCTCCAGGTCAAAGGTGGGTGAGGGGACGCCAAGAGTCCCC GCGGTTAGTGAG
NaA43E-Col-Cy3	A*C*GTCCATCTCCAGGTCAAAGGTGGGTGAGGGGACGCCAAGAGTCCC CGCGGTTAGTG*A*G/3Cy3ph

* represents phosphorothioate modification

Table 4.5 Intracellular imaging oligos

Name	Sequence of Oligonucleotide (5' to 3')
Active NaA43E-IBQ	A*C*GTCCATCTCCAGGTCAAAGGTGGGTGAGGGGACGCCAAGA GTCCCCGCGGTTAGTG*A*G/3IABkFQ
FAM-caged NaA43S-BHQ	6-FAM/ACTCACTAT/iNiBenz-rA/GGAAGAGATGGACGTG/BHQ_1
FAM-non-cleavable NaA43S-BHQ	6-FAM/ACTCACTATAGGAAGAGATGGACGTG/BHQ_1
Active NaA43E-IBRQ	A*C*GTCCATCTCCAGGTCAAAGGTGGGTGAGGGGACGCCAAGA GTCCCCGCGGTTAGTG*A*G/IAbRQSp
TAMRA-caged NaA43S-BHQ2	6-TAMN/ACTCACTAT/iNiBenz-rA/GGAAGAGATGGACGTG/BHQ_2
Inactive NaA43E-IBRQ	A*C*GTCCATCTCCAGGACAAAGGTGGGTGAGGGGACGCCAAGA GTCCCCGCGGTTAGTG*A*G/IAbRQSp

* represents phosphorothioate modification

4.2.2 Methods

4.2.2.1 *In Vitro* Selection

The same initial selection pool was used for both selections and was generated through template-directed extension followed by two PCR amplifications. For each selection, the extension reaction was carried out in two steps. In the first step, 300 pmol of DNA template and 300 pmol of primer P1 were mixed in 60 × 50 µl reaction mixtures and extended for two thermal cycles (1 min at 94°C, 1.5 min at 58°C and then 3 min at 72°C). Second step was carried out by addition of 450 pmol of primer P2 and two more thermal cycles. The reaction buffer also included 0.1 units/µl of Taq DNA polymerase (New England Biolabs (NEB)), 1.5 mM $MgCl_2$, 50 mM KCl, 10 mM Tris-HCl (pH 8.3 at 25°C), and 0.2 mM of each dNTP. After two-step extension, 150 pmol of P2 and 3 nmol of P1 were added to the mixture reaction for ten additional amplification cycles (PCR1). Next, second PCR amplification was carried out by addition of 3 nmol of P3 and ten more thermal cycles to incorporate the rA cleavage site into the PCR product. Amplification of the isolated DNA at the end of each selection round was carried out by two PCR reactions. In PCR1 isolated DNA was amplified with skewed ratio of P1 (1.0 µM) to P2 (0.1 µM). 10% of PCR1 reaction was used as template in PCR2 and amplified with skewed ratio of P3 (1.0 µM) to P1 (0.1 µM). PCR2 products were internally labeled with [α-^{32}P]-dATP (PerkinElmer) to keep track of DNA pools and cleavage products through selection process via liquid scintillation counting and denaturing PAGE analysis.

PCR amplified pools were immobilized on NeutrAvidin agarose beads using buffer A (10 mM Bis-Tris (pH 7.0 at 24 °C) and 1 mM EDTA) over 10 minutes (Fig. S1). Single stranded DNA pools were generated by washing beads with buffer B (150 mM NaOH and 2 mM EDTA) at 45 °C for 1 min followed by three more washing steps with ice cold buffer B and then ice cold distilled

water. Background cleavage was collected using buffer C (50 mM Bis-Tris (pH 7.0 at 24 °C) and 1 mM EDTA). Two parallel selections were carried out using two different sodium concentrations. In selection A active DNAzymes were collected by incubating immobilized pool with a solution containing 50 mM Bis-Tris (pH=7.0 at 24 °C), 1 mM EDTA, 10 mM sodium citrate and 105 mM NaCl (total of ~135 mM Na^+). Selection B was carried out using a solution containing 50 mM Bis-Tris (pH=7.0 at 24 °C), 1 mM EDTA, 10 mM sodium citrate and 370 mM NaCl (total of ~ 400 mM Na^+).

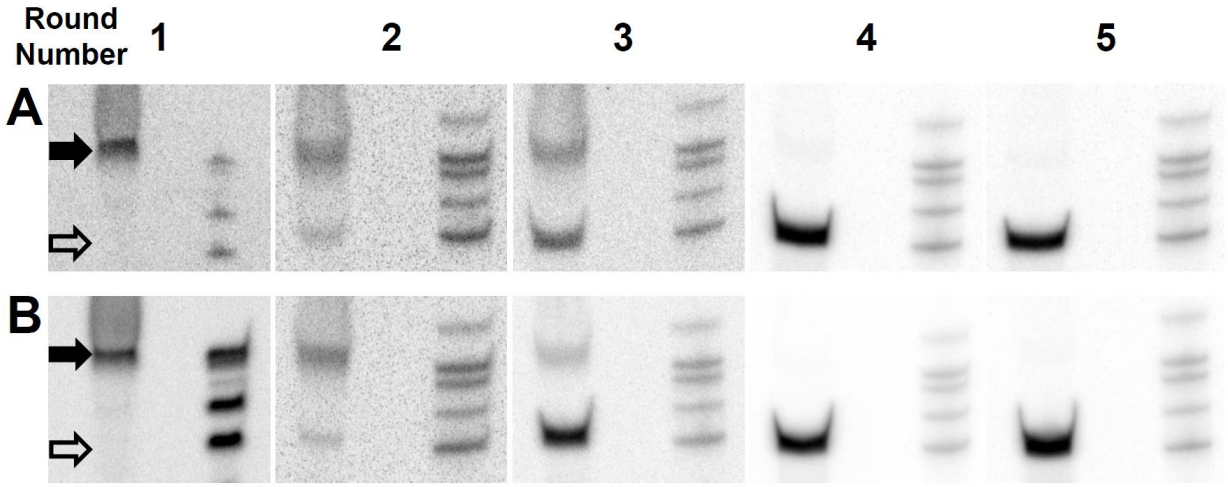

Figure 4.1 PAGE purification results of the first five rounds of Na^+-specific DNAzyme selection (A: selection A and B: selection). In the first round of the *in vitro* selection active sequences (open arrows) that are eluted from selection columns are below detection limit of phosphorimaging and only nonspecific detachment of uncleaved DNA is observed (filled arrows). From the second round of selections, cleavage products are detectable in phosphorimaged gels. Ratio of nonspecific detachment of DNA over active DNA cleavage increases significantly in the subsequent rounds. These results indicate that PAGE purification steps in our *in vitro* selection strategy are important to remove inactive sequences from eluted DNA at the end of each selection round and before amplification of active sequences.

Selected DNA sequences were PAGE purified and used as PCR template to generate pools for the next round of the selection. As it is shown in Figure 4.1, PAGE purification was an important part of the selection to remove nonspecific detachment of uncleaved sequences from

beads. The PAGE purification step was critical especially at early rounds of the selection (Figure 4.1). Immobilized DNA pools were incubated with selection buffers for 2 h at the first and the second rounds of the selection and incubation time was reduced subsequently to 45 seconds at round 15. Selection progress was monitored by using four independent means: 1- Calculating fraction cleaved DNA relative to the initial pool which was eluted from selection columns (via liquid scintillation counting and denaturing PAGE analysis), 2- measuring selection signal over background 3- Calculating fraction of cleaved DNA relative to the initial pool over 3 h reaction time, and 4- testing activity of the selected pools every other round (started at round 5) at different Na^+ concentrations. Amplification of selected pools for analysis of their activity were carried out by using P4 and P5 primers instead of P1 and P3, respectively. P4 contained a hexaethyleneglycol spacer which served as a DNA polymerization termination site, followed by 5′-GACAACAACAACAAC-3′, which resulted in formation of two strands of unequal lengths as PCR products. Amplified DNA pools contained rA cleavage site were separated from the longer PCR product via denaturing PAGE and precipitated with ethanol. Selected pools from the last three rounds of selections were tested further to find the most active pools for cloning and sequencing experiments. Selected pools from round 13 and 15 were chosen for cloning for selection condition A and B, respectively. TA-TOPO Cloning Kit (Invitrogen) was used for cloning experiments. The vectors were transformed into E. coli competent cells through heat-shock and ampicillin resistant transformants were selected on ampicillin containing LB plates. From each selection total of 50 randomly chosen colonies were grown in 5 ml LB culture with 100 μg ml^{-1} ampicillin at 37°C. DNA was extracted using Miniprep Kits (QIAGEN) and eluted into water. All clones were submitted to the University of Illinois Sequencing Center. Sequence analysis and

alignment were performed by Vector NTI Advance 11.0 (Invitrogen). Secondary structure of DNAzymes were predicted using UNAFold and DINAMelt packages (1, 2).

4.2.2.2 *In Vitro* Selection

Activity of selected pools and *cis*-cleavage form of the DNAzyme was tested in 50 mM Bis-Tris (pH 7.0) and the reaction was initiated by addition of Na^+ at desired concentration. DNA sequences were internally labeled during PCR amplification with [α-^{32}P]-dATP (PerkinElmer). Selectivity of *trans*-cleavage form of NaA43 DNAzyme for Na^+ over Cu^{2+} and Hg^{2+} was tested under single turn-over condition using final concentration of 2 μM and 10 nM for the enzyme and substrate, respectively. The substrate was labeled at 5´-end with [γ-^{32}P]-ATP (PerkinElmer) using T4 polynucleotide kinase from NEB. The DNAzyme complex containing the NaA43E and ^{32}P-labeled NaA43S was denatured by heating the mixture at 90°C for 3 min and annealed in buffer C (50 mM Bis-Tris (pH 7.0) containing 90 mM LiCl) by gradual cooling to room temperature over 30 min. For all activity assay experiments, reaction sample were quenched by addition of 2 μl of reaction mixture to 30 μl of a "stop solution" containing 9 M urea, 1× TBE and 0.05 % each bromophenol blue and xylene cyanol. It has been verified that using a large volume (15×) of stop solution with high urea concentration which would dilute Na^+ concentration significantly is an effective method to quench the DNAzyme reaction (data not shown). The zero time point samples were mixed with the stop solution at the end of the activity assay to test the cleavage in the absence of Na^+. The cleaved and uncleaved DNA were separated by 10% or 20% denaturing PAGE and gel images were taken by Molecular Dynamics Storm 430 phosphorimager (from Amersham Biosciences). Kinetic curves were plotted using OriginLab 9.1 and fit to the equation of

$$\%P_{cleavage,t} = \%P_{max} (1 - e^{-kt})$$

where $\%P_{max}$ is the maximum percent of cleavage product at the end of the reaction and *k* is the rate of cleavage (k_{obs}) (7).

4.2.2.3 Preparation of Sensor and Na+ Detection

The enzyme-substrate complex was formed by annealing a mixture of NaA43E and NaA43S (1.2 to 1 ratio) in buffer C. Concentrated Na^+ or other metal solutions in buffer C were mixed with annealed complex before recording fluorescence change. Final concentration of the sensor complex was calculated to be 50 nM. Fluorescence change was continuously monitored by a FluoroMax-2 fluorometer (Horiba Jobin Yvon, Inc., Edison, NJ) every 12 s for at least 15 min. The excitation wavelength was 490 nm and emission was monitored at 520 nm. The initial rate of fluorescence enhancement, attributed to release of the cleaved substrate was measured by plotting the change in fluorescence intensity for the first 2 min after addition of Na^+ using a linear fit. Other metal salts used as in material section of supporting information. Selectivity of the sensor for Na^+ over other metal ions was tested in the presence of 22 different metal salts. Sensor response to monovalent competing cations (Li^+, K^+, Rb^+, Cs^+, NH_4^+) was tested at 100 mM, while divalent (Mg^{2+}, Ca^{2+}, Sr^{2+}, Ba^{2+}, Mn^{2+}, Co^{2+}, Ni^{2+}, Cu^{2+}, Zn^{2+}, Cd^{2+}, Hg^{2+}, Pb^{2+}) and trivalent (In^{3+}, La^{3+}, Eu^{3+}, Sm^{3+}, Yb^{3+}) metal ions were tested at 2 mM and 0.2 mM, respectively.

4.2.2.4 Activity of the Intracellular Sensor in Buffer

Active NaE-IBRQ and TAMRA-caged NaS-BHQ2 were mixed in Buffer K (12.5 mM HEPES, 140 mM KCl, 10 mM Glucose, 1.2 mM $MgCl_2$, 1 mM $CaCl_2$, pH 7.4) at a final concentration of 10 μM. The two strands were annealed by heating the solution to 75°C for 2 min followed by slowly cooling down to room temperature over 1h. To restore the activity of the caged substrate strand, the solution was added into one of the wells in a 12-well plate, and exposed to UV light at 365 nm for 30 min. Buffer solutions with different concentrations of Na^+ were prepared

by mixing Buffer K with Buffer Na (12.5 mM HEPES, 140 mM NaCl, 10 mM Glucose, 1.2 mM $MgCl_2$, 1 mM $CaCl_2$, pH 7.4) at different ratios. Buffer solutions were spiked with the sensor solution after the decaging process, and fluorescence change was monitored using a fluorometer (Jobin Yvon FluoroMax-P) at 541 nm excitation and 568 nm emission over a time period of 20 min.

4.2.2.5 Cell Culture, Sensor Delivery and Co-localization Study

HeLa cells were cultured in Dulbecco's modification of Eagle's medium (DMEM) supplemented with 10% Fetal Bovine Serum (FBS), 100 U/mL penicillin, and 100 µg/mL streptomycin, on 25 cm^2 culture flasks at 37°C in a humidified 5% CO_2 incubator. Before imaging, cells were plated in 35 mm glass-bottom dishes (MatTek) and grown to 70-90% confluence.

For the delivery of DNAzyme sensors using cationic helical polypeptide G8, the corresponding NaA43E and NaA43S (final concentration of 0.1 mM) were mixed in the buffer containing 20 mM MOPS, 100 mM NaCl with pH at 7.1. To anneal the DNAzyme for better hybridization, the mixture was heated to 75°C for 2 min and slowly cooled down to room temperature for 30 min. G8 polypeptide (degree of polymerization=50) was dissolved in water at 0.2 mg/ml and the pH of the solution was adjusted to 6 using diluted HCl for better solubility. 45 µl of polypeptide G8 was mixed and incubated with 2 µl of the aforementioned NaA43ES construct for another 30 min to allow the formation of polymer-DNA complex (G8-NaA43ES). Normal cell culture medium was replaced with OPTI-MEM before the G8-NaA43ES complex solution was added to the cells grown in the plates.

After incubating HeLa cells with G8-NaA43ES complex for 4 hours, cells were washed thoroughly with PBS to remove excess amount of G8-NaA43ES complex in the medium. Specific

organelles inside cells were stained with commercial dyes, such as Hoechst 33258, LysoTracker Red DND-99, MitoTracker Red CMXRos, and ER tracker Red. Images were obtained using a Zeiss LSM 710 NLO confocal microscope at 63x magnification equipped with a Mai-Tai Ti-Sapphire laser. Fluorescence emission of Hoechst 33258 was measured over 450-520 ranges, with excitation at 401 nm. Fluorescence of LysoTracker, MitoTracker and ER tracker was obtained by exciting at 561 nm and measuring over 575-620 nm, 585-630 nm, and 600-650 nm, respectively. The pinhole and gain settings were kept constant throughout the whole imaging process. Z-stack images were also obtained to confirm that the fluorescent signal was inside cells.

4.2.2.6 Intracellular Sodium Imaging and Flow Cytometry

HeLa cells were cultured in glass bottom dishes until about 80% confluence. After treatment with corresponding NaA43ES construct for 4 hours, cells were washed thoroughly with DPBS. Then cells were immersed in DPBS and irradiated with UV lamp at 365 nm for 30 minutes. Immediately after UV treatment, stock solutions of gramicidin D, monensin and ouabain were added to the cells at final concentrations of 3 μM, 10 μM and 100 μM, respectively. Fluorescent images as well as bright field images were taken every 5 minutes immediately after addition of ionophores.

Cells were cultured in 12-well plates until about 80-90% confluence. 22.5 μl of 0.2 mg/ml G8 polypeptide and 1 μl of 0.1 mM NaA43ES DNA were mixed and pre-incubated for 30 minutes before being added to each well. After 4-hour incubation, cells were washed thoroughly with DPBS. Then cells were immersed in 500 ul of DPBS and UV irradiation was applied to the cells for 30 minutes using a UV hand lamp. For the group of cells with elevated concentration of Na^+, final concentrations of 3 μM gramicidin D, 10 μM monensin and 100 μM ouabain were added

immediately after UV irradiation. After 30-minute incubation in DPBS, cells were treated with 0.25% trypsin for suspension, and the fluorescence of cells was detected by flow cytometry.

4.2.2.7 Synthesis and Characterization of DNA-Invertase Conjugate

The DNA−Invertase conjugate was synthesized by the maleimide-thiol reaction using heterobifunctional linker sulfo-SMCC (sulfosuccinimidyl-4-(N-maleimidomethyl)cyclohexane-1-carboxylate). Briefly, 30 µL of 1 mM thiol-DNA, 2 µL of 1 M PBS buffer (pH 5.5), and 2 µL of 30 mM TCEP (Tris(2-carboxyethyl)phosphine hydrochloride) were mixed and incubated at room temperature for 1 hour. Then, the thiol-DNA was purified by Amicon-10K using PBS buffer by 8 times. For Invertase conjugation, 400 µL of 20 mg mL^{-1} Invertase in PBS buffer was mixed with 1 mg of sulfo-SMCC. After vortexing for 5 minutes, the solution was placed on a shaker for 1 hour at room temperature. The mixture was then purified by Amicon-10K using PBS buffer by 8 times. The purified solution of sulfo-SMCC-activated Invertase was mixed with the above solution of thiol-DNA. The resulting solution was kept at room temperature for 48 hours. To remove un-reacted thiol-DNA, the solution was purified by Amicon-30K 8 times using Bis-Tris buffer (pH 7, 0.01 M Bis-Tris, 50 mM LiCl, 0.05% Tween-20).

4.2.2.8 Na^+ Detection using the PGM (Personal Glucose Meter) System

For the Na^+ sensor, a portion of 2 mL 1.2 mg/mL solution of MBs was placed close to a magnetic rack for 1 minute. The clear solution was discarded and replaced by 1 mL of Bis-Tris buffer. This buffer exchange procedure was repeated twice. Then, 12 µL 0.5 mM Biotin-DNA was added to the MBs solution and well mixed for 30 minutes at room temperature. After that, the MBs were washed twice using Bis-Tris buffer to remove excess biotin-DNA. Later, 12 µL of 1.0 mM Na^+-DNAzyme and Na+-Substrate were mixed and incubated at 80 ^{o}C for 1 min, and cooled to room temperature for 30 min. After that, the mixture was added to the MB solution and well mixed

for 30 minutes at room temperature. After three times washing using Bis-Tris buffer to remove excess DNA, 200 µL of DNA−Invertase conjugate (~20 mg/mL) was added to the solution and well mixed at room temperature for 60 minutes. Excess DNA−Invertase conjugate was washed off by Bis-Tris buffer three times and was recycled for further use by condensing the washing solutions using an Amicon-30K. The DNA−Invertase immobilized MBs were then dispersed in 1 mL of Bis-Tris Buffer. After the removal of Bis-Tris buffer, the MBs (~100 µL) were well mixed with 25 µL of Na^+ samples in human serum for 30 minutes. After that, the solution was separated and the supernatant (18 µL) was incubated with 6 µL of sucrose solution prepared in pH 4.0 potassium acetate buffer for 30 min, and detected using PGM.

For Na^+ detection in human serum and calf blood, the samples were diluted using Bis-Tris buffer, and the concentration of Na^+ in each samples were calculated using ICP method. For lower concentration of Na^+ detection in human serum (0-3.2 mM), the DNA−Invertase immobilized MBs were incubated with Na^+ samples for 2 hours, and then the supernatant was incubated with 6 µL of sucrose solution prepared in pH 4.0 potassium acetate buffer for 45 min.

4.3 Results and Discussions

4.3.1 *In Vitro* Selection of Na^+-specific DNAzyme

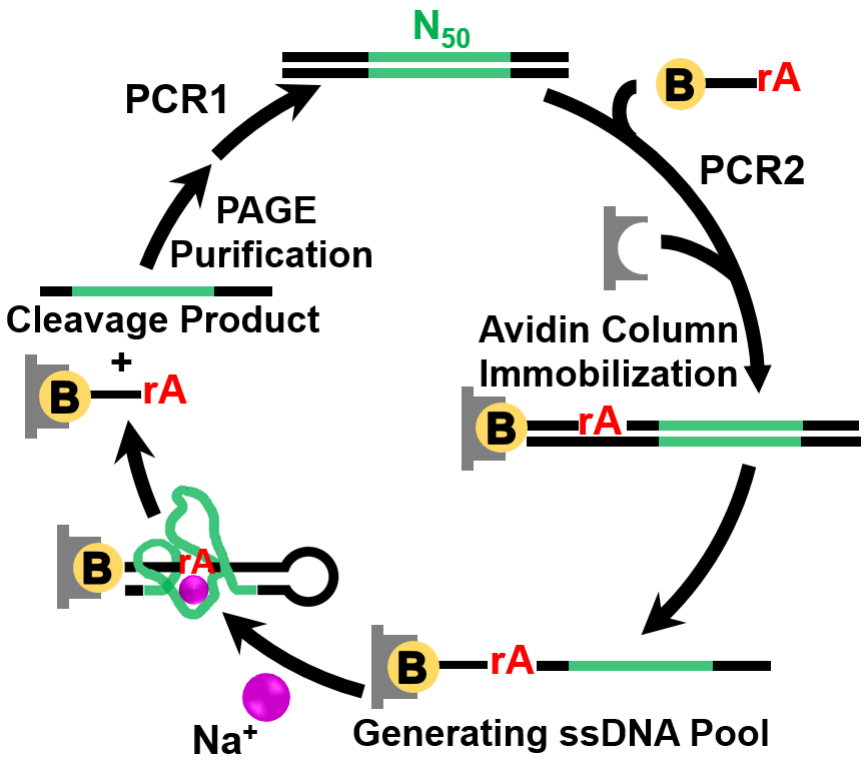

Figure 4.2 *In vitro* selection of a Na^+-specific DNAzyme. Scheme of *in vitro* selection strategy.

With the goal of selecting Na^+-specific DNAzymes, I carried out two parallel experiments using a column-based *in vitro* selection method reported previously (Figure 4.2) (35, 46), one in the presence of 135 mM total Na^+ (selection A) and another in the presence of 400 mM total Na^+ (selection B). Each selection employed a 110-mer oligonucleotide containing a 50 nucleotide random sequence (Figure 4.3), flanked by conserved sequences at both sides as primer-binding regions for polymerase chain reaction (PCR) amplification. The intended cleavage site, a single adenosine ribonucleotide (rA) was contained in the 5'-conserved region of the library sequence. Two distinct pairing regions were designed in the library to confine the folded random region to

be in proximity of the rA cleavage site (Figure 4.3). For both selections A and B, the positive selection buffers contained 10 mM citrate and 1 mM EDTA to minimize the likelihood of selecting DNAzymes that could catalyze cleavage of the rA site in the presence of multivalent metal ions.

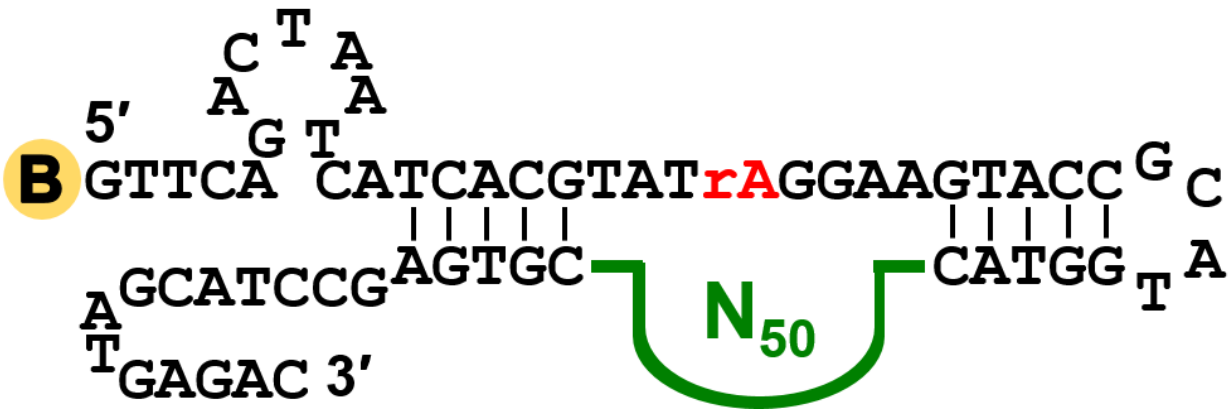

Figure 4.3 Design of the initial pool sequence used for selection of Na^+-specific DNAzyme.

Initially, the selection pools were immobilized on NeutrAvidin columns through the 5′-biotin moiety on the DNA molecules. Functional sequences that could catalyze cleavage of the RNA bond in the presence of Na^+ were eluted off the columns, amplified by PCR and used to initiate successive rounds of selection. Selective-amplification cycles (Figure 4.2) were repeated until the DNA pools were enriched with Na^+-specific DNAzymes (see Supporting Information for detailed protocols). To increase the stringency of the selection and thus search for more efficient DNAzymes, the reaction time was gradually decreased from 2 h in round 1, to 45 s in round 14 (Figure 4.4). Selection progress and enrichment of the DNA pools with Na^+-specific DNAzymes were monitored using several methods.

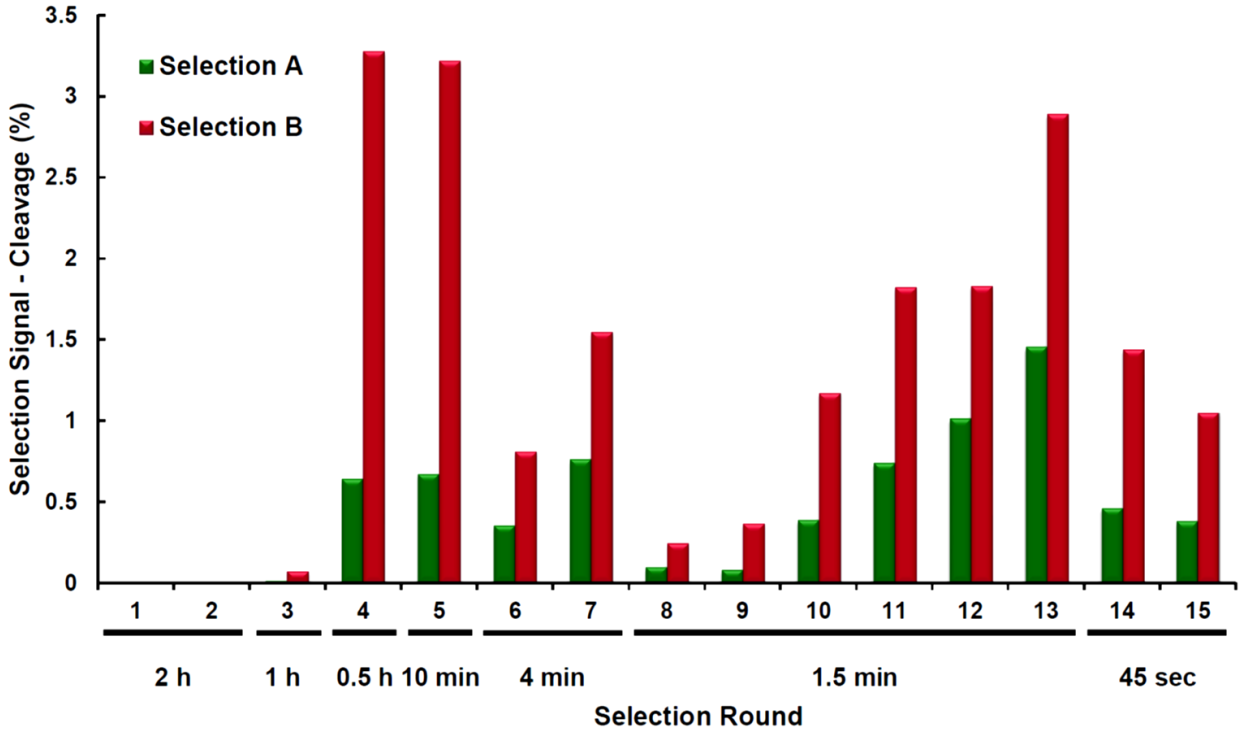

Figure 4.4 *In vitro* selection progress at each specific round represented in percentage fraction of cleaved DNA eluted off the column versus initial immobilized pool. Incubation time is displayed for each round.

Several methods were used to monitor selection progress and enrichment of the DNA pools with Na^+-specific DNAzymes. First, the fraction of the cleaved versus the initial population of the pool was calculated at each round of selection (Figure 4.4). Second, the signal to background ratio was measured at each round of the selection, by comparing the amount of cleavage that occurred in buffer without Na^+, with the cleavage from each round of selection (Figure 4.5). Third, since the reaction time was shortened through increasing rounds of selection, to offer fair assessment of enriching the selection pool with Na^+-DNAzymes, a parallel experiment was conducted with a constant reaction time, beginning from the fourth round of the selection (Figure 4.6). Lastly, starting at round five, the activity of the selected pools was tested every other round at different

Na^+ concentrations and the observed rate constants (k_{obs}) for the cleavage were plotted versus selection rounds (Figure 4.7).

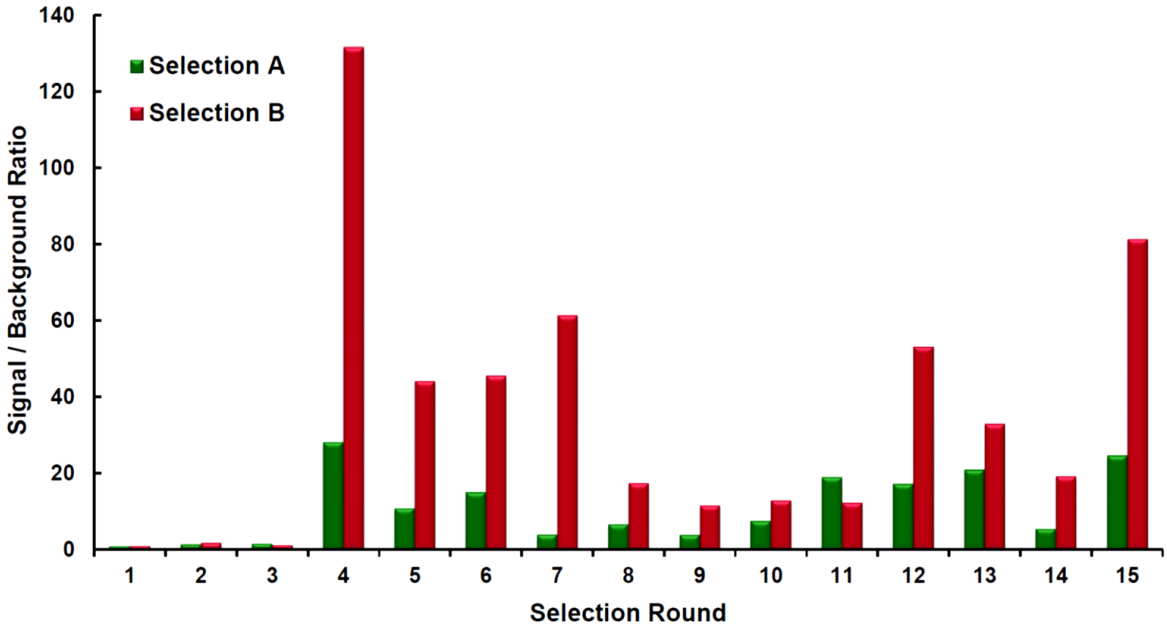

Figure 4.5 *In vitro* selection progress at each specific round represented in signal over background cleavage ratio. At each round signal is the fraction of DNA which is cleaved and eluted in presence of Na^+ and background is the fraction DNA which is cleaved and eluted in the absence of Na^+.

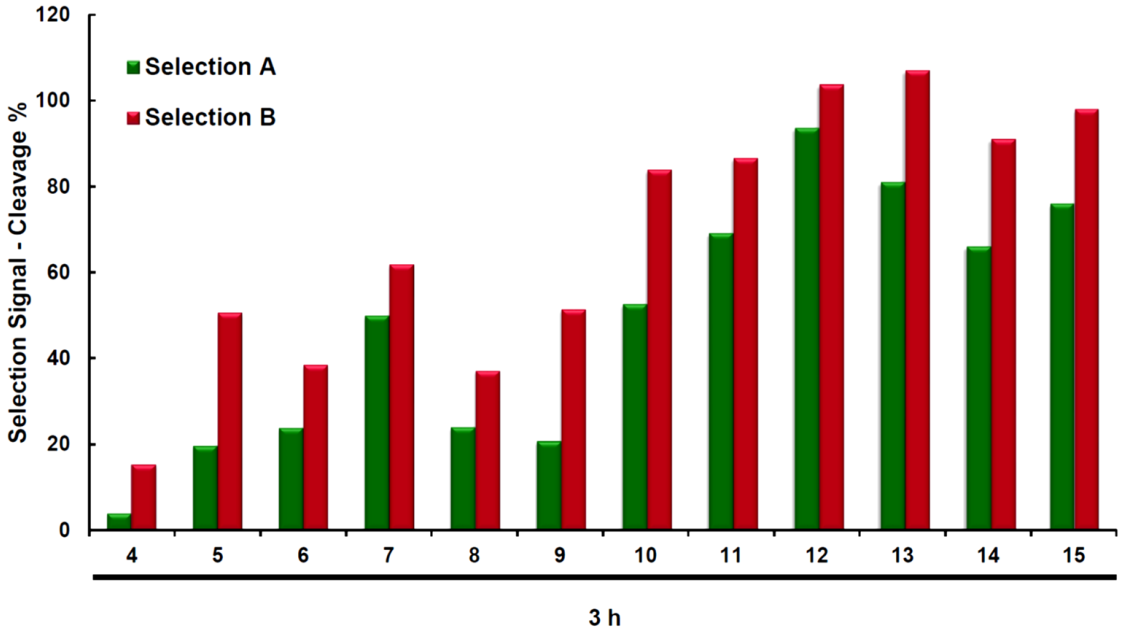

Figure 4.6 *In vitro* selection progress monitored from round four by determining percentage fraction of cleaved DNA eluted off the column versus initial immobilized pool over the course of three hours incubation with Na^+ in selection buffer.

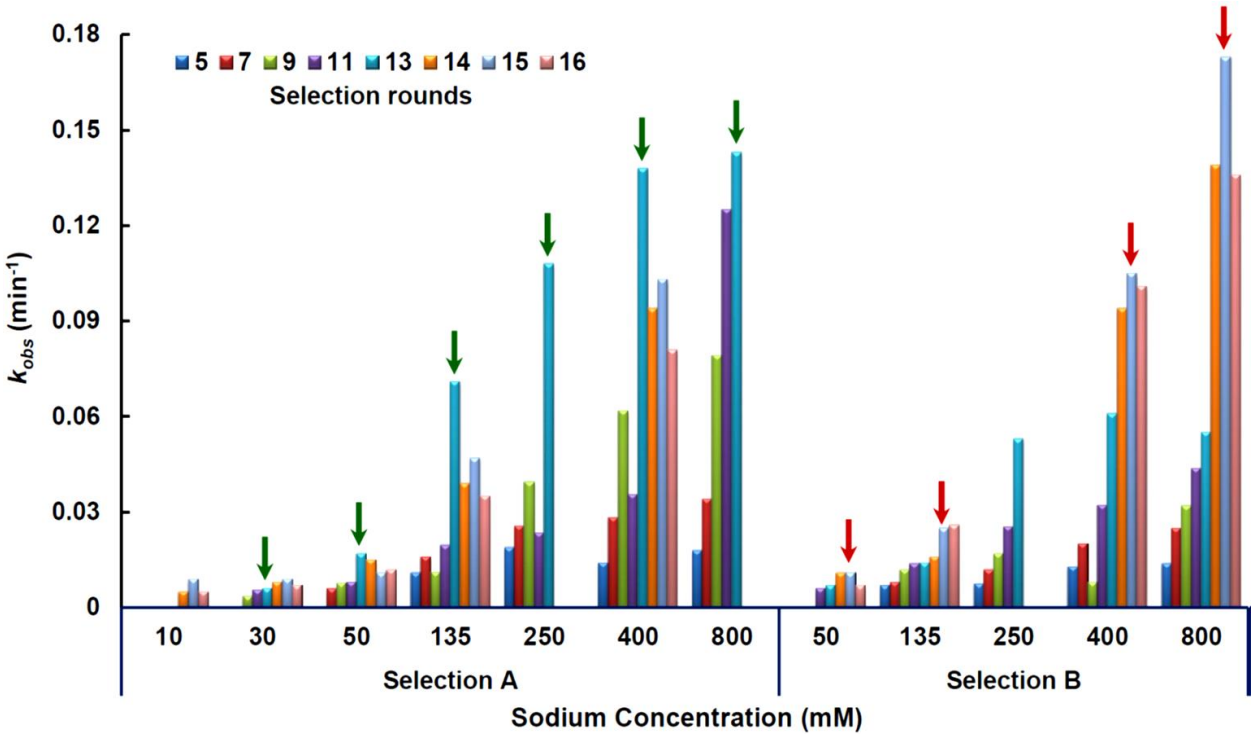

Figure 4.7 *In vitro* selection progress is followed from round 5 by calculating the observed rate constants (k_{obs}) of selected pools at different Na^+ concentrations. Specific pools from selection A and B showing overall highest activity are marked by arrows.

To monitor selectivity of the pool for Na^+, the activity of the selected pools was tested in the presence of other monovalent ions including Li^+, K^+, Rb^+, Cs^+, or NH_4^+ at 500 mM, cobalt hexamine at 40 mM or 1 mM Pb^{2+}. The cobalt hexammine was used as an inert metal complex and a divalent metal ion mimic (3), while the Pb^{2+}-dependent activity was tested due to the persistent presence of the 8-17 DNAzyme motif, which shows fast reaction rate in the presence of Pb^{2+} (4). It has been shown that undesired cross-reactivity with other metal ions could be minimized through counter-selection and removing cross-reactive species (5, 6). Due to the absence of cross reactivity with competing metal ions in our systems, no counter-selection step was incorporated into the selections. Interestingly, the selection B pools had higher signal over background and more cleavage than the selection A pools (Figures 4.4-4.6), probably because the concentration of Na^+

in selection B was ~ 3 times higher than in selection A. On the other hand, selected pools from selection A have shown higher rates of cleavage at lower Na^+ concentrations and better sensitivity (Figure 4.7).

In total, 48 and 47 sequences were obtained from cloning and sequencing of active pools from selection A and B, respectively. On the basis of sequence similarities, the obtained clones from selection A and B could be classified into two and three major classes, respectively (Figures 4.8 and 4.9). The Class A-II members showed a high degree of sequence similarity to class B-I. The Class A-II and B-I shared a common consensus sequence in the 50 nucleotides random-region (Figure 4.10). After screening the activity of individual clones from different classes, we found that the DNAzyme with highest activity belongs to class A-II.

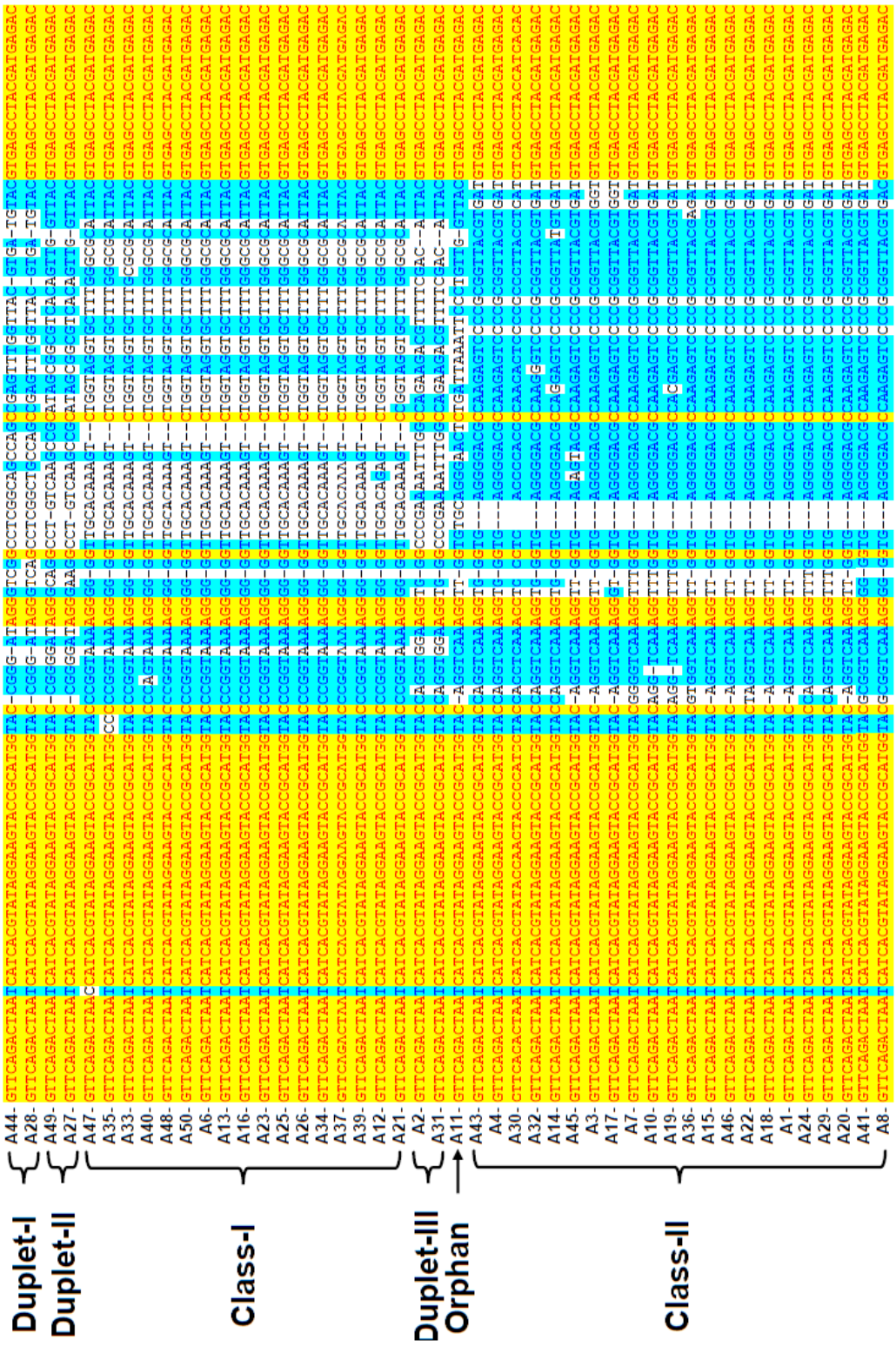

Figure 4.8 47 individual clones resulting from sequencing the selected pool from selection A. The sequence alignment was carried out by Vector NTI. Obtained sequences from Selection A fall into two major classes. Clone A43 was chosen for subsequent studies.

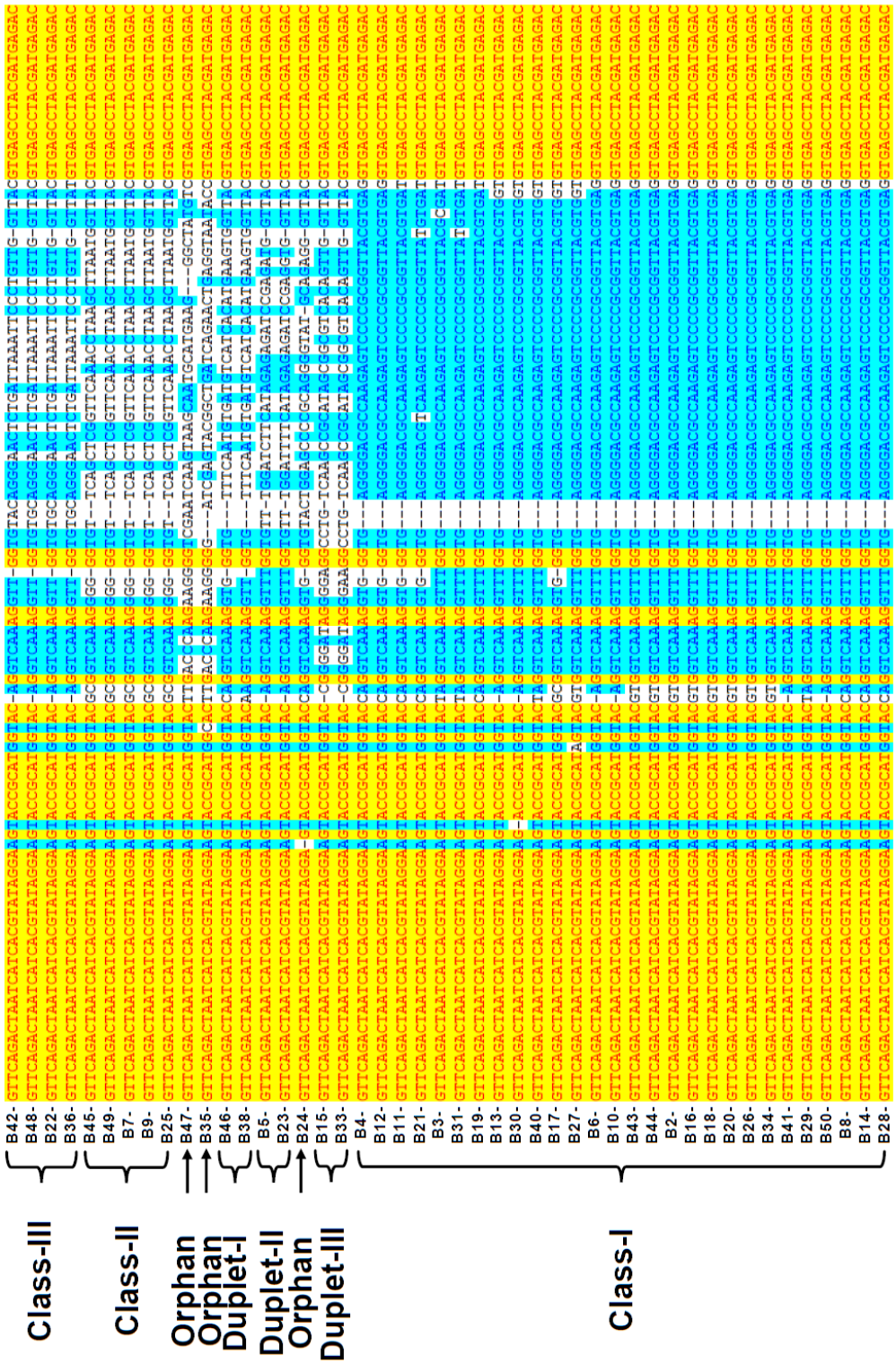

Figure 4.9 48 individual clones resulting from sequencing the selected pool from selection B. Sequence alignment was carried out by Vector NTI. Obtained sequences from Selection B fall into three major classes and the majority of them belong to class I.

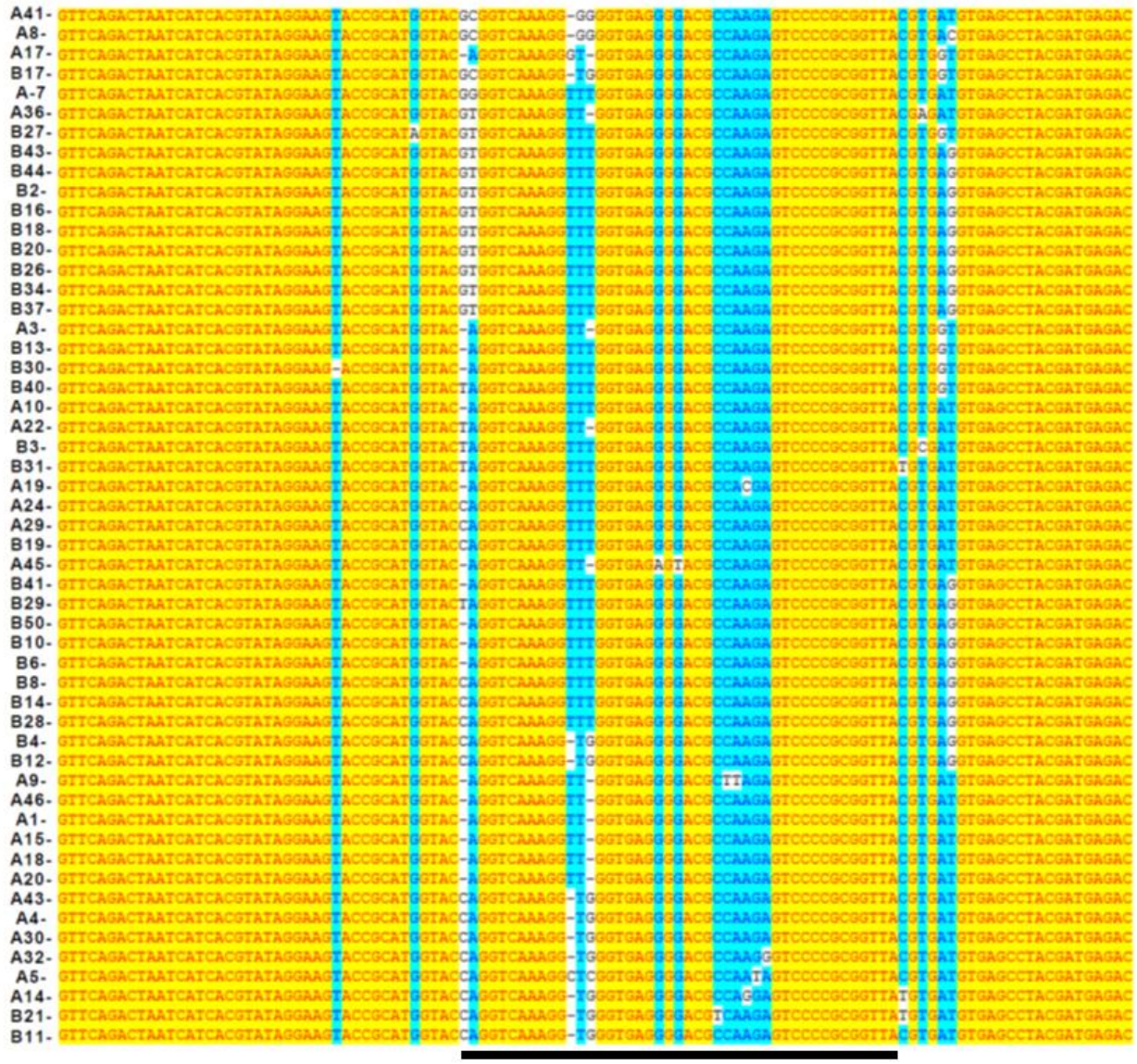

Figure 4.10 The sequence alignment of selection A class-II and selection B class-I. These two classes sharing significant similarity in the N_{50} random-region (marked with a black line).

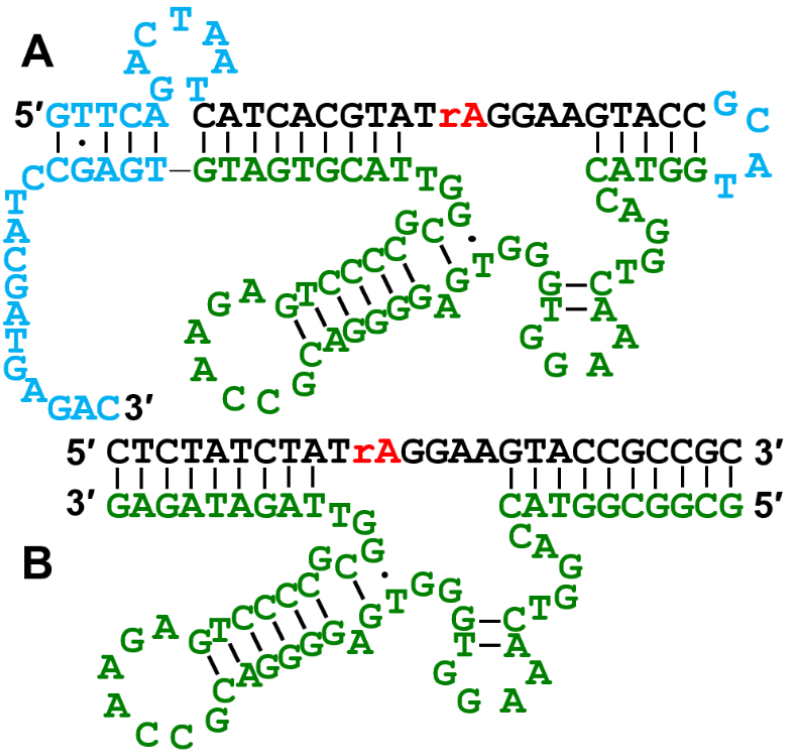

Figure 4.11 The sequence and secondary structure of the NaA43 DNAzyme (A) Secondary structure of an *in vitro* selected Na^+-specific DNAzyme (A43 clone) in its *cis*-cleaving form. Regions that are colored in blue were removed by truncation. (B) Secondary structure of the trans-cleaving NaA43 DNAzyme.

The most active pools from selection A (round 13) and B (round 15) were chosen for cloning and sequencing to find the best DNAzymes based on the percentage of the pool cleaved, the signal to background ratio, and the k_{obs} of different pools (Figures 4.4-4.7). Analysis of 95 resulting sequences revealed the existence of two and three major classes of similar sequences in selection A and B, respectively (Figures 4.8 and 4.9). The Class A-II and B-I shared a common consensus sequence in the 50 nucleotide random region (Figure 4.10). The catalytic activity of obtained sequences was then screened to find the most active DNAzyme. One such clone, named NaA43 (Figure 4.11A), displayed a k_{obs} of 0.11 ± 0.01 min^{-1} in the presence of 400 mM Na^+ at 20 °C, which is about two to three orders of magnitude faster than those of other divalent-independent

DNAzymes reported previously (53-55). The NaA43 DNAzyme achieved a rate enhancement of ~ 10^9-fold over uncatalyzed cleavage of a single RNA phosphodiester bond under similar conditions (59, 60). No noticeable difference was observed in the activity of the Na^+-dependent NaA43 DNAzyme in the presence or absence of 50 mM EDTA (Figure 4.12), suggesting that the DNAzyme activity was not caused by any trace multivalent metal ions in the buffer.

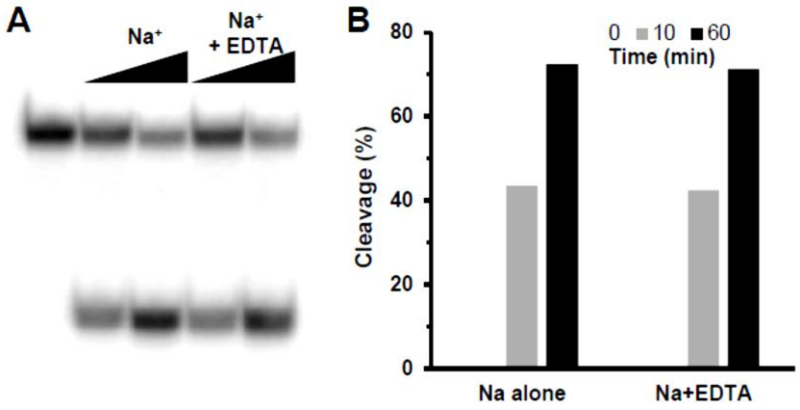

Figure 4.12 Activity of the NaA43 DNAzyme in the presence of EDTA (A) Gel image of NaA43 DNAzyme activity assay after incubation with 100 mM Na^+ in presence or absence of 50 mM EDTA. First lane is before addition of Na^+. (B) Quantification of the gel data in A.

Based on the secondary structure of the *cis*-cleaving NaA43 DNAzyme (Figure 4.11A), predicted by the UNAFold web package (61), the NaA43 DNAzyme was truncated into the minimal catalytic sequence by removing the sequences in blue and converted into to a true enzyme with catalytic turnover (*trans*-form), by removing the connecting loop between the substrate strand (NaA43S) and the enzyme strand (NaA43E) and then extending the double stranded arm to ensure efficient hybridization (Figure 4.11B). The green strand in Figure 4.11B represents NaA43E (DNAzyme strand) and the black strand shows the substrate. The cleavage site is a single rA nucleotide which is shown in red.

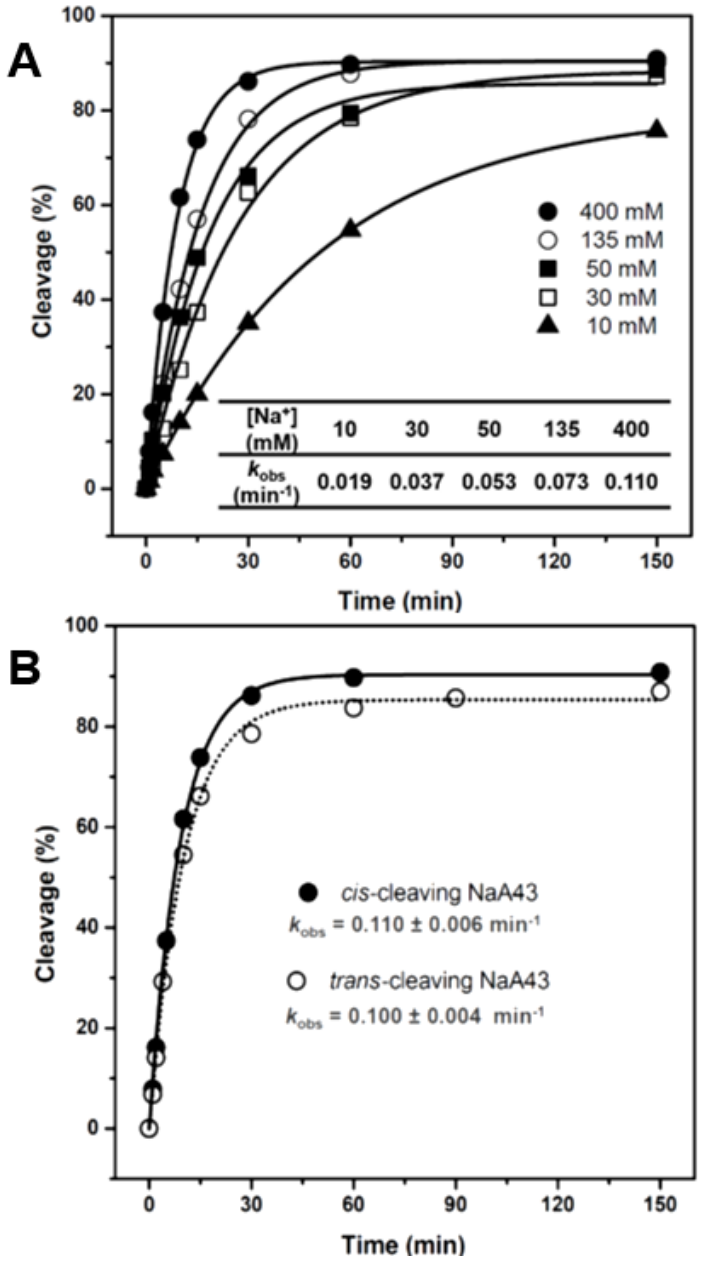

Figure 4.13 Activity of the *cis*-cleaving NaA43 DNAzyme (A) Plot of the fraction of DNA cleavage product (%) versus the incubation time (min) for *cis*-cleaving NaA43 DNAzyme at different concentrations of Na^+. (Inset) k_{obs} values for NaA43 DNAzyme obtained at different concentrations of Na^+. The calculated standard deviation was less than 10% for all samples. (B) Activity assay results of *cis*-cleaving and *trans*-cleaving forms of the NaA43 DNAzyme in the presence of 400 mM NaCl showing little difference in the activity of the two forms.

Activity assays (Figure 4.13) indicate that the truncation has little effect on the activity of the NaA43 DNAzyme. It is known that the substrate-binding arms of different DNAzymes, such as those of 8-17 and 10-23, are interchangeable and that their sequences do not play a significant role in the DNAzymes activity (42, 62). Similarly, the NaA43 DNAzyme showed no significant change in activity when tested with four different substrate-binding arms (Figure 4.14).

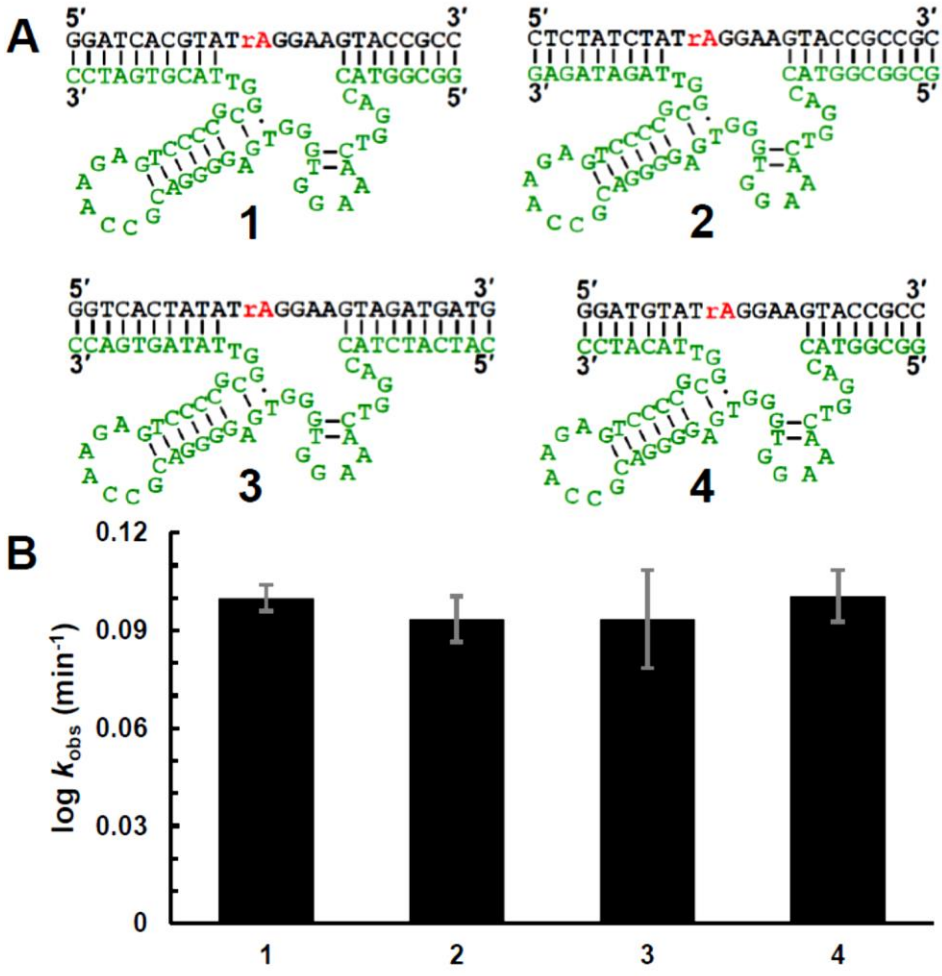

Figure 4.14 The effect of DNAzyme binding arm on its activity (A) NaA43 DNAzyme is represented with four different binding arms. (B) Activity of the four different versions of NaA43 DNAzyme was tested at 400 mM Na^+ and k_{obs} values were obtained from at least two independent experiments. Error bars are represented by the standard deviation of the repeats performed.

4.3.2 Converting the DNAzyme into a Fluorescent Sensor for Na^+ Ion

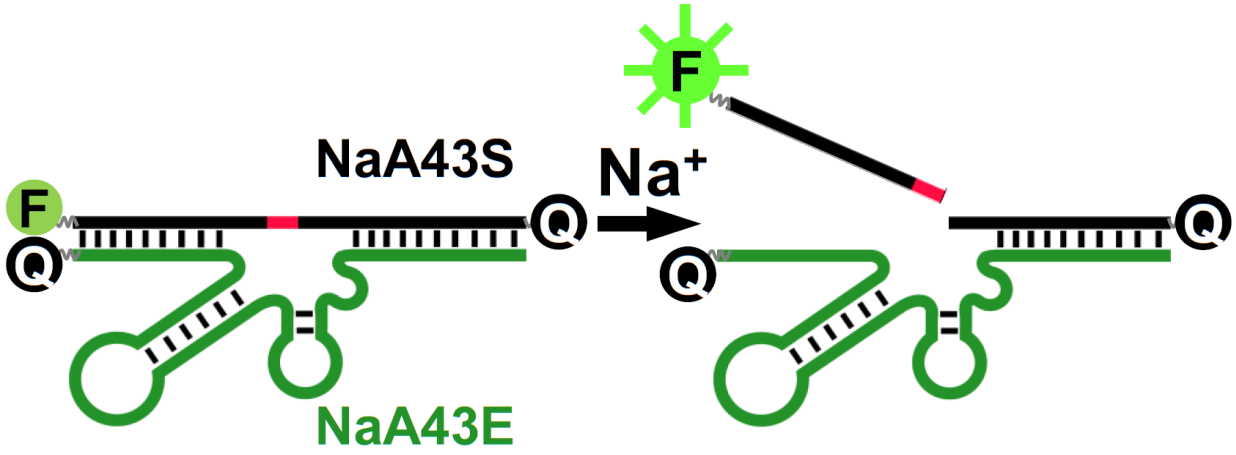

Figure 4.15 Design of the DNAzyme beacon with a fluorophore and two quenchers. In the presence of Na^+, cleavage of the substrate results in fluorescence enhancement.

To convert the Na^+-dependent catalytic activity of the NaA43 DNAzyme into a turn-on fluorescence response, we next designed a catalytic beacon by labeling the NaA43S with a 6-carboxyfluorescein fluorophore (FAM) at its 5′ end and the NaA43E with an Iowa Black FQ quencher at its 3′ end (63) (Figure 4.15). In addition, a second quencher was added at the 3′ end of the NaA43S to minimize background fluorescence (Figure 4.15) (64). To ensure stable duplex formation at room temperature, the 3′ arm of NaA43S was extended by 5 nucleotides and designed to have a high (~ 80%) GC-content. To ensure the release of the product fragment containing the fluorophore after cleavage, the 5′ end of NaA43S was designed with a much lower (33%) GC-content. In the presence of sufficient Li^+, the NaA43S-NaA43E complex was formed because it has a melting temperature higher than room temperature (>44 °C). As a result, the fluorescence signal was quenched due to the close proximity of the fluorophore and quencher. Upon addition of Na^+, NaA43S was cleaved at the rA in the middle. Since the melting temperature of the

fluorophore-containing arm after cleavage is below room temperature (~10 °C), dehybridization causes the fluorophore to release from its quenchers, resulting in fluorescence increase (47, 63).

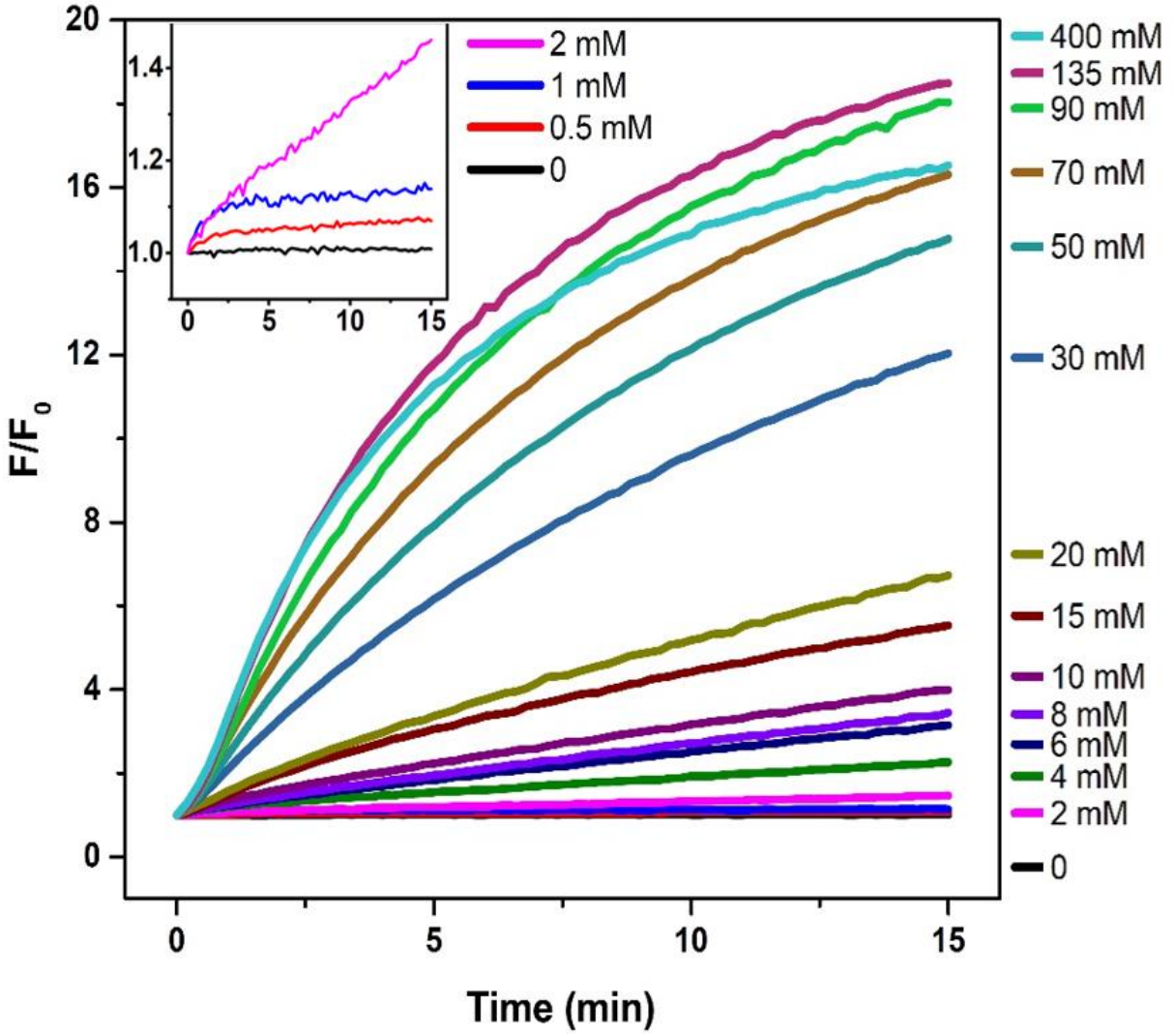

Figure 4.16 Time-dependent fluorescence increases over the background signal at varying Na^+ concentrations. The DNAzyme sensor concentration was 60 nM in buffer containing 10 mM Bis-Tris (pH=7.0) and 90 mM LiCl, to assist formation of the NaA43E-NaA43S complex. (Inset) Sensor response to Na^+ concentrations below 2 mM.

Indeed, as shown in Figure 4.16 and 4.17, the observed rate of fluorescence increase was accelerated with additional Na^+, until saturation at ~ 135 mM Na^+, with an apparent dissociation

constant (K_d) of 39.1±2.3 mM (Fig. S9). The limit of detection was determined to be 135 μM or 3.1 parts per million (3σ/slope), with dynamic range up to 50 mM (Figure 4.17, inset). This range covers the likely cellular concentrations of Na^+ very well (65, 66).

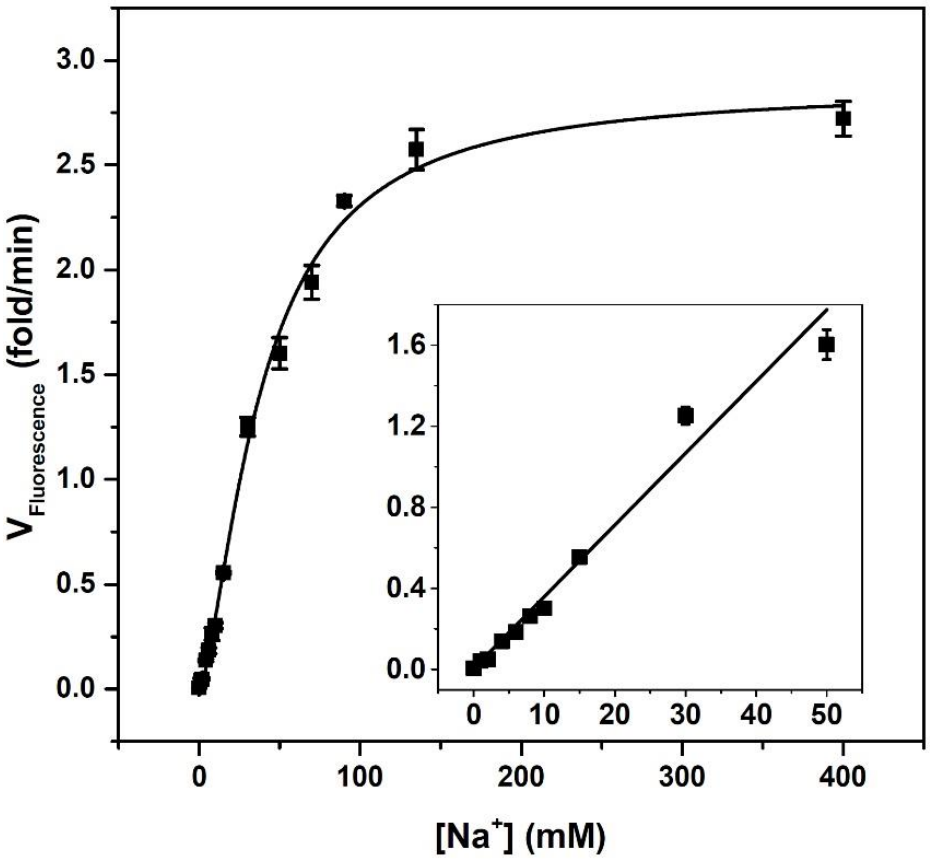

Figure 4.17 Na^+ detection based on the initial rate of fluorescence enhancement which is plotted versus Na^+ concentration. (Inset) Linear response at Na^+ concentrations lower than 50 mM. The error bars represent the standard deviation calculated from three independent experiments.

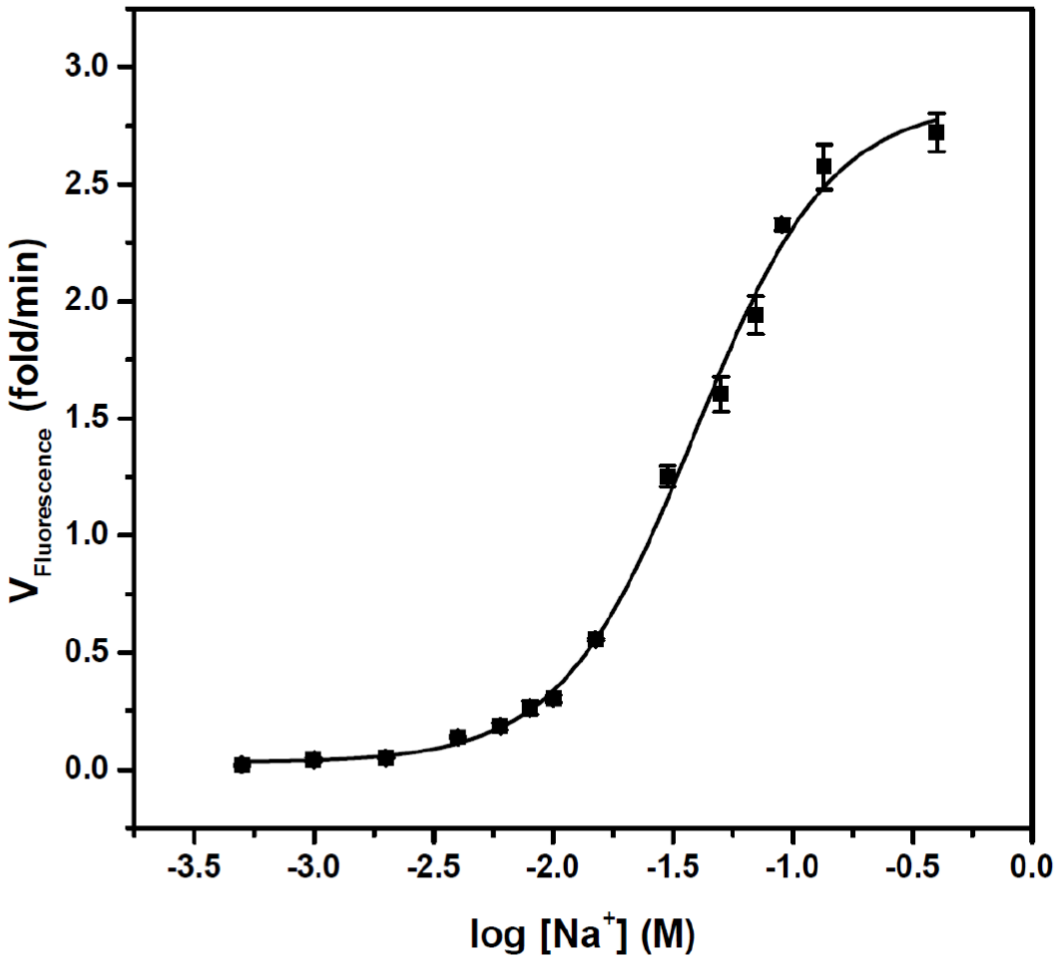

Figure 4.18 Rate of the initial fluorescence enhancement was calculated for different Na^+ concentration up to 400 mM. The change in the initial fluorescence enhancement leads to a K_d = 39.1 ± 2.3 mM. The error bars represent the standard deviation calculated from three independent experiments.

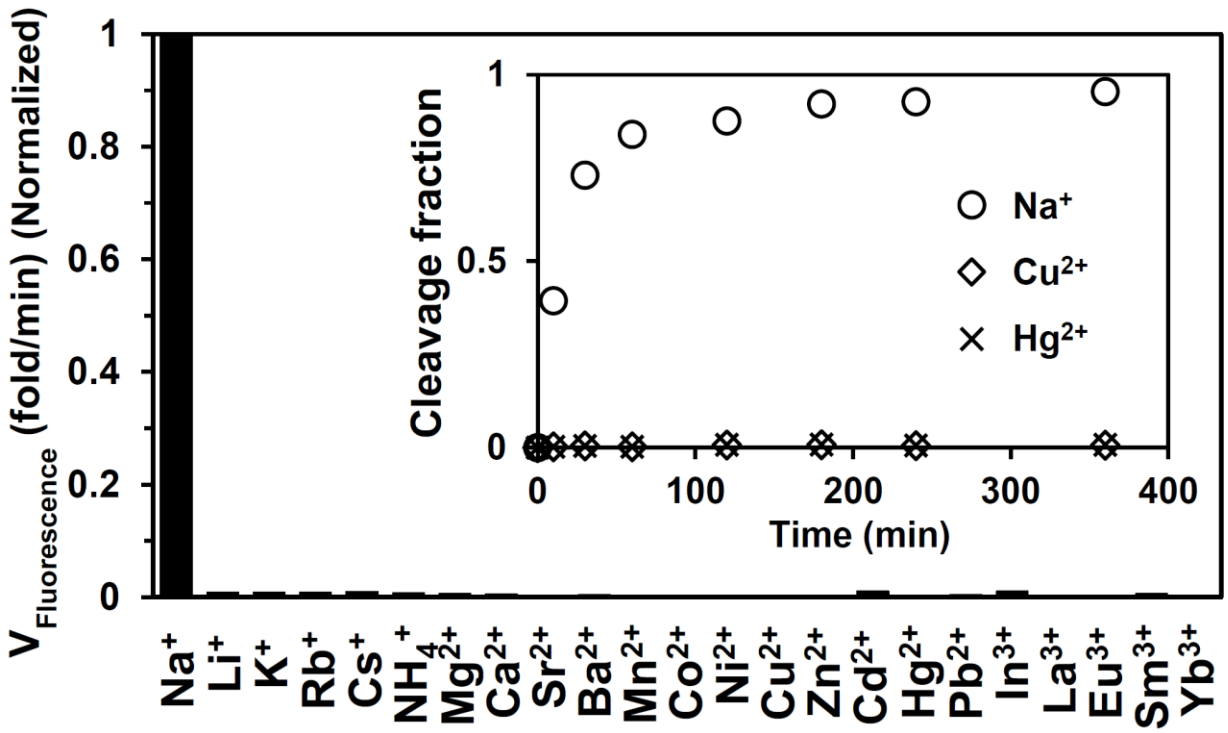

Figure 4.19 Response of the sensor to different competing metal ions. Sensor complex was formed in 90 mM LiCl and the rate of fluorescence enhancement was measured in presence of 100 mM, 2 mM and 0.2 mM of mono-, di- and trivalent metal ions, respectively. (Inset) Cleavage fraction of the substrate in a gel-based assay with ^{32}P radiolabeled substrate in the presence of Na^+, Cu^{2+} and Hg^{2+}.

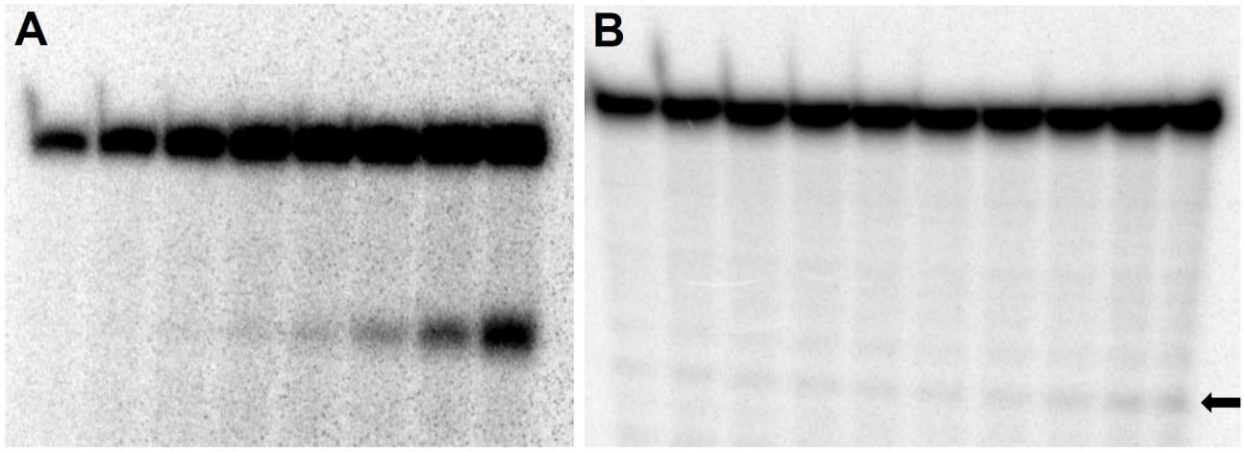

Figure 4.20 Activity of NaA43 was tested in the presence of 0.5 mM Na^+ (A) and 5 M Li^+ (B) over 25 h reaction time. Although 0.5 mM Na^+ results in ~ 20% cleavage after 25 h (last lane in A), 5 M Li^+ shows negligible cleavage over the same time period. Cleavage product (5′ cleavage fragment) in B is marked by a black arrow.

To determine the selectivity of the sensor for Na^+ over other metal ions, we monitored sensor response to 22 different metal ions. None of the tested metal ions showed a significant change in fluorescence signal (Figure 4.19), suggesting that the NaA43 DNAzyme based sensor has excellent selectivity for Na^+, with at least 10,000-fold better activity versus the next best competing metal ion (Li^+) (Figure 4.20). It is known that metal ions such as Cu^{2+} and Hg^{2+} induce a strong quenching on FAM (5), therefore the performance of the sensor with Cu^{2+} and Hg^{2+} was tested using a gel-based method. No cleavage was observed in response to either Cu^{2+} or Hg^{2+}, while incubation with Na^+ resulted in a significant increase in cleavage (Figure 4.19, inset). Interference of other monovalent metal ions and a few intracellularly abundant divalent metal ions was tested on sensor response to Na^+. The sensor remained selective in the presence of a mixture of 100 mM Na^+ and other mono- or divalent metal ions in their physiologically relevant concentrations (Figure 4.21).

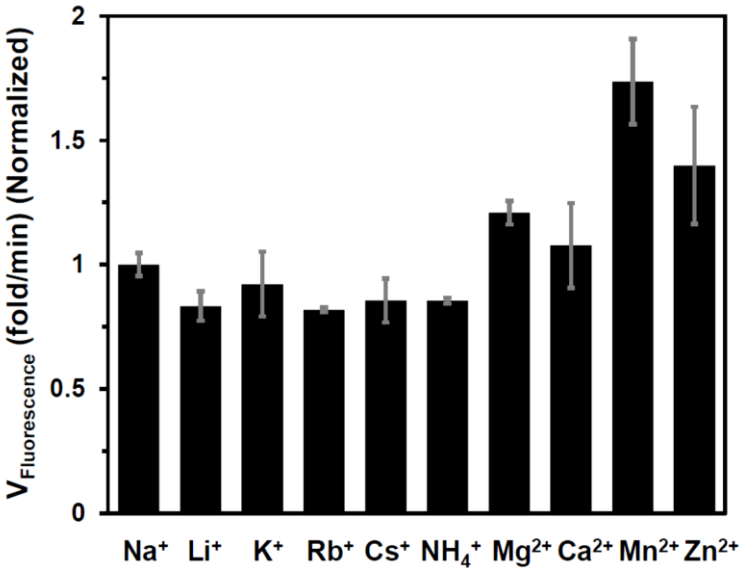

Figure 4.21 The rates of fluorescent increase of the NaA43 DNAzyme sensor in the presence of a mixture of 100 mM Na^+ and either 100 mM Li^+, Rb^+, Cs^+ or NH_4^+, 140 mM K^+, 0.5 mM Mg^{2+}, 1 µM Ca^{2+}, 100 µM Mn^{2+} or 100 µM Zn^{2+}. Error bars are represented by the standard deviation of the repeats performed (at least two independent experiments).

4.3.3 Intracellular Na^+ Imaging Using the NaA43 DNAzyme

Having demonstrated detection of Na^+ in a buffer, we then explored application of the Na^+-specific DNAzyme for imaging Na^+ in living cells. To prevent cleavage of NaA43S during the delivery of the DNAzyme into cells so that the activation of the sensor for Na^+ detection can be controlled with temporal resolution, we employed a photocaging strategy, in which the 2′-hydroxyl (2′-OH) group at the rA cleavage site in the substrate strand (NaA43S) was modified with a photolabile *o*-nitrobenzyl group (Figure 4.22) (67). The caging of the 2′-OH group prevents the cleavage of NaA43S by blocking the activity of 2′-OH as a nucleophile in a transesterification reaction (62). The caging group can be readily removed upon brief irradiation at 365 nm, which switches the substrate from being non-cleavable to cleavable, in a controllable manner.

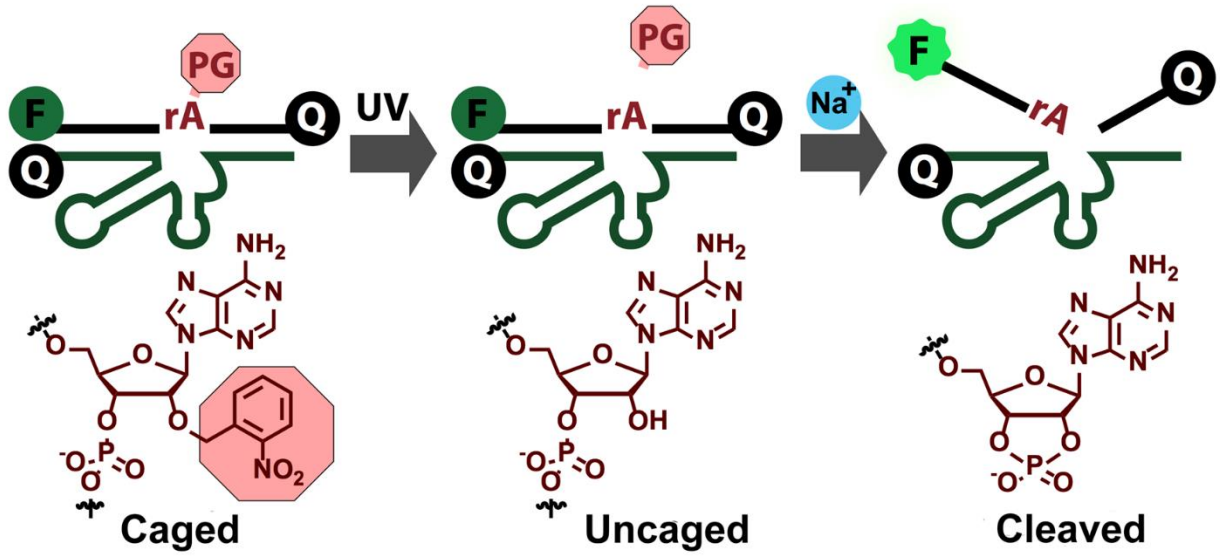

Figure 4.22 Scheme of the decaging process for the photolabile Na^+-specific DNAzyme.

To convert the caged DNAzyme into a fluorescent sensor, fluorophore and quenchers were attached to the DNAzyme in the same way as shown in Figure 4.15. The caged DNAzyme showed

no activity even in the presence of a high concentration of Na^+ (300 mM) (Figure 4.23). After 365 nm irradiation for 30 minutes, ~ 80% of the DNAzymes were decaged, estimated based on HPLC (51). Two saline solutions, commonly used for *in vivo* calibration of Na^+ probes (68) were made for testing the performance of the decaged DNAzyme. One solution contains 12.5 mM HEPES (pH 7.4), 140 mM NaCl, 10 mM glucose, 1.2 mM $MgCl_2$, and 1 mM $CaCl_2$. The other buffer has the same components except that 140 mM NaCl was replaced by 140 mM KCl. A mixture of these two solutions was used to generate buffers with a range of different concentrations of Na^+. Increased fluorescent signal with increasing concentrations of Na^+ was observed, indicating that the activity of the DNAzyme can be restored after reactivation by 365 nm irradiation (Figure 4.23).

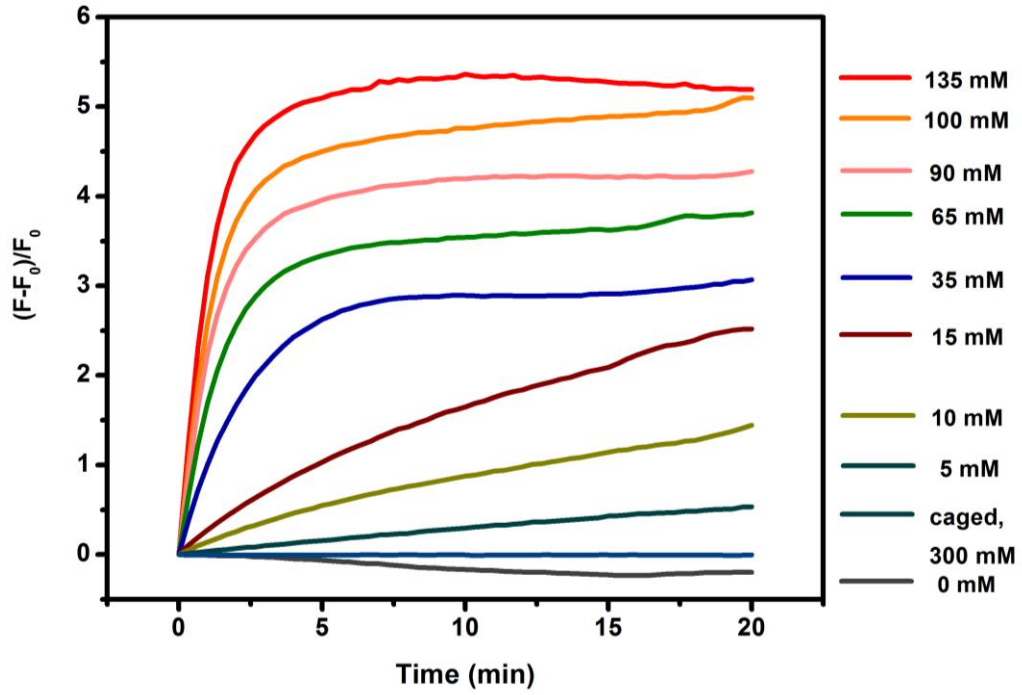

Figure 4.23 Turn-on fluorescence of NaA43ES sensor in buffer solution with different concentrations of Na^+. Active NaE-IBRQ and TAMRA-caged NaS-BHQ2 were used as the constructs of the sensor, and activity was measured after decaging the sensor at 365 nm for 30 min.

To use the photocaged Na^+-specific DNAzyme to image Na^+ in cells, a delivery method that can transport DNA into the cytoplasm of cells without accumulation in specific sub-cellular organelles is required. To achieve this goal, we chose an α-helical cationic polypeptide family, G8 (Figure 4.24A), which contains guanidine side chains that are known to play a crucial role in cell penetration efficiency (69). It has been demonstrated that G8 forms an ultrastable helical structure within a pH range of 1-9, and has sufficient water solubility. By maintaining its helical structure at both neutral and acidic pH, G8 was able to penetrate cell membranes as well as escape from endosomes and lysosomes, resulting in highly efficient gene delivery (Figure 4.24B) (69).

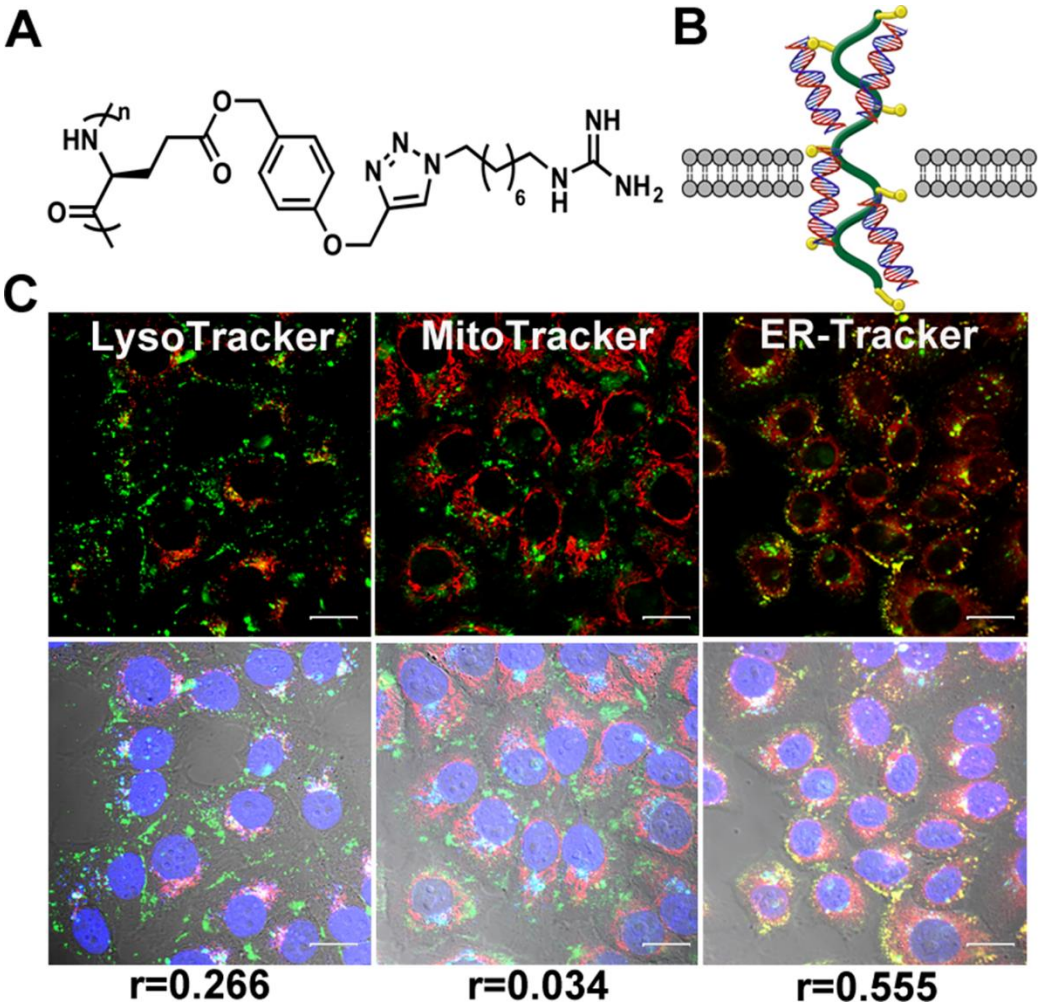

Figure 4.24 Intracellular delivery of NaA43ES DNAzymes into HeLa cells by G8 polypeptide. (A) Chemical structure of G8; (B) Scheme of the hypothesized delivery mechanism; (C) Internalization of FAM-labeled NaA43ES and its co-localization with LysoTracker (left), MitoTracker (middle) and ER-Tracker (right). (r refers to the Pearson correlation coefficients. Scale bar = 20 μm)

Using G8 polypeptide, we achieved high delivery efficiency of the NaA43ES DNAzymes into the cytoplasm of living HeLa cells after a 4 h incubation (Figure 4.24C). To further investigate localization of the DNAzymes inside cells, FAM-labeled non-cleavable NaA43S, in which the rA at cleavage site was substituted by deoxyribonucleic adenosine (dA), was used to form complex with NaA43E and was delivered using G8. Staining using organelle-specific dyes was carried out subsequently. The degree of co-localization of two fluorophores was quantified by Pearson

correlation coefficient as a standard technique (70). As suggested by both this calculation and microscopic images (Figure 4.24C), NaA43ES was mainly located inside the cytoplasm of the cell, without showing organelle localization in lysosomes, mitochondria, or the endoplasmic reticulum.

Given the fact that G8 polypeptide is a very efficient carrier for NaA43ES, we used it to deliver the caged NaA43ES complex into living HeLa cells (Figure 4.25A and B) for the detection of Na^+. The sensor showed minimal background fluorescence after its delivery, indicating that most of the caged NaA43S remained intact during the delivery process. After washing the cells to remove excess probes and G8 in the culture medium, the cells were incubated in Dulbecco's Phosphate-Buffered Saline (DPBS) solution and irradiated with light at 365 nm for 30 minutes in order to uncage the DNAzyme complex. Immediately after uncaging, the intracellular Na^+ level was elevated by adding gramicidin, monensin and ouabain. The combination of these three ionophores is known to equilibrate the intracellular Na^+ concentration with extracellular concentration within several minutes (22, 30). The influx of Na^+ from extracellular medium caused the fluorescence inside cells to gradually increase over a time course of 30 minutes (Figure 4.25A). In comparison, with the same treatment, but using a non-cleavable NaA43S, the turn-on fluorescence was not observed inside cells (Figure 4.26).

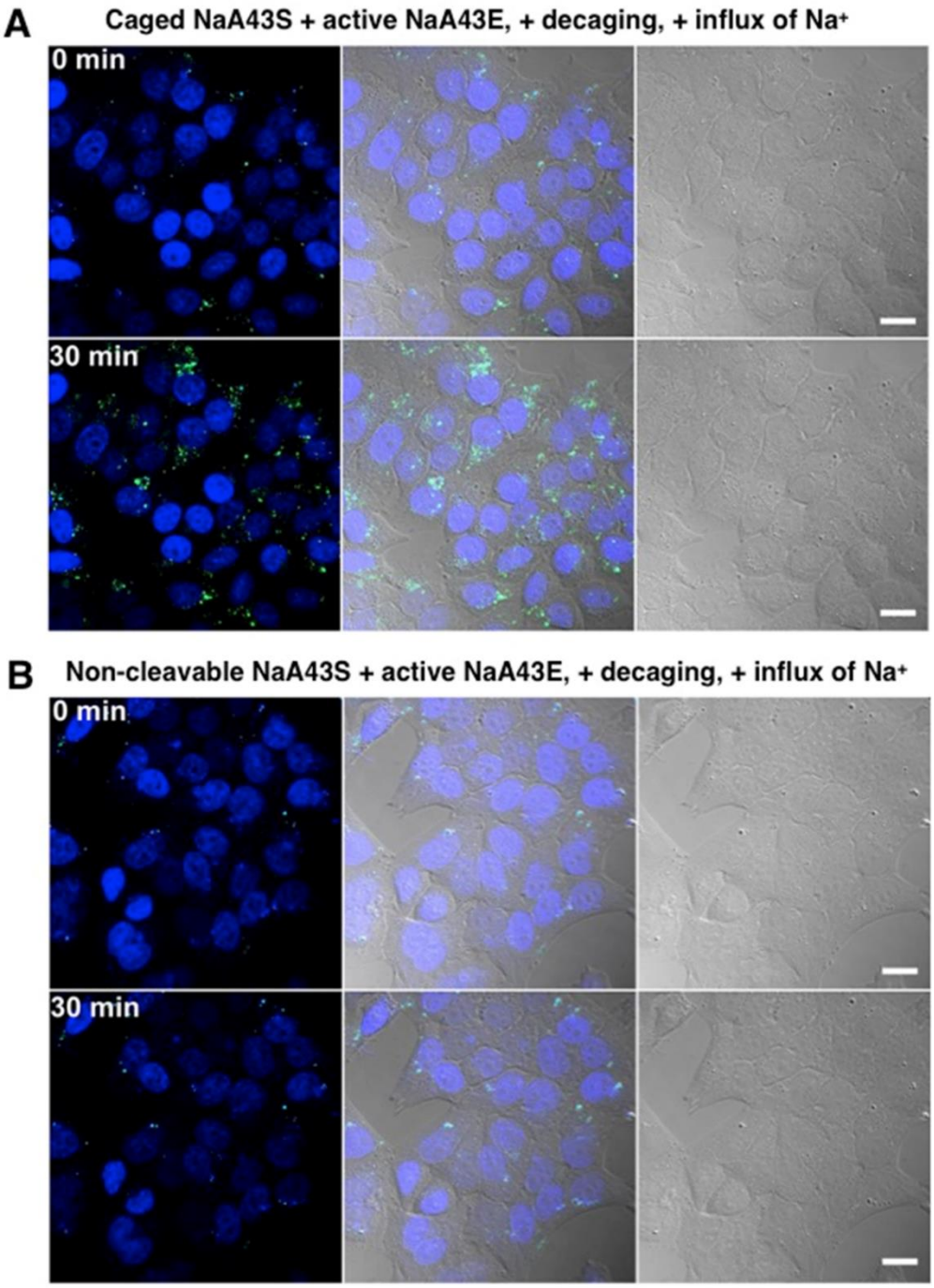

Figure 4.25 Confocal microscopy images of HeLa cells transfected with (A) caged NaA43ES complex and (B) Non-cleavable NaA43S in complex with NaA43E. After transfection, both groups were irradiated with light at 365 nm for 30 min, followed by induced Na^+ influx. The images show the fluorescence of the probe inside cells before and 30 minutes after Na^+ influx, respectively. (Scale bar =20 μm)

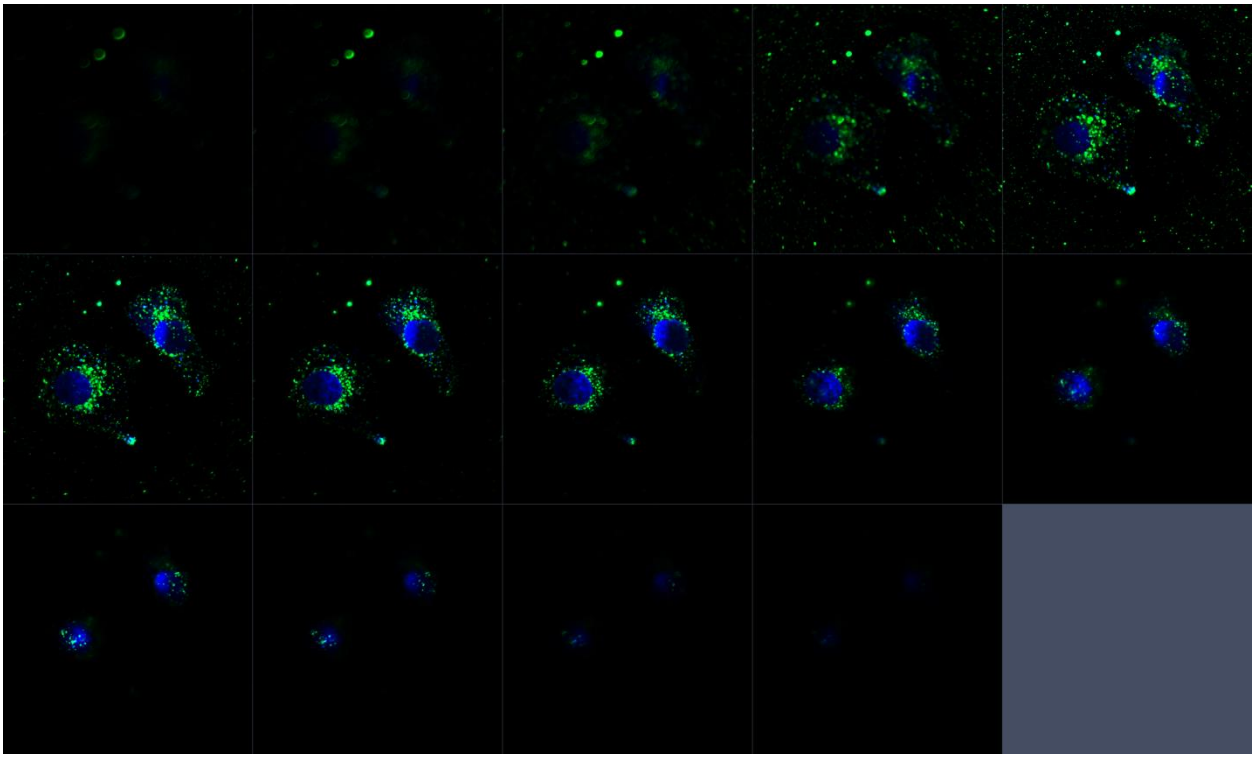

Figure 4.26 Z-stack images of HeLa cells with G8-NaA43ES complex. The green channel is FAM fluorescence from FAM-labeled non-cleavable NaA43S. The blue channel is Hoechst 33258 for nuclear staining.

To further confirm that the turn-on fluorescence was a result from the cleavage of uncaged NaA43S by active NaA43E, we also used the combination of caged NaA43S with an inactive variant of NaA43E as a negative control (forming catalytically inactive NaA43ES complex). The inactive NaA43E contains a single point mutation, which completely abolishes the DNAzyme activity. In this case, fluorescence from the probes was maintained at a constant background level over 30 minutes (Figure 4.27), which strongly suggests that the turn-on fluorescence we observed from the active NaA43ES resulted from successful decaging and subsequent Na^+-specific DNAzyme cleavage activity.

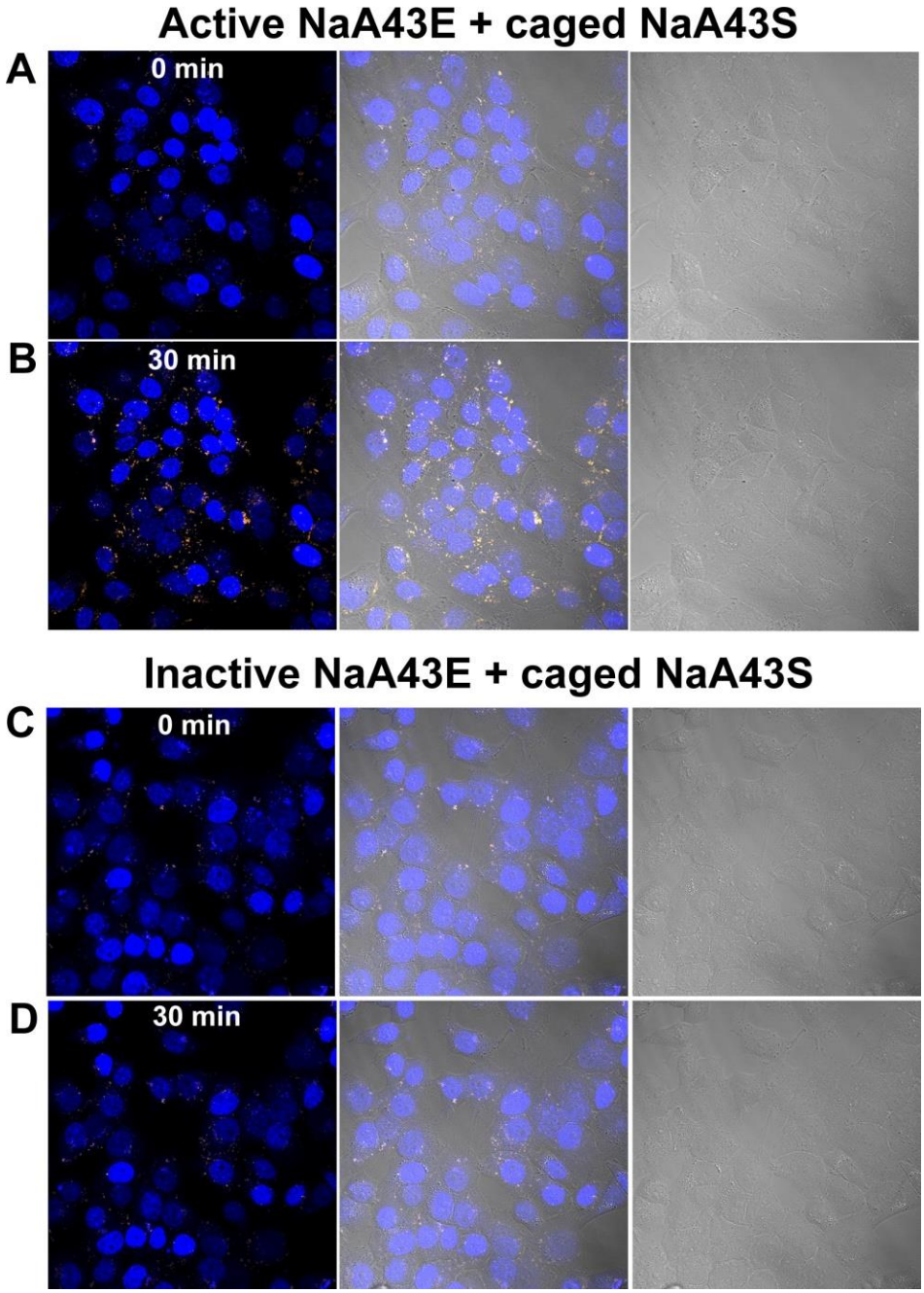

Figure 4.27 Confocal images of Na^+ sensing using TAMRA-caged NaA43S-BHQ2 as the substrate. To confirm the activity of NaA43E after decaging process, an inactive NaA43E construct that contains a single-point mutation was used as the control group. (A, B) Fluorescent and bright field images of cells delivered with active NaA43E-IBRQ and TAMRA-caged NaA43S-BHQ2 construct. Images were taken (A) immediately after adding ionophores or (B) after 30 minutes. (C, D) Fluorescent and bright field images of cells delivered with inactive NaA43E-IBRQ and TAMRA-caged NaA43S-BHQ2 construct. Images were taken (C) immediately after adding ionophores, or (D) after 30 minutes.

To support that the increased fluorescence intensity with Na^+ uptake noted in confocal imaging applies to the whole cell population, we employed flow cytometry. As shown in Figure 4.28, cells incubated with active NaA43ES and an influx of 143 mM Na^+ were the only group that showed a significant increase in fluorescence, after photo-decaging. In contrast, cells incubated with caged NaA43ES delivered to them showed a shift in fluorescence intensity from that of blank cells that can be attributed to background fluorescence. Additionally, without an influx of Na^+, cells delivered with active NaA43ES did not show increased fluorescence, suggesting that the fluorescent signal came from the Na^+-dependent activity of the probe rather than from any degradation of the DNAzyme probe by endogenous nucleases. Moreover, no turn-on fluorescence was observed in the populations of cells delivered with inactive NaA43ES, regardless of whether the Na^+ level inside cells was elevated or not, which is a strong indication that the fluorescent signal resulted from the activity of DNAzymes inside cells.

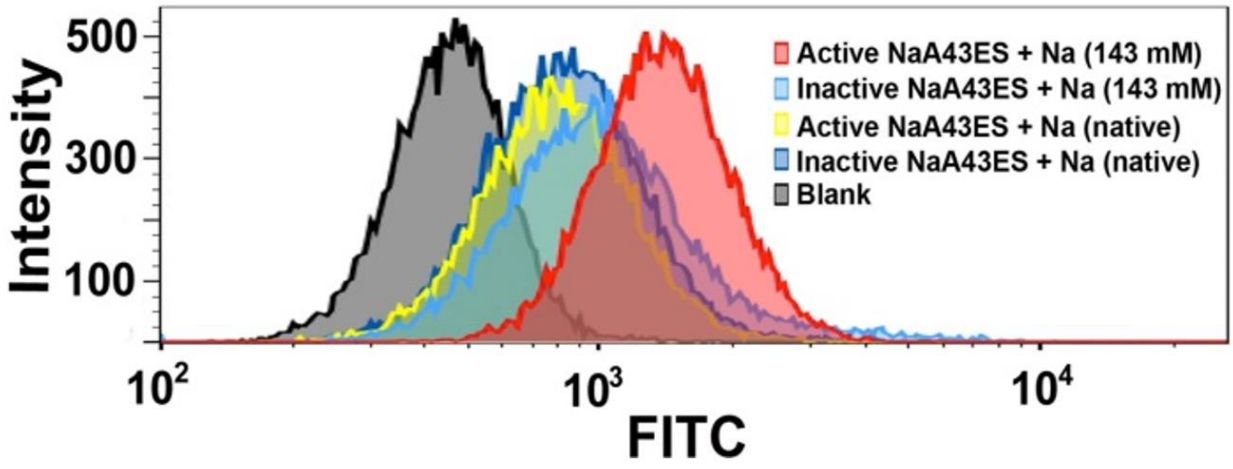

Figure 4.28 Flow cytometric quantification of cell associated fluorescence.

4.3.4 Developing a Point of Care Na^+ Sensor

Current commercial systems monitoring of Na^+ are mainly based on ion-selective electrode sensors and still suffer from issues of interferences from ions such as Br^- (71, 72). In addition, most of them are expensive and not pocket-able. Our group has shown previously that DNAzymes can be employed with personal glucose meter (PGM) to make quantitative, highly selective, easy to use, and portable sensors (73). In this general approach a DNAzyme-invertase conjugate is used to convert the metal-specific DNAzyme activity into the production of glucose, allowing the use of glucose concentration to quantify metal ions such as UO_2^{2+} and Pb^{2+} by PGM (73, 74). As shown in Figure 4.29, addition of Na^+ to the beads activates the DNAzyme, resulting in cleavage of the substrate into two shorter product strands at the rA position. Like our previous fluorescent sensor, the cleavage product had a much lower melting temperature to the enzyme strand than that of the substrate strand, leading to dehybridization and thus release of the invertase from the beads into the supernatant. Addition of the released invertase into a sucrose solution and subsequent conversion of sucrose into glucose, allowed to detect produced glucose by PGM.

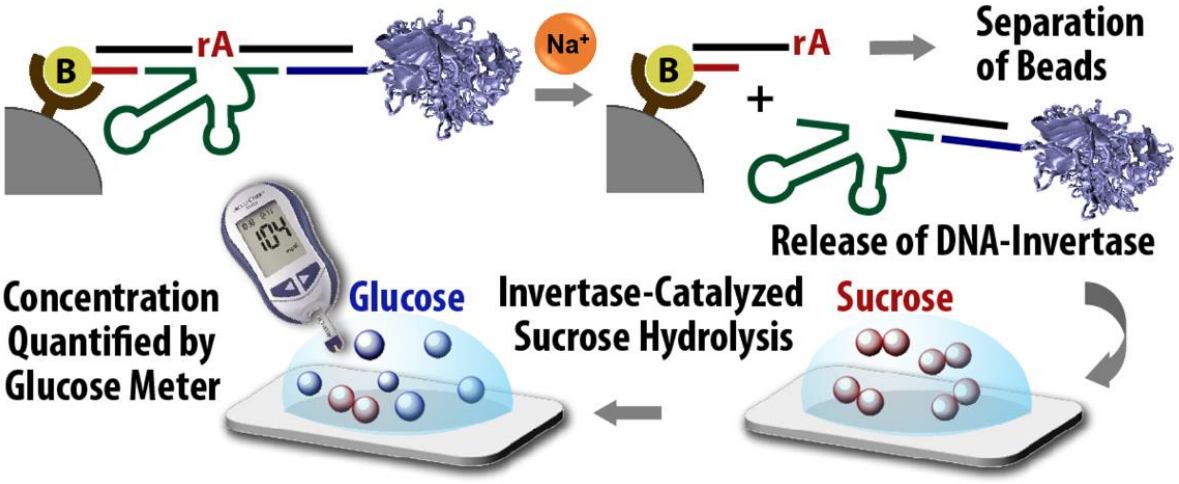

Figure 4.29 Solution assay of Na^+ based on DNAzyme-invertase conjugation. Schematic showing the release of the invertase in the presence of Na^+ and detection using PGM (image is made by Li Huey Tan).

First we have tested the performance of the DNAzyme-PGM based sensor for Na^+ human serum. Samples were incubated for only 30 minutes with the beads followed by 30 minutes incubation of the released invertase with the sucrose solution for 30 minutes. Produced glucose was monitored for each sample using PGM and the obtained PGM signals were plotted versus Na^+ concentrations in the samples. A dynamic range from 8.0 to 120 mM Na^+ (Figure 4.30) was obtained.

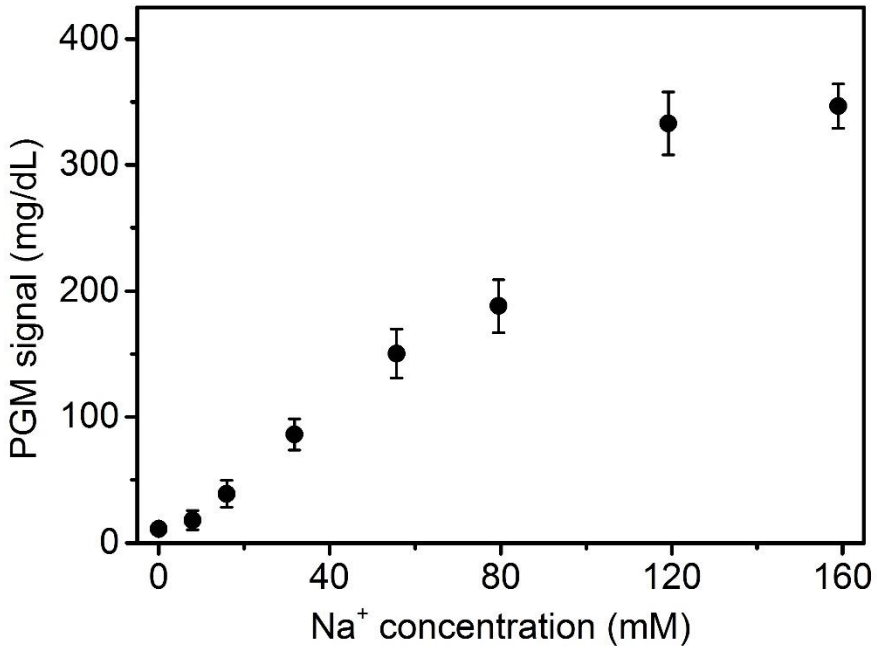

Figure 4.30 Na^+ detection in human serum dynamic range from 8.0 to 120 mM.

To further verify the accuracy and reliability of our DNAzyme-PGM-based sensor, we compared obtained data from our system to inductively coupled plasma mass spectrometry (ICP-MS) method (Figure 4.31). A series of human serum samples with different Na^+ levels were examined. A direct correlation between these two methods was found with a linear correlation coefficient of 0.99, demonstrating that the results from the two methods matched within the

experimental error (Figure 4.31A). In addition, we also tested our DNAzyme-PGM-based system in detecting Na^+ in calf blood. A direct correlation between these two methods was found with a linear correlation coefficient of 0.99 (Figure 4.31B), indicating an acceptable results for sodium sensing in animal blood using our system. These results demonstrate that the accuracy of the DNAzyme-PGM-based Na^+ detection method is as good as that of ICP-MS. Our results suggest reliability of using DNAzyme-PGM-based system as an alternative method for Na^+ detection that is simple and user-friendly.

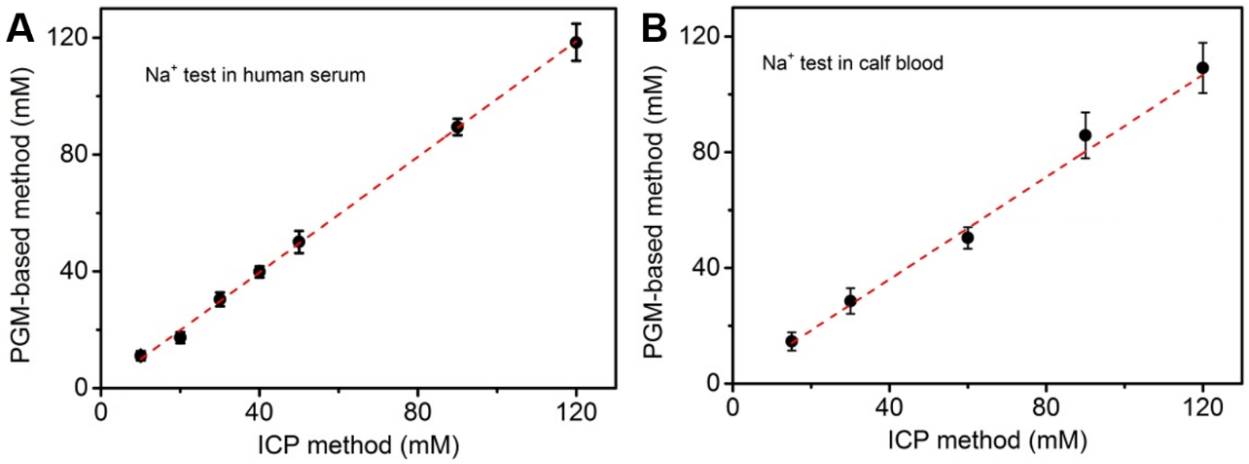

Figure 4.31 Validation of DNAzyme-PGM-based sensor for Na^+ in human serum (A) and calf blood (B) with ICP-MS.

4.4 Conclusions

In conclusion, we have obtained the first Na^+-specific RNA-cleaving DNAzyme (NaA43ES) with fast catalytic rate and exceptionally high selectivity over other metal ions, and demonstrated the use of this DNAzyme for sensing and imaging intracellular Na^+ in living cells, by adopting an efficient DNAzyme delivery method using a cationic polypeptide, together with a photo-caging strategy to allow controllable activation of the probe inside cells. In the field of sensing monovalent metal ions, in particular Na^+, obtaining highly selective sensors with proper sensitivity and selectivity has been a major challenge. Most previously developed Na^+ fluorescent sensors suffer from poor sensitivity or are also responsive to other metal ions such as K^+. The *in vitro* selection of DNAzymes selective for Na^+ has allowed for the identification of a fluorescent sensor with exceptional selectivity and sensitivity, further validating this method for the simple identification of sensors for many other metal ions, even where existing design strategies may be lacking. Finally, cellular sensing of sodium using DNAzyme sensors will allow for greater insight into the mechanisms and importance of sodium homeostasis in biology.

Furthermore, we applied the NaA43 DNAzyme to design a simple Na+ sensor based on personal glucose meter. We demonstrated that the DNAzyme-PGM-based method can be used for accurate detection of Na^+ in biological samples such as human serum. Such a simple and accurate detection method will facilitate monitoring of Na^+ level in a user-friendly fashion.

4.5 References

1. Guengerich FP (2008) Thematic Series: Metals in Biology. *J Biol Chem* 284(2):709-709.

2. Domaille DW, Que EL, & Chang CJ (2008) Synthetic fluorescent sensors for studying the cell biology of metals. *Nat Chem Biol* 4(3):168-175.

3. Fu D & Finney L (2014) Metalloproteomics: challenges and prospective for clinical research applications. *Expert Rev Proteomics* 11(1):13-19.

4. Gray HB (2003) Biological inorganic chemistry at the beginning of the 21st century. *Proc Natl Acad Sci U S A* 100(7):3563-3568.

5. Grant FD, *et al.* (2002) Low-renin hypertension, altered sodium homeostasis, and an alpha-adducin polymorphism. *Hypertension* 39(2):191-196.

6. Baartscheer A, *et al.* (2005) Chronic inhibition of Na/H-exchanger attenuates cardiac hypertrophy and prevents cellular remodeling in heart failure. *Cardiovasc Res* 65(1):83-92.

7. Moritz ML & Ayus JC (2010) Disorders of water and sodium homeostasis. *Oxford Textbook of Medicine*, eds Warrell D, Cox T, Firth J (Oxford University Press), pp 3818-3831.

8. Hollenberg NK (2006) The influence of dietary sodium on blood pressure. *J Am Coll Nutr* 25(3 Suppl):240S-246S.

9. Aronson PS, Boron WF & Boulpaep EL (2009) Transport of solutes and water. *Medical physiology: a cellular and molecular approach*, eds Boron WF, Boulpaep EL (Elsevier), pp 106-146.

10. Ferre-D'Amare AR & Winkler WC (2011) The roles of metal ions in regulation by riboswitches. *Met Ions Life Sci* 9:141-173.

11. Jaitovich A & Bertorello AM (2010) Intracellular sodium sensing: SIK1 network, hormone action and high blood pressure. *Biochim Biophys Acta* 1802(12):1140-1149.

12. Malloy CR, *et al.* (1990) Influence of global ischemia on intracellular sodium in the perfused rat heart. *Magn Reson Med* 15(1):33-44.

13. Grubman A, *et al.* (2014) X-ray fluorescence imaging reveals subcellular biometal disturbances in a childhood neurodegenerative disorder. *Chem Sci* 5(6):2503.

14. Ivanics T, Blum H, Wroblewski K, Wang DJ, & Osbakken M (1994) Intracellular sodium in cardiomyocytes using 23Na nuclear magnetic resonance. *Biochim Biophys Acta* 1221(2):133-144.

15. Kikuchi K (2010) Design, synthesis and biological application of chemical probes for bio-imaging. *Chem Soc Rev* 39(6):2048-2053.

16. Fahrni CJ & O'Halloran TV (1999) Aqueous coordination chemistry of quinoline-based fluorescence probes for the biological chemistry of zinc. *J Am Chem Soc* 121(49):11448-11458.

17. McRae R, Bagchi P, Sumalekshmy S, & Fahrni CJ (2009) In situ imaging of metals in cells and tissues. *Chem Rev* 109(10):4780-4827.

18. Chang CJ, Jaworski J, Nolan EM, Sheng M, & Lippard SJ (2004) A tautomeric zinc sensor for ratiometric fluorescence imaging: application to nitric oxide-induced release of intracellular zinc. *Proc Natl Acad Sci U S A* 101(5):1129-1134.

19. Qiu L, *et al.* (2014) A turn-on fluorescent Fe(3+) sensor derived from an anthracene-bearing bisdiene macrocycle and its intracellular imaging application. *Chem Commun (Camb)* 50(35):4631-4634.

20. Wegner SV, Arslan H, Sunbul M, Yin J, & He C (2010) Dynamic copper(I) imaging in mammalian cells with a genetically encoded fluorescent copper(I) sensor. *J Am Chem Soc* 132(8):2567-2569.

21. Carter KP, Young AM, & Palmer AE (2014) Fluorescent Sensors for Measuring Metal Ions in Living Systems. *Chem Rev* 114(8):4564-4601.

22. Donoso P, Mill JG, O'Neill SC, & Eisner DA (1992) Fluorescence measurements of cytoplasmic and mitochondrial sodium concentration in rat ventricular myocytes. *J Physiol* 448:493-509.

23. Amorino GP & Fox MH (1995) Intracellular Na+ measurements using sodium green tetraacetate with flow cytometry. *Cytometry* 21(3):248-256.

24. Meier SD, Kovalchuk Y, & Rose CR (2006) Properties of the new fluorescent Na+ indicator CoroNa Green: comparison with SBFI and confocal Na+ imaging. . *J Neurosci Methods* 155(2):251-259.

25. Jayaraman S, Song Y, Vetrivel L, Shankar L, & Verkman AS (2001) Noninvasive in vivo fluorescence measurement of airway-surface liquid depth, salt concentration, and pH. *J Clin Invest* 107(3):317-324.

26. Kim MK, *et al.* (2010) Sodium-Ion-Selective Two-Photon Fluorescent Probe for In Vivo Imaging. *Angew Chem Int Ed Engl* 49(2):364-367.

27. Sarkar AR, Heo CH, Park MY, Lee HW, & Kim HM (2014) A small molecule two-photon fluorescent probe for intracellular sodium ions. *Chem Commun* 50(11):1309-1312.

28. Martin VV, Rothe A, & Gee KR (2005) Fluorescent metal ion indicators based on benzoannelated crown systems: a green fluorescent indicator for intracellular sodium ions. *Bioorg Med Chem Lett* 15(7):1851-1855.

29. Dubach JM, Lim E, Zhang N, Francis KP, & Clark H (2011) In vivo sodium concentration continuously monitored with fluorescent sensors. *Integr Biol (Camb)* 3(2):142-148.

30. Bernardinelli Y, Azarias G, & Chatton JY (2006) In situ fluorescence imaging of glutamate-evoked mitochondrial Na+ responses in astrocytes. *Glia* 54(5):460-470.

31. Kenmoku S, *et al.* (2004) Rational design of novel photoinduced electron transfer type fluorescent probes for sodium cation. *Tetrahedron* 60(49):11067-11073.

32. Gunnlaugsson T, Nieuwenhuyzen M, Richard L, & Thoss V (2002) Novel sodium-selective fluorescent PET and optically based chemosensors: towards Na+ determination in serum. *J Chem Soc Perkin Trans 2* (1):141-150.

33. Leray I, Valeur B, O'Reilly F, Jiwan JLH, & Soumillion JP (1999) A new calix[4]arene-based fluorescent sensor for sodium ion. *Chem Commun* (9):795-796.

34. Leray I, Lefevre JP, Delouis JF, Delaire J, & Valeur B (2001) Synthesis and photophysical and cation-binding properties of mono- and tetranaphthylcalix[4]arenes as highly sensitive and selective fluorescent sensors for sodium. *Chemistry* 7(21):4590-4598.

35. Breaker RR & Joyce GF (1994) A DNA enzyme that cleaves RNA. *Chem Biol* 1(4):223-229.

36. Xiang Y & Lu Y (2014) DNA as sensors and imaging agents for metal ions. *Inorg Chem* 53(4):1925-1942.

37. Chiuman W & Li Y (2007) Simple fluorescent sensors engineered with catalytic DNA 'MgZ' based on a non-classic allosteric design. *PLoS One* 2(11):e1224.

38. Schlosser K & Li Y (2010) A versatile endoribonuclease mimic made of DNA: characteristics and applications of the 8-17 RNA-cleaving DNAzyme. *Chembiochem* 11(7):866-879.

39. Joyce GF (2004) Directed evolution of nucleic acid enzymes. *Annu Rev Biochem* 73:791-836.

40. Ihms HE & Lu Y (2012) In vitro selection of metal ion-selective DNAzymes. *Methods Mol Biol* 848:297-316.

41. Wu P, Hwang K, Lan T, & Lu Y (2013) A DNAzyme-gold nanoparticle probe for uranyl ion in living cells. *J Am Chem Soc* 135(14):5254-5257.

42. Santoro SW & Joyce GF (1997) A general purpose RNA-cleaving DNA enzyme. *Proc Natl Acad Sci U S A* 94(9):4262-4266.

43. Deibler K & Basu P (2013) Continuing issues with Lead: Recent Advances in Detection. *Eur J Inorg Chem* 2013(7):1086-1096.

44. Carmi N, Shultz LA, & Breaker RR (1996) In vitro selection of self-cleaving DNAs. *Chem Biol* 3(12):1039-1046.

45. Carmi N, Balkhi SR, & Breaker RR (1998) Cleaving DNA with DNA. *Proc Natl Acad Sci U S A* 95(5):2233-2237.

46. Li J, Zheng W, Kwon AH, & Lu Y (2000) In vitro selection and characterization of a highly efficient Zn(II)-dependent RNA-cleaving deoxyribozyme. *Nucleic Acids Res* 28(2):481-488.

47. Liu J, *et al.* (2007) A catalytic beacon sensor for uranium with parts-per-trillion sensitivity and millionfold selectivity. *Proc Natl Acad Sci U S A* 104(7):2056-2061.

48. Hollenstein M, Hipolito C, Lam C, Dietrich D, & Perrin DM (2008) A Highly Selective DNAzyme Sensor for Mercuric Ions. *Angew Chem Int Ed Engl* 47(23):4346-4350.

49. Torabi SF & Lu Y (2014) Functional DNA nanomaterials for sensing and imaging in living cells. *Curr Opin Biotechnol* 28:88-95.

50. Zhang L, Huang H, Xu N, & Yin Q (2014) Functionalization of cationic poly(p-phenylene ethynylene) with dendritic polyethylene enables efficient DNAzyme delivery for imaging Pb2+ in living cells. *J Mater Chem B* 2:4935-4942.

51. Hwang K, *et al.* (2014) Photocaged DNAzymes as a General Method for Sensing Metal Ions in Living Cells. *Angew Chem Int Ed Engl* .

52. Meng H-M, *et al.* (2014) DNA Dendrimer: An Efficient Nanocarrier of Functional Nucleic Acids for Intracellular Molecular Sensing. *ACS Nano* 8(6):6171-6181.

53. Faulhammer D & Famulok M (1997) Characterization and divalent metal-ion dependence of in vitro selected deoxyribozymes which cleave DNA/RNA chimeric oligonucleotides. *J Mol Biol* 269(2):188-202.

54. Geyer CR & Sen D (1997) Evidence for the metal-cofactor independence of an RNA phosphodiester-cleaving DNA enzyme. *Chem Biol* 4(8):579-593.

55. Carrigan MA, Ricardo A, Ang DN, & Benner SA (2004) Quantitative Analysis of a RNA-Cleaving DNA Catalyst Obtained via in Vitro Selection. *Biochemistry* 43(36):11446-11459.

56. Hollenstein M, Hipolito CJ, Lam CH, & Perrin DM (2009) A self-cleaving DNA enzyme modified with amines, guanidines and imidazoles operates independently of divalent metal cations (M2+). *Nucleic Acids Res* 37(5):1638-1649.

57. Smuga D, Majchrzak K, Sochacka E, & Nawrot B (2010) RNA-cleaving 10–23 deoxyribozyme with a single amino acid-like functionality operates without metal ion cofactors. *New J Chem* 34(5):934.

58. Hollenstein M, Hipolito CJ, Lam CH, & Perrin DM (2013) Toward the combinatorial selection of chemically modified DNAzyme RNase A mimics active against all-RNA substrates. *ACS Comb Sci* 15(4):174-182.

59. Weinstein LB, Earnshaw DJ, Cosstick R, & Cech TR (1996) Synthesis and Characterization of an RNA Dinucleotide Containing a 3‘-S-Phosphorothiolate Linkage. *J Am Chem Soc* 118(43):10341-10350.

60. Matsumoto Y & Komiyama M (1990) Efficient cleavage of adenylyl(3'-5')adenosine by triethylenetetraminecobalt(III). *J Chem Soc Chem Commun* (15):1050-1051.

61. Markham NR & Zuker M (2008) UNAFold: software for nucleic acid folding and hybridization. *Methods Mol Biol* 453:3-31.

62. Brown AK, Li J, Pavot CM, & Lu Y (2003) A lead-dependent DNAzyme with a two-step mechanism. *Biochemistry* 42(23):7152-7161.

63. Li J & Lu Y (2000) A Highly Sensitive and Selective Catalytic DNA Biosensor for Lead Ions. *J Am Chem Soc* 122(42):10466-10467.

64. Liu J & Lu Y (2003) Improving fluorescent DNAzyme biosensors by combining inter- and intramolecular quenchers. *Anal Chem* 75(23):6666-6672.

65. Murphy E & Eisner DA (2009) Regulation of intracellular and mitochondrial sodium in health and disease. *Circ Res* 104(3):292-303.

66. Cinelli AR, Efendiev R, & Pedemonte CH (2008) Trafficking of Na-K-ATPase and dopamine receptor molecules induced by changes in intracellular sodium concentration of renal epithelial cells. *Am J Physiol Renal Physiol* 295(4):F1117-1125.

67. Chaulk SG & MacMillan AM (2007) Synthesis of oligo-RNAs with photocaged adenosine 2'-hydroxyls. *Nat Protoc* 2(5):1052-1058.

68. Donoso P, Mill JG, O'Neill SC, & Eisner DA (1992) Fluorescence measurements of cytoplasmic and mitochondrial sodium concentration in rat ventricular myocytes. *J Physiol* 448:493-509.

69. Zhang R, Zheng N, Song Z, Yin L, & Cheng J (2014) The effect of side-chain functionality and hydrophobicity on the gene delivery capabilities of cationic helical polypeptides. *Biomaterials* 35(10):3443-3454.

70. Radford RJ, Chyan W, & Lippard SJ (2013) Peptide-based Targeting of Fluorescent Zinc Sensors to the Plasma Membrane of Live Cells. *Chem Sci* 4(8):3080-3084.

71. Privett, B. J., Shin, J. H., and Schoenfisch, M. H. (2008) Electrochemical sensors, *Anal Chem* 80, 4499-4517.

72. Jain, A., Subhan, I., and Joshi, M. (2009) Comparison of the point-of-care blood gas analyzer versus the laboratory auto-analyzer for the measurement of electrolytes, *Int J Emerg Med* 2, 117-120.

73. Xiang, Y., and Lu, Y. (2011) Using personal glucose meters and functional DNA sensors to quantify a variety of analytical targets, *Nat Chem* 3, 697-703.

74. Xiang, Y., and Lu, Y. (2012) Portable and quantitative detection of protein biomarkers and small molecular toxins using antibodies and ubiquitous personal glucose meters, *Anal Chem* 84, 4174-4178.

5 Chapter 5. Biochemical Characterization of a Na^+-specific DNAzyme

5.1 Introduction

The discovery of ribozymes in early 1980s followed by the isolation of short DNA molecules with catalytic activity in 1994 fundamentally changed biochemists' understanding about the ways biomolecules catalyze reactions (*1-3*). Deoxyribozymes (DNAzymes or catalytic DNA) are obtained by a combinatorial process known as *in vitro* selection, a powerful approach to identify oligonucleotides from a large library of random sequences (up to 10^{14}). These DNAzymes are single stranded DNA molecules that can catalyze a variety of chemical reactions including RNA/DNA cleavage, RNA/DNA ligation, phosphoryl transfer, peptide bond formation, peptide-nucleic acid conjugation, and porphyrin metallation (*4-11*). Since DNA is a negatively charged and relatively functionality-poor biopolymer, most identified DNAzymes require multivalent metal ions or other cofactors for efficient catalysis. It is suggested that ribozymes and DNAzymes require metal ions for proper folding and/or catalytic activity (*4*, *11*, *12*). Due to the high metal specificity displayed by RNA-cleaving DNAzymes, they are the most extensively used class of DNAzymes in designing biosensors for metal ions (*13-15*).

In contrast to metal-dependent DNAzymes, it has been shown that amino acid functionalities can be used as a cofactor in DNAzymes. A histidine-dependent DNAzyme has been suggested to utilize the imidazole group of histidine for catalysis in a way analogous to the catalytic mechanism of RNase A (*16*). Additionally, several divalent metal-independent DNAzymes have been reported by equipping DNAzymes with one or multiple protein-like functionalities (*e.g.* amines, guanidinium, and imidazole) (*17-20*). These DNAzymes perform catalysis independent of

any divalent metal ions or small molecule cofactors and are similar to the other cofactor-independent DNAzymes isolated previously (*21, 22*). Different DNAzymes have been obtained for catalysis with several metal ions including Pb^{2+} (*3*), Mg^{2+} (*23*), Ca^{2+} (*24*), Mn^{2+} (*25*), Co^{2+} (*26*), Zn^{2+} (*27*), Hg^{2+} (*28*), UO_2^{2+} (*29*), and lanthanides (*30*). Although many metal-dependent DNAzymes have been reported so far, few examples are highly selective for a specific metal cofactor (*viz.* UO_2^{2+}-dependent DNAzyme (17), Pb^{2+}-dependent DNAzyme (GR5) (4), and Hg^{2+}-dependent DNAzyme (18)). The most extensively studied DNAzymes, 10-23 and 8-17, are active with several divalent metal ions (*23, 31-33*). Other metal dependent DNAzymes perform reactions with different divalent metal ions with partial preference for one over another (*24-26, 34, 35*) or with trivalent metal ions with no preference for a specific metal ion (*30*).

I have recently selected, to the best of our knowledge, the first Na^+-specific DNAzyme with a fast catalytic rate ($k_{obs} \sim 0.1\ min^{-1}$). Na^+ is the most abundant metal ion in biological systems and is among the most abundant metal ions in the intracellular environment (*36*). A variety of biological processes are influenced by Na^+ through the activation of signal transduction pathways, or indirectly through the action of hormones (*37*). Na^+ is tightly regulated in the body and its imbalance is associated with several health conditions including hypertension (*38*), heart failure (*39*), and diabetes insipidus (*40*). To identify a Na^+-specific DNAzyme that can recognize Na^+ selectively from the other metal ions, an *in vitro* selection experiment was performed using Na^+ as the only cofactor. A fluorescent sensor was designed based on NaA43, one of the selected DNAzymes, with a remarkable selectivity (> 10,000-fold) for Na^+ over competing metal ions and with a detection limit of 135 μM.

Although the above preliminary studies showed some of the unique properties of the Na^+-specific DNAzyme such as high rate of catalysis without aid of divalent metal ion cofactors and

high specificity for Na^+, the structure and mechanism of this DNAzyme is not known. Here I report a comprehensive study on the mechanism of the NaA43 DNAzyme by thoroughly investigating catalytically important nucleotides and conserved sequence of NaA43; metal binding affinity and specificity; kinetic properties; pH dependence of the catalysis in the presence of Na^+; and the effect of other metal ions on DNAzyme activity. Studying the mechanistic properties of the NaA43 DNAzyme provides a better understanding on how these and other DNAzymes function and will help in the design of better biosensors.

5.2 Materials and Methods

5.2.1 Materials

All oligonucleotides were purchased from Integrated DNA Technology Inc. (IDT) and purified by denaturing (8 M urea) 10 % polyacrylamide gel electrophoresis (PAGE) before use. Sensor oligonucleotides were synthesized and HPLC-purified by IDT. Details of the nucleotide sequences are provided in Sequences section. Other metal salts used included the following: $LiCl.H_2O$ (Alfa Aesar, 99.996%), NaCl (Alfa Aesar, 99.999%), KCl ((Alfa Aesar, 99.995%), RbCl (Alfa Aesar, 99.975%), CsCl (Alfa Aesar, 99.999%), $NH_4CH_3CO_2$ (Aldrich, 99.999%), $MgCl_2.6H_2O$ (Alfa Aesar, 99.999%), $Ca(NO_3)_2.6H_2O$ (Alfa Aesar, 99.995%), $SrCl_2.6H_2O$ (Alfa Aesar, 99.996%), $BaCl_2.2H_2O$ (Alfa Aesar, 99.997%), $Mn(CH_3CO_2)_2.4H_2O$ (Alfa Aesar, 99.999%), $CoCl_2.6H_2O$ (Alfa Aesar, 99.9%), $NiCl_2.6H_2O$ (Alfa Aesar, 99.995%), $Cu(NO_3)_2.H_2O$ (Alfa Aesar, 99.999%), $ZnCl_2.H_2O$ (Alfa Aesar, 99.99%), $Cd(NO_3)_2.4H_2O$ (Alfa Aesar, 99.999%), $HgCl_2$ (Alfa Aesar, 99.999%), $Pb(CH_3CO_2)_2.3H_2O$ (Aldrich, 99.999%), $InCl_3$ (Aldrich, 99.999%), $La(NO_3)_3.6H_2O$ (Aldrich, 99.999%), $EuCl_3.6H_2O$ (Aldrich, 99.999%), $SmCl_3.6H_2O$ (Aldrich, 99.99%), and $YbCl_3.6H_2O$ (Aldrich, 99.998%). Salts and solutions used to adjust pH of buffer solutions included the following: $LiOH.H_2O$ (Alfa Aesar, 99.996%) $NaOH.H_2O$ (Alfa Aesar, 99.996%), KOH (Fisher Scientific), and 36.5% HCl (Alfa Aesar, 99.999%). Other chemicals used to prepare different solutions included the following: Ethylenediaminetetraacetic acid, sodium free (EDTA) (Fluka, 99.0%), $EDTA.2Na.2H_2O$ (Fisher Scientific), Trisodium citrate (Alfa Aesar, 99%), urea (Affymetrix, MB grade), Tris (Affymetrix, MB grade), boric acid (Fisher Scientific, electrophoresis grade), and Bis-Tris (Sigma, 99.0%). Acrylamide/bisacrylamide 40% solution (29:1) was obtained from Bio-Rad. *Taq* DNA polymerase with standard *Taq* buffer, T4-polynucletide kinase, and deoxynucleotide (dNTP) solution mix were obtained from New England

Biolabs. ^{32}P labeled γ-ATP for DNA radiolabeling was obtained from Perkin-Elmer. All buffer, metal ion and gel stock solutions were prepared with Milli-Q water. The pH of the buffers was measured with a Fisher Scientific Accumet AB15 pH meter.

5.2.2 Methods

5.2.2.1 Gel-Based Activity Assays

Activity assay experiments were carried out using *cis*-cleaving Na+ DNAzymes obtained from cloning and sequencing experiments. Single stranded DNAzymes were PCR amplified using a primer with Taq-stopper and internally labeled with ^{32}P with the same protocol mentioned earlier. No annealing step was carried out before testing the activity of individual pools or *cis*-cleaving DNAzymes. DNA samples were dissolved in 20 mM Bis-Tris pH 7.0 and 50 mM Li^+ (reaction buffer) and tested with different concentrations of Na^+ or other metal ions. Each reaction was initiated by the addition of 10 µl of 2X Na^+ solution to 10 µl of the DNA in 1X reaction buffer. At known time points, 2 µl aliquots of the reaction mixture were withdrawn and added to 18 µl of a stop solution containing 0.1 mM EDTA, 9.2 M Urea, 1X TBE, 0.05 % xylene cyanol and 0.05 % bromophenol blue. Since Na^+ DNAzymes use Na^+ as a cofactor and EDTA cannot chelate Na^+, a combination of dilution and unfolding in high concentration of denaturant (urea) was used to quench reactions. It was shown that this procedure quenches the reactions even when high concentrations of Na^+ were used in reaction medium. The fraction of cleavage at each time point was monitored after separation on a 10 % PAGE gel (36 W, 1.5h). The gel was then wrapped and exposed to a phosphorimager cassette. The cassette was then imaged using a Molecular Dynamics Storm 430 Phosphorimager (from Amersham Biosciences) and the fraction of cleavage was calculated using ImageQuant software (Molecular Dynamics). To monitor activity of *trans*-cleaving DNAzymes, each substrate was radioactively labeled with [γ-^{32}P]-dATP using T4 kinase

from NEB. The labeling mixture contained 10 pmol of the substrate, 1X forward reaction buffer, 0.5 µL of T4 kinase and 1 µl of [γ-^{32}P]-dATP, the total volume being 20 µl. This solution incubated at 37 °C for 1.5 h. *Trans*-cleaving Na^+ DNAzyme activity was monitored under single-turnover conditions (NaA43E : NaA43S > 200:1) unless otherwise stated. The NaA43ES complex was annealed at 80 °C for 3 minutes and cooled down to room temperature over 20 minutes. Reactions were initiated as mentioned earlier. To separate cleavage product from uncleaved substrate DNA samples were separated on a 20 % PAGE gel. If gels were used for a single loading they were run at 40 W for 1.5 h.; if used for double loading, the first loaded samples ran at 40 W for 1h 10min and after subsequent loading samples were run for another 1 h at 40 W. Timing for double loading depends on the size of cleaved products and uncleaved substrate.

Rate of cleavage was determined by plotting cleavage percentage versus time and fitting the data points to the following equation:

$$Y_t = Y_0 + Y_\infty (1\text{-}e^{-kobs \times t}) \quad (1)$$

In this equation Y_0 is the initial percent of cleavage product (t = 0), Y_∞ is the % of product at the end point of the reaction (t = ∞) Y_t is the % of product at time t, and k_{obs} is the apparent rate of cleavage.

5.2.2.2 pH Profile

Cleavage activity of the NaA43 DNAzyme was monitored at saturating concentration of Na^+ (400 mM) at different pH values to study the effect of pH on the activity of NaA43. Different buffers were used including: acetate (for pH between 4.0 to 5.5), Bis-Tris (for pH between 6.0 to 7.0), MOPS (for pH 7.5), Tris-HCl (for pH 8.0 to 9.0), and CHES (for pH 9.5 to 10.0). No buffer dependency was found when activity of the DNAzyme was tested at pH 7.0 with Bis-Tris or MOPS

buffer. Rate of cleavage was obtained using equation (1). To determine apparent pK_a of the general base form the pH profile following equation is used:

$$k_{obs,pH} = k_{obs,min} + \frac{k_{obs,max} - k_{obs,min}}{1 + 10^{\,n(pk_a - pH)}} \qquad (2)$$

In this equation, $k_{obbs,min}$ and $k_{obs,max}$ are the rate constant values at the lower and upper limit of the rate in the plot, respectively; pK_a is the apparent acidic constant for the general base; and n is the number of deprotonation events in the catalysis.

5.2.2.3 Metal Concentration-Dependent Activity

Activity of the NaA43 DNAzyme in the presence of different concentrations of several metal ions were tested at pH 7.0 in 20 mM Bis-Tris and 50 mM Li^+ as the background ionic strength required for proper formation of the NaA43ES complex. All activity assays were carried out as mentioned earlier. To determine the apparent dissociation constant for different metal ions, the dependence of k_{obs} was measured at pH 7.0 and plotted versus logarithm of a desired metal ion. Obtained rate constants at different concentrations of the metal ion were fit to the following equation:

$$k_{obs,log[M^{n+}]} = k_{obs,min} + \frac{k_{obs,max} - k_{obs,min}}{1 + 10^{\,n(\log Kd - \log[M^{n+}])}} \qquad (3)$$

In this equation, $k_{obs,min}$ and $k_{obs,max}$ are the rate constant values at the lower and upper limit of the rate in the plot, respectively; K_d is the apparent dissociation constant for the tested metal ion; and n is the Hill slope, in which is an index of the number of metal ions associated with the DNAzyme.

To determine the Hill coefficient, n, a linear plot was derived by representing $\log(k_{obs} \div (k_{obs.max} - k_{obs}))$ versus $\log[M^{n+}]$.

5.2.2.4 Kinetics of PS Substrate Cleavage

The oligonucleotides containing the PS modifications were obtained as racemic mixtures, containing both the R_P and S_P stereoisomers, and were used without further separation. ^{32}P labeling and purification of the substrates were carried out as stated before.

Rate of cleavage for PS substrate (rA48PS) was determined by plotting cleavage percentage versus time and fitting the data points to a double exponential equation:

$$Y_t = Y + A \times e^{-k_{obs,1} \times t} + B \times e^{-k_{obs,2} \times t} \quad (4)$$

In this equation Y is the percentage of the substrate cleaved at completion ($t = \infty$), Y_t is the % product at time t, −A and −B are the amplitude of the observed cleavage at each at each phase. $k_{obs,1}$ and $k_{obs,2}$ are the observed first-order rate constants for the fast and slow phases.

Thio effect was calculated based on the following equation:

$$\textbf{thio effect} = \frac{k_{obs,OXO}}{k_{obs,PS}} \quad (5)$$

In this equation $k_{obs,OXO}$ is the rate of cleavage for the oxo substrate and $k_{obs,PS}$ is the rate of cleavage for the phosphorothioate substrate.

$$\textbf{metal ion rescue} = \left(\frac{k_{obs,PS}{}^{M^{2+}}}{k_{obs,PS}{}^{Ca^{2+}}}\right) \Big/ \left(\frac{k_{obs,OXO}{}^{M^{2+}}}{k_{obs,OXO}{}^{Ca^{2+}}}\right) \quad (6)$$

5.3 Results and Discussion

5.3.1 Sequence Similarity and Activity Analysis

Na^+-specific RNA-cleaving DNAzymes were obtained through fifteen rounds of *in vitro* selection at two different sodium concentrations: selection A at 135 mM Na^+ and selection B at 400 mM Na^+. As shown in Figure 5.1, the reaction time was gradually decreased from 2 hours to 45 seconds, as described previously (chapter 4). Both selections were carried out in pH 7.0, 50 mM Bis-Tris buffer in the presence of 10 mM citrate and 1 mM EDTA to minimize the likelihood of multivalent metal ions being able to participate in the cleavage reaction. The most active pools were cloned and sequenced, and a total of 95 individual sequences were obtained. Multiple sequence alignment was used to divide individual clones from each selection into different classes based on sequence similarities. A Na^+-specific sensor was designed recently based on the sequence of clone A43, which was found to be the most active of the isolated sequences. Clone A43 was converted into a *trans*-cleaving DNAzyme, named NaA43. The NaA43 complex is consisted of an enzyme strand (NaA43E, Figure 5.2) and a substrate strand (NaA43S, Figure 5.2). The substrate is a chimeric RNA/DNA sequence with a single RNA nucleotide (rA) as the cleavage site, and the DNAzyme complex forms through the hybridization of two Watson-Crick base-pairing arms. Similar to previously reported RNA-cleaving DNAzymes NaA43 is predicted to fold into a three-way-junction structure (Figure 5.2) (*27*, *29*).

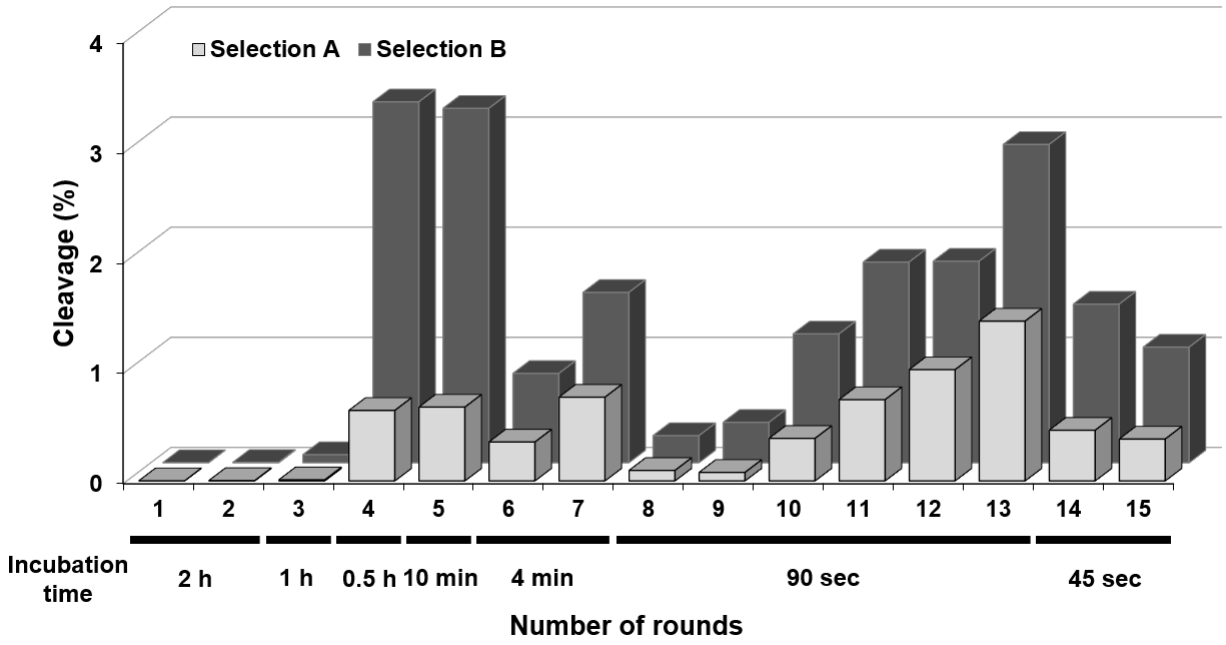

Figure 5.1 Progress of *in vitro* selection at each specific round represented in percentage fraction of the cleavage product eluted off the column during reaction time. Incubation time is displayed for each round.

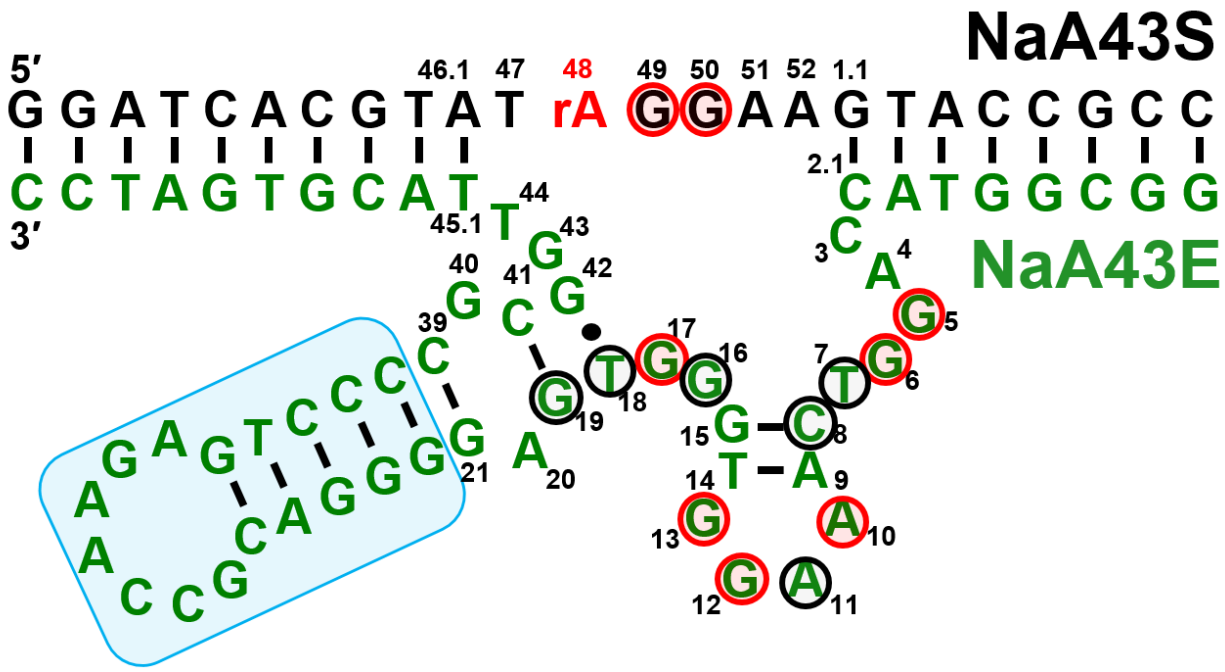

Figure 5.2 Predicted secondary structure of the *trans*-cleaving A43 DNAzyme, called NaA43 DNAzyme. The enzyme strand is shown in green and the substrate strand in black. Nucleotides in the core of the enzyme and substrata are numbered. Cleavage site is a single rA which is shown in red. Structural motif is boxed in blue. Absolutely critical nucleotides for catalytic activity are circled in red. The most highly conserved nucleotides are circled in black.

Sequence similarity of obtained sequences were represented using Sequence Similarity Networks (SSN), originally utilized for organizing sequence similarity of protein sequences (*41*). In contrast to multiple sequence alignment and phylogenic trees, SSN presents interconnected sequences as clusters within 2D space, which provides a visual representation of sequence similarity relationships. In Figure 5.3 the SSN of all sequences obtained from both selection conditions, A and B, is shown. Each sequence is represented by a node and two sequences are connected via a line if their pair-wise BLAST E-value is below a cutoff of 10^{-45}. The designated cutoff could be adjusted to more stringent values to group sequences with higher similarities into clusters. As shown in Figure 5.3, 24 and 29 sequences obtained from selection A and B, respectively, are grouped into the same cluster (shown at top-left). Observing high similarity between more than half of the sequences obtained from two different selection conditions may imply that a common motif is responsible for the activity of these Na^+-specific DNAzymes.

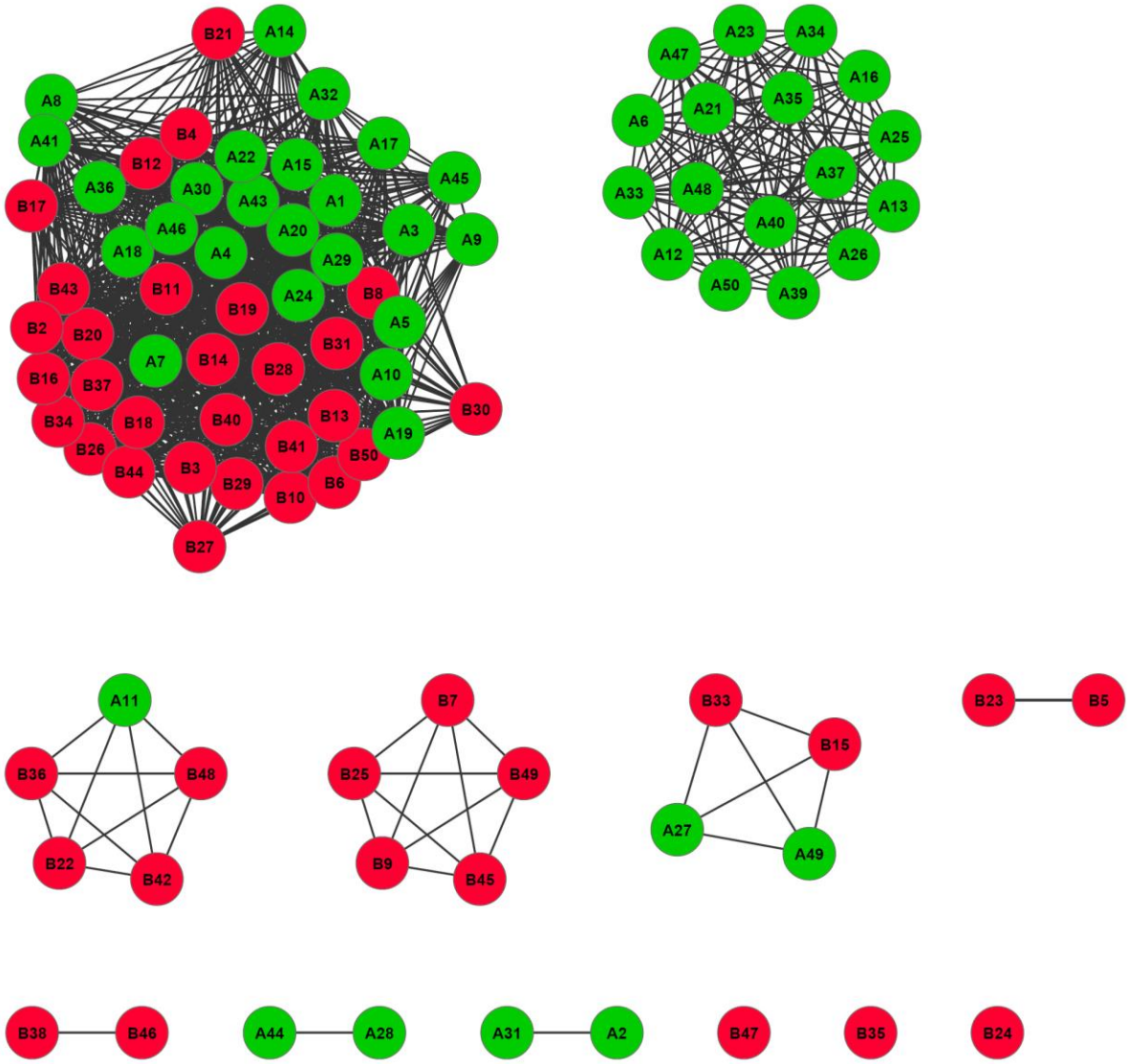

Figure 5.3 Sequence similarity network including 95 sequences obtained from selection conditions A (green) and B (red). This network used a threshold set at a BLAST E-value of 10^{-45}: only edges associated with E-values more significant than e^{-45} are included in the network. Lengths of connecting edges correlate with the relative dissimilarities of each pair of sequences. Although 24 and 29 sequences obtained from Selection A and B, respectively, are clustered in the largest group, the proximity of the nodes with the same color shows higher sequence similarity in each selected pool than in between the two different pools.

Table 5.1 Comparison of the values for k_{obs} for different *cis*-cleaving DNAzymes from selection condition A and B. Only clones which their relative activities in reference to A43are higher than 40% and 30% are represented.

Clones	k_{obs} (min^{-1})	$k_{relative}$	Class/Subclass	
A32	0.115	1.03	A-II/C	
A4, A30, A43, B11[1]	0.111	1.00	B-I/C	
B21	0.108	0.97	A-II/C & B-I/C	
A14[2]	0.104	0.94	A-II/E	
A9	0.074	0.67	A-II/E	
A1, A15, A18, A20, A46[3]	0.062	0.56	A-II/A	
A24, A29, B19	0.059	0.53	A-II/B	
B2, B16, B18, B20, B26, B34, B37, B43, B44	0.056	0.50	B-I/A	
A10	0.054	0.49	A-II/C	
B17	0.052	0.47	B-I/C	
A3[4]	0.045	0.40	A-II/A	≥40%
B22, B48[5]	0.043	0.39	B-III	
A5[6]	0.040	0.36	A-II/E	
A6, A13, A16, A23, A25, A26, A34, A37, A39, A48, A50[7]	0.037	0.33	A-I	
B38[8]	0.036	0.32	B-V	
B23[9]	0.035	0.31	B-VI	
A33	0.033	0.30	A-I	≥30%

[1] There is an identical duplet (B4 and B12) very similar to this cluster of four identical clones. The duplet contains a single nucleotide mismatch in the 3′-arm of the enzyme. [2] A14, B21 and A32 show very high sequence similarity to A43. There is a single mutation in each sequence in the loop region: C28T, A31G, and A33G in B21, A14 and A32, respectively. In addition, both A14 and B21 have a C to T mutation in the 3′-arm of the enzyme which results in the formation of a G-T wobble base-pair instead of a C-G Watson-Crick base-pair in the arm. [3] Sequences and predicted secondary structures of this group of five clones is very similar to the sequence and secondary structure of A43, except for an extra T at position 14. A22 is another clone with very high sequence similarity to this group of five clones, except for one extra nucleotide in the catalytic region (C3 replaced with CT). Clone A17 is also highly similar to this group of five clones except for an extra G in between G12 and G13 and a mismatch in the 3′-arm of the enzyme. [4] A3 belongs to pool A Class II – Subclass A which has seven members including six identical clones and A3. Clone A3 is different from the other six identical clones by having a G-T wobble base-pair in the 3′-arm of the enzyme. [5] B22 and B48 belong to pool B class III. There are two more members in this class including B36 with a G-T wobble base-pair in the 3′-arm of the enzyme and B42, which contains a G21A mutation. [6] A5 is one of the clones from pool A Class II – Subclass E, which contains four members. Activity of the all four clones from Subclass E have been tested and A14 was found to be the most active clone. A5 has several changes in the catalytic core (an extra C in between G13 and T14, G15C and G32T mutations, and a mismatch in the 3′-arm of the enzyme. [7] This group of clones belongs to pool A class I which contains 17 individual members including 11 identical clones, which are represented in the table. Other sequences from class A-I that are not represented in the table were found to have less than 30% of the activity of A43. [8] B38 and B46 are unclassified and belong to pool B duplet I. Their sequences are different in two different positions, C3 and G15. Although their sequences are not highly similar to A43, their predicted secondary structures are similar to the structure of A43. [9] B5 and B23 are unclassified and belong to pool B duplet II. They do not share high sequence similarity with NaA43, although their secondary structures are similar to the structure of A43.

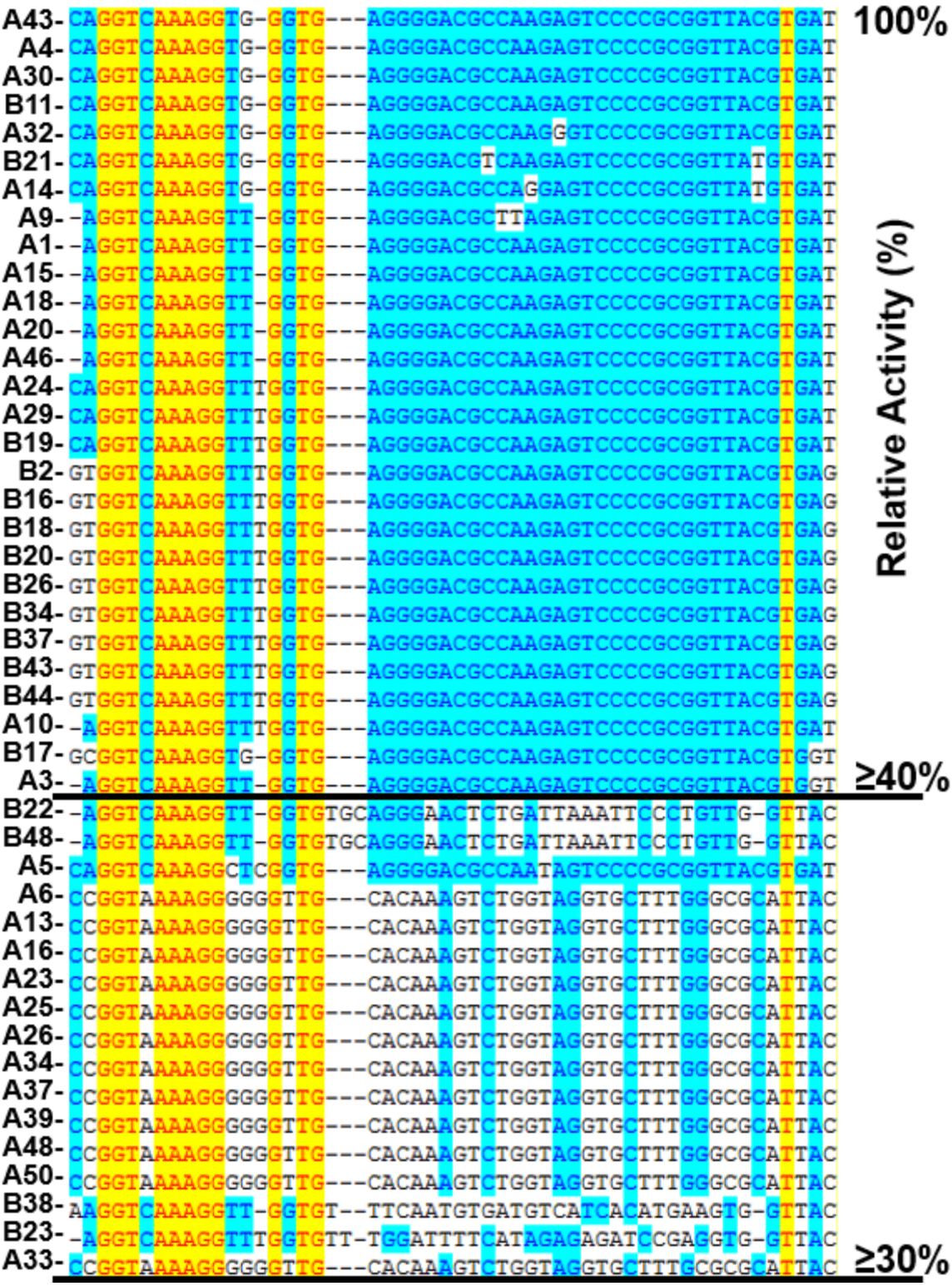

Figure 5.4 Multiple sequence alignment of sequences with apparent rate of catalysis equal or higher than 30% of clone A43. Identical nucleotides are represented in red text with yellow background and conserved regions are shown in dark blue text with light blue background. Non-similar nucleotides are in black text with white background.

The activity of a number of sequences including representatives of all different clusters have been tested in *cis*-cleaving format to understand the sequence-function relationship of the isolated DNAzymes. In Table 5.1, the apparent cleavage rate (k_{obs}) and relative activity of 45 individual clones have been summarized into two categories. The first category includes sequences with relative activity more than 40% of A43, while the second one represents sequences with activity higher than 30% but lower than 40%. Multiple sequence alignment of the corresponding random region from this group of highly active DNAzymes is shown in Figure 5.4. Sequences with relative activity higher than 40% shares a very high similarity all over the random region. However, relative activity lower than 40% is linked to a low sequence similarity in the 3′ end of the random region. All active sequences were found to share a highly conserved region close to the 5′ end of the random region. Interestingly, even sequences with relative activity lower than 40% that share low sequence similarity are able to form a similar secondary structure (Figure 5.5). Formation of a highly similar secondary structure by active sequences suggests that Na^+-specific DNAzymes have a highly conserved motif that can utilize Na^+ ion for catalysis. One of the clones, A45, which showed very high sequence similarity with A43 was found to be barely active. As shown in Figure 5.6, A45 was found to be different from A43 in few positions including two guanosines (G22 and G24) that are changed to A and T, respectively. Since G22 and G24 are necessary for Watson-Crick base-pairing in the stem region of a long hairpin (T18-G42 region) formed in A43, the sequence of A45 cannot form a stable stem. Restoring Watson-Crick base-pairing in the long hairpin of A45 resulted in a significant increase in the activity of the DNAzyme (Figure 5.6D). These results suggest that the 3′ end of the random region forms a structural motif and sequence identity of this region may not be critical for the Na^+-DNAzyme activity as long as the hairpin/stem-loop structure is retained.

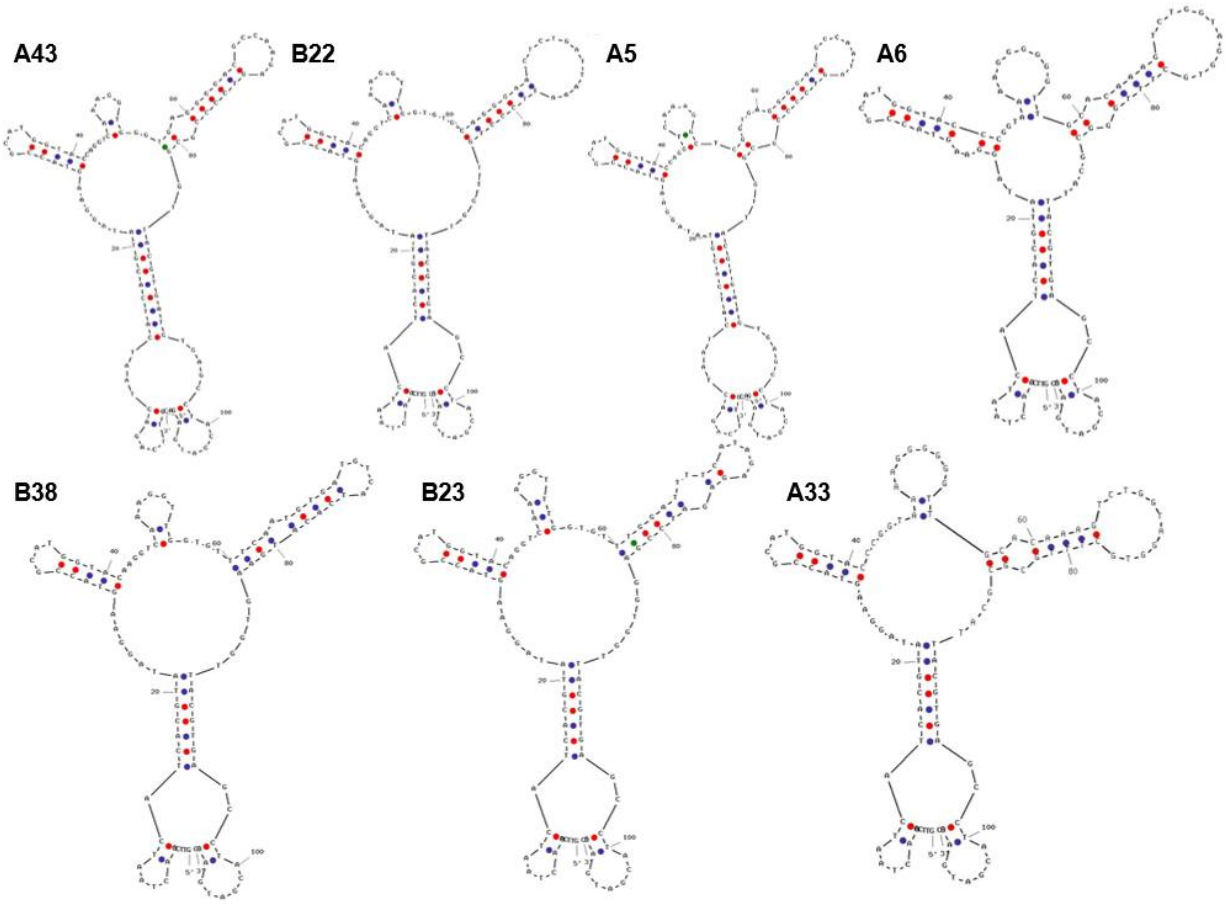

Figure 5.5 Predicted secondary structure of A43 and 6 clones that have relative activity lower than 40% (bottom part of Figure 5.4). All of these 6 clones share low sequence similarity to A43 at the 3′ region of the catalytic core.

To further investigate the sequence requirements for catalytic activity of the Na^+-specific DNAzyme I designed mutated *trans*-cleaving DNAzymes based on A43 (Figure 5.2). These mutational studies included a number of single point mutations, deletions, and multiple mutations (or shuffling). Based on sequence similarities of active clones, single point mutations were introduced at the 3′ end of catalytic region (Table 5.2). All nucleotides that were found to be conserved in the highly active clones have been systematically mutated to all other three possible

nucleotides. Interestingly, I found six nucleotides (G5, G6, A10, G12, G13, and G17) in the A43E DNAzyme that are absolutely required for DNAzyme activity. Any one of the possible single point mutations at each of these six sites completely abolishes the activity of the NaA43 DNAzyme. Additionally, six other nucleotides have been identified (T7, C8, A11, G16, T18 and G19) in which single point mutations resulted in a drastic reduction of the activity (at least 100-fold reduction in the pseudo-first-order rate constant for cleavage, k_{obs}). Among single point mutations in the most highly conserved nucleotides within the catalytic region, A9 mutations were particularly different. Although A9C and A9T mutations caused significant reduction in catalytic activity of NaA43 (~ 370 and 740-fold, respectively), A9G was nearly as active as the wild type NaA43 (~ 55% activity).

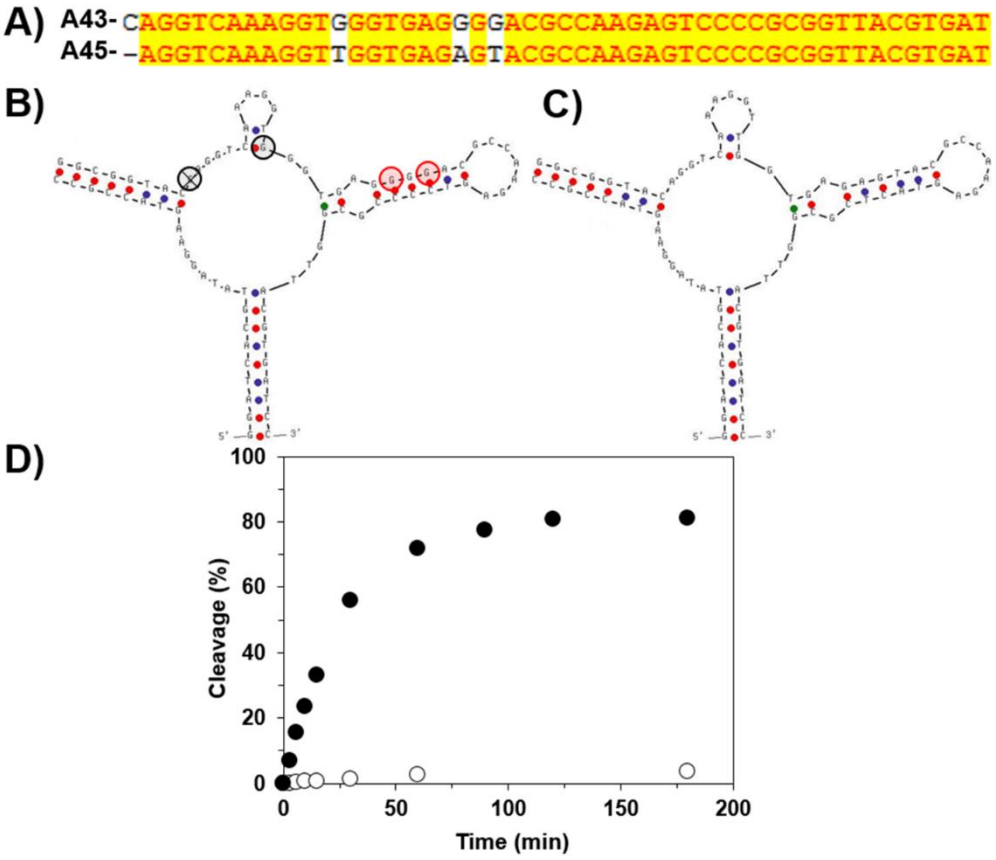

Figure 5.6 Clone A45 sequence similarity with A43. (A) Sequence alignment of random region from clone A43 and A45. (B) Predicted secondary structure of A43 in *trans*-cleaving form. There are four positions in which A45 is different from A43. Deletion of a cytosine which is shown with a crossed black circle. Two of the three mutated guanosines are located in a region which is predicted to form a long hairpin in A43 with Watson-Crick base-pairing (red circles). (C) Predicted secondary structure of A45 in *trans*-cleaving form after introducing two mutations in the stem region to restore Watson-Crick base-paring. (D) Cleavage activity of A45 DNAzyme before (open circles) and after (closed circles) restoring Watson-Crick base-paring in the stem region. In the modified A45 DNAzyme only Watson-Crick base-pairing is restored in the stem region by replacing G22 and G24 with A and T, respectively.

The role of the secondary structural elements shared between the NaA43 DNAzyme (Figure 5.2) and other active DNAzymes (Figure 5.5) was investigated further. Formation of common secondary structural elements was predicted by the UNAFold web package (*42, 43*). In all active DNAzymes, there is a short and a long hairpin formed at the 3′ and 5′ ends of the catalytic

region, respectively. To investigate the structural role of these hairpins in the activity of the NaA43 DNAzyme, several mutations made either by shuffling nucleotide positions or by multiple mutations have been tested. Mutations in the stem region of the short hairpin (C8-G15 region) resulted in loss of activity (Table 5.3). This finding is consistent with single point mutation results showing that C8 and A9 are critical nucleotides for catalytic activity of NaA43 (with an exception of A9G). Our results suggest that nucleotide identity and position in the short hairpin is critical for catalytic activity of NaA43. I next studied the role of the long hairpin (T18-G42 region) which contains an internal loop based on the predicted secondary structure. Converting the internal loop to a Watson-Crick base-pair in M6 variant (A20T/G40A) resulted in a 10-fold reduction in catalytic activity. Shuffling the nucleotides in the stem (G22-C26 and G34-C38; M8 variant) or in the loop region (G27-A33; M9 variant) of the predicted long hairpin caused no significant change in the cleavage rate of the NaA43 DNAzyme (no more than 30% reduction in k_{obs}). Additionally, complete shuffling of the G22-C38 region in M10 variant reduced the activity by only 50%. Furthermore, in order to investigate the role of G21:C39 base-pair, I designed the M11 variant from M10 by addition of G21C/C39G retro-mutations. I found that M11 activity is 10-fold less than M10. In addition, I found that G21T/C31A multiple mutation in the M7 variant resulted in more than a 10-fold reduction in the activity of the NaA43 DNAzyme. Altogether, our results show that the region between A20 and G40 of the long hairpin is tolerant to mutations that do not disrupt its overall secondary structure (Figure 5.2, boxed in blue). In addition, G22-C38 region is highly tolerant to the same type of mutations with no more than 50% reduction in the activity after mutation(s). Therefore, it is suggested that the long hairpin may not be critical for catalysis and may only play a structural role in the catalytic activity of the NaA43 DNAzyme, especially in the

G22-C38 region. Such structural motifs have been observed previously in other *in vitro* selected DNAzymes (*4*, *29*).

Table 5.2 List of single point mutations examined in the enzyme core of NaA43. Activity represents log ($10^5 \times k_{obs}$).

	3										13										23										33										43			Activity
A43E	C	A	G	G	T	C	A	A	A	G	G	T	G	G	G	T	G	A	G	G	G	G	A	C	G	C	C	A	A	G	A	G	T	C	C	C	C	G	C	G	G	T	**4.00**
C3A	A	-	-	-	-	-	-	-	-	-	-	-	-	-	-	-	-	-	-	-	-	-	-	-	-	-	-	-	-	-	-	-	-	-	-	-	-	-	-	-	-	-	**3.68**
A4G	-	G	-	-	-	-	-	-	-	-	-	-	-	-	-	-	-	-	-	-	-	-	-	-	-	-	-	-	-	-	-	-	-	-	-	-	-	-	-	-	-	-	**3.29**
A4T	-	T	-	-	-	-	-	-	-	-	-	-	-	-	-	-	-	-	-	-	-	-	-	-	-	-	-	-	-	-	-	-	-	-	-	-	-	-	-	-	-	-	**3.09**
G5A	-	-	A	-	-	-	-	-	-	-	-	-	-	-	-	-	-	-	-	-	-	-	-	-	-	-	-	-	-	-	-	-	-	-	-	-	-	-	-	-	-	-	**None**
G5C	-	-	C	-	-	-	-	-	-	-	-	-	-	-	-	-	-	-	-	-	-	-	-	-	-	-	-	-	-	-	-	-	-	-	-	-	-	-	-	-	-	-	**None**
G5T	-	-	T	-	-	-	-	-	-	-	-	-	-	-	-	-	-	-	-	-	-	-	-	-	-	-	-	-	-	-	-	-	-	-	-	-	-	-	-	-	-	-	**None**
G6A	-	-	-	A	-	-	-	-	-	-	-	-	-	-	-	-	-	-	-	-	-	-	-	-	-	-	-	-	-	-	-	-	-	-	-	-	-	-	-	-	-	-	**None**
G6C	-	-	-	C	-	-	-	-	-	-	-	-	-	-	-	-	-	-	-	-	-	-	-	-	-	-	-	-	-	-	-	-	-	-	-	-	-	-	-	-	-	-	**None**
G6T	-	-	-	T	-	-	-	-	-	-	-	-	-	-	-	-	-	-	-	-	-	-	-	-	-	-	-	-	-	-	-	-	-	-	-	-	-	-	-	-	-	-	**None**
T7A	-	-	-	-	A	-	-	-	-	-	-	-	-	-	-	-	-	-	-	-	-	-	-	-	-	-	-	-	-	-	-	-	-	-	-	-	-	-	-	-	-	-	**None**
T7C	-	-	-	-	C	-	-	-	-	-	-	-	-	-	-	-	-	-	-	-	-	-	-	-	-	-	-	-	-	-	-	-	-	-	-	-	-	-	-	-	-	-	**0.63**
T7G	-	-	-	-	G	-	-	-	-	-	-	-	-	-	-	-	-	-	-	-	-	-	-	-	-	-	-	-	-	-	-	-	-	-	-	-	-	-	-	-	-	-	**None**
C8A	-	-	-	-	-	A	-	-	-	-	-	-	-	-	-	-	-	-	-	-	-	-	-	-	-	-	-	-	-	-	-	-	-	-	-	-	-	-	-	-	-	-	**1.88**
C8G	-	-	-	-	-	G	-	-	-	-	-	-	-	-	-	-	-	-	-	-	-	-	-	-	-	-	-	-	-	-	-	-	-	-	-	-	-	-	-	-	-	-	**1.57**
C8T	-	-	-	-	-	T	-	-	-	-	-	-	-	-	-	-	-	-	-	-	-	-	-	-	-	-	-	-	-	-	-	-	-	-	-	-	-	-	-	-	-	-	**1.52**
A9C	-	-	-	-	-	-	C	-	-	-	-	-	-	-	-	-	-	-	-	-	-	-	-	-	-	-	-	-	-	-	-	-	-	-	-	-	-	-	-	-	-	-	**1.44**
A9G	-	-	-	-	-	-	G	-	-	-	-	-	-	-	-	-	-	-	-	-	-	-	-	-	-	-	-	-	-	-	-	-	-	-	-	-	-	-	-	-	-	-	**3.74**
A9T	-	-	-	-	-	-	T	-	-	-	-	-	-	-	-	-	-	-	-	-	-	-	-	-	-	-	-	-	-	-	-	-	-	-	-	-	-	-	-	-	-	-	**1.13**
A10C	-	-	-	-	-	-	-	C	-	-	-	-	-	-	-	-	-	-	-	-	-	-	-	-	-	-	-	-	-	-	-	-	-	-	-	-	-	-	-	-	-	-	**None**
A10G	-	-	-	-	-	-	-	G	-	-	-	-	-	-	-	-	-	-	-	-	-	-	-	-	-	-	-	-	-	-	-	-	-	-	-	-	-	-	-	-	-	-	**None**
A10T	-	-	-	-	-	-	-	T	-	-	-	-	-	-	-	-	-	-	-	-	-	-	-	-	-	-	-	-	-	-	-	-	-	-	-	-	-	-	-	-	-	-	**None**
A11C	-	-	-	-	-	-	-	-	C	-	-	-	-	-	-	-	-	-	-	-	-	-	-	-	-	-	-	-	-	-	-	-	-	-	-	-	-	-	-	-	-	-	**1.33**
A11G	-	-	-	-	-	-	-	-	G	-	-	-	-	-	-	-	-	-	-	-	-	-	-	-	-	-	-	-	-	-	-	-	-	-	-	-	-	-	-	-	-	-	**None**
A11T	-	-	-	-	-	-	-	-	T	-	-	-	-	-	-	-	-	-	-	-	-	-	-	-	-	-	-	-	-	-	-	-	-	-	-	-	-	-	-	-	-	-	**None**
G12A	-	-	-	-	-	-	-	-	-	A	-	-	-	-	-	-	-	-	-	-	-	-	-	-	-	-	-	-	-	-	-	-	-	-	-	-	-	-	-	-	-	-	**None**
G12C	-	-	-	-	-	-	-	-	-	C	-	-	-	-	-	-	-	-	-	-	-	-	-	-	-	-	-	-	-	-	-	-	-	-	-	-	-	-	-	-	-	-	**None**
G12T	-	-	-	-	-	-	-	-	-	T	-	-	-	-	-	-	-	-	-	-	-	-	-	-	-	-	-	-	-	-	-	-	-	-	-	-	-	-	-	-	-	-	**None**
G13A	-	-	-	-	-	-	-	-	-	-	A	-	-	-	-	-	-	-	-	-	-	-	-	-	-	-	-	-	-	-	-	-	-	-	-	-	-	-	-	-	-	-	**None**
G13C	-	-	-	-	-	-	-	-	-	-	C	-	-	-	-	-	-	-	-	-	-	-	-	-	-	-	-	-	-	-	-	-	-	-	-	-	-	-	-	-	-	-	**None**
G13T	-	-	-	-	-	-	-	-	-	-	T	-	-	-	-	-	-	-	-	-	-	-	-	-	-	-	-	-	-	-	-	-	-	-	-	-	-	-	-	-	-	-	**None**
T14G	-	-	-	-	-	-	-	-	-	-	-	G	-	-	-	-	-	-	-	-	-	-	-	-	-	-	-	-	-	-	-	-	-	-	-	-	-	-	-	-	-	-	**3.27**
G15T	-	-	-	-	-	-	-	-	-	-	-	-	T	-	-	-	-	-	-	-	-	-	-	-	-	-	-	-	-	-	-	-	-	-	-	-	-	-	-	-	-	-	**3.56**
G16A	-	-	-	-	-	-	-	-	-	-	-	-	-	A	-	-	-	-	-	-	-	-	-	-	-	-	-	-	-	-	-	-	-	-	-	-	-	-	-	-	-	-	**None**
G16C	-	-	-	-	-	-	-	-	-	-	-	-	-	C	-	-	-	-	-	-	-	-	-	-	-	-	-	-	-	-	-	-	-	-	-	-	-	-	-	-	-	-	**0.79**
G16T	-	-	-	-	-	-	-	-	-	-	-	-	-	T	-	-	-	-	-	-	-	-	-	-	-	-	-	-	-	-	-	-	-	-	-	-	-	-	-	-	-	-	**1.55**
G17A	-	-	-	-	-	-	-	-	-	-	-	-	-	-	A	-	-	-	-	-	-	-	-	-	-	-	-	-	-	-	-	-	-	-	-	-	-	-	-	-	-	-	**None**
G17C	-	-	-	-	-	-	-	-	-	-	-	-	-	-	C	-	-	-	-	-	-	-	-	-	-	-	-	-	-	-	-	-	-	-	-	-	-	-	-	-	-	-	**None**
G17T	-	-	-	-	-	-	-	-	-	-	-	-	-	-	T	-	-	-	-	-	-	-	-	-	-	-	-	-	-	-	-	-	-	-	-	-	-	-	-	-	-	-	**None**
T18A	-	-	-	-	-	-	-	-	-	-	-	-	-	-	-	A	-	-	-	-	-	-	-	-	-	-	-	-	-	-	-	-	-	-	-	-	-	-	-	-	-	-	**1.06**
T18C	-	-	-	-	-	-	-	-	-	-	-	-	-	-	-	C	-	-	-	-	-	-	-	-	-	-	-	-	-	-	-	-	-	-	-	-	-	-	-	-	-	-	**1.00**
T18G	-	-	-	-	-	-	-	-	-	-	-	-	-	-	-	G	-	-	-	-	-	-	-	-	-	-	-	-	-	-	-	-	-	-	-	-	-	-	-	-	-	-	**1.06**
G19A	-	-	-	-	-	-	-	-	-	-	-	-	-	-	-	-	A	-	-	-	-	-	-	-	-	-	-	-	-	-	-	-	-	-	-	-	-	-	-	-	-	-	**1.34**
G19C	-	-	-	-	-	-	-	-	-	-	-	-	-	-	-	-	C	-	-	-	-	-	-	-	-	-	-	-	-	-	-	-	-	-	-	-	-	-	-	-	-	-	**2.10**
G19T	-	-	-	-	-	-	-	-	-	-	-	-	-	-	-	-	T	-	-	-	-	-	-	-	-	-	-	-	-	-	-	-	-	-	-	-	-	-	-	-	-	-	**2.17**
A20T	-	-	-	-	-	-	-	-	-	-	-	-	-	-	-	-	-	T	-	-	-	-	-	-	-	-	-	-	-	-	-	-	-	-	-	-	-	-	-	-	-	-	**3.06**
G40C	-	-	-	-	-	-	-	-	-	-	-	-	-	-	-	-	-	-	-	-	-	-	-	-	-	-	-	-	-	-	-	-	-	-	-	-	-	-	-	C	-	-	**2.61**
C41T	-	-	-	-	-	-	-	-	-	-	-	-	-	-	-	-	-	-	-	-	-	-	-	-	-	-	-	-	-	-	-	-	-	-	-	-	-	-	-	-	T	-	**3.31**
G42A	-	-	-	-	-	-	-	-	-	-	-	-	-	-	-	-	-	-	-	-	-	-	-	-	-	-	-	-	-	-	-	-	-	-	-	-	-	-	-	-	-	A	**2.99**
G42T	-	-	-	-	-	-	-	-	-	-	-	-	-	-	-	-	-	-	-	-	-	-	-	-	-	-	-	-	-	-	-	-	-	-	-	-	-	-	-	-	-	T	**3.05**
G43A	-	-	-	-	-	-	-	-	-	-	-	-	-	-	-	-	-	-	-	-	-	-	-	-	-	-	-	-	-	-	-	-	-	-	-	-	-	-	-	-	-	-	**2.55**
G43T	-	-	-	-	-	-	-	-	-	-	-	-	-	-	-	-	-	-	-	-	-	-	-	-	-	-	-	-	-	-	-	-	-	-	-	-	-	-	-	-	-	-	**2.28**
T44A	-	-	-	-	-	-	-	-	-	-	-	-	-	-	-	-	-	-	-	-	-	-	-	-	-	-	-	-	-	-	-	-	-	-	-	-	-	-	-	-	-	-	**3.33**
T44C	-	-	-	-	-	-	-	-	-	-	-	-	-	-	-	-	-	-	-	-	-	-	-	-	-	-	-	-	-	-	-	-	-	-	-	-	-	-	-	-	-	-	**2.51**

Table 5.3 List of multiple mutations/shuffling examined in the enzyme core of NaA43. Activity represents log ($10^5 \times k_{obs}$).

	3										13										23										33										43	**Activity**
A43E	C	A	G	G	T	C	A	A	A	G	G	T		G		G	G	T	G	A	G	G	G	G	A	C	G	C	C	A	A	G	A	G	T	C	C	C	C	G	C	G	T	**4.00**
M1	-	-	-	-	-	-	T	-	-	-	-	A		-		-	-	-	-	-	-	-	-	-	-	-	-	-	-	-	-	-	-	-	-	-	-	-	-	-	-	-	**None**
M2	-	-	-	-	-	G	T	-	-	-	-	A		C		-	-	-	-	-	-	-	-	-	-	-	-	-	-	-	-	-	-	-	-	-	-	-	-	-	-	-	**None**
M3	-	-	-	-	-	G	C	-	-	-	-	G		C		-	-	-	-	-	-	-	-	-	-	-	-	-	-	-	-	-	-	-	-	-	-	-	-	-	-	-	**None**
M4	G	A	-	-	-	-	-	-	-	-	-	-		T	T	-	-	-	-	-	-	-	-	-	-	-	-	-	-	-	-	-	-	-	-	-	-	-	-	-	-	-	**3.06**
M5	-	-	-	-	-	-	-	-	-	-	-	-		-		-	-	-	A	-	-	-	-	-	-	-	-	-	-	-	-	-	-	-	-	-	-	-	-	T	-	-	**1.07**
M6	-	-	-	-	-	-	-	-	-	-	-	-		-		-	-	-	-	T	-	-	-	-	-	-	-	-	-	-	-	-	-	-	-	-	-	-	-	A	-	-	**2.94**
M7	-	-	-	-	-	-	-	-	-	-	-	-		-		-	-	-	-	-	T	-	-	-	-	-	-	-	-	-	-	-	-	-	-	-	-	-	-	A	-	-	**2.96**
M8	-	-	-	-	-	-	-	-	-	-	-	-		-		-	-	-	-	-	-	C	C	C	T	G	-	-	-	-	-	-	-	C	A	G	G	G	-	-	-	-	**3.87**
M9	-	-	-	-	-	-	-	-	-	-	-	-		-		-	-	-	-	-	-	-	-	-	-	-	G	A	G	C	C	A	A	-	-	-	-	-	-	-	-	-	**3.87**
M10	-	-	-	-	-	-	-	-	-	-	-	-		-		-	-	-	-	-	-	A	C	A	G	G	T	T	T	C	T	T	T	C	C	T	G	T	-	-	-	-	**3.76**
M11	-	-	-	-	-	-	-	-	-	-	-	-		-		-	-	-	-	-	-	C	A	C	A	G	G	T	T	T	C	T	T	T	C	C	T	G	T	G	-	-	-	**2.72**
M12	A	T	-	-	-	-	-	-	-	-	-	-		-		-	-	-	-	-	G	C	A	C	A	G	G	T	T	T	C	T	T	T	C	C	T	G	T	G	A	-	-	T	C	**None**

It can be observed from the sequence alignment of active DNAzymes in Figure 5.4 that the size of the catalytic region has remained almost the same, although there are some sequences with an enzyme region one nucleotide shorter than A43. To further evaluate whether a specific sequence length of the enzyme region is required for the activity of the NaA43 DNAzyme, I constructed several deletion variants (Table 5.4). As it was expected, all variants with deletions in G5-G19 region are completely inactive. Interestingly, the D7 variant which has G22-C38 deleted, was found to be completely inactive. This region, which was deleted in the D7 variant, was the region of the hairpin tolerant to mutations and shuffling. This finding shows that although this region of the DNAzyme is tolerant to mutation, it cannot be deleted. Additionally, it was found that shorting the loop region or stem region of the long hairpin as long as it remains stable is still tolerated. The D12 variant, shortened in the long hairpin by 11 nucleotides, remained active, although the activity was reduced by ~ 25-fold compared to the NaA43 DNAzyme. In another variant, the split DNAzyme, the loop region of the long hairpin was completely removed and the DNAzyme split in two halves. Interestingly, the split DNAzyme (Table 5.4) can still catalyze the cleavage reaction as efficient as NaA43 with a rate constant of ~0.08 min^{-1}, which is only 20% less than the catalytic rate of NaA43. Therefore, deletion experiments confirmed that the long hairpin serves as a structural element for the activity of NaA43 and can be used as a scaffold to design allosteric DNAzymes or functional nucleic acids.

Table 5.4 List of deletions examined in the enzyme core of NaA43. Activity represents log $(10^5 \times k_{obs})$.

	3										13										23										33										43		**Activity**
A43E	C	A	G	G	T	C	A	A	A	G	G	T	G	G	G	T	G	A	G	G	G	G	A	C	G	C	C	A	A	G	A	G	T	C	C	C	C	G	C	G	G	T	**4.00**
D1	X	-	-	-	-	-	-	-	-	-	-	-	-	-	-	-	-	-	-	-	-	-	-	-	-	-	-	-	-	-	-	-	-	-	-	-	-	-	-	-	-	-	**3.728**
D2	-	-	-	-	-	-	-	-	-	-	-	-	-	-	-	-	-	-	-	-	-	-	-	-	-	-	-	-	-	-	-	-	-	-	-	-	-	-	-	-	-	X	**2.457**
D3	-	-	X	X	X	X	X	X	X	X	-	-	-	-	-	-	-	-	-	-	-	-	-	-	-	-	-	-	-	-	-	-	-	-	-	-	-	-	-	-	-	-	**None**
D4	-	-	-	-	-	-	X	X	X	X	X	X	-	-	-	-	-	-	-	-	-	-	-	-	-	-	-	-	-	-	-	-	-	-	-	-	-	-	-	-	-	-	**None**
D5	-	-	-	-	-	X	X	X	X	X	X	X	X	X	X	X		-	-	-	-	-	-	-	-	-	-	-	-	-	-	-	-	-	-	-	-	-	-	-	-	-	**None**
D6	-	-	-	-	-	X	X	X	X	X	X	X	X	X	X	X	X	-	-	-	-	-	-	-	-	-	-	-	-	-	-	-	-	-	-	-	-	-	-	-	-	-	**None**
D7	-	-	-	-	-	-	-	-	-	-	-	-	-	-	-	-	-	-	-	X	X	X	X	X	X	X	X	X	X	X	X	X	X	X	X	X	-	-	-	-	-	-	**None**
D8	-	-	-	-	-	-	-	-	-	-	-	-	-	-	-	-	-	X	X	X	X	X	X	X	X	X	X	X	X	X	X	X	X	X	X	X	X	X	X	X	-	-	**None**
D9	-	-	-	-	-	-	-	-	-	-	-	-	-	-	-	-	-	-	-	-	X	-	-	-	-	-	-	-	-	-	-	-	-	-	X	-	-	-	-	-	-	-	**3.843**
D10	-	-	-	-	-	-	-	-	-	-	-	-	-	-	-	-	-	-	-	-	X	X	-	-	-	-	-	-	-	-	-	-	-	X	X	-	-	-	-	-	-	-	**3.668**
D11	-	-	-	-	-	-	-	-	-	-	-	-	-	-	-	-	-	-	-	-	X	X	-	-	-	-	X	X	X	-	-	-	-	X	X	-	-	-	-	-	-	-	**3.809**
D12	-	-	-	-	-	-	-	-	-	-	-	-	-	-	-	-	-	-	-	-	X	X	X	X	-	-	X	X	X	-	-	X	X	X	X	-	-	-	-	-	-	-	**2.588**
D13	-	-	-	-	-	-	-	-	-	-	-	-	-	-	-	-	-	X	X	X	X	X	X	-	-	-	-	-	-	-	-	-	X	X	X	X	X	-	-	-	-	-	**None**
D14	-	-	-	-	-	-	-	-	-	-	-	-	-	-	-	-	-	-	X	X	X	X	X	X	-	-	-	-	-	-	X	X	X	X	X	X	X	X	-	-	-	-	**1.719**
Split	-	-	-	-	-	-	-	-	-	-	-	-	-	-	-	-	-	-	-	-	-	-	-	-	3′						5′	-	-	-	-	-	-	-	-	-	-	-	**3.877**

Table 5.5 List of single point mutations examined in the substrate junction of NaA43S. Activity represents log $(10^5 \times k_{obs})$. In the A43rS all of the other nucleotides in the arms were also ribonucleotides.

							Activity
A43S	T	rA	G	G	A	A	**4.00**
T47C	C	-	-	-	-	-	**2.99**
rA48C	-	rC	-	-	-	-	**2.20**
rA48G	-	rG	-	-	-	-	**3.03**
rA48U	-	rU	-	-	-	-	**2.37**
G49A	-	-	A	-	-	-	**None**
G49C	-	-	C	-	-	-	**None**
G49T	-	-	T	-	-	-	**None**
G50A	-	-	-	A	-	-	**None**
G50C	-	-	-	C	-	-	**None**
G50T	-	-	-	T	-	-	**None**
A51T	-	-	-	-	T	-	**3.99**
A52T	-	-	-	-	-	T	**3.93**
A43rS-RNA	rU	rA	rG	rG	rA	rA	**1.80**
A43dS-DNA	-	A	-	-	-	-	**None**

The identity of nucleotides in the substrate junction plays a critical role in RNA-cleaving DNAzyme catalysis (*25*, *44*), while the sequence of binding arms in DNAzymes and their substrates is not specific for catalysis (*32*). To explore the role of the substrate junction in catalysis, I conducted mutational analysis on six nucleotides in NaA43S (Table 5.5). It was found that catalysis rate is not influenced by the identity of nucleotides at positions 51 and 52 as the DNAzyme cleaved A51T and A52T substrates as efficiently as unmutated NaA43S. The T47C mutation remained active although its activity was reduced by ~ 10-fold versus NaA43S. In contrast, I found that G49 and G50 were absolutely critical for catalysis and their systematic single point mutation to any other possible nucleotide completely prohibits catalysis. Cleavage site, rA48, was the optimal ribonucleotide for the NaA43 DNAzyme and its substitution with the other three ribonucleotides resulted in a noticeable reduction in the rate of cleavage (rA>>rG>>rU>rC). In addition, I examined the ability of NaA43 DNAzyme to cleave an all-RNA substrate (NaA43rS). Cleavage of the all-RNA substrate was found to be about two orders of magnitude slower than the wild type NaA43S. Previously isolated DNAzymes were found to be inactive or ~ 1000-fold less active toward all-RNA substrate (*27*). Not surprisingly, NaA43 was unable to cleave all-DNA substrate (NaA43dS). It is known that 2′-OH acts as a nucleophile in a transesterification reaction and is required for cleavage of RNA phosphodiester bond (*32*).

5.3.2 Na^+-Dependent Activity of NaA43

The activity of a fluorescent sensor designed based on NaA43 at varying concentrations of Na^+ was tested and it was shown that the sensor responds linearly to increasing Na^+ concentration with a dynamic range from 135 μM to 50 mM under optimal conditions (chapter 4). To investigate Na^+-dependent activity of the DNAzyme I carried out activity assay experiments under single-

turnover conditions with approximately 1 nM ^{32}P labeled NaA43S and 200 nM NaA43E. First, I tested Na^+-dependent activity in the presence of only Na^+ as a source of ionic strength as well as catalytic cofactor of the cleavage reaction. The NaA43ES complex was annealed in the presence of buffer and the reaction was initiated by addition of varying concentrations of Na^+. As shown in Figure 5.7, NaA43 is barely active at 4 mM Na^+ and subsequent increases in Na^+ concentration resulted in higher k_{obs} until a plateau at 400 mM at which point no more change was observed by further increase in Na^+ concentration. The activity of NaA43 dropped significantly when decreasing Na^+ concentration from 15 to 10 mM by more than one order of magnitude. Testing a variant of the NaA43 DNAzyme with elongated binding arms resulted in a significant increase in catalytic activity of the DNAzyme at low Na^+ concentrations (data not shown).

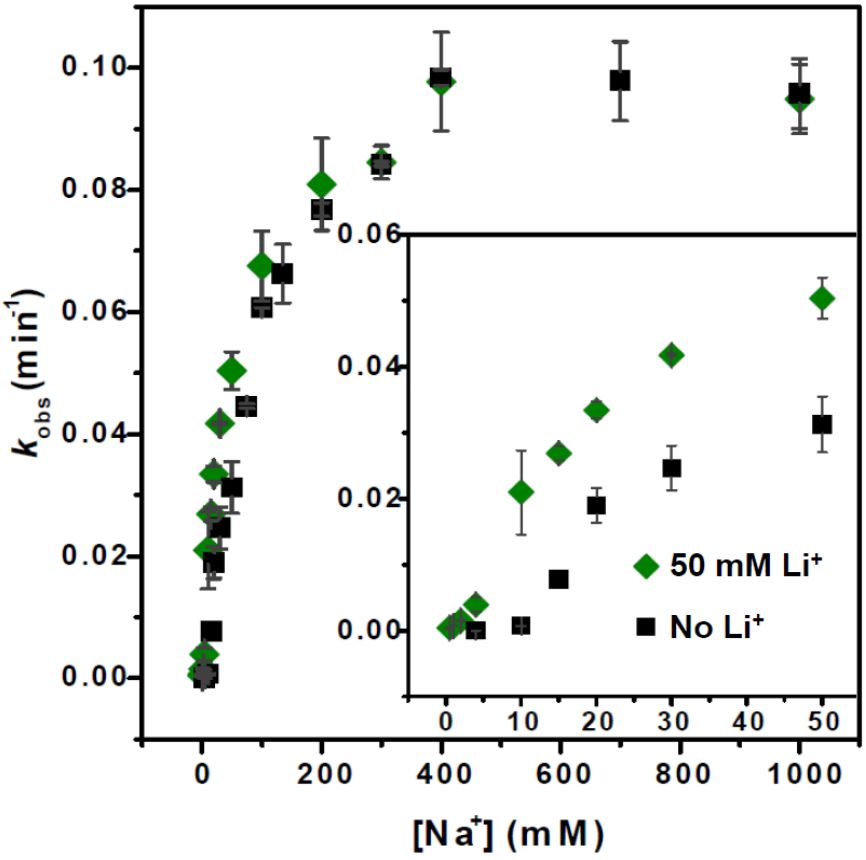

Figure 5.7 Na^+-dependent activity of the NaA43 DNAzyme at varying concentrations of Na^+ from 0.5 to 1000 mM in the absence (black squares) or presence (green diamond) of 50 mM Li^+. (Inset)

NaA43 cleavage rate at Na^+ concentrations lower than 50 mM. The error bars represent the standard deviation calculated from three independent experiments.

Since formation of the NaA43ES complex requires sufficient hybridization of the binding arms, I have tested the effect of introducing ionic strength from other sources such as Li^+, K^+, Rb^+, Cs^+, and NH_4^+. The kinetic profile of NaA43 at different concentrations of different monovalent ions was studied (Figure 5.8). To initiate the cleavage reactions 4 mM final concentration of Na^+ was added. This relatively low concentration of Na^+ has a minimal contribution to the overall ionic strength of the solution (~10% or lower), which made it possible to study optimal conditions for monitoring Na^+-dependent activity of the DNAzyme at very low concentrations of Na^+. As shown in Figure 5.8, activity of NaA43 at 50 mM Li^+ was higher than the other conditions. $NH4^+$ was found to be as efficient as Li^+, although other monovalent metal ions showed lower activity even at higher concentrations, which may be due to their inhibitory effect on the activity of the NaA43 DNAzyme. Therefore, Na^+-dependent activity of the NaA43 DNAzyme was tested at 50 mM Li^+ as an optimal condition to monitor rate of the cleavage reaction. Although presence of 50 mM Li^+ made no significant difference in the rate of reactions carried out at 100 mM Na^+ or higher, Li^+ was shown to increase k_{obs} significantly at Na^+ concentrations lower than 50 mM (*i.e.* ~ 20-fold increase in rate at 10 mM Na^+) (Figure 5.7, inset). In addition, the apparent dissociation constant ($K_{d,app}$) of the NaA43 DNAzyme decreased from 77.8 ± 8.7 mM in the absence of Li^+ to 41.2 ± 4.8 mM in 50 mM Li^+ (Figure 5.9A). The obtained K_d is in good agreement with binding constants obtained from fluorescence assays (chapter 4). The Hill-coefficient of 1.3 and 1.2 was obtained for Na^+-dependent cleavage in the absence and presence of 50 mM Li^+, respectively (Figure 5.9B). These Hill-coefficients suggest that binding of Na^+ in both conditions does not occur in a cooperative fashion and at least one Na^+ ion is required for catalysis.

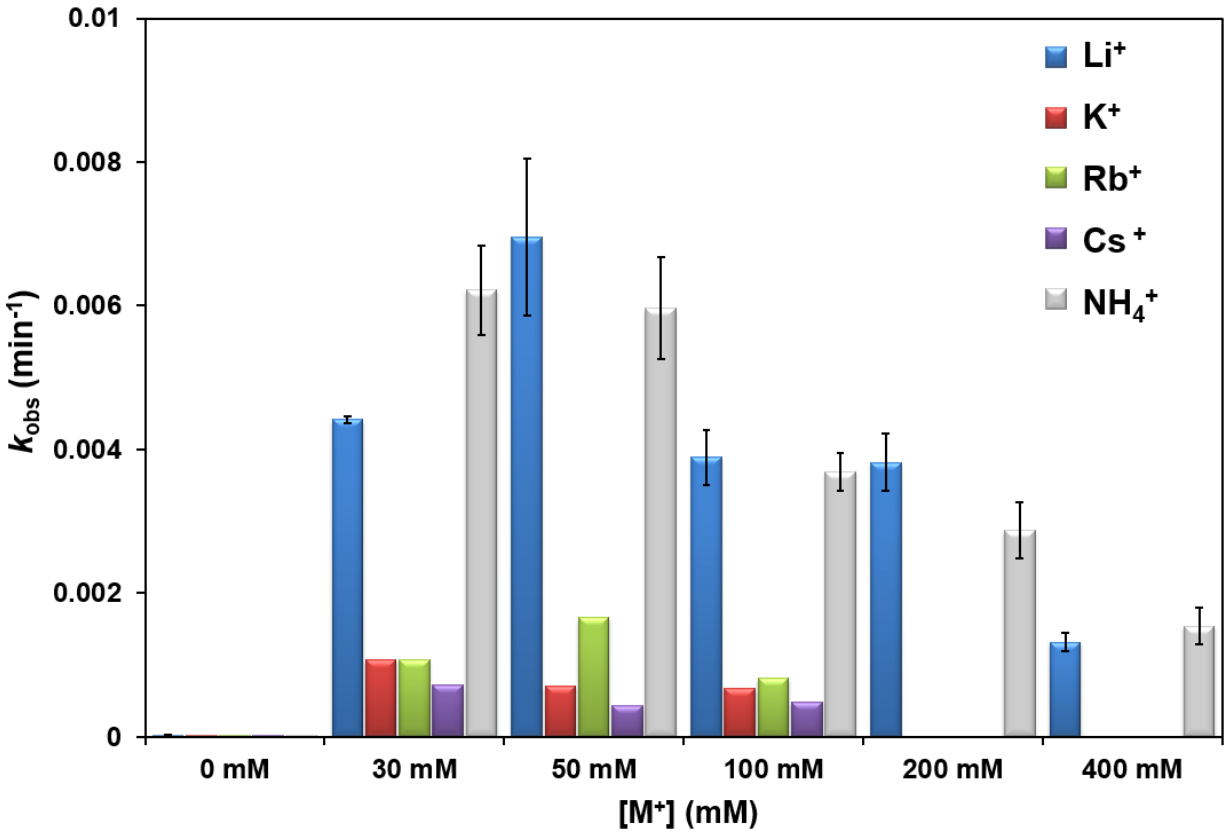

Figure 5.8 Activity of NaA43 in the presence of different concentrations of other monovalent ions at constant (4 mM) concentration of Na^+. k_{obs} values was obtained under single-turnover condition. The error bars represent the standard deviation calculated from at least two independent experiments (Li^+ and NH_4^+ conditions).

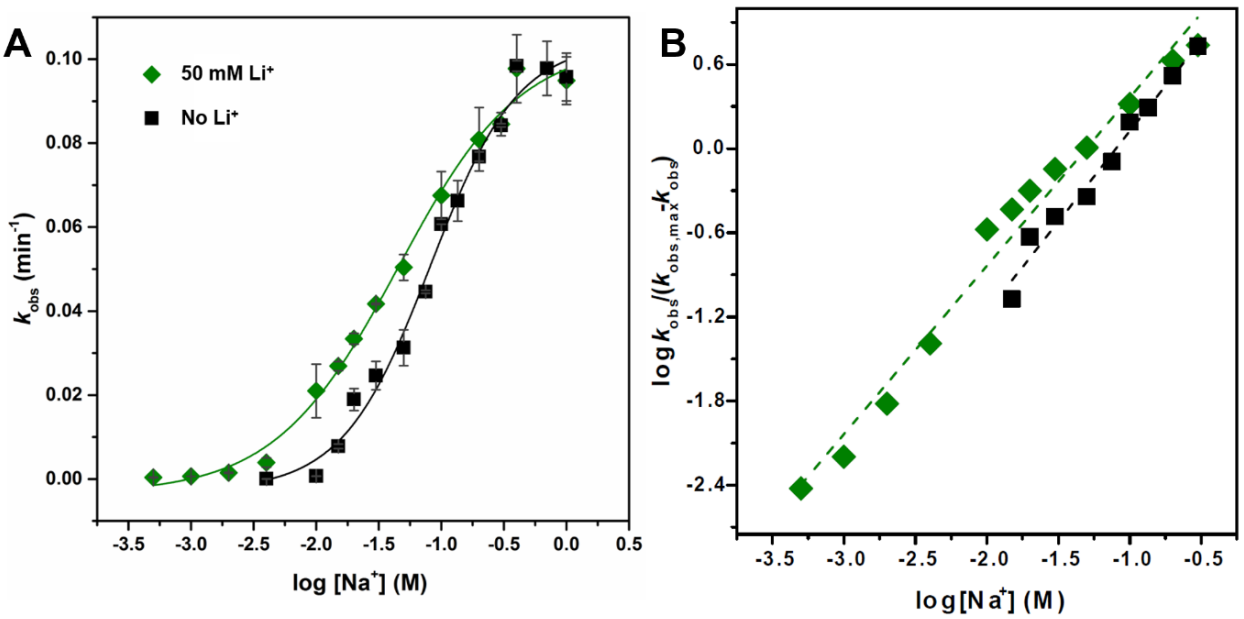

Figure 5.9 Apparent dissociation constants of the NaA43 DNAzyme for Na^+. (A) Rate of cleavage catalyzed by NaA43 was calculated for different Na^+ concentration in the presence or absence of 50 mM Li^+. k_{obs} values were obtained under single-turnover condition. The change in activity leads to a K_d = 77.8 ± 8.7 mM in the absence of Li^+ (black square) and K_d = 41.2 ± 4.8 mM in the presence of 50 mM Li^+ (green diamonds). The error bars represent the standard deviation calculated from at least two independent experiments. (B) Hill plots for the NaA43 DNAzyme activity in varying concentrations of Na^+ (in the absence of Li^+: 15-300 mM, in 50 mM Li^+: 0.5-300 mM). The obtained Hill coefficients for the NaA43 DNAzyme are 1.3 (R^2=0.98) and 1.2 (R^2=0.98) in the absence and presence of 50 mM Li^+, respectively.

It was shown previously that the activity of the fluorescent sensor based on NaA43 slightly increases in the presence of divalent metal ions and decreases at high concentrations of monovalent metal ions such as Rb^+ (chapter 4). To further examine Na^+-dependent activity of NaA43, I studied the activity of NaA43 with varying concentrations of Na^+ and at a constant concentration of Rb^+ or Mg^{2+}, as a representative of metal ions with inhibitory or acceleratory effect on the rate of NaA43 catalysis. The maximum rate of cleavage in the presence of 1 M Rb^+ was reduced by ~ 30% and in the presence of 1 mM Mg^{2+} the obtained maximum k_{obs} was increased by ~ 60% (Figure 5.10). Although no significant change was observed in the maximum rate of catalysis, the apparent

K_d for Na^+ increased to 268 ± 34 mM in the presence of 1 M Rb^+ and decreased to 13.3 ± 1.0 mM in the presence of 1 mM Mg^{2+} (Figure 5.11). In addition, the slope of the Hill plot for Na^+ has increased to 1.8 and 2.0 in the presence of Rb^+ and Mg^{2+}, respectively. These data indicate that at least two Na^+ ions are needed for the Na^+-dependent catalysis in the presence of Rb^+ and Mg^{2+}. The increase in the cooperativity might suggest that in the presence of Rb^+ and Mg^{2+} NaA43 cooperatively binds to one more Na^+ ion. The partial inhibitory effect of high concentrations of metal ions such as Rb^+ on NaA43 activity and increase in the apparent K_d for Na^+ might be due to their competition with Na^+ over the Na^+ binding sites (*45*). On the other hand, the observed decrease in apparent K_d in the presence of Mg^{2+} may suggest stabilization of the Na^+ binding site or a structure that prefers Na^+ over Mg^{2+} (*45*, *46*).

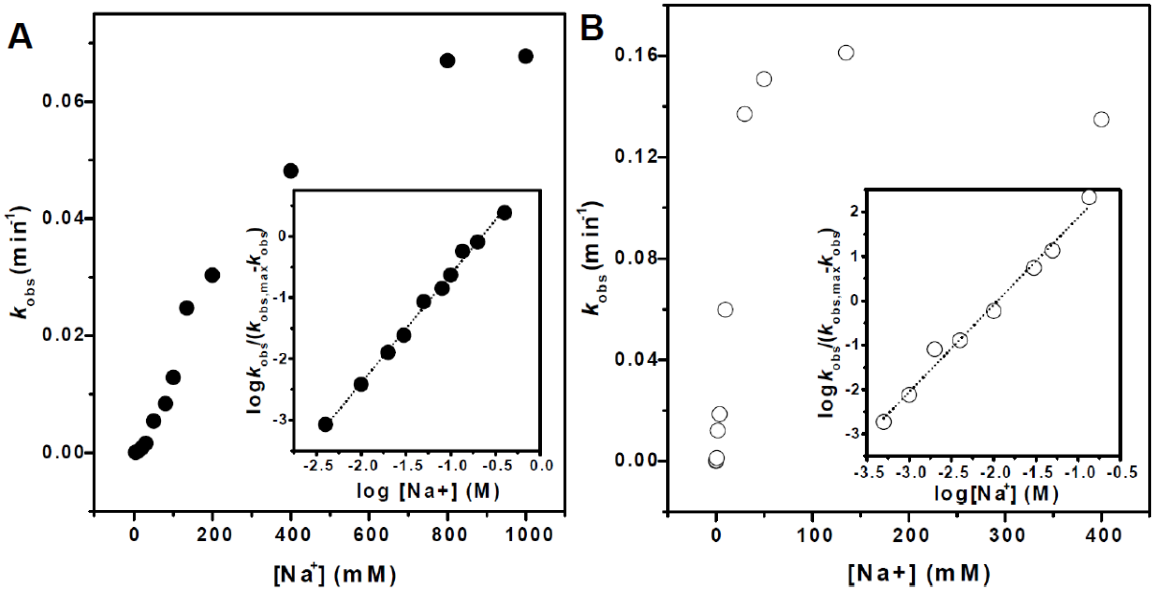

Figure 5.10 Na^+-dependent activity of the NaA43 DNAzyme in the presence of 1 M Rb^+ (A) or 1 mM Mg^{2+} (B). (Insets) Na^+ cooperativity in the presence of Rb^+ (A) or Mg^{2+} (B). The Hill coefficients were 1.8 (R^2=0.99) and 2.0 (R^2=0.99) for the reaction in Rb^+ and Mg^{2+}, respectively.

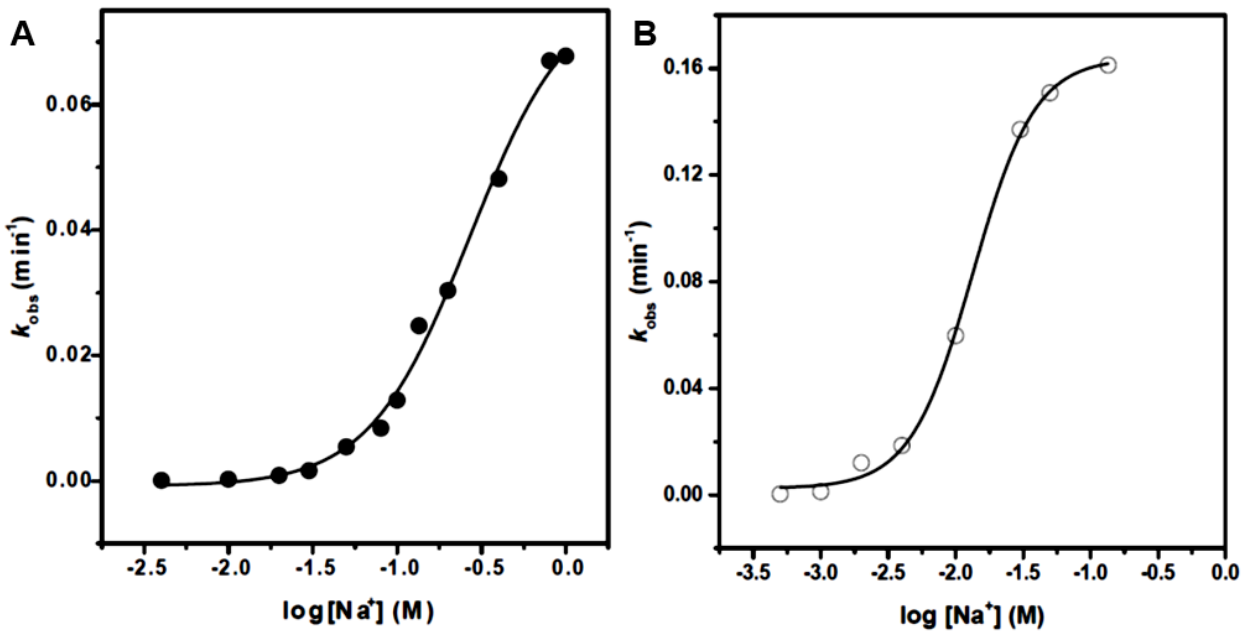

Figure 5.11 Plot of k_{obs} as a function of log Na^+ concentration in the presence of 1 M Rb^+ (A) or 1 mM Mg^{2+} (B). Apparent association constant of NaA43 for Na^+ was calculated to be 268 ± 34 mM and 13.3 ± 1.0 mM in the presence of Rb^+ and Mg^{2+}, respectively.

The apparent binding affinity of NaA43 for Na^+ is much stronger compared to the affinity of other DNAzymes or ribozymes that show activity in the presence of monovalent metal ions such as Na^+. Previous attempts in selecting DNAzymes active with only monovalent metal ions have resulted in divalent-independent DNAzymes, with no selectivity for a specific monovalent metal ion and activity in the range of ~500 mM to molar concentrations of Na^+ (*22*, *47*). It is also known that hammerhead, hairpin and hepatitis delta virus (HDV) ribozymes require very high concentrations of monovalent metal ions (as high as 4 M) to show catalytic activity (*10*, *46*, *48*). Therefore, in contrast to previously reported DNAzymes and ribozymes, NaA43 is the first example that can utilize Na^+ ion at relatively low concentrations and in a very selective manner to catalyze cleavage of RNA phosphodiester bonds. Interestingly, $K_{d,app}$ of the NaA43 DNAzyme is

even better than that of commercially available sodium indicators CoroNa Green and CoroNa Red, which have K_d values of ~ 80 and ~ 200 mM, respectively (*11, 49*).

5.3.3 Na^+ the only Cofactor for NaA43 Catalysis

NaA43 was selected in the presence of 1 mM EDTA and 10 mM citrate. Since all salt sources used to prepare solutions were ultra-pure and selection was carried out in the presence of EDTA and citrate, it is reasonably unlikely that trace multivalent metal ions caused the observed cleavage reaction. Analysis of the selection buffers by ICP-MS cannot be performed due to their high ionic strength. Diluted samples were tested by ICP-MS and all cations, except Na^+, were below the detection limit of the instrument. Based on the metal analysis data provided by Alfa Aesar, supplier of the metal-basis sodium chloride (99.999%), metal ion contaminants are no more than 2 ppm. The NaA43 DNAzyme activity was tested in the presence and absence of 50 mM EDTA and no noticeable difference was observed between the two conditions (Figure 5.12). All components of the reaction except Na^+ were heat-denatured in presence of EDTA and allowed to cool down gradually to room temperature. Therefore, even if there was any trace multivalent metal ion kinetically trapped in the structure of the DNAzyme, after heat-denaturation in the presence of EDTA it should not remain bound to the DNAzyme. EDTA chelates multivalent metal ions with high potency (*50*). Mg^{2+} might be the most likely multivalent contaminant in our solutions and its complex with EDTA is one the weakest among other multivalent metal ions. Since 50 mM EDTA was present in the solution (Mg^{2+}-EDTA; log K = 8.7)(*50*) and only 1 nM NaA43ES complex was used, affinity of DNA for Mg^{2+} should be remarkably stronger (*i.e.* 10^7-fold) than the affinity of EDTA for Mg^{2+} to outcompete EDTA. Moreover, NaA43 showed no activity in presence of other monovalent metal ions (Li^+, K^+, Rb^+, Cs^+), Mg^{2+} (up to 40 mM), and cobalt hexammine (40 mM). Similarly, no cleavage activity was observed when NaA43 was incubated in the presence of 4 M

Li^+. We previously demonstrated that a fluorescent sensor based on NaA43 was significantly selective for Na^+ over any other metal ions tested in fluorescence-based assay (chapter 4). Here I used gel-based assay to study cleavage of ^{32}P labeled NaA43S in the presence of different metal ions, which prohibits artifacts of metal-fluorophore interactions that might occur in the fluorescence-based assay. No cleavage was observed in the presence of 50 mM Li^+ and 1 mM of a divalent metal ion (Mg^{2+}, Ca^{2+}, Sr^{2+}, Br^{2+}, Mn^{2+}, Co^{2+}, Ni^{2+}, Cu^{2+}, Zn^{2+}, Cd^{2+}, Hg^{2+} and Pb^{2+}) or 100 μM of a trivalent metal ion (La^{3+} and Ce^{3+}). The combined evidence strongly suggests that the NaA43 DNAzyme carries out catalysis in a Na^+-specific manner and that no metal ion other than Na^+ can serve as a metal cofactor in this catalysis.

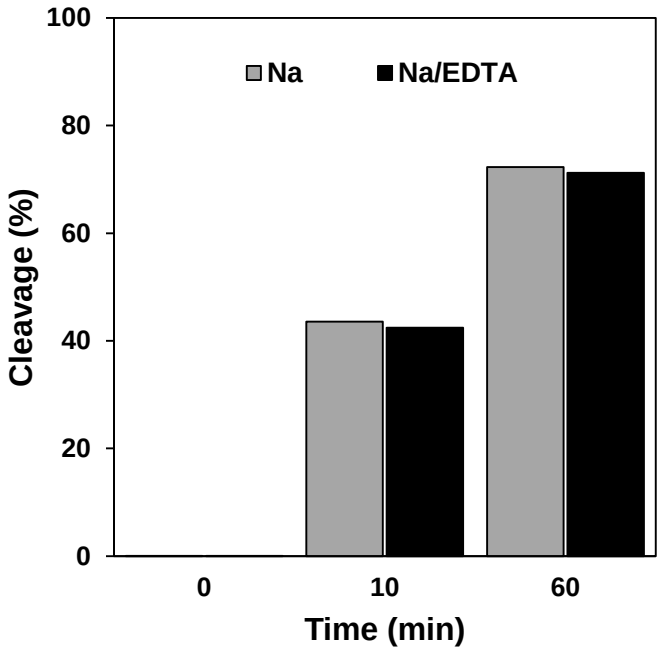

Figure 5.12 Sodium dependent activity of NaA43 in the presence or absence of 50 mM ETDA.

5.3.4 Catalytic Rate Enhancement

NaA43 catalyzes cleavage of its substrate at the embedded RNA site with a rate constant of ~ 0.1 min^{-1}. To estimate the rate enhancement obtained by NaA43 DNAzyme over the uncatalyzed reaction, the spontaneous reaction rate at background level is needed. Spontaneous RNA cleavage at 23° C, pH 7, 250 mM K^+, and 5 mM Mg^{2+} for ApG has been projected to be ~1×10^{-8} min^{-1} (*51*). It has been very well known that divalent metal ions such as Mg^{2+} strongly promote the RNA cleavage reaction. Similarly, an increase in ionic strength will increase the spontaneous rate of RNA degradation. The NaA43 DNAzyme does not require divalent metal ions, thus the proper conditions for measuring background reaction rate is a solution without divalent metals. Uncatalyzed rate of RNA hydrolysis under similar conditions was reported to be ~ 10^{-10} min^{-1} (*52, 53*). Therefore, rate enhancement obtained by the NaA43 DNAzyme over spontaneous cleavage of a single RNA phosphodiester bond is ~ 10^9-fold. NaA43 rate constant is 2-3 orders of magnitude higher than that of previously reported divalent-independent DNAzymes (*21, 22, 47*). Additionally, NaA43 has a similar or better rate of catalysis compared to several divalent-independent DNAzymes which have numerous modified nucleosides with protein-like functionalities (*e.g.* guanidinium, ammonium, and imidazole) (*18, 20, 54*).

Several ribozymes catalyze the RNA cleavage reaction in the absence of divalent metal ions, although they need high concentrations of monovalent metal ions. Hammerhead and hairpin ribozymes catalyze their reactions with a rate of ~ 10^{-1} min^{-1} in 4 M Li^+, at pH 8.0 (*10, 48*). Similarly, HDV ribozymes were reported with rate constants ranging from 10^{-2} to 10^{-1} min^{-1} in 4 M Li^+, at pH 6.3 (*46*). In addition, the cleavage rates of the aforementioned ribozymes in 4 M Na^+ do not exceed 10^{-3} min^{-1} (*12, 46, 48*). Thus, the cleavage rate of the NaA43 DNAzyme is at least two orders of magnitude higher than that of ribozymes under similar conditions.

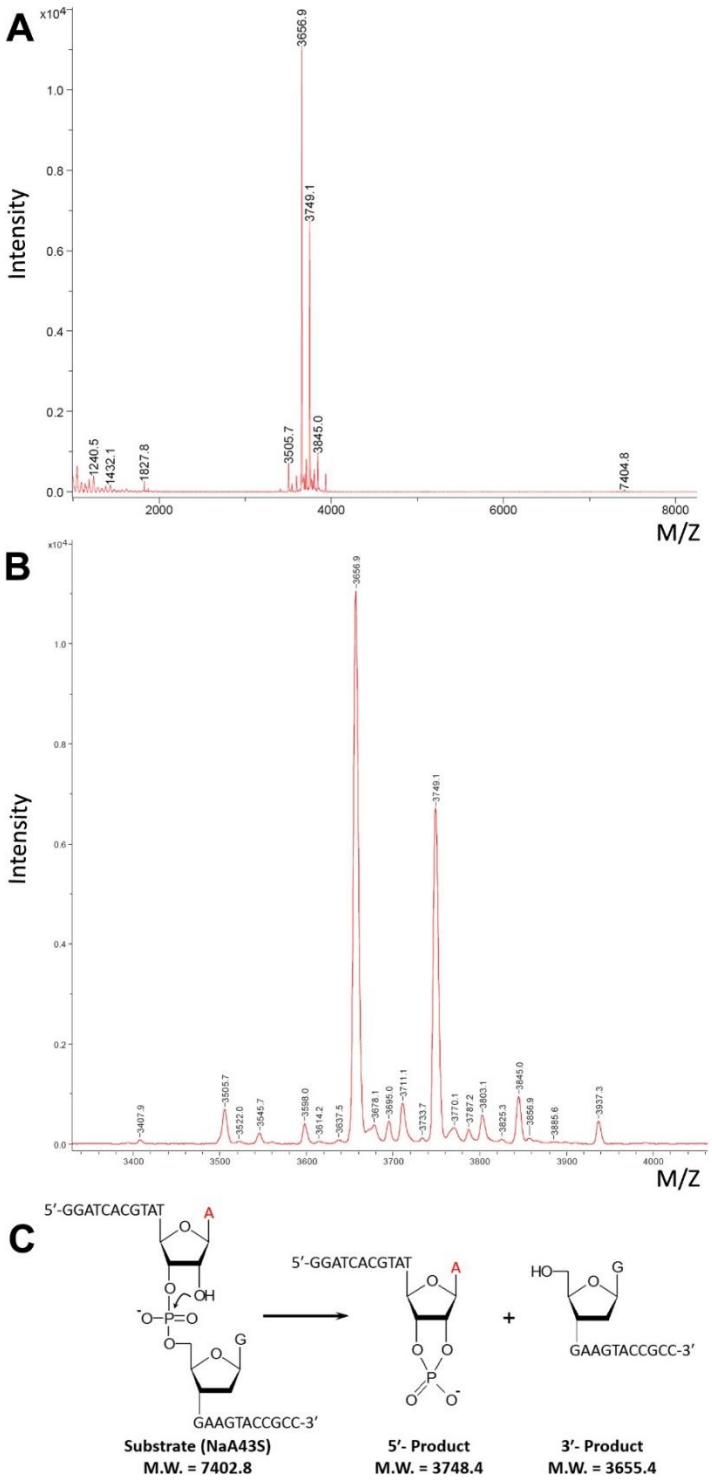

Figure 5.13 Mass spectrometry data of NaA43 reaction mixture contained 200 pmol NaA43S and 400 pmol NaA43E in 400 mM Na^+ (20 mM Bis-Tris, pH 7.0). A) The whole spectra showing negligible amount of uncleaved NaA43S is remained (M.W. 7402.8). B) Zoomed in spectra from (A) showing presence of 5′-end (3748.4) and 3′-end (3655.4) cleavage products. C) Proposed reaction mechanism of substrate cleavage by the NaA43 DNAzyme in the presence of Na^+. The calculated molecular weights (M.W.) of uncleaved substrate and cleavage products are indicated.

5.3.5 Characterization of Cleavage Product by Mass Spectrometry

MALDI mass spectrometry was used to identify cleavage products of the reaction using a DNA/RNA chimeric substrate (NaA43S). As it is shown in the mass spectrum of the reaction products produced from the cleavage of NaA43S by NaA43E, uncleaved NaA43S with the mass of 7404.8 (calculated m/z: 7402.8, Δ = + 0.03%) was barely detectable (Figure 5.13A). Two major signals were identified for the cleavage products with mass of 3656.9 and 3749.1 corresponding to the 3′-fragment which contains a free 5′-hydroxyl group (calculated m/z: 3655.4, Δ = + 0.04%) and the 5′-fragment with 2′,3′-cyclic phosphate end (calculated m/z: 3748.4, Δ = + 0.02%) (Figure 5.13B and C). Identification of a 2′,3′-cyclic phosphate product in the cleavage reaction is in agreement with an internal transesterification mechanism, in which a phosphoester bond is transferred to an adjacent 2′-OH group through in-line attack of the hydroxyl group towards the scissile phosphate and subsequent release of the second product with a 5′-OH group (*55*). This mechanism is similar to the generally accepted mechanism in ribozymes such as hammerhead (*39*), hairpin (*31*), HDV (*40*), glmS (*38*) and twister (*33*) as well as other RNA-cleaving DNAzymes isolated previously (*2, 27*).

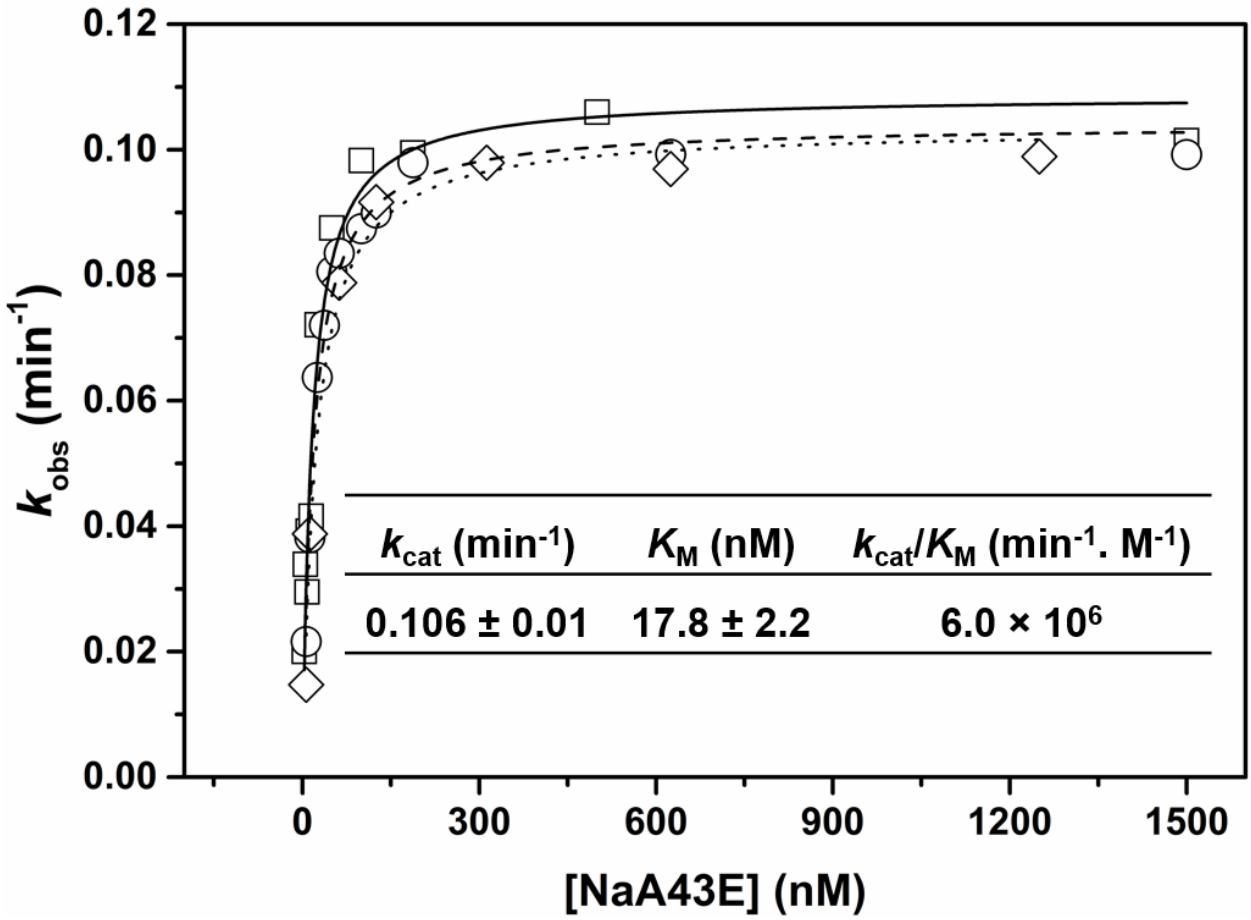

Figure 5.14 Activity of the NaA43 DNAzyme under pre-steady-state conditions. Plots of k_{obs} versus NaA43E concentration in the presence of 400 mM Na^+ at 21 °C with 1 nM NaA43S (5′-^{32}P labeled) from three independent experiments. (Inset) Kinetic parameters.

5.3.6 Pre-Steady-State Reactions

In Figure 5.14 single turnover rate constants of the NaA43 DNAzyme were plotted versus different NaA43E concentrations. This plot is used to determine kinetic parameters of NaA43 under pre-steady-state conditions (NaA43E>>NaA43S). All the experiments were carried out in 400 mM Na+. Cleavage reactions mostly proceeded until 85-95% of NaA43S cleavage, which may indicate that most of the NaA43 DNAzymes in NaA43ES complex were in a catalytically active form. A small fraction of uncleaved substrate, which may be due to the presence of inactive

conformations of the enzyme, has been observed previously for other DNAzymes (*27, 32*). To determine the apparent k_{cat} and K_M values, trace amounts of ^{32}P labeled NaA43S were reacted with increasing enzyme concentrations (Figure 5.14 and inset). The k_{cat} and K'_M were determined to be 0.106 ± 0.01 min-1 and 17.8 ± 2.2 nM, respectively, for the wild-type NaA43 DNAzyme at pH 7.0 and 21 °C. The obtained k_{cat}/K'_M of the NaA43 DNAzyme is similar or slightly higher than the values reported for Pb^{2+} (*27, 32*) and UO_2^{2+}-dependent DNAzymes (*4*).

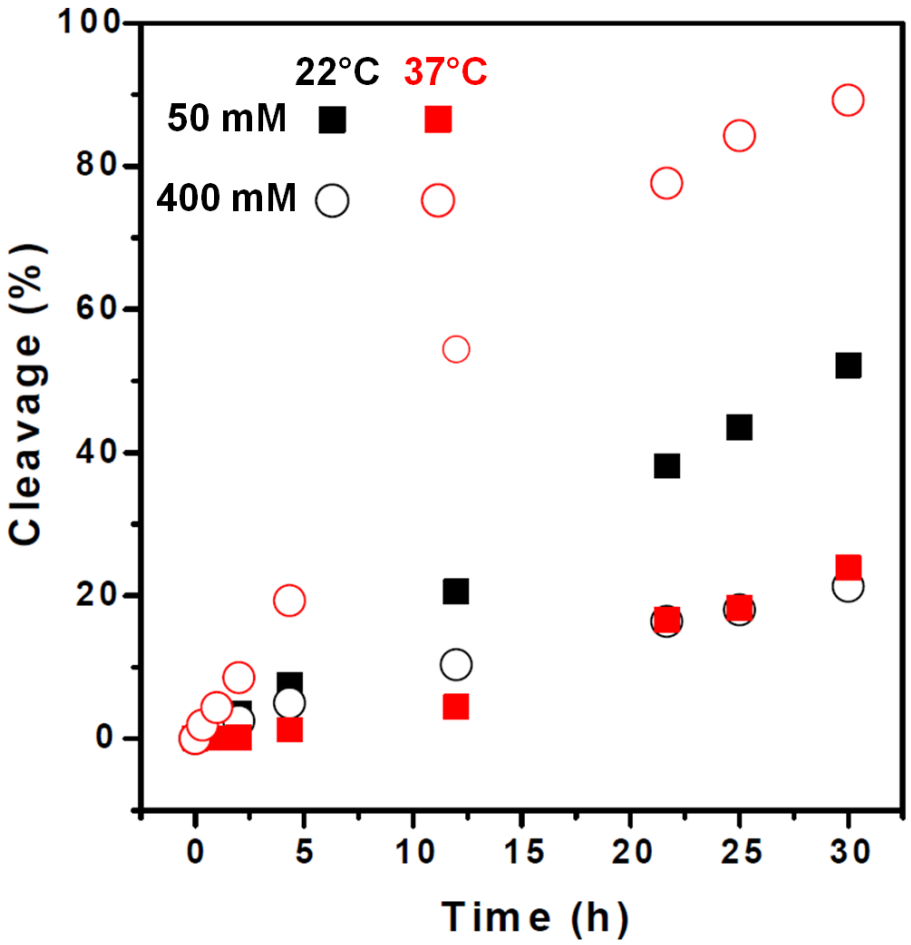

Figure 5.15 Cleavage reaction under multiple-turnover conditions in which NaA43S concentration was ~100 times higher than NaA43E. Reactions carried out using two different temperatures (22 in black and 37 °C in red) and two different Na^+ concentrations (50 mM filled squares and 400 mM empty circles).

5.3.7 Multiple-Turnover Reactions

To explore whether the NaA43 DNAzyme can catalyze the cleavage reaction under multiple-turnover conditions, assays were carried out using 20 nM NaA43E and 2000 nM NaA43S (Figure 5.15). Reactions were started by the addition of Na^+ at a final concentration of 50 or 400 mM at 22 or 37 °C. Nearly maximal turnover numbers were obtained at 400 mM Na^+ and 37 °C. However, NaA43 was found to reach higher turnover numbers in the presence of 50 mM Na^+ at 22 °C. Cleavage products should dissociate to allow NaA43E to form a new NaA43ES complex with an uncleaved substrate for multiple turnovers. Therefore, the melting temperature (T_m) of binding arms in NaA43ES complex plays a critical role in turnover number that is achievable under a certain condition. T_m of the 5′ cleavage product under reaction condition, predicted by the DINAMelt web server (*42*), is 21.4 and 29.8 °C in 50 and 400 mM Na^+, respectively (Table 5.6). Since dissociation of the cleavage product at 400 mM Na^+ is inefficient at < 30 °C, fewer turnovers is achieved in 400 mM Na^+ at room temperature. It is expected that NaA43ES with shorter binding arms, which makes dissociation of cleavage products faster than catalytic step, provide similar kinetics under single- and multiple-turnover conditions (*23, 56*).

Table 5.6 T_m of the 5′ and 3′ cleavage products under multiple-turnover conditions, predicted by DINAMelt web server, at 50 and 400 mM Na^+.

[Na^+] (mM)	5′ cleavage product	3′ cleavage product
50	21.4 °C	15.1 °C
400	29.8 °C	22.6 °C

5.3.8 Rate-pH Profile

The dependence of reaction rate (k_{obs}) on pH (pH/log k_{obs} profile) in the presence of Na^+ was studied in five different buffers spanning a broad range of pH from 4.0 to 10.0 under single-turnover conditions. Investigating the pH/log k_{obs} profile helps to identify whether the chemical-cleavage step or conformational change is the rate-limiting step (*57*, *58*). As shown in Figure 5.16, the log value of k_{obs} increased linearly with a slope of 1.03 as pH increased in the range of pH from 4.0 to 6.5. No significant change in the reaction rate was observed as pH increased further from 6.5 to 10.0. Since no noticeable change in the cleavage rate was observed after increase in the concentration of NaA43E (*e.g.* 300 nM to 600 nM, Figure 5.14) it is suggested that conformational changes do not play a major role in the rate of catalysis (*45*, *59*). In addition, observing a slope of unity in pH profile of NaA43 indicates that the rate-limiting step of the reaction is cleavage step and the obtained k_{obs} represents the rate of chemical cleavage (*59*). This pH dependency of the NaA43 DNAzyme may show that a general base or acid is involved in the catalysis. Since the 2′,3′-cyclic phosphate product was identified as one of the products in the cleavage reaction and catalytic activity of NaA43 increases by pH linearly until plateaus, it is likely that a functional group in the DNAzyme acts as a general base in the catalysis. This functional group might assist in deprotonation or partial deprotonation of the 2′-hydroxyl group which results in the formation of 2′-oxyanion which is a better nucleophile by ~ 10^{10} times than 2′-hydroxyl group (*55*). In this catalytic strategy the amount of rate enhancement is proportional to the extent of 2′-oxyanion formation. The pH profile of NaA43 and the slope of 1 at pH below 6.5 indicates titration of a functional unprotonated form of one general base with apparent p*K*a value ~ 6.1. Therefore, the cleavage reaction proceeds faster as pH increases up to the point in which the base is fully deprotonated and further increase in pH (>6.5) causes no significant change in the cleavage rate.

Observing the slope of zero at higher pH values (>6.5) may also imply that concentration of one species increases while another decreases by the same extent. Our results cannot exclude the possibility that the unperturbed pK_a of 2′-hydroxyl group has been shifted from 13.7 (*51*) to 6.1 in the cleavage site of NaA43.

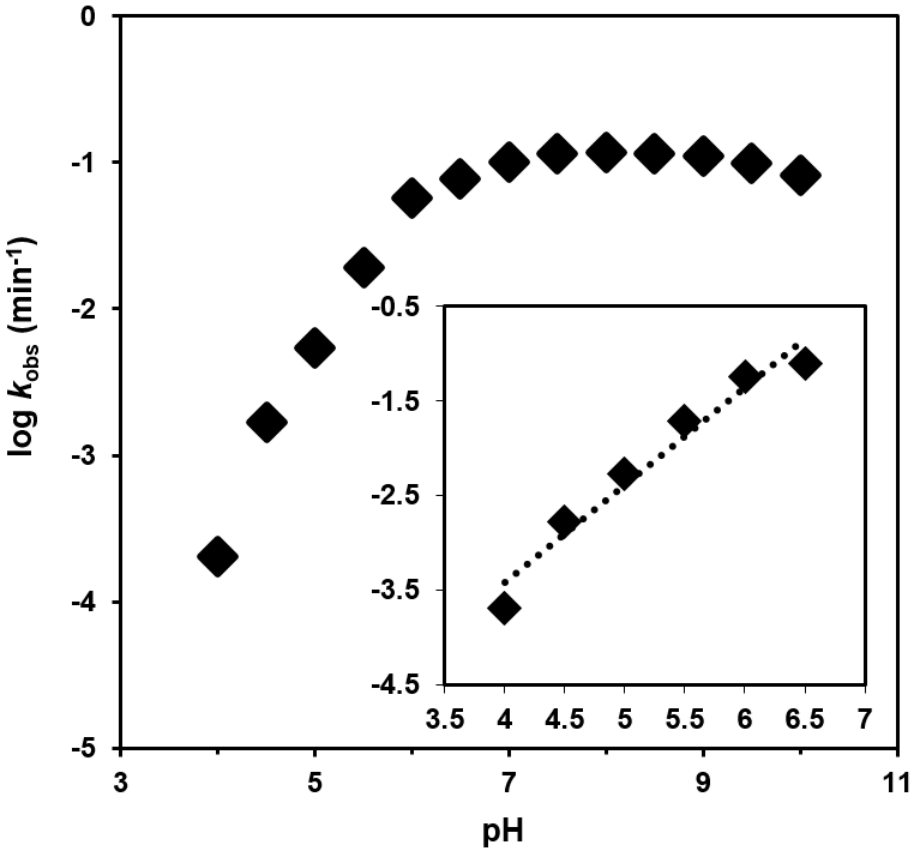

Figure 5.16 Rate-pH profile for the *trans*-cleaving NaA43 DNAzyme. Single-turnover cleavage rates were obtained in the presence of 400 mM Na^+ and plotted as a function of pH. Individual k_{obs} represent the average of at least three independent reactions. (Inset) Linear portion of the rate-pH profile (pH = 4.0 – 6.5) slope of 1.03 and R^2 value of 0.96.

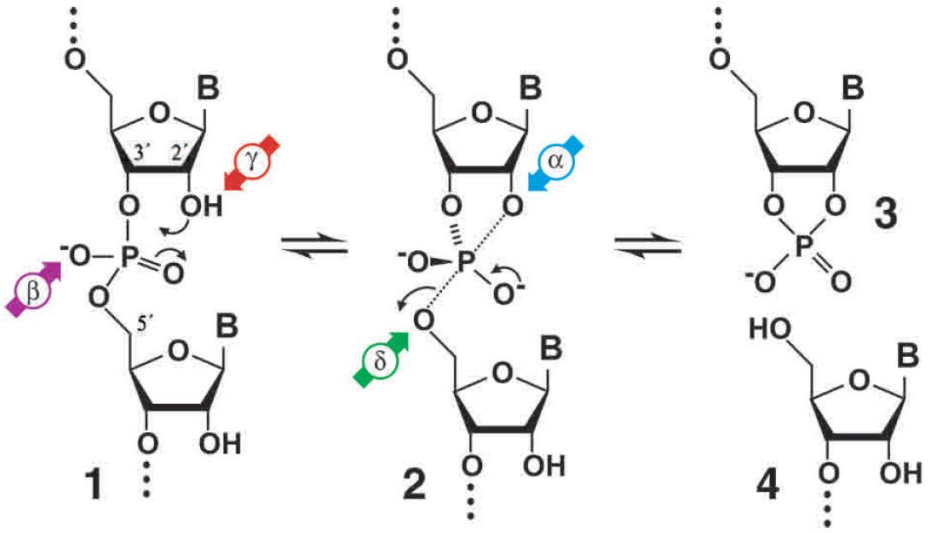

Figure 5.17 Proposed mechanisms for RNA cleavage by ribozymes and DNAzymes (borrowed from (*55*)). 3 and 4 are observed as products in the NaA43 reaction. Four different catalytic strategies are represented: α (blue) is in-line geometry of nucleophilic attack; ß (purple) is neutralization of the negative charge on a nonbridging phosphate oxygen; γ (red) is deprotonation of the 2′-hydroxyl group; and δ (green) is neutralization of the negative charge on the 5′-oxygen atom.

When RNA cleavage by internal phosphoester transfer involves only deprotonation of the 2′-hydroxyl group as the only mechanism for rate enhancement (γ catalysis, Figure 5.17), the maximum values for the rate constant can reach 0.01 min^{-1} at pH 14 (*55*). Another mechanism that affects RNA cleavage rate is the formation of in-line attack geometry that occurs when the 2′-oxygen and 5′-oxygen are positioned in-line with the phosphorus center (α catalysis, Figure 5.17). The rate enhancement obtained by in-line configuration has been determined to be in the order of 10 to 100-fold (*60*). As NaA43 DNAzyme catalyzes RNA cleavage by at least one order of magnitude faster than the maximum rate obtained by γ catalysis, it is likely that other mechanisms such as in-line attack geometry are also involved in the catalysis. The combination of both α and

γ catalysis to accelerate rate of RNA cleavage has been proposed to be utilized by other ribozymes or DNAzymes (*61*).

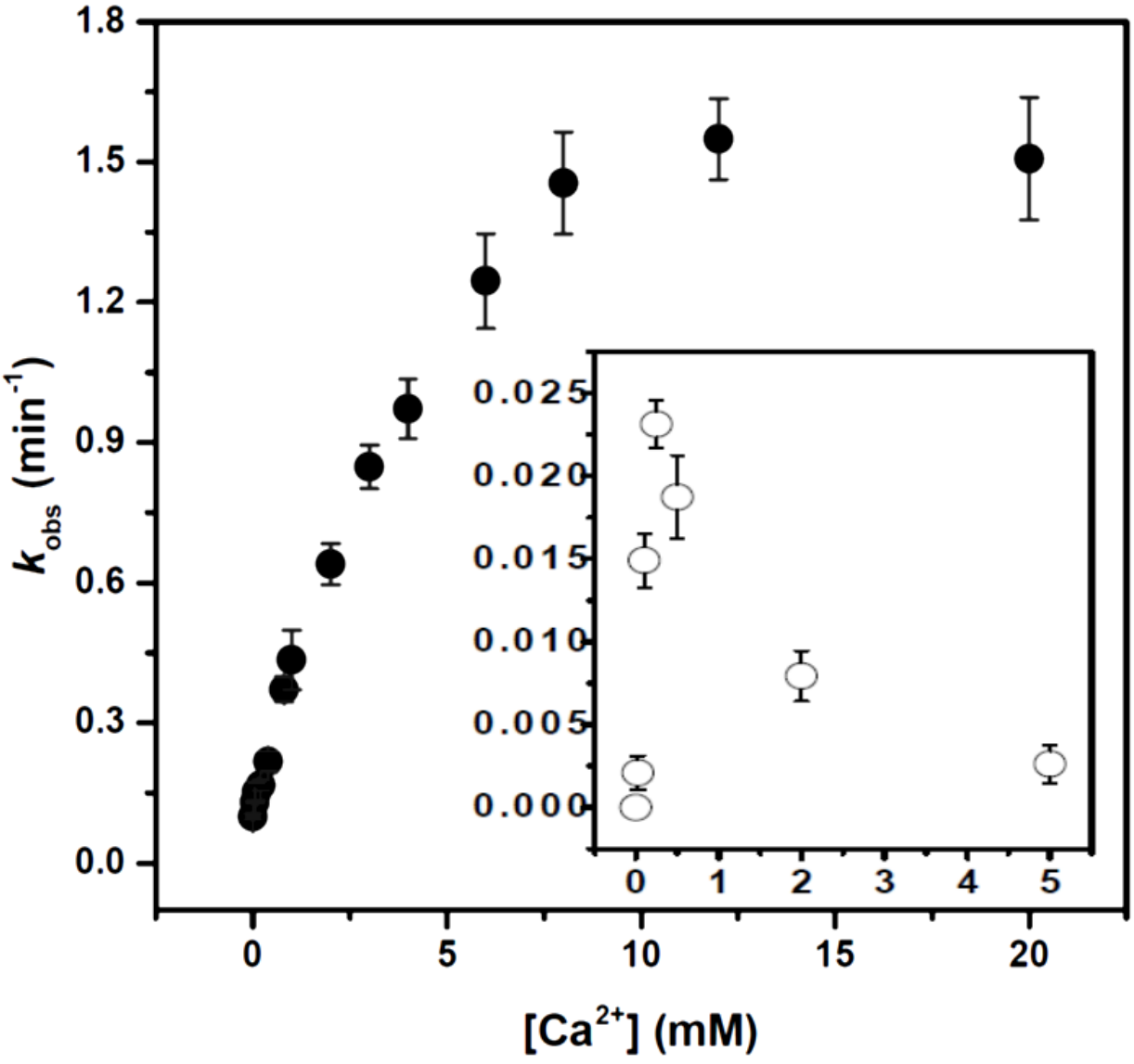

Figure 5.18 Acceleration of Na^+-dependent activity of the NaA43 DNAzyme by Ca^{2+}. Rate of cleavage reaction in 400 mM Na^+ with increasing concentrations of Ca^{2+}. Apparent dissociation constant for Ca^{2+} was calculated to be 3.9 ± 0.5 mM. The inset is a plot of NaA43 activity in 0.25 mM Na^+ with increasing concentrations of Ca^{2+}. Maximum acceleration was obtained at 0.25 mM Ca^{2+}. The error bars represent the standard deviation calculated from at least two independent experiments.

5.3.9 Effect of Ca^{2+} on the Cleavage Rate

Most of the currently reported hydrolytic ribozymes and DNAzymes require multivalent metal ions for catalytic activity (*12*). Multivalent-independent catalytic activity of ribozymes and DNAzymes requires very high concentration of monovalent metal ions to display relatively low catalytic rates (*22, 46-48*). NaA43 catalysis in the absence of divalent metal ions has one the highest divalent-independent rate of catalysis. Although NaA43 does not need any multivalent metal ion for catalysis, we found that Ca^{2+} significantly accelerates Na^{+}-mediated catalysis (Figure 5.18). In the absence of Na^{+} increase in the Ca^{2+} concentration up to 20 mM resulted in no cleavage activity, because Na^{+} is the obligate cofactor of the NaA43 DNAzyme and no catalysis occurs in the absence of Na^{+}. To further explore Ca^{2+}-mediated acceleration of the NaA43 DNAzyme reaction, we tested cleavage rate under single-turnover condition at saturated concentration of Na^{+} (400 mM), in the presence of Ca^{2+} in the range of 0.1 to 20 mM. As shown in Figure 5.18, the reaction rate increases with the addition of Ca^{2+} by more than 15-fold until the rate plateaus at approximately 8 mM Ca^{2+}. To evaluate cooperativity, these results are presented in a linear form (the Hill plot) in Figure 5.19. The slope of the Hill plot of Ca^{2+}-mediated rate acceleration reveals a Hill coefficient of ~ 1.0, which suggests that one Ca^{2+} ion is involved in the transition state of the cleavage reaction and Ca^{2+} binding is non-cooperative. The apparent dissociation constant for Ca^{2+} was determined by plotting the dependence of k_{obs} versus log [Ca^{2+}] using fitting equation 3, explained in the Materials and Methods section. The apparent dissociation constant was found to be 3.9 ± 0.5 mM, which is tighter than reported affinities of ribozymes and DNAzymes for Ca^{2+} (*32, 59, 62*). In addition, we tested Ca^{2+}-mediated rate acceleration at low Na^{+} concentrations (0.25 mM). At this condition rate acceleration showed a bell-shaped response to the increase of Ca^{2+} concentration with highest acceleration at 0.25 mM (two orders of magnitude acceleration). Bell-

shaped responses in cleavage activity with increasing multivalent metal concentration have been reported for other DNAzymes (*56, 63*). Nonspecific metal/DNA interactions were proposed as a cause of the inhibitory effect at higher metal concentrations. Here, the inhibitory effect of higher concentrations of Ca^{2+} was observed at a Na^{+} concentration much lower than the apparent dissociation constant of NaA43 for Na^{+}, ~40 mM. Additionally, such an effect was not observed at 400 mM Na^{+}. Therefore it is likely that high concentrations of Ca^{2+} disrupt Na^{+}/DNA interactions when Na^{+} is present at lower concentrations (much lower than saturating concentrations) (*45*). Similar inhibitory effects were observed with high Mg^{2+} concentrations in combination with Na^{+} at concentrations below the apparent dissociation constant (data not shown).

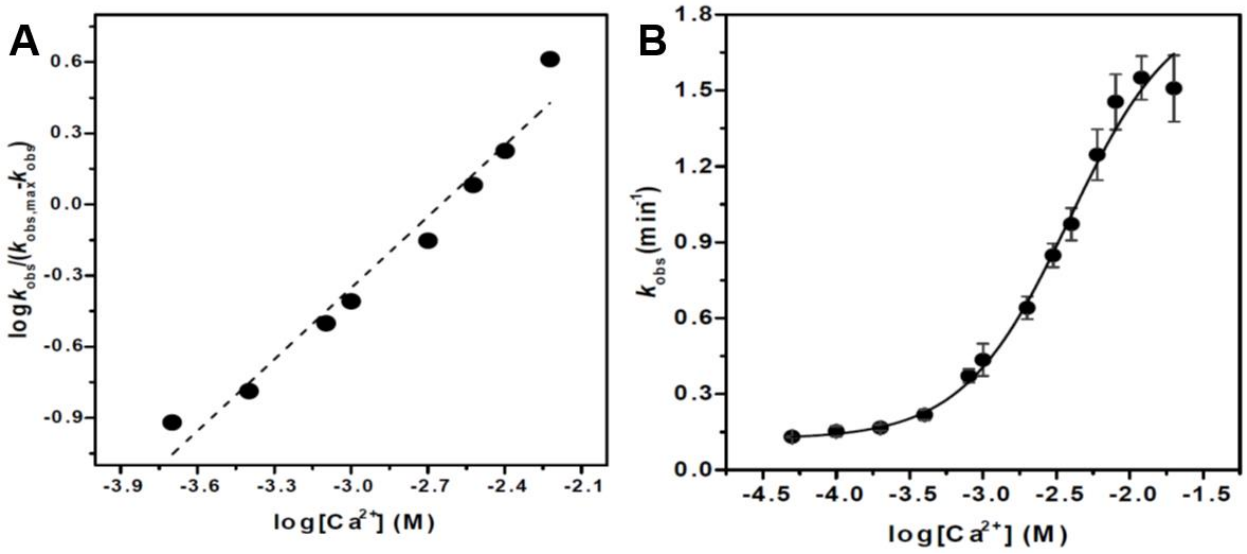

Figure 5.19 Ca^{2+} cooperativity in the presence of 400 mM Na^{+}. (A) The Hill coefficients of 1.0 ($R^2 = 0.96$) was obtained. (B) Plot of k_{obs} as a function of Ca^{2+} concentration in the presence of 400 mM Na^{+}. Apparent dissociation constant of NaA43 for Ca^{2+} was calculated to be 3.9 ± 0.5 mM.

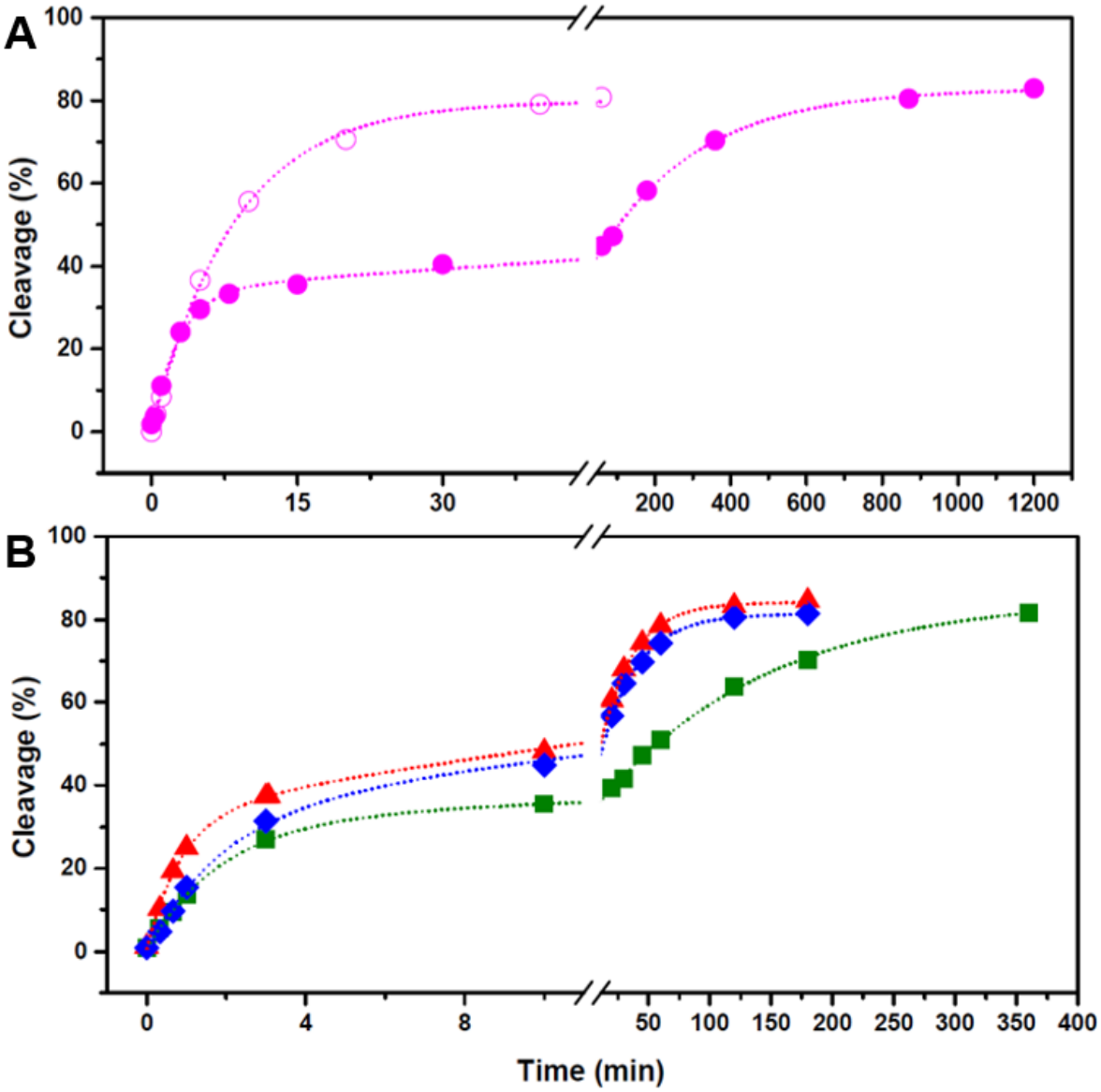

Figure 5.20 Observing thio effect with PS modified NaA43S. (A) Cleavage % versus time traces of the oxo NaA43S (open circles) and PS NaA43S (closed circles) with 400 mM Na^+. Equation 1 was used for fitting oxo data and PS data were fitted using equation 4. The oxo substrate reacts monophasically and close to completion, with k_{obs} value of 0.1 min^{-1}. In contrast, the PS substrate reacts biphasically with the first phase being faster (0.3 min^{-1}) and the second phase slower (0.005 min^{-1}) than the oxo substrate. (B) Cleavage % versus time trances of PS substrate with 1 mM Ca^{2+} (green squares), 1 mM Cd^{2+} (red triangles), or 1 mM Zn^{2+} (blue diamonds) in the presence of 400 mM Na^+. As in (A) the PS substrate reacts biphasically. All experiments carried out at pH 7.0. Rate constants and thio effects are represented in Table 5.7.

5.3.10 Thio Effect Observation with Phosphorothioate Substitution

In the presence of both Na^+ and Ca^{2+} cleavage rate is increased up to ~ 15-fold in comparison to the original catalytic rate in the absence of Ca^{2+}. It is proposed that when the rate of RNA-cleavage reaction exceeds unity, one possible catalytic strategy which is utilized by nucleic acid enzymes is neutralization of the negative charge on a nonbridging oxygen of the scissile phosphate (*55*). To further investigate Ca^{2+}-mediated acceleration, I studied effects of sulfur substitution at nonbridging phosphate oxygens. The phosphorothioate (PS) NaA43S which is a diastereomeric mixture of R_P and S_P, with near equal distribution, was used to probe potential coordination of Ca^{2+} with nonbridging oxygens in the cleavage site (*46, 61, 64*). It is known that sulfur binds to thiophilic metal ions such as Cd^{2+} and Zn^{2+} with much higher affinity than Ca^{2+}. Therefore, if Ca^{2+} is coordinated with nonbridging oxygens, it is expected to observe less efficient Ca^{2+}-mediated acceleration with at least of the diastereomers. This reduction in activity upon sulfur replacement is known as "thio effect". In addition, reduction of thio effect is anticipated when a thiophilic metal ion is used in place of Ca^{2+} (*46, 61*).

All of these experiments were carried out in the presence of 400 mM Na^+ under single-turnover conditions at pH 7.0. The PS substrate, in contrast to the oxo substrate (NaA43S with no PS modification), showed a biphasic kinetic profile (Figure 5.20A). An inverse thio effect by factor of ~ 0.3 was observed for the fast phase and in the slow phase the PS substrate reacted ~ 20-fold slower than the oxo substrate (Table 5.7). The biphasic kinetic profile of PS substrate cleavage showed no difference when the reaction was carried out in the absence of 50 mM Li^+ or in the presence of 50 mM K^+ or NH_4^+ (Figure 5.21). Therefore, presence of 50 mM Li^+ in the reaction had no effect on the cleavage rate and kinetic profile of PS substrate.

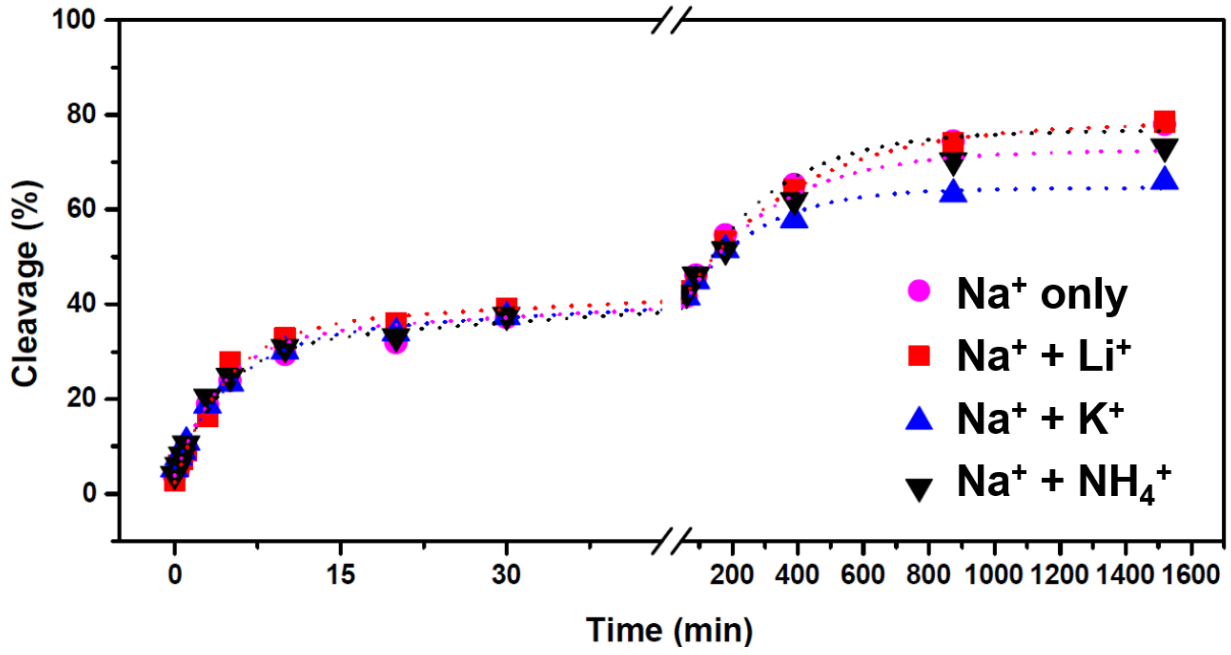

Figure 5.21 Observing thio effect with PS modified NaA43S with 400 mM Na^+ in the absence of monovalent metal ions (no background ionic strength) or in the presence of 50 mM Li^+, K^+, or NH_4^+ at pH 7.0. No significant difference was observed in the rate of both phases.

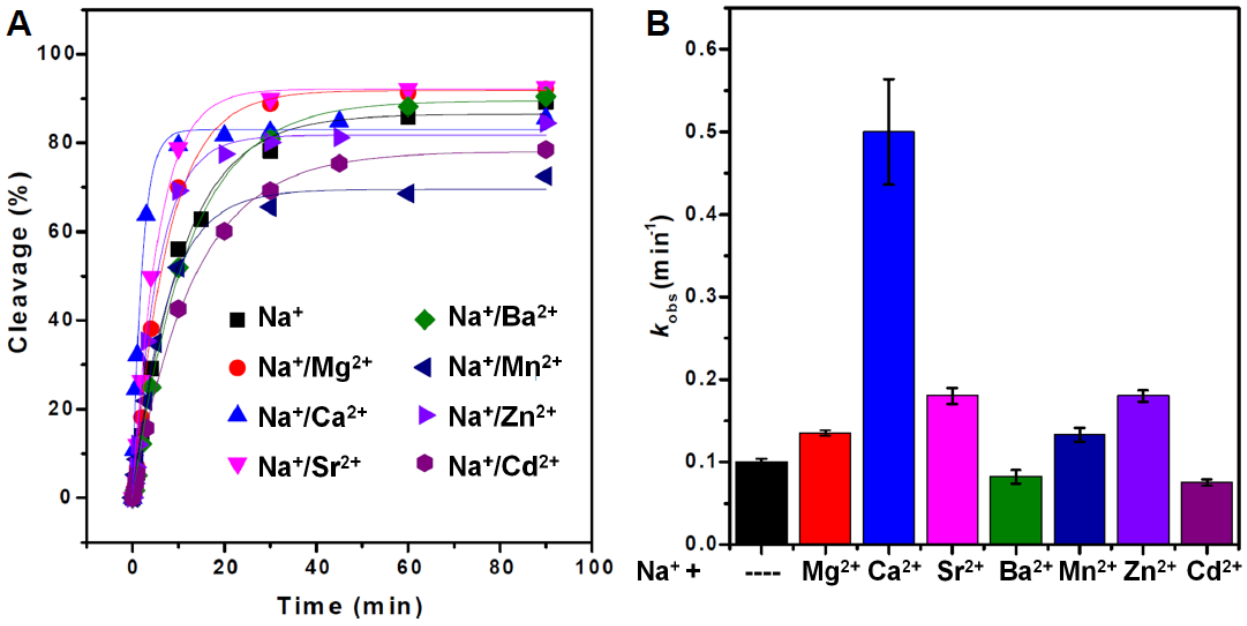

Figure 5.22 Effect of 1 mM divalent metal ions on NaA43 activity at 400 mM Na^+. (A) Kinetic plots of NaA43 cleavage activity at pH 7.0 in the presence of 400 mM Na^+ and 1 mM divalent metal ion at 22 °C. Data points were fitted to first-order kinetics. (B) k_{obs} values for different conditions in (A) were plotted. Error bars represent standard deviation from at least two independent experiments.

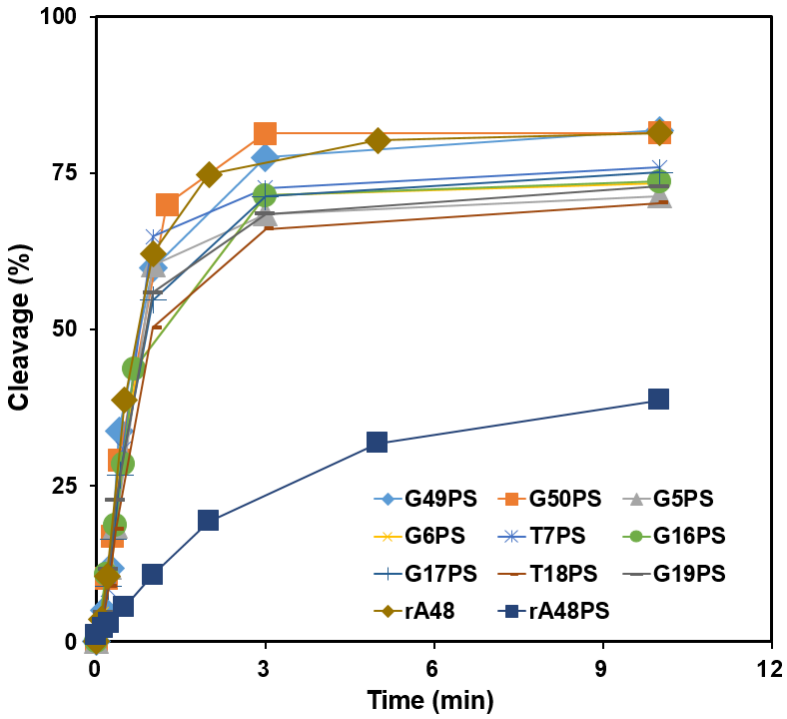

Figure 5.23 PS modification at positions other than rA48, cleavage site, does not affect rate of catalysis with 20 mM Ca^{2+} in the presence of 400 mM Na^{+} at pH 7.0.

Inverse thio effect was observed previously for HDV ribozyme in the presence of divalent (*65*) or monovalent metal ions (*46*). It was proposed that the active site geometry in one of the diastereomers is more favorable with thiophosphate than phosphate, thus the cleavage rate of the fast phase was faster than the cleavage rate of the oxo substrate (*46*). The origin of the inverse thio effect is still not clear. Cleavage rate of PS and oxo substrates was monitored in the presence of 400 mM Na^{+} and 1 mM Ca^{2+}, Zn^{2+}, or Cd^{2+} at pH 7.0 (Figure 5.20B and 22). PS substrate cleavage followed biphasic kinetics in the presence of divalent metal ions. Although in the presence of Ca^{2+} no thio effect was observed for the fast phase, a large thio effect was obtained in the slow phase (56 ± 9-fold). The thio effect for the slow phase showed 10- or 30-fold rescue in the presence of 1 mM Zn^{2+} or Cd^{2+}, respectively. These rescue values are in the typical range of 10-100 as previously

reported in the literature (*65*). In addition, I tested the effect of introducing PS modification in several other positions such as catalytically critical nucleotides in the DNAzyme and substrate. No significant difference was observed in the kinetic profile of cleavage reaction by introducing PS modification in positions other than the rA48 cleavage site (Figure 5.23). Results of phosphorothioate rescue experiments in the presence of 1 mM or 10 mM thiophilic metal ions at pH 6.0 were consistent with the experiments carried out at pH 7.0 (Table 5.8). Therefore, our data suggest that direct interaction of Ca^{2+} with nonbridging oxygens and subsequent neutralization of the negative charges might be the source of Ca^{2+}-mediated acceleration (*46, 55, 61*).

Table 5.7 Thiophosphate substitutions at the rA48 cleavage site, thio effect and metal ion rescue for the NaA43 DNAzyme in the presence of 400 mM Na^+ at pH 7.0 [a]

Ionic condition	Substrate	k_{obs} (min^{-1})	End point (%)	k_O/k_S [b]	Metal ion rescue [c]
400 mM Na^+	oxo	0.102 ± 0.004	85 ± 10	N/A	N/A
	PS fast	0.32 ± 0.028	38 ± 8	0.32 ± 0.04	N/A
	PS slow	0.005 ± 0.001	46 ± 4	21 ± 2.6	N/A
400 mM Na^+	oxo	0.49 ± 0.06	85 ± 6	N/A	N/A
+ 1 mM Ca^{2+}	PS fast	0.50 ± 0.04	31 ± 6	0.98 ± 0.01	N/A
	PS slow	0.008 ± 0.001	41 ± 10	56 ± 9	N/A
400 mM Na^+	oxo	0.17 ± 0.01	80 ± 5	N/A	N/A
+ 1 mM Zn^{2+}	PS fast	0.50 ± 0.06	32 ± 4	0.34 ± 0.02	2.9 ± 0.2
	PS slow	0.030 ± 0.005	43 ± 10	5.6 ± 0.4	10 ± 1.0
400 mM Na^+	oxo	0.070 ± 0.007	78 ± 4	N/A	N/A
+ 1 mM Cd^{2+}	PS fast	1.1 ± 0.08	29 ± 7	0.065 ± 0.001	15 ± 0.5
	PS slow	0.036 ± 0.002	47 ± 7	2.0 ± 0.2	30 ± 1.1

[a] All rate constants measured in the background of 400 mM Na^+ at 37 °C and pH 7.0 (20 mM Bis-Tris). [b] The thio effect (k_O/k_S) is the ratio of k_{obs} for the oxo substrate over the k_{obs} for the phosphorothioate substrate at 400 mM Na^+ (equation 5). [c] Metal rescue values for each condition is calculated based on the equation described in materials and methods (equation 6). Represented errors are standard deviation of two to more independent experiments.

In nucleic acid enzymes that require coordination of a metal ion with nonbridging oxygens for catalysis, only one of the nonbridging oxygens is coordinated with the metal ion which is imposed by active site geometry (*61*). Such enzymes cleave 50% of the PS substrate in which consists of equal ratio of R_P and S_P diastereomers in the absence of thiophilic metal ions. Therefore, the fraction of total substrate cleaved in the presence of an oxophilic metal ion such as Ca^{2+} will be half of what is cleaved in the presence of a thiophilic metal ion such as Cd^{2+} (*61, 64*). Since NaA43 cleavage proceeds to completion in the absence of divalent metal ions, monitoring fraction of cleaved PS substrate in the presence of Ca^{2+} or Cd^{2+} at earlier stages of each phase might show preference of Cd^{2+} for PS substrate over Ca^{2+}. As demonstrated in (Figure SX) at two time points such as 1 and 30 minutes that are well in the linear stages of the biphasic kinetic profiles, fraction of cleaved PS in the presence of Ca^{2+} was approximately half of what was cleaved in the presence of Cd^{2+}. These data indicate that at linear region of each phase Cd^{2+} is about twice as efficient as Ca^{2+} in accelerating cleavage reaction, which indicates the importance of the interaction between nonbridging oxygens and the Ca^{2+} ion.

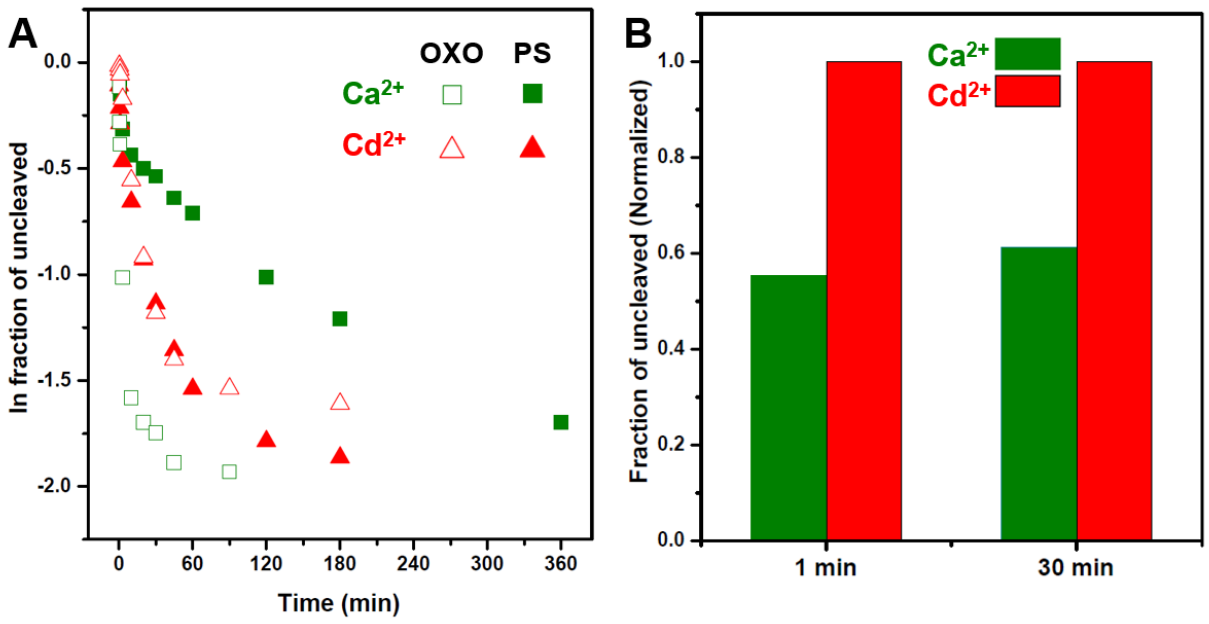

Figure 5.24 Kinetic characteristics of the NaA43 DNAzyme with 400 mM Na^+ in the presence of 1 mM Ca^{2+} (empty and filled squares for oxo and PS substrate, respectively) or 1 mM Cd^{2+} (empty and filled triangles for oxo and PS substrate, respectively) at pH 7.0. The bar graph on left represents the fraction of cleaved substrate in the presence of Ca^{2+} or Cd^{2+} at the indicated time points.

Table 5.8 Thiophosphate substitutions at the rA48 cleavage site, thio effect and metal ion rescue for the NaA43 DNAzyme in the presence of 400 mM Na^+ at pH 6.0

Ionic condition	**Substrate**	k_{obs} **(min^{-1})**	**End point (%)**	k_O/k_S [b]	**Metal ion rescue** [c]
		pH 6.0	Conditions		
400 mM Na^+	oxo	0.055 ± 0.003	74 ± 4	N/A	N/A
	PS fast	0.207 ± 0.021	31 ± 2	0.26 ± 0.04	N/A
	PS slow	0.003 ± 0.0001	45 ± 4	19 ± 0.4	N/A
400 mM Na^+	oxo	0.26	81	N/A	N/A
+ 1 mM Ca^{2+}	PS fast	0.23	32	1.1	N/A
	PS slow	0.004	41	57	N/A
400 mM Na^+	oxo	0.13	82	N/A	N/A
+ 1 mM Zn^{2+}	PS fast	0.25	31	0.53	2.1
	PS slow	0.007	44	20	2.9
400 mM Na^+	oxo	0.047	84	N/A	N/A
+ 1 mM Cd^{2+}	PS fast	0.82	23	0.058	19
	PS slow	0.017	55	2.8	21
400 mM Na^+	oxo	0.65	77	N/A	N/A
+ 10 mM Ca^{2+}	PS fast	0.20	31	3.3	N/A
	PS slow	0.011	47	62	N/A
400 mM Na^+	oxo	0.020	76	N/A	N/A
+ 10 mM Zn^{2+}	PS fast	0.042	32	0.50	6.9
	PS slow	0.003	46	7.5	8.3
400 mM Na^+	oxo	0.018	74	N/A	N/A
+ 10 mM Cd^{2+}	PS fast	0.19	27	0.091	36
400 mM Na^+	PS slow	0.021	48	0.86	72

5.4 Conclusions

In conclusion, we have characterized a Na^+-specific RNA-cleaving DNAzyme called NaA43. Sequence alignment and DNAzyme/substrate mutations revealed sequence requirements of the NaA43 DNAzyme for catalysis. This DNAzyme is consisted of two main motifs; a highly conserved region and a structural motif. The presence of a structural motif that tolerates replacement with other functional nucleic acids makes the NaA43 DNAzyme a perfect platform for the design of allosteric biosensors. Additionally, Na^+ specificity of the DNAzyme was investigated and it was confirmed that Na^+ is an obligate cofactor for catalysis by NaA43. This is a unique feature of NaA43 as no previous report has shown a high specificity for a monovalent metal ion in RNA-cleaving DNAzymes. It further demonstrates that the *in vitro* selection process can be applied as a general method to many metal ions of interest.

Studying the pH profile of the NaA43 DNAzyme demonstrated a catalytic mechanism which utilize a general base in catalysis with single deprotonation event in the rate-limiting step of the reaction. The achieved rate of reaction suggests that NaA43 DNAzyme utilize at least two different catalytic strategies in cleaving the RNA phosphodiester bond. Analysis of the cleavage products imply phosphoester bond transfer to the 2′-OH group of the rA in the cleavage site, in agreement with the generally accepted mechanism for RNA-cleaving ribozymes. Although NaA43 was selected in the absence of divalent metal ions, it was found that the DNAzyme has at least one catalytic binding site for Ca^{2+} in which results in ~ 15-fold rate acceleration at saturating Na^+ concentration. Phosphorothioate studies suggest that Ca^{2+} may directly interact with one of the nonbridging oxygens of the scissile phosphate. Taken together, the results presented here provide important information about the mechanism and function of the NaA43 DNAzyme. Further studies can define the identity and location of the general base used for catalysis. Moreover, structural

studies can provide insight into the source of extreme selectivity of the NaA43 DNAzyme over other monovalent metal ions.

5.5 References

1. Guerrier-Takada, C., Gardiner, K., Marsh, T., Pace, N., and Altman, S. (1983) The RNA moiety of ribonuclease P is the catalytic subunit of the enzyme, *Cell 35*, 849-857.

2. Kruger, K., Grabowski, P. J., Zaug, A. J., Sands, J., Gottschling, D. E., and Cech, T. R. (1982) Self-splicing RNA: autoexcision and autocyclization of the ribosomal RNA intervening sequence of Tetrahymena, *Cell 31*, 147-157.

3. Breaker, R. R., and Joyce, G. F. (1994) A DNA enzyme that cleaves RNA, *Chem Biol 1*, 223-229.

4. Schlosser, K., and Li, Y. (2009) Biologically inspired synthetic enzymes made from DNA, *Chem Biol 16*, 311-322.

5. Silverman, S. K. (2008) Catalytic DNA (deoxyribozymes) for synthetic applications-current abilities and future prospects, *Chem Commun (Camb)*, 3467-3485.

6. Franzen, S. (2010) Expanding the catalytic repertoire of ribozymes and deoxyribozymes beyond RNA substrates, *Curr Opin Mol Ther 12*, 223-232.

7. Silverman, S. K. (2010) DNA as a versatile chemical component for catalysis, encoding, and stereocontrol, *Angew Chem Int Ed Engl 49*, 7180-7201.

8. Chu, C. C., Wong, O. Y., and Silverman, S. K. (2014) A generalizable DNA-catalyzed approach to peptide-nucleic acid conjugation, *Chembiochem 15*, 1905-1910.

9. Chandrasekar, J., and Silverman, S. K. (2013) Catalytic DNA with phosphatase activity, *Proc Natl Acad Sci U S A 110*, 5315-5320.

10. Gu, H., Furukawa, K., Weinberg, Z., Berenson, D. F., and Breaker, R. R. (2013) Small, highly active DNAs that hydrolyze DNA, *J Am Chem Soc 135*, 9121-9129.

11. Lu, Y. (2002) New transition-metal-dependent DNAzymes as efficient endonucleases and as selective metal biosensors, *Chemistry 8*, 4589-4596.

12. Ward, W. L., Plakos, K., and DeRose, V. J. (2014) Nucleic acid catalysis: metals, nucleobases, and other cofactors, *Chem Rev 114*, 4318-4342.

13. Xiang, Y., and Lu, Y. (2014) DNA as sensors and imaging agents for metal ions, *Inorganic chemistry 53*, 1925-1942.

14. Liu, J., Cao, Z., and Lu, Y. (2009) Functional nucleic acid sensors, *Chemical Reviews 109*, 1948-1998.

15. Lan, T., and Lu, Y. (2012) Metal ion-dependent DNAzymes and their applications as biosensors, *Metal ions in life sciences 10*, 217-248.

16. Roth, A., and Breaker, R. R. (1998) An amino acid as a cofactor for a catalytic polynucleotide, *Proc Natl Acad Sci U S A 95*, 6027-6031.

17. Ting, R., Thomas, J. M., Lermer, L., and Perrin, D. M. (2004) Substrate specificity and kinetic framework of a DNAzyme with an expanded chemical repertoire: a putative RNaseA

mimic that catalyzes RNA hydrolysis independent of a divalent metal cation, *Nucleic acids research 32*, 6660-6672.

18. Hollenstein, M., Hipolito, C. J., Lam, C. H., and Perrin, D. M. (2013) Toward the combinatorial selection of chemically modified DNAzyme RNase A mimics active against all-RNA substrates, *ACS combinatorial science 15*, 174-182.

19. Hollenstein, M., Hipolito, C. J., Lam, C. H., and Perrin, D. M. (2009) A self-cleaving DNA enzyme modified with amines, guanidines and imidazoles operates independently of divalent metal cations (M2+), *Nucleic acids research 37*, 1638-1649.

20. Hollenstein, M., Hipolito, C. J., Lam, C. H., and Perrin, D. M. (2009) A self-cleaving DNA enzyme modified with amines, guanidines and imidazoles operates independently of divalent metal cations (M2+), *Nucleic acids research 37*, 1638-1649.

21. Faulhammer, D., and Famulok, M. (1997) Characterization and divalent metal-ion dependence of in vitro selected deoxyribozymes which cleave DNA/RNA chimeric oligonucleotides, *Journal of molecular biology 269*, 188-202.

22. Geyer, C. R., and Sen, D. (1997) Evidence for the metal-cofactor independence of an RNA phosphodiester-cleaving DNA enzyme, *Chemistry & biology 4*, 579-593.

23. Santoro, S. W., and Joyce, G. F. (1997) A general purpose RNA-cleaving DNA enzyme, *Proceedings of the National Academy of Sciences of the United States of America 94*, 4262-4266.

24. Faulhammer, D., and Famulok, M. (1996) The Ca2+ Ion as a Cofactor for a Novel RNA-Cleaving Deoxyribozyme, *Angewandte Chemie International Edition in English 35*, 2837-2841.

25. Cruz, R. P., Withers, J. B., and Li, Y. (2004) Dinucleotide junction cleavage versatility of 8-17 deoxyribozyme, *Chem Biol 11*, 57-67.

26. Nelson, K. E., Ihms, H. E., Mazumdar, D., Bruesehoff, P. J., and Lu, Y. (2012) The importance of peripheral sequences in determining the metal selectivity of an in vitro-selected Co(2+) -dependent DNAzyme, *Chembiochem 13*, 381-391.

27. Li, J., Zheng, W., Kwon, A. H., and Lu, Y. (2000) In vitro selection and characterization of a highly efficient Zn(II)-dependent RNA-cleaving deoxyribozyme, *Nucleic acids research 28*, 481-488.

28. Hollenstein, M., Hipolito, C., Lam, C., Dietrich, D., and Perrin, D. M. (2008) A Highly Selective DNAzyme Sensor for Mercuric Ions, *Angewandte Chemie International Edition 47*, 4346-4350.

29. Liu, J., Brown, A. K., Meng, X., Cropek, D. M., Istok, J. D., Watson, D. B., and Lu, Y. (2007) A catalytic beacon sensor for uranium with parts-per-trillion sensitivity and millionfold selectivity, *Proceedings of the National Academy of Sciences of the United States of America 104*, 2056-2061.

30. Huang, P. J., Lin, J., Cao, J., Vazin, M., and Liu, J. (2014) Ultrasensitive DNAzyme beacon for lanthanides and metal speciation, *Anal Chem 86*, 1816-1821.

31. Peracchi, A. (2000) Preferential activation of the 8-17 deoxyribozyme by Ca(2+) ions. Evidence for the identity of 8-17 with the catalytic domain of the Mg5 deoxyribozyme, *J Biol Chem 275*, 11693-11697.

32. Brown, A. K., Li, J., Pavot, C. M., and Lu, Y. (2003) A lead-dependent DNAzyme with a two-step mechanism, *Biochemistry 42*, 7152-7161.

33. Sugimoto, N., Okumoto, Y., and Ohmichi, T. (1999) Effect of metal ions and sequence of deoxyribozymes on their RNA cleavage activity, *Journal of the Chemical Society, Perkin Transactions 2*, 1381-1386.

34. Liu, Z., Mei, S. H., Brennan, J. D., and Li, Y. (2003) Assemblage of signaling DNA enzymes with intriguing metal-ion specificities and pH dependences, *J Am Chem Soc 125*, 7539-7545.

35. Feldman, A. R., Leung, E. K., Bennet, A. J., and Sen, D. (2006) The RNA-cleaving bipartite DNAzyme is a distinctive metalloenzyme, *Chembiochem 7*, 98-105.

36. Ferre-D'Amare, A. R., and Winkler, W. C. (2011) The roles of metal ions in regulation by riboswitches, *Metal ions in life sciences 9*, 141-173.

37. Jaitovich, A., and Bertorello, A. M. (2010) Intracellular sodium sensing: SIK1 network, hormone action and high blood pressure, *Biochimica et Biophysica Acta (BBA) - Molecular Basis of Disease 1802*, 1140-1149.

38. Goh, K. P. (2004) Management of hyponatremia, *Am Fam Physician 69*, 2387-2394.

39. Madan, V. D., Novak, E., and Rich, M. W. (2011) Impact of change in serum sodium concentration on mortality in patients hospitalized with heart failure and hyponatremia, *Circ Heart Fail 4*, 637-643.

40. Babey, M., Kopp, P., and Robertson, G. L. (2011) Familial forms of diabetes insipidus: clinical and molecular characteristics, *Nat Rev Endocrinol 7*, 701-714.

41. Atkinson, H. J., Morris, J. H., Ferrin, T. E., and Babbitt, P. C. (2009) Using sequence similarity networks for visualization of relationships across diverse protein superfamilies, *PLoS One 4*, e4345.

42. Markham, N. R., and Zuker, M. (2005) DINAMelt web server for nucleic acid melting prediction, *Nucleic acids research 33*, W577-581.

43. Markham, N. R., and Zuker, M. (2008) UNAFold: software for nucleic acid folding and hybridization, *Methods in molecular biology 453*, 3-31.

44. Santoro, S. W., and Joyce, G. F. (1998) Mechanism and utility of an RNA-cleaving DNA enzyme, *Biochemistry 37*, 13330-13342.

45. Zhou, J. M., Zhou, D. M., Takagi, Y., Kasai, Y., Inoue, A., Baba, T., and Taira, K. (2002) Existence of efficient divalent metal ion-catalyzed and inefficient divalent metal ion-independent channels in reactions catalyzed by a hammerhead ribozyme, *Nucleic Acids Res 30*, 2374-2382.

46. Perrotta, A. T., and Been, M. D. (2006) HDV ribozyme activity in monovalent cations, *Biochemistry 45*, 11357-11365.

47. Carrigan, M. A., Ricardo, A., Ang, D. N., and Benner, S. A. (2004) Quantitative Analysis of a RNA-Cleaving DNA Catalyst Obtained via in Vitro Selection†, *Biochemistry 43*, 11446-11459.

48. Curtis, E. A., and Bartel, D. P. (2001) The hammerhead cleavage reaction in monovalent cations, *RNA 7*, 546-552.

49. Meier, S. D., Kovalchuk, Y., and Rose, C. R. (2006) Properties of the new fluorescent Na+ indicator CoroNa Green: comparison with SBFI and confocal Na+ imaging, *Journal of neuroscience methods 155*, 251-259.

50. Flora, S. J., and Pachauri, V. (2010) Chelation in metal intoxication, *Int J Environ Res Public Health 7*, 2745-2788.

51. Li, Y., and Breaker, R. R. (1999) Kinetics of RNA Degradation by Specific Base Catalysis of Transesterification Involving the 2‘-Hydroxyl Group, *Journal of the American Chemical Society 121*, 5364-5372.

52. Matsumoto, Y., and Komiyama, M. (1990) Efficient cleavage of adenylyl(3?-5?)adenosine by triethylenetetraminecobalt(III), *Journal of the Chemical Society, Chemical Communications*, 1050-1051.

53. Weinstein, L. B., Earnshaw, D. J., Cosstick, R., and Cech, T. R. (1996) Synthesis and Characterization of an RNA Dinucleotide Containing a 3‘-S-Phosphorothiolate Linkage, *Journal of the American Chemical Society 118*, 10341-10350.

54. Hollenstein, M., Hipolito, C. J., Lam, C. H., and Perrin, D. M. (2009) A DNAzyme with three protein-like functional groups: enhancing catalytic efficiency of M2+-independent RNA cleavage, *Chembiochem : a European journal of chemical biology 10*, 1988-1992.

55. Emilsson, G. M., Nakamura, S., Roth, A., and Breaker, R. R. (2003) Ribozyme speed limits, *RNA 9*, 907-918.

56. Brown, A. K., Liu, J., He, Y., and Lu, Y. (2009) Biochemical characterization of a uranyl ion-specific DNAzyme, *Chembiochem 10*, 486-492.

57. Dahm, S. C., Derrick, W. B., and Uhlenbeck, O. C. (1993) Evidence for the role of solvated metal hydroxide in the hammerhead cleavage mechanism, *Biochemistry 32*, 13040-13045.

58. Zhou, D. M., Zhang, L. H., and Taira, K. (1997) Explanation by the double-metal-ion mechanism of catalysis for the differential metal ion effects on the cleavage rates of 5'-oxy and 5'-thio substrates by a hammerhead ribozyme, *Proc Natl Acad Sci U S A 94*, 14343-14348.

59. Chowrira, B. M., Berzal-Herranz, A., and Burke, J. M. (1993) Ionic requirements for RNA binding, cleavage, and ligation by the hairpin ribozyme, *Biochemistry 32*, 1088-1095.

60. Soukup, G. A., and Breaker, R. R. (1999) Relationship between internucleotide linkage geometry and the stability of RNA, *RNA 5*, 1308-1325.

61. Breaker, R. R., Emilsson, G. M., Lazarev, D., Nakamura, S., Puskarz, I. J., Roth, A., and Sudarsan, N. (2003) A common speed limit for RNA-cleaving ribozymes and deoxyribozymes, *RNA 9*, 949-957.

62. Dahm, S. C., and Uhlenbeck, O. C. (1991) Role of divalent metal ions in the hammerhead RNA cleavage reaction, *Biochemistry 30*, 9464-9469.

63. Carmi, N., and Breaker, R. R. (2001) Characterization of a DNA-cleaving deoxyribozyme, *Bioorg Med Chem 9*, 2589-2600.

64. Nawrot, B., Widera, K., Wojcik, M., Rebowska, B., Nowak, G., and Stec, W. J. (2007) Mapping of the functional phosphate groups in the catalytic core of deoxyribozyme 10-23, *FEBS J 274*, 1062-1072.

65. Thaplyal, P., Ganguly, A., Golden, B. L., Hammes-Schiffer, S., and Bevilacqua, P. C. (2013) Thio effects and an unconventional metal ion rescue in the genomic hepatitis delta virus ribozyme, *Biochemistry 52*, 6499-6514.

6 Chapter 6. Development of a New Colorimetric Sensor for Hg^{2+}

Note: This chapter is the basis of a published manuscript, "Small-molecule diagnostics based on functional DNA nanotechnology: a dipstick test for mercury" Seyed-Fakhreddin Torabi and Yi Lu Faraday Discuss., 2011, 149, 125-135.

6.1 Introduction

6.1.1 Importance of Detecting Small Molecule Targets

Novel analytical techniques improve diagnostics and theranostics for applications in healthcare and related fields (*1-3*). In contrast to the tremendous progress in nucleic acid and protein detection, small molecule analysis of disease markers and inorganic or organic cofactors in biological pathways, has lagged behind (*4-6*). These targets are just as important as their larger counterparts, as they play critical roles in biological function or disease development. For example, for many years a protein-based marker called prostate-specific antigen (PSA) has been used as a marker for prostate cancer (*7*). However, it has been recognized that PSA is a poor marker for the disease because it gives high rates of false positives and false negatives (*8*). On the other hand, a recent report demonstrated that sacrosine, a small organic molecule similar to glycine, may be a better marker for the onset of prostate cancer than PSA (*9*). Therefore, detecting small molecule targets is a major but exciting challenge in bioanalytical chemistry and medical diagnostics.

6.1.2 Importance of Detecting Metal Ions

Among the small molecule targets, metal ions such as calcium or iron are known to benefit human health while other metal ions, such as lead and mercury, are deleterious. With the exception of a few metal ions such as calcium, we know very little about the mechanisms by which metal ions are transported into cells, speciated into different forms, and enabled to carry out their

beneficial or deleterious functions (*10*). Tsien and others' calcium sensors are an excellent example of how metal-ion sensors can revolutionize biochemistry, cellular biology, and related fields (*11*).

6.1.3 Challenges in Detecting Small Molecular Targets Such as Metal Ions

More than half of the elements in the periodical table form metal ions that are found in biological systems and the environment, and some metals form many different oxidation states. Unlike nucleic acid and protein detection where nucleic acid or antibody arrays can be used to detect almost any biomolecular target, there are few general sensing strategies that can be used to produce a sensor for any metal ion or a specific oxidation state of a given metal ion (*12*). Antibodies that can be raised against large molecular targets such as proteins often fail to recognize metal ions; they are too small to elicit a strong immunological response, and some metal ions are too toxic for animals or cells to produce antibodies against them (*13*). Recently, several whole-cell bacterial biosensors were developed to detect metal ions such as mercury. However, most of them were insufficiently selective (*14, 15*). Also, whole-cell biosensors are limited by the expense, fragility, growth requirements of cells, and the specialized training needed to handle them (*16, 17*).

6.1.4 Functional DNA or RNA as an Excellent Alternative in Detecting Small Molecular Targets Such as Metal Ions

Functional DNA and RNA are nucleic acids with either enzymatic or specific binding activities.(*18*) Examples of functional DNA include ribozymes and deoxyribozymes (also called DNAzymes), which are similar to protein enzymes, and riboswitches and aptamers, which are similar to antibodies. Ribozymes and riboswitches have been isolated from cells while DNAzymes and DNA aptamers are obtained by *in vitro* selection (*19, 20*), which is also known as the Systematic Evolution of Ligands by Exponential Enrichment (SELEX) (*21, 22*). The selection process can be tailored to obtain functional DNA or RNA to bind almost any target of interest,

making it, like antibody selection, a general method for obtaining sensing molecules (*23*). Unlike antibody selections, however, these functional DNA and RNA have been shown to bind selectively not only to large molecules, but also to small molecule targets, with affinities down to the picomolar range for the binding constant. In particular, functional DNAs are much more stable than antibodies and can be denatured and renatured many times without losing their function (*12*). Because of these advantages, we and others have developed functional nucleic acid sensors for a wide range of targets including metal ions, small organic molecules, proteins, and cells (*18*). By combining the functional DNA with fluorophores/quenchers, gold nanoparticles, carbon nanotubes, quantum dots, and iron oxide nanoparticles, we have developed highly sensitive and selective, fluorescent, colorimetric, and electrochemical sensors and MRI contrast agents, with detection limits as low as 45 pM (11 ppt) and over million-fold selectivities (*24-28*).

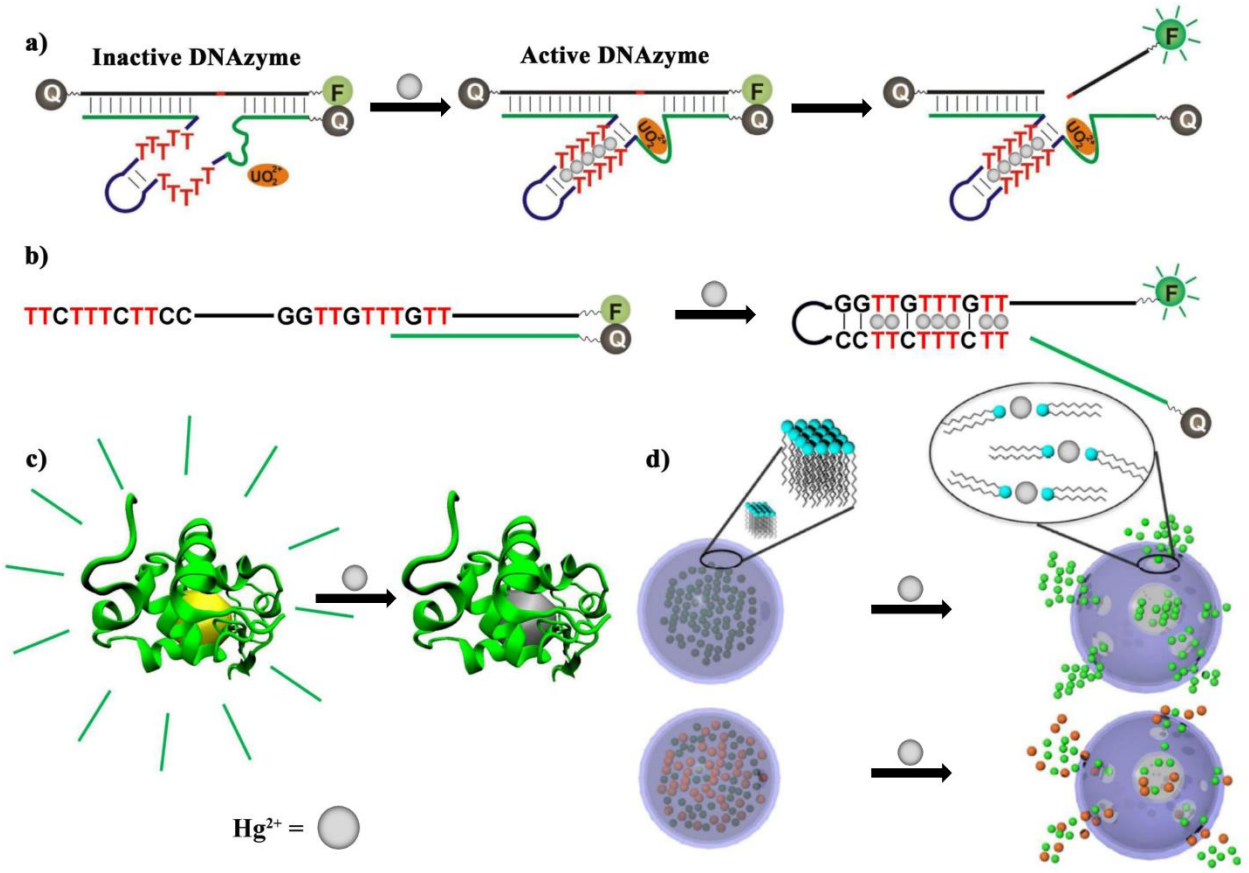

Figure 6.1 Schematic illustration of sensors and theranostic agents for mercury. a) a mercury sensor based on allosteric enhancement of uranium-specific DNAzyme activity by Hg^{2+} binding.(*29*) b) A simplified "turn-on" mercury sensor based on structure-switching DNA that releases quencher modified DNA in the presence of Hg^{2+}.(*27*) c) A lysozyme-stabilized gold fluorescent cluster as A Hg^{2+} sensor.(*30*) d) A theranostic agent for Hg^{2+} based on Hg^{2+}-responsive PEG-liposomes that results in the release of both fluorescent probe and detoxifying agent.(*31*)

6.1.5 Functional DNA Sensors for Mercury

Mercury is a highly toxic heavy metal ion that can cause a number of severe adverse health effects such as damage to the nervous, immune, and excretory systems. Sensors that can detect mercury *in situ* and in real time can greatly increase our understanding of its toxicity and prevent its toxic effects. Toward this goal, we have designed a highly sensitive and selective catalytic beacon sensor for Hg^{2+} using the thymine-mercury-thymine interaction to modulate DNAzyme activities through allosteric interactions (Figure 6.1a) (*29*). Its detection limit of 2.4 nM is lower than the 10 nM maximum contamination level defined by the U.S. EPA for drinking water. We then further simplified the sensor by using the thymine-mercury-thymine interaction without the DNAzyme to create a "turn-on" fluorescent sensor for mercury. This only slightly changed the sensor's properties, giving it a detection limit of 3.2 nM and high selectivity (Figure 6.1b) (*27*). In addition to DNA molecules, we also used proteins in lysozyme-stabilized gold fluorescent clusters Hg^{2+} sensors, which also had a similar detection limit (10 nM) (Figure 6.1c) (*30*). These results complement those of other groups who have developed Hg^{2+} sensors using functional DNA and lysozyme-stabilized gold fluorescent clusters (*32-36*). Finally, we also developed a Hg^{2+} theranostic agent that can simultaneously detect and detoxify mercury using an ion-responsive PEG liposome (Figure 6.1d) (*31*). Since the distribution of mercury in a patient can be location- and time-specific, treating a patient exposed to Hg^{2+} can be challenging. Using a Hg^{2+} detoxification agent at too high a concentration can lead to side-effects, and in any case a single dose of such an agent may be inefficient in dealing with the Hg^{2+} concentration distribution throughout the patient's tissues. The novel liposome-based system shown in Figure 6.1d can detect and respond to Hg^{2+} at concentrations as low as 10 nM. This system adjusts the release of Hg^{2+} chelators to the local concentration of Hg^{2+}, releasing more chelators in regions of high Hg^{2+}

concentration and no chelators in regions of low concentration. This "budgeted" release profile will be particularly useful in situations where the local Hg^{2+} contamination levels vary, or fluctuate over time.

6.1.6 Developing Dipstick Tests for Small Molecular Targets Such as Metal Ions

While these functional nucleic acid sensors are useful as analytical tools to understand biological systems and serve as diagnostics and theranostics in healthcare, they are not without their limitations. For example, the techniques described thus far require the precise transfer of solutions containing reagents (*18*), and thus are not suitable to address a major unmet need in healthcare: rapid, on-site and real-time detection and quantification of small molecule targets. To overcome this limitation, we have transformed the functional nucleic acid sensors into dipstick tests using lateral flow devices (*37, 38*). Similar to a pregnancy test that uses antibodies as the diagnostic agent, we used aptamers and DNAzymes that are much more stable than antibodies and gold nanoparticles (AuNPs) whose extinction coefficient is 10-100 times greater than the most intense organic dyes currently used in commercial dipstick tests (*39*). More importantly, we took advantage of the distance-dependent color changes of AuNPs that are due to surface plasmon effects. As a result, when the target is absent, the aggregated AuNPs will appear blue, but when the target is introduced the AuNPs will appear red (*38*). While this unique concept made adenosine and cocaine detection in aptamer-AuNP-based lateral flow devices possible, it has not been feasible to detect metal ions using an analogous DNAzyme system. Instead, AuNPs serve only as a color-labeling agent (*37, 40*). To take full advantage of the distance-dependent optical changes of AuNPs, we herein describe a new dipstick test that changes color in the presence of mercury.

6.2 Materials and Methods

6.2.1 Materials

All DNA samples were purchased from Integrated DNA Technologies Inc. (Coralville, IA). The linker DNA molecules were purified by gel electrophoresis, whereas the thiol–modified DNA molecules were purified by HPLC. Streptavidin was purchased from Promega. AuNP's (13 nm diameter) were synthesized by the citrate reduction method (*41*). Thiol–modified DNA was activated with two equivalents of tris(2–carboxyethyl) phosphine hydrochloride (TCEP). TCEP–activated thiol–modified DNA and AuNP's were mixed at room temperature for at least 16 h (typically 9 μL of 1 mM DNA was added to 3 mL of AuNP's), and NaCl (100 mM) was added to the solution. The solution was left at room temperature for another two days, and the DNA–functionalized AuNP's were purified by centrifugation and removal of supernatant before use.

6.2.2 Methods

6.2.2.1 Sensor Preparation

Solutions of thiol–modified DNA AuNP's were mixed in the presence of $NaNO_3$ (300 mM), MOPS (3–(Nmorpholino) propanesulfonic acid) buffer (10 mM; pH 7.2), and 45–mer linker DNA (varying concentrations). The samples were annealed by heating at 75 °C for 2 minutes and cooling down to room temperature over ~ 1 h and then were stored at 4 °C for 2 h. AuNP's aggregated and changed color from red to purple in this process. The samples were centrifuged, and the precipitates were collected and dispersed in a buffer containing 150 mM $NaNO_3$; 10 mM MOPS; pH 7.2.

6.2.2.2 Dipstick Test Sample Preparation

The Millipore Hi–Flow Plus Assembly Kit (Millipore Corporation, Bedford, MA) was used. The kit contains a Hi–Flow Plus Cellulose Ester Membrane with a nominal capillary flow

time of 240 seconds/4 cm, an absorption pad, a wicking, and a glass fiber conjugation pad. The device assembly was shown in Fig. 1b. One of the DNA arms contained a biotin moiety at 5′ end, whereas the other did not contain a biotin. The purified AuNP aggregates were dispersed in designated buffer solutions (8% sucrose, 150 mM $NaNO_3$, 10 mM MOPS; pH 7.2) and agitated vigorously with a pipette. AuNP aggregates (4 µL) were spotted on each conjugation pad, and 10 mg mL^{-1} streptavidin (1.5 µL) was applied on the membrane by a 2 µL pipette to form a thin line. The loaded strips were stored in a drawer overnight before use.

6.2.2.3 Detection

To detect Hg^{2+} using solution−based sensor, a small volume of concentrated Hg^{2+} solution was added to 100 µL of the AuNP aggregates suspension. The color change was monitored with a UV–Vis spectrophotometer (Hewlett–Packard 8453) at room temperature. For dipstick tests, varying concentrations Hg^{2+} were dissolved in a flow buffer containing 150 mM $NaNO_3$, 10 mM MOPS, pH 7.2. The wicking pad part of each device was dipped into the solutions for ca. two minutes when the conjugation pad was fully hydrated and the liquid started to migrate on the membrane. Then the device was placed horizontally on a plastic surface for the flow to continue. A digital camera was used to take pictures of the devices after ca. 10 minutes.

6.3 Results and Discussions

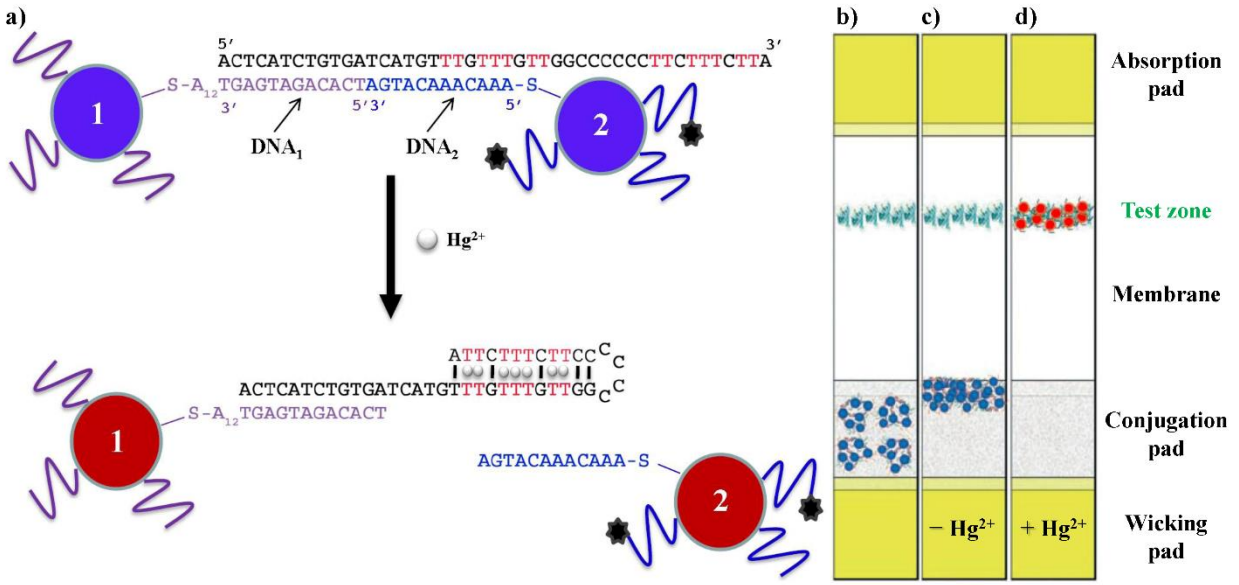

Figure 6.2 Design of colorimetric sensor for mercury. a) Schematic representation of colorimetric detection of Hg^{2+}. The DNA sequences are shown, the A_{12} in DNA_1 (pink) denotes a 12–mer polyadenine chain and biotin is denoted as black stars (✹). AuNPs 1 and 2 are functionalized with two different DNA molecules through thiol−gold chemistry. The two kinds of AuNPs are linked by 45–mer linker DNA strand (in black) containing several thymine residues (in red). In the presence of Hg^{2+}, the aggregates disassemble to give dispersed red AuNPs. b) Assembled lateral flow device loaded with the AuNP aggregates (on the conjugation pad) and streptavidin (on the membrane in cyan color) before use. c) Negative control. In the absence of Hg^{2+}, unreacted AuNP aggregates are stuck on the boundary between the conjugation pad and the membrane. d) Positive test. In the presence of Hg^{2+}, AuNP aggregates are disassembled and dispersed AuNP's product migrates to be captured at the test zone through biotin−streptavidin interaction and the red line is produced.

We constructed a colorimetric mercury sensor as shown in Figure 6.2a. It is based on our recent fluorescent Hg^{2+} sensor that uses structure-switching DNA and on colorimetric sensors for adenosine and cocaine using aptamers and AuNPs (*27*, *38*, *42*). The sensor system consists of two sets of 13-nm AuNPs, with each set of AuNP functionalized with either DNA_1 (in purple) or DNA_2 (in blue). A 45-mer linker DNA is then used to bring the two sets of DNA-functionalized AuNPs together. This linker contains three segments. The first segment is complementary to DNA_1, the

second segment is complementary to DNA_2, and the third segment remains in single-stranded form. Critical to this sensor design is the presence of seven thymine-thymine mismatched pairs (T-T, shown in red) separated by five self-complementary base pairs located within the second and third segments of the linker DNA. In this way, the addition of the linker DNA should aggregate the AuNPs functionalized with DNA_1 and DNA_2 to form blue- or purple-colored aggregates due to the surface plasmon effect. Since Hg^{2+} is known to form strong thymine-Hg^{2+}-thymine base pairs (*32*, *43*), the presence of Hg^{2+} would induce the folding of the last two segments of the linker DNA into a hairpin structure as shown in Figure 6.2a. As a result, only five base pairs would remain between DNA_2 and the linker DNA, which is not enough to keep both strands in a stable double-stranded form at room temperature. Therefore, DNA_2 and the attached AuNPs would be released from the linker DNA, the AuNPs would disassemble, and their color would change from purple to red. This phenomenon can be monitored by measuring changes in the solution absorbance at 520 and 700 nm, with a high ratio indicating red-colored disassembled AuNPs and a low ratio indicating purple-colored aggregated AuNPs (*42*).

The colorimetric spectra of the sensor system during the four minutes after adding 1.5 μM Hg^{2+} is shown in Figure 6.3a. The assembly of AuNP aggregates was studied using different linker DNA concentrations from 4 nM to 100 nM. The concentration of AuNPs was 8 nM (4 nM each of DNA_1- and DNA_2-functionalized AuNPs). Although 40 nM of linker DA was sufficient to aggregate all the AuNPs, AuNPs aggregated with 20 nM of linker DNA were found to be the most sensitive toward Hg^{2+}-induced disassembly. At 20 nM linker DNA, ~ 85% of AuNPs were removed in the form of aggregated particles after 2 minutes of centrifugation at 400 × *g*. As a result, each AuNP was connected to the AuNPs by approximately six linker DNAs.

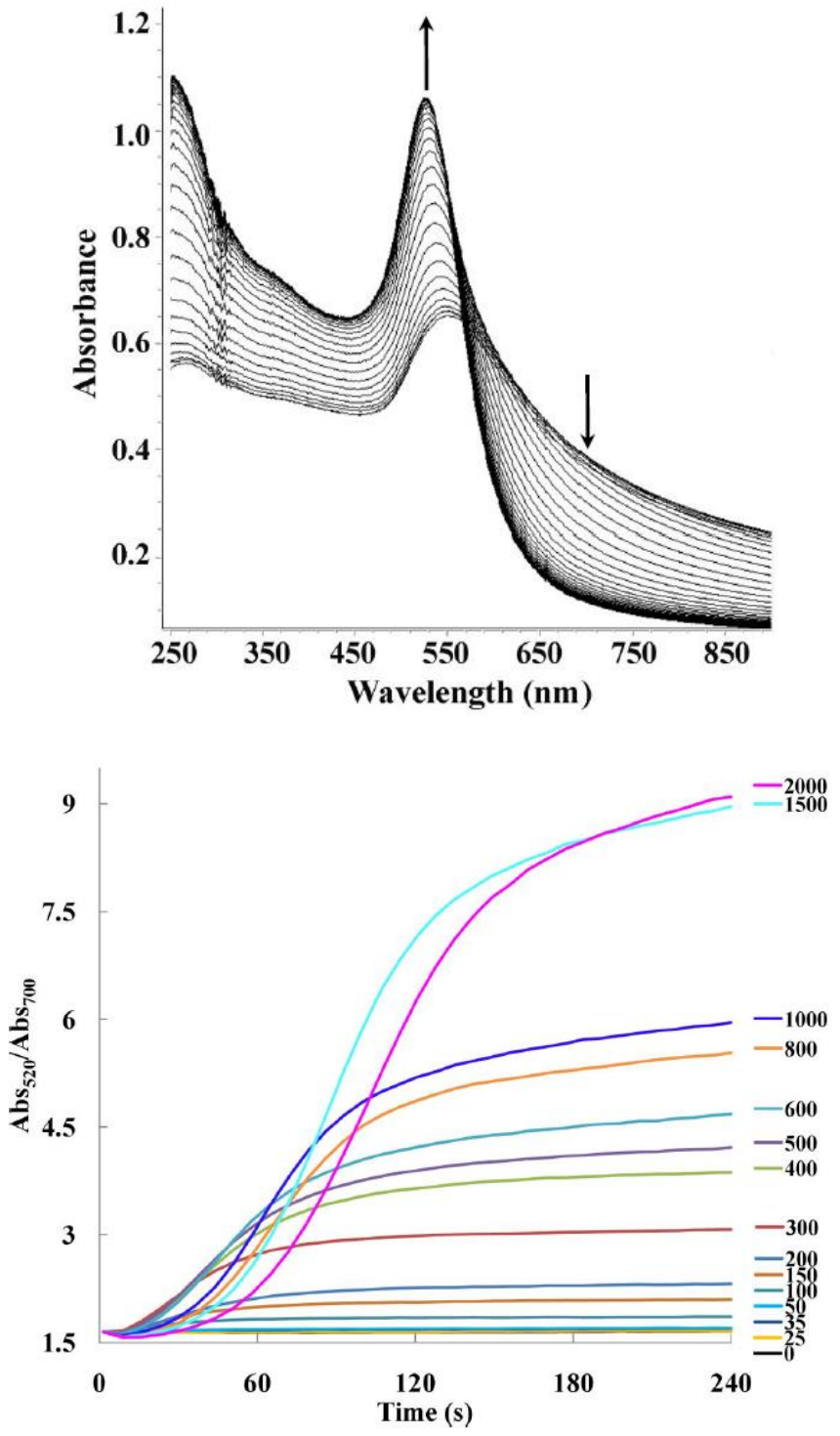

Figure 6.3 Kinetics of the color change at various concentrations of Hg^{2+}. a) UV–Vis spectra of the colorimetric mercury sensor upon addition of 1.5 μM of mercury during a four–minute time course. Decrease in the absorbance at 700 nm and its increase at 520 nm is shown. b) Kinetics of the absorbance ratio increase in the presence of varying concentrations of Hg^{2+} ion.

To study the Hg^{2+}-induced disassembly of AuNP aggregates, the sensor solutions were treated with Hg^{2+} ions of various concentrations and the kinetics of their color changes were monitored by UV-Vis spectroscopy (Figure 6.3b). Higher concentrations of Hg^{2+} ions increased the rate at which the solution changed to red. Quantitative analysis was carried out by monitoring the increase in the absorbance ratio four minutes after adding different Hg^{2+} concentrations. As illustrated in Figure 6.4, a linear relationship between the absorbance ratio and Hg^{2+} concentration was observed in the wide range of Hg^{2+} concentrations from 0-1500 nM. The sensor has a detection limit of 5.4 nM based on 3σ/slope, which is about two times lower than the maximum contaminant level of 10 nM defined by the U.S. EPA for drinking water. At very low Hg^{2+} concentrations, because there were around six linkages for each AuNP and each linkage contains seven T-T mismatches, only a small fraction of the AuNPs was released from the aggregates. Therefore, the absorbance ratio could not substantially increase in the presence of the high background absorbance of the remaining aggregates. Despite this limitation, the sensitivity of the current detection system is comparable to our recent fluorescent-based detection method (*27*), and is greater than those of the previously-reported Hg^{2+} sensors (*32, 44-46*).

To determine the selectivity of the sensor, 1 μM of each metal ion was individually added to the sensor solution and the absorbance ratio change was monitored. As shown in Figure 6.5 (blue bars), among the metal ions tested (Zn^{2+}, Pb^{2+}, Cu^{2+}, Co^{2+}, Cd^{2+}, Mn^{2+}, Ba^{2+}, Ca^{2+}, $Mg^{2+}$and Hg^{2+}), only Hg^{2+} resulted in a significant increase in the absorbance ratio. In addition, 1 μM of Hg^{2+} and 1 μM of another divalent metal ion were added together to the sensor solution. The absorbance ratio of the Hg^{2+}-M^{2+} pair (Figure 6.5 red bars) indicates that the sensor has a high selectivity for Hg^{2+} against a background of competing analytes. The excellent selectivity of the

sensor is likely due to the high specificity of the interaction between T-T mispairs and Hg^{2+} which has been previously demonstrated (*47*).

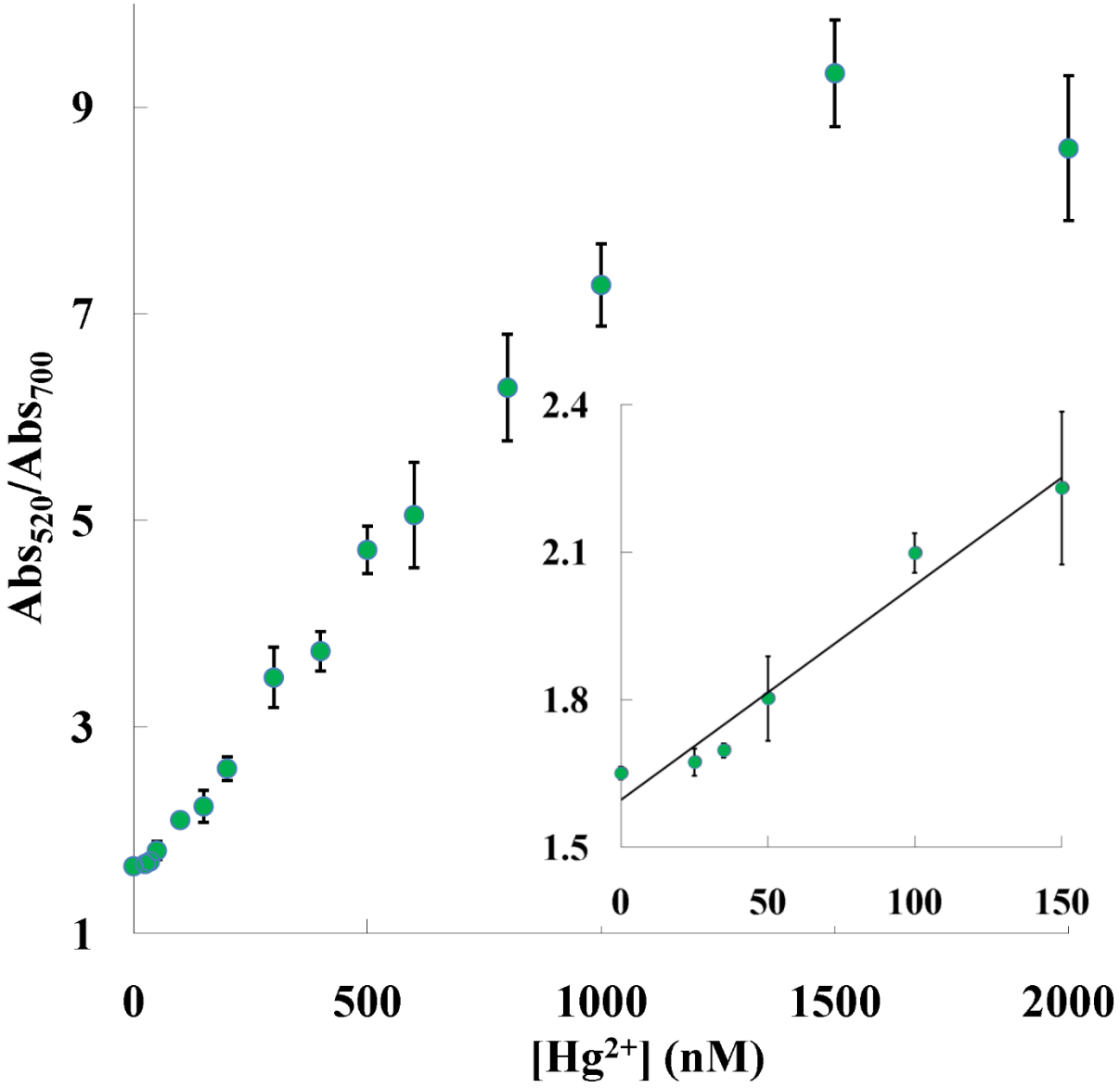

Figure 6.4 Quantifying the Hg^{2+} concentration by monitoring the absorbance ratio four minutes after adding mercury. The calibration curve of the colorimetric mercury sensor saturated at concentrations higher than 1500 nM. A linear relationship between the absorbance ratio and Hg^{2+} concentration was observed for a wide concentration range (0–1500 nM). The data were obtained from three independent measurements and the error bars indicate the standard deviation.

Since it had exhibited exquisite sensitivity and selectivity in buffer solutions, our sensor was further tested with pond water collected on the University of Illinois campus. Using the standard addition method, Hg^{2+} ions were added to the sensor solution in the pond water up to a final concentration of 1 μM. The sensor responded to Hg^{2+} very similarly, whether it was in pure or pond water (Figure 6.5). Similar responses were also obtained with 100 and 300 nM mercury in pure and pond water. This is an indicator that our sensor is able to detect Hg^{2+} in pond water with little interference.

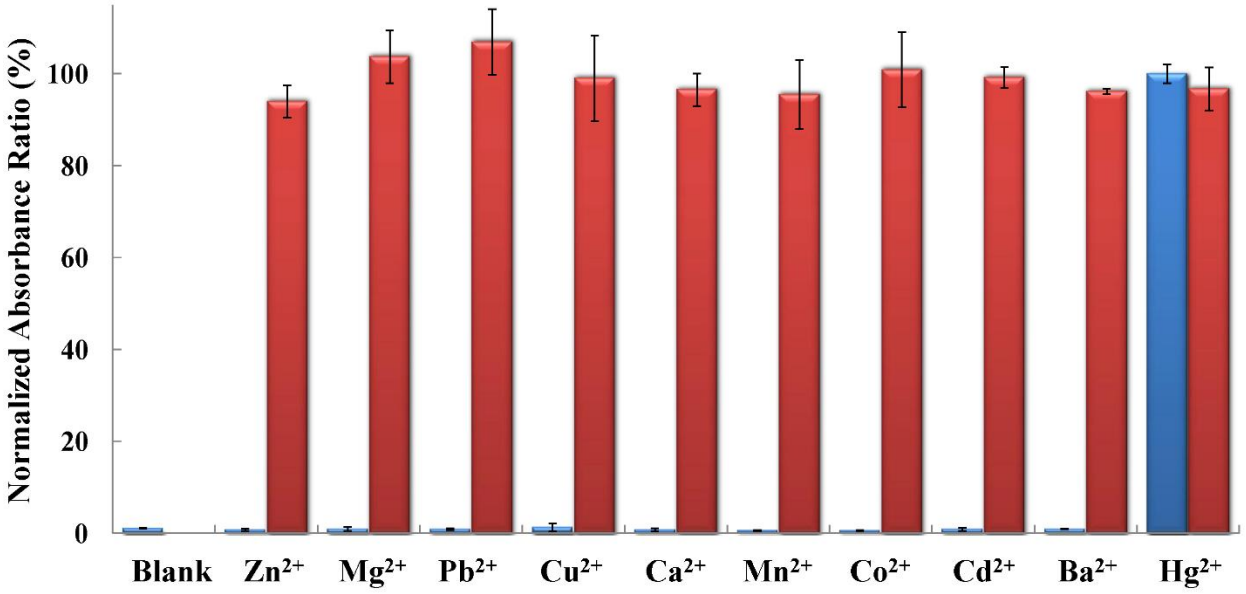

Figure 6.5 Selectivity of the Hg^{2+} sensor. Blue bars represent normalized absorbance ratios four minutes after adding 1 μM of the other metal ions (from left to right: blank, Zn^{2+}, Mg^{2+}, Pb^{2+}, Cu^{2+}, Ca^{2+}, Mn^{2+}, Co^{2+}, Cd^{2+}, Ba^{2+} and Hg^{2+}). Red bars represent sensor responses after adding 1 μM of Hg^{2+} and 1 μM of another metal ion. The last red bar represents the sensor response when 1 μM of mercury was added to the pond water; the dilution factor was 1.5.

Although the success of this Hg^{2+} colorimetric sensor is an important step toward real-time sensing, the next step would be to convert this sensor into an even simpler Hg^{2+} dipstick test that does not require instruments such as a UV-Vis spectrophotometer. As in the colorimetric sensing

system, Hg^{2+}-responsive AuNP aggregates containing two kinds of DNA-functionalized AuNPs and a 45-mer linker DNA were prepared. In this case, two kinds of thiol-modified DNA_2 (biotinylated and non-biotinylated) were used to functionalize particle 2. Biotin modifications on the DNA strands (●) allowed the AuNPs to be captured by streptavidin. The optimal 1:1 ratio between two DNA molecules, which has been shown in our previous work (*38*), was used in this study.

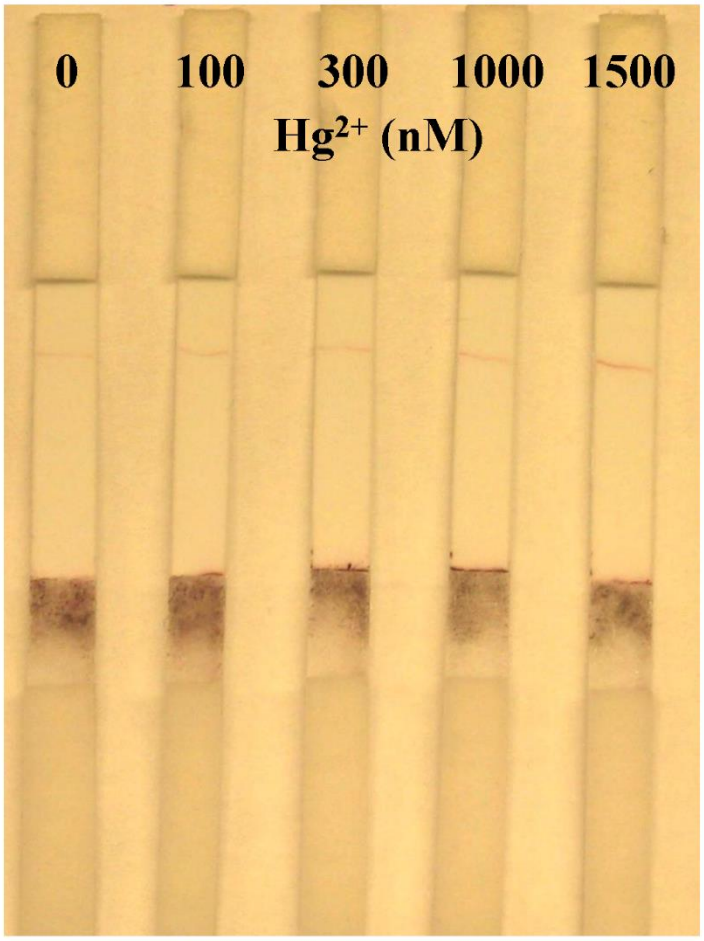

Figure 6.6 Lateral flow-based detection of Hg^{2+}. Test of the mercury-sensing lateral flow device with varying concentrations of Hg^{2+}.

Four overlapping pads of a lateral flow device were attached to a paper backing as follows (from top to bottom): absorption pad, HiFlow Plus membrane, glass fiber conjugation pad, and wicking pad. Aggregated AuNPs were prepared in a buffer containing 10 mM MOPS (pH 7.2), 150 mM $NaNO_3$, and 8% sucrose, producing a dark purple-colored solution. Sucrose was added to the buffer to keep the DNA hybridized and facilitate the rehydration of the aggregates. The lateral flow device was allowed to dry for 8 h. Aggregated AuNPs were spotted onto the conjugation pad, and streptavidin was applied to the HiFlow Plus membrane as a thin line (Figure 6.2b). When the bottom of the dipstick was placed into the sample solution, the Hg^{2+} ions migrated to the aggregates and disassembled the aggregated particles. While the large size of the aggregates prevented them from migrating onto the conjugation pad (*42*), the small size of the dispersed AuNPs allowed them to migrate freely with the solution flow and be captured by streptavidin. Their capture and immobilization formed a thin red line that indicated the presence of Hg^{2+}.

In order to test the performance of the lateral flow device, the dipstick was placed into flow buffers containing varying Hg^{2+} concentrations. In all cases, a dark band at the boundary between the conjugation pad and the membrane was observed (Figure 6.6). The unreacted aggregates on the boundary provided a useful control which was due to the aggregated AuNPs that are so large they can no longer migrate along the membrane (*38, 42*). As shown in Figure 6.6, the intensity of the red line at the streptavidin capture zone increased as the concentration of Hg^{2+} increased. While colorimetric tests monitor a change in color, dipstick tests measure the intensity of a single color. Thus, the dipstick test can provide qualitative or semiquantitative results. In fact, for most lateral-flow-based detections, such as the pregnancy test, only a yes or no answer is required.

6.4 Conclusions

In summary, we have designed a highly sensitive and selective colorimetric sensor for mercury that is based on structure-switching DNA that contains mismatched thymine residues. The sensor is easy-to-use, shows a fast color change, and has a detection limit of 5.4 nM, which is lower than the 10 nM EPA limit for Hg^{2+} in drinking water. Furthermore, we have immobilized AuNP aggregates onto a lateral flow device, resulting in the first easy-to-use dipstick test for mercury. Their simple design makes the highly sensitive and selective colorimetric sensor and corresponding dipstick tests capable of carrying out real-time mercury detection in environmental and medical applications.

6.5 References

1. Cheng, A. K., Sen, D., and Yu, H. Z. (2009) Design and testing of aptamer-based electrochemical biosensors for proteins and small molecules, *Bioelectrochemistry 77*, 1-12.

2. Lindon, J. C., Holmes, E., and Nicholson, J. K. (2004) Metabonomics: systems biology in pharmaceutical research and development, *Curr Opin Mol Ther 6*, 265-272.

3. Famulok, M., Hartig, J. S., and Mayer, G. (2007) Functional aptamers and aptazymes in biotechnology, diagnostics, and therapy, *Chem Rev 107*, 3715-3743.

4. Majidi, J., Barar, J., Baradaran, B., Abdolalizadeh, J., and Omidi, Y. (2009) Target therapy of cancer: implementation of monoclonal antibodies and nanobodies, *Hum Antibodies 18*, 81-100.

5. Majumdar, D., Peng, X. H., and Shin, D. M. (2010) The Medicinal Chemistry of Theragnostics, Multimodality Imaging and Applications of Nanotechnology in Cancer, *Curr Top Med Chem*.

6. Lu, B., Smyth, M. R., and O'Kennedy, R. (1996) Oriented immobilization of antibodies and its applications in immunoassays and immunosensors, *Analyst 121*, 29R-32R.

7. Wu, G., Datar, R. H., Hansen, K. M., Thundat, T., Cote, R. J., and Majumdar, A. (2001) Bioassay of prostate-specific antigen (PSA) using microcantilevers, *Nat Biotechnol 19*, 856-860.

8. Semjonow, A., Oberpenning, F., Weining, C., Schon, M., Brandt, B., De Angelis, G., Heinecke, A., Hamm, M., Stieber, P., Hertle, L., and Schmid, H. P. (2001) Do modifications of nonequimolar assays for total prostate-specific antigen improve detection of prostate cancer?, *Clin Chem 47*, 1472-1475.

9. Sreekumar, A., Poisson, L. M., Rajendiran, T. M., Khan, A. P., Cao, Q., Yu, J., Laxman, B., Mehra, R., Lonigro, R. J., Li, Y., Nyati, M. K., Ahsan, A., Kalyana-Sundaram, S., Han, B., Cao, X., Byun, J., Omenn, G. S., Ghosh, D., Pennathur, S., Alexander, D. C., Berger, A., Shuster, J. R., Wei, J. T., Varambally, S., Beecher, C., and Chinnaiyan, A. M. (2009) Metabolomic profiles delineate potential role for sarcosine in prostate cancer progression, *Nature 457*, 910-914.

10. Yokel, R. A., Lasley, S. M., and Dorman, D. C. (2006) The speciation of metals in mammals influences their toxicokinetics and toxicodynamics and therefore human health risk assessment, *J Toxicol Environ Health B Crit Rev 9*, 63-85.

11. Palmer, A. E., Jin, C., Reed, J. C., and Tsien, R. Y. (2004) Bcl-2-mediated alterations in endoplasmic reticulum Ca2+ analyzed with an improved genetically encoded fluorescent sensor, *Proc Natl Acad Sci U S A 101*, 17404-17409.

12. O'Sullivan, C. K. (2002) Aptasensors--the future of biosensing?, *Anal Bioanal Chem 372*, 44-48.

13. Hilvert, D. (2000) Critical analysis of antibody catalysis, *Annu Rev Biochem 69*, 751-793.

14. Ivask, A., Virta, M., and Kahru, A. (2002) Construction and use of specific luminescent recombinant bacterial sensors for the assessment of bioavailable fraction of cadmium, zinc, mercury and chromium in the soil, *Soil Biol Biochem 34*, 1439-1447.

15. Nolan, E. M., and Lippard, S. J. (2008) Tools and tactics for the optical detection of mercuric ion, *Chemical Reviews 108*, 3443-3480.

16. Fishman, H. A., Greenwald, D. R., and Zare, R. N. (1998) Biosensors in chemical separations, *Annu Rev Biophys Biomol Struct 27*, 165-198.

17. Zhao, J., Jedlicka, S. S., Lannu, J. D., Bhunia, A. K., and Rickus, J. L. (2006) Liposome-doped nanocomposites as artificial-cell-based biosensors: detection of listeriolysin O, *Biotechnol Prog 22*, 32-37.

18. Liu, J., Cao, Z., and Lu, Y. (2009) Functional nucleic acid sensors, *Chem Rev 109*, 1948-1998.

19. Breaker, R. R., and Joyce, G. F. (1994) A DNA enzyme that cleaves RNA, *Chem Biol 1*, 223-229.

20. Robertson, D. L., and Joyce, G. F. (1990) Selection in vitro of an RNA enzyme that specifically cleaves single-stranded DNA, *Nature 344*, 467-468.

21. Ellington, A. D., and Szostak, J. W. (1990) In vitro selection of RNA molecules that bind specific ligands, *Nature 346*, 818-822.

22. Tuerk, C., and Gold, L. (1990) Systematic evolution of ligands by exponential enrichment: RNA ligands to bacteriophage T4 DNA polymerase, *Science 249*, 505-510.

23. Bunka, D. H., and Stockley, P. G. (2006) Aptamers come of age - at last, *Nat Rev Microbiol 4*, 588-596.

24. Lan, T., Furuya, K., and Lu, Y. (2010) A highly selective lead sensor based on a classic lead DNAzyme, *Chem Commun (Camb)*.

25. Lee, J. H., Wang, Z., Liu, J., and Lu, Y. (2008) Highly sensitive and selective colorimetric sensors for uranyl (UO2(2+)): development and comparison of labeled and label-free DNAzyme-gold nanoparticle systems, *J Am Chem Soc 130*, 14217-14226.

26. Lee, J. H., Yigit, M. V., Mazumdar, D., and Lu, Y. (2010) Molecular diagnostic and drug delivery agents based on aptamer-nanomaterial conjugates, *Adv Drug Deliv Rev*.

27. Wang, Z., Heon Lee, J., and Lu, Y. (2008) Highly sensitive "turn-on" fluorescent sensor for Hg2+ in aqueous solution based on structure-switching DNA, *Chem Commun (Camb)*, 6005-6007.

28. Liu, J., Lee, J. H., and Lu, Y. (2007) Quantum dot encoding of aptamer-linked nanostructures for one-pot simultaneous detection of multiple analytes, *Anal Chem 79*, 4120-4125.

29. Liu, J., and Lu, Y. (2007) Rational design of "turn-on" allosteric DNAzyme catalytic beacons for aqueous mercury ions with ultrahigh sensitivity and selectivity, *Angew Chem Int Ed Engl 46*, 7587-7590.

30. Wei, H., Wang, Z., Yang, L., Tian, S., Hou, C., and Lu, Y. (2010) Lysozyme-stabilized gold fluorescent cluster: Synthesis and application as Hg(2+) sensor, *Analyst 135*, 1406-1410.

31. Yigit, M. V., Mishra, A., Tong, R., Cheng, J., Wong, G. C., and Lu, Y. (2009) Inorganic mercury detection and controlled release of chelating agents from ion-responsive liposomes, *Chem Biol 16*, 937-942.

32. Ono, A., and Togashi, H. (2004) Highly selective oligonucleotide-based sensor for mercury(II) in aqueous solutions, *Angew Chem Int Ed Engl 43*, 4300-4302.

33. Lee, J. S., Han, M. S., and Mirkin, C. A. (2007) Colorimetric detection of mercuric ion (Hg2+) in aqueous media using DNA-functionalized gold nanoparticles, *Angew Chem Int Ed Engl 46*, 4093-4096.

34. Xue, X., Wang, F., and Liu, X. (2008) One-step, room temperature, colorimetric detection of mercury (Hg2+) using DNA/nanoparticle conjugates, *J Am Chem Soc 130*, 3244-3245.

35. Li, D., Wieckowska, A., and Willner, I. (2008) Optical analysis of Hg2+ ions by oligonucleotide-gold-nanoparticle hybrids and DNA-based machines, *Angewandte Chemie-International Edition 47*, 3927-3931.

36. Xie, J. P., Zheng, Y. G., and Ying, J. Y. (2010) Highly selective and ultrasensitive detection of Hg2+ based on fluorescence quenching of Au nanoclusters by Hg2+-Au+ interactions, *Chemical Communications 46*, 961-963.

37. Mazumdar, D., Liu, J., Lu, G., Zhou, J., and Lu, Y. (2010) Easy-to-use dipstick tests for detection of lead in paints using non-cross-linked gold nanoparticle-DNAzyme conjugates, *Chem Commun (Camb) 46*, 1416-1418.

38. Liu, J., Mazumdar, D., and Lu, Y. (2006) A simple and sensitive "dipstick" test in serum based on lateral flow separation of aptamer-linked nanostructures, *Angew Chem Int Ed Engl 45*, 7955-7959.

39. Mirkin, C. A. (2000) Programming the assembly of two- and three-dimensional architectures with DNA and nanoscale inorganic building blocks, *Inorg Chem 39*, 2258-2272.

40. Zhao, W., Ali, M. M., Aguirre, S. D., Brook, M. A., and Li, Y. (2008) Paper-based bioassays using gold nanoparticle colorimetric probes, *Anal Chem 80*, 8431-8437.

41. Liu, J., and Lu, Y. (2006) Preparation of aptamer-linked gold nanoparticle purple aggregates for colorimetric sensing of analytes, *Nat Protoc 1*, 246-252.

42. Liu, J., and Lu, Y. (2005) Fast colorimetric sensing of adenosine and cocaine based on a general sensor design involving aptamers and nanoparticles, *Angew Chem Int Ed Engl 45*, 90-94.

43. Tanaka, Y., Oda, S., Yamaguchi, H., Kudo, M., Kondo, Y., Kojima, C., and Ono, A. (2006) Structural analyses on the mercuryII-mediated T-T base pair, *Nucleic Acids Symp Ser (Oxf)*, 47-48.

44. Kumar, M., Dhir, A., Bhalla, V., Sharma, R., Puri, R. K., and Mahajan, R. K. (2010) Highly effective chemosensor for mercury ions based on bispyrenyl derivative, *Analyst*.

45. Zhang, L., Li, T., Li, B., Li, J., and Wang, E. (2010) Carbon nanotube-DNA hybrid fluorescent sensor for sensitive and selective detection of mercury(II) ion, *Chem Commun (Camb) 46*, 1476-1478.

46. Wang, H., Wang, Y., Jin, J., and Yang, R. (2008) Gold nanoparticle-based colorimetric and "turn-on" fluorescent probe for mercury(II) ions in aqueous solution, *Anal Chem 80*, 9021-9028.

47. Miyake, Y., Togashi, H., Tashiro, M., Yamaguchi, H., Oda, S., Kudo, M., Tanaka, Y., Kondo, Y., Sawa, R., Fujimoto, T., Machinami, T., and Ono, A. (2006) MercuryII-mediated formation of thymine-HgII-thymine base pairs in DNA duplexes, *J Am Chem Soc 128*, 2172-2173.